

The role of Eg5 in EML4-ALK driven lung cancer

Thesis submitted for the degree of
Doctor of Philosophy
at the University of Leicester

by

Sarah Louise Pashley

Department of Molecular and Cell Biology
The University of Leicester

June 2023

The role of Eg5 in EML4-ALK driven lung cancer

Sarah Louise Pashley

Abstract

EML4-ALK fusions are found in approximately 5% of lung cancer patients. Multiple variants of the EML4-ALK fusion exist due to alternate breakpoints in the *EML4* gene. EML4-ALK variant 3 (V3) is a significant clinical risk factor being associated with accelerated metastasis, heightened resistance to ALK inhibitor treatment and worse survival rates compared to other common variants, such as V1. Interestingly, EML4-ALK V3 but not V1 binds interphase microtubules. Cells expressing EML4-ALK V3 display a more mesenchymal-like morphology and exhibit enhanced migration. These phenotypic changes rely on EML4-ALK V3 interaction and activation of the NEK9 and NEK7 kinases. However, the downstream substrates of this pathway and how they contribute to oncogenic progression remain unclear.

Here, we have tested the hypothesis that the mitotic kinesin, Eg5, is a downstream substrate of the EML4-ALK V3:NEK9:NEK7 pathway. NEK7 is known to phosphorylate Eg5 to promote centrosome separation in mitosis and dendrite extension in post-mitotic neurons. Strikingly, we found that in proliferating cells, Eg5 is recruited to interphase microtubules in cells expressing EML4-ALK V3 but not V1. Furthermore, this recruitment was reduced upon depletion of NEK7 from V3 cells. The mesenchymal morphology of V3 cells was also lost upon chemical inhibition of Eg5 or expression of a phosphonull-Eg5 mutant. We therefore propose that Eg5 is a downstream substrate of the EML4-ALK V3:NEK9:NEK7 pathway that contributes to microtubule-dependent morphological changes in cells expressing V3.

We also investigated whether EML4-ALK V3 has a role at the centrosome based on recent published findings that cells expressing V3 exhibit centrosome amplification and enhanced microtubule nucleation. Strikingly, we found EML4-ALK V3 but not V1 co-localised with interphase centrosomes but that this was not associated with recruitment of Eg5. Together, our data provide new mechanistic insights that reveal novel therapeutic opportunities for treatment of lung cancer patients with EML4-ALK V3.

Acknowledgements

I'd firstly like to thank my supervisor Professor Andrew Fry for his support and guidance throughout my PhD. Your knowledge and experience is so inspiring and I'm so grateful that you have shared that with me. Thank you so much for the patience, kindness and care you have shown me over the last four years. You really are the most amazing supervisor!

I'd also like to thank my second supervisor Dr Sally Prigent and my committee panel Dr Sue Shackleton and Professor Karen Brown for the helpful discussions and feedback they provided throughout my project. Thank you also to Dr Raj Patel for being an additional lifeline and for giving me my first lab experience when I was a young summer student a few moons ago!

Thank you also to the rest of the Fry lab for their friendship and support and to Natasha Beasley, our fantastic summer student for her enthusiasm and strong work ethic and her contribution to our work.

A huge thank you to Dr Kees Straatman for his support with many many things! I really can't thank you enough for the number of hours you have spent with me and the amount I have learned from you.

Thank you to the MRC IMPACT DTP for funding my PhD and providing me with so many exciting and exceptional opportunities. Thank you to Louise, Dan, Karen and Vikki and also to the 2019 cohort for always providing me with a source of positivity and for the friendships we have made.

Lastly, I'd like to thank my incredible parents for giving me the confidence and freedom to follow my dreams and supporting me no matter how big and scary they are. I was truly blessed to be born into your family and to have you as my life guides.

COVID-19 impact statement

Research undertaken in this thesis was carried out during the COVID-19 pandemic. As a result of the pandemic, access to the lab was significantly affected where initially no access was allowed at all for a period of five months (April 2020 – August 2020) and later only restricted part-time access was allowed for a period of around ten months due to building occupancy limits. Thus, the number of experiments performed during this period was greatly reduced. Additionally, there were also COVID-related delays in receiving some reagents and general lab stocks which further contributed to the disruption of research undertaken in this thesis.

Table of Contents

Abstract	I
Acknowledgments	II
COVID-19 impact statement	III
Table of contents	IV
List of tables	VIII
List of figures	VIII
Abbreviations	XI
CHAPTER 1: Introduction	1
1.1. Lung cancer	2
1.1.1. Incidence, classification and diagnosis	2
1.1.2. Oncogenic drivers of lung adenocarcinoma	2
1.1.3. Current treatments of lung cancer	6
1.2. EML4-ALK fusions.....	7
1.2.1. Discovery and occurrence in cancer	7
1.2.2. Echinoderm microtubule-associated protein-like (EML) proteins	8
1.2.3. Anaplastic Lymphoma Kinase (ALK).....	13
1.2.4. EML4-ALK fusion proteins.....	15
1.2.5. ALK inhibitors in current therapies.....	21
1.3. Mammalian NEK kinases.....	23
1.3.1. Never In Mitosis A (NIMA) protein	23
1.3.2. The NEK kinase family.....	23
1.3.2.1. NEK9	24
1.3.2.2. NEK6 and NEK7	27
1.3.3. The NEK9-NEK6/NEK7 signalling cascade	30
1.4. Microtubules.....	33
1.4.1. Microtubule structure, organisation and function.....	33
1.4.2. Microtubule motors.....	36
1.4.3. The centrosome and microtubule nucleation	39
1.4.4. Microtubule post-translational modifications.....	42
1.5. The Eg5 kinesin	44

1.5.1. Eg5 structure and function	44
1.5.2. Eg5 in centrosome separation and spindle formation	45
1.5.3. Eg5 in neurons	47
1.5.4. Eg5 as a microtubule polymerase.....	50
1.5.5. Eg5 in cancer.....	50
1.5.6. Eg5 inhibitors	52
1.6. Cell migration.....	54
1.6.1. Mesenchymal cell migration.....	54
1.6.2. Epithelial to mesenchymal transition.....	59
1.6.3. The role of microtubules in cell migration	61
1.7. Aims and objectives	64
CHAPTER 2: Materials and methods.....	66
2.1. Materials and reagents	67
2.2. Methods.....	73
2.2.1. Cell culture	73
2.2.1.1. Cell maintenance	73
2.2.1.2. Cell storage	73
2.2.1.3. Induction of proteins in inducible cell lines.....	73
2.2.1.4. FuGENE transfection	74
2.2.1.5. siRNA depletion	74
2.2.1.6. Embedding in collagen for 3D cell culture.....	75
2.2.1.7. Collagen-coated coverslips	75
2.2.1.8. Microtubule depolymerisation and regrowth assay	75
2.2.2. Preparation of Eg5 constructs	76
2.2.3. Cell lysis, SDS-PAGE and Western blotting.....	76
2.2.4. Fixed and live cell microscopy	77
2.2.4.1. Immunofluorescence staining	77
2.2.4.2. Confocal microscopy.....	78
2.2.4.3. Super-resolution imaging.....	78
2.2.4.4. Live cell imaging	78
2.2.5. Quantitative analyses	78
2.2.5.1. Imaris co-localisation analysis.....	78

2.2.5.2. Fiji co-localisation analysis	79
2.2.5.3. Fluorescence intensity analysis.....	79
2.2.5.4. Cell length analysis.....	80
2.2.5.5. Single cell migration analysis	80
2.2.5.6. Western blot quantification.....	80
2.2.5.7. Statistical analysis	81
CHAPTER 3: EML4-ALK V3 promotes recruitment of Eg5 to interphase microtubules downstream of NEK7	82
3.1. Introduction	83
3.2. Results.....	85
3.2.1. Characterisation of EML4-ALK variant expression in cell lines used in this study85	
3.2.2. Analysis of Eg5 expression in EML4-ALK cell lines.....	87
3.2.3. Localisation of Eg5 to the mitotic spindle in cells expressing EML4-ALK variants	89
3.2.4. Comparison of methods for measuring co-localisation	89
3.2.5. Eg5 is recruited to interphase microtubules in EML4-ALK V3 expressing cells....	94
3.2.6. NEK7 depletion reduces Eg5 localisation to interphase microtubules in V3 expressing cells	97
3.2.7. Phosphomimetic Eg5 localises to interphase microtubules in cells expressing EML4-ALK V1	100
3.2.8. Eg5 is not recruited to phase separated foci formed by EML4-ALK variants.....	106
3.3. Discussion.....	109
CHAPTER 4: The morphology of cells expressing EML4-ALK V3 is dependent on phosphorylation and motor activity of Eg5	113
4.1. Introduction	114
4.2. Results.....	117
4.2.1. Characterising Eg5 inhibitors in EML4-ALK expressing cells.....	117
4.2.2. Eg5 inhibitors reduce the cell length of cells expressing EML4-ALK V3	123
4.2.3. Eg5 inhibitors did not alter migration of EML4-ALK V3 cells embedded in collagen.....	127
4.2.4. NEK7 phosphorylation of Eg5 on S1033 regulates cell length	133
4.2.5. NEK7 depletion reduces microtubule stability of EML4-ALK V3 cells	134

4.2.6. It is unclear whether microtubule stability is regulated by phosphorylation of Eg5	137
4.3. Discussion.....	143
CHAPTER 5: EML4-ALK V3 has a role at the centrosome independent of NEK7 and Eg5..	148
5.1. Introduction	149
5.2. Results.....	151
5.2.1. EML4-ALK V3 localises to the centrosome in interphase BEAS-2B cells	151
5.2.2. Neither NEK7 nor Eg5 are recruited to centrosomes in BEAS-2B:EML4-ALK V3 cells	157
5.2.3. EML4-ALK V3 expressing BEAS-2B cells have increased microtubule nucleation capacity.....	158
5.3. Discussion.....	167
CHAPTER 6: Discussion	171
6.1. Summary	172
6.2. EML4-ALK biology and current treatment of ALK rearranged NSCLC	172
6.3. Eg5 is a downstream substrate of the EML4-ALK V3:NEK9:NEK7 signalling module	174
6.4. Eg5 activity is required for altered cell morphology in EML4-ALK V3 cells	176
6.5. Could Eg5 inhibitors be used in the treatment of lung cancer?.....	180
6.6. EML4-ALK V3 promotes microtubule nucleation at the centrosome	181
6.7. Implications and future perspectives	183
6.8. Concluding statement.....	185
CHAPTER 7: Bibliography	186

List of Tables

Table 2.1.1. Reagents and materials.....	67
Table 2.1.2. Plasmids	69
Table 2.1.3. Sequencing primers.....	69
Table 2.1.4. Cell lines	69
Table 2.1.5. Cell culture reagents	70
Table 2.1.6. Cell culture materials	70
Table 2.1.7. Drugs	71
Table 2.1.8. siRNAs.....	71
Table 2.1.9. Primary antibodies	71
Table 2.1.10. Secondary antibodies.....	72

List of Figures

Chapter 1

Figure 1.1. Histological classification of lung cancer	3
Figure 1.2. Incidence of oncogenic drivers of lung adenocarcinoma.....	5
Figure 1.3. EML proteins	10
Figure 1.4. The ALK tyrosine kinase receptor	14
Figure 1.5. EML4-ALK variants	17
Figure 1.6. Current working model of EML4-ALK V3:NEK9:NEK7 pathway.....	20
Figure 1.7. Comparison of <i>Aspergillus</i> NIMA and human NEK kinase domain organisation	25
Figure 1.8. Mechanism of NEK7 activation.....	32
Figure 1.9. Dynamic instability of microtubules	35
Figure 1.10. Phylogenetic tree of the mouse kinesin superfamily	37
Figure 1.11. The centrosome duplication cycle	41
Figure 1.12. Schematic diagram of Eg5 domain structure.....	46
Figure 1.13. NEK7 phosphorylation of Eg5 at S1033 promotes dendrite extension in neurons	49
Figure 1.14. Mechanisms of Eg5 inhibitors.....	53

Figure 1.15. Four steps of mesenchymal cell migration.....	56
--	----

Chapter 3

Figure 3.1. Expression of EML4-ALK variants in cell lines used in this study.....	86
Figure 3.2. Eg5 expression in EML4-ALK cell lines	88
Figure 3.3. Eg5 localises to the mitotic spindle in cells expressing EML4-ALK variants	91
Figure 3.4. Imaris software was used for co-localisation analysis.....	92
Figure 3.5. Schematic diagram showing why the PlotMultiColor macro is not appropriate for measuring co-localisation of punctate staining patterns	93
Figure 3.6. Eg5 co-localises with interphase microtubules in BEAS-2B cells expressing EML4-ALK V3	95
Figure 3.7. Eg5 co-localises with interphase microtubules in H2228 cells	96
Figure 3.8. NEK7 depletion reduces Eg5 recruitment to interphase microtubules in BEAS-2B:EML4-ALK V3 cells	98
Figure 3.9. NEK7 depletion reduces Eg5 recruitment to interphase microtubules in H2228 cells.....	102
Figure 3.10. More S1033D Eg5 localises with interphase microtubules in BEAS-2B:EML4-ALK V1 cells than WT Eg5	104
Figure 3.11. Eg5 is not recruited to phase separated foci in BEAS-2B:EML4-ALK cell lines.....	107
Figure 3.12. Eg5 is not recruited to phase separated foci in NSCLC patient cell lines	108

Chapter 4

Figure 4.1. Eg5 inhibitors arrest BEAS-2B:EML4-ALK cells in mitosis	119
Figure 4.2. Eg5 inhibitors arrest H2228 cells in mitosis.....	120
Figure 4.3. Eg5 inhibitors result in the formation of monopolar spindles	122
Figure 4.4. The length of BEAS-2B:EML4-ALK V3 cells is significantly reduced by Eg5 inhibitors filanesib and BRD9876.....	124
Figure 4.5. The length of H2228 (V3) cells is significantly reduced by Eg5 inhibitors filanesib and BRD9876	126
Figure 4.6. BEAS-2B:EML4-ALK V3 cells travel further and faster than V1 cells.....	128
Figure 4.7. Eg5 inhibitors have no effect on migration of BEAS-2B:EML4-ALK V3 cells	129
Figure 4.8. BRD9876 reduced distance and speed of migration in H2228 cells.....	132

Figure 4.9. Phosphorylation of Eg5 on S1033 regulates cell length of BEAS-2B cells	135
Figure 4.10. S1033D Eg5 rescues the length of BEAS-2B V3 cells after NEK7 depletion	136
Figure 4.11. NEK7 depletion reduces acetylated tubulin intensity in BEAS-2B:EML4-ALK V3 cells	139
Figure 4.12. NEK7 depletion reduced acetylated tubulin intensity in H2228 (V3) cells	140
Figure 4.13. Eg5 phospho-mutants do not rescue acetylated tubulin intensity after NEK7 depletion	141

Chapter 5

Figure 5.1. A combination nocodazole and cold treatment was performed in BEAS-2B and NSCLC cell lines	152
Figure 5.2. EML4-ALK V3 co-localises with the centrosome in BEAS-2B:EML4-ALK V3 cells	154
Figure 5.3. There is little recruitment of EML4-ALK variants to the centrosome in NSCLC cell lines	156
Figure 5.4. NEK7 is not selectively recruited to interphase centrosomes in BEAS-2B:EML4-ALK V3 cells.....	159
Figure 5.5. Eg5 is not selectively recruited to interphase centrosomes in BEAS-2B:EML4-ALK V3 cells.....	160
Figure 5.6. Time course of microtubule repolymerisation in BEAS-2B cells	162
Figure 5.7. BEAS-2B V3 cells have larger nucleation sites than parental cells	163
Figure 5.8. Time course of microtubule regrowth in NSCLC cell lines.....	165
Figure 5.9. H2228 (V3) cells have a higher microtubule nucleation capacity than H3122 (V1) cells	166

Chapter 6

Figure 6.1. Schematic figure of how the EML4-ALK V3:NEK9:NEK7 complex may regulate microtubule and actin associated proteins.....	179
---	-----

Abbreviations

ABL1 – Abelson murine leukaemia
ADP – Adenosine diphosphate
ALAD – alanine-leucine-alanine-aspartic acid
ALCL – anaplastic large cell lymphoma
ALK – Anaplastic Lymphoma Kinase
APC – adenomatous polyposis coli
aPKC – atypical protein kinase C
APS – ammonium persulfate
Arp2/3 – actin related protein 2/3
 α TAT1 – α -tubulin acetyltransferase 1
ATP – adenosine triphosphate
Ba/F3 – murine interleukin-3 dependent pro-B cell line
BASS – bipolar assembly
BEAS – bronchial epithelial cells
BRD9876 - 6-(1,1-dimethylethyl)-2,3-naphthalenedicarbonitrile
BSA – bovine serum albumin
CDC25B – cell division cycle 25B
CDK1 – cyclin dependent kinase 1
cDNA – complementary DNA
CHK1/2 – checkpoint kinase 1/2
ch-TOG – cytoskeleton-associated protein 5
CLASP1 – cytoplasmic linker-associated protein 1
CLIP170 – cytoplasmic linker protein 170
DMEM – Dulbecco's Modified Eagle Media
DMSO – dimethyl sulfoxide
DNA – deoxyribose nucleic acid
DTT – dithiothreitol

ECL – enhanced chemiluminescence

ECM – extracellular matrix

EDTA – ethylenediaminetetraacetic acid

EGFR – epidermal growth factor receptor

ELP – EMAP like proteins

EMAP – Echinoderm microtubule associated protein

EML(1-6) – Echinoderm microtubule associated protein like (1-6)

EML2-L – EML2 long isoform

EML2-S – EML2 short isoform

EMT – epithelial to mesenchymal transition

ERK – extracellular signal-regulated kinase

FAK – focal adhesion kinase

FBS – foetal bovine serum

FBXO11 – F-box only protein 11

FCPT - 2-[1-(4-fluorophenyl)cyclopropyl]-4-(pyridin-4-yl)thiazole

FDA – Food and Drug Administration (USA)

FLAG – DYKDDDDK tag

GADD54A – growth arrest and DNA-damage-inducible protein

γ TuRC – γ -tubulin ring complex

GAPDH – glyceraldehyde-3-phosphate dehydrogenase

GCP – γ -tubulin complex protein

GEF – guanine nucleotide exchange factor

GTP – Guanine triphosphate

HCl – hydrochloric acid

HDAC6 – histone deacetylase 6

HELP – hydrophobic EML protein

HEPES – 4-(2-hydroxyethyl)-1-piperazineethanesulfonic acid

HRP – horseradish peroxidase

HSP72/90 – heat shock protein 72/90

HUVEC – human umbilical vein endothelial cells
IHC – Immunohistochemistry
IQGAP1 – Ras GTPases-activating-like protein IQGAP1
JAK – Janus kinase
KCl – potassium chloride
KH₂PO₄ – monopotassium phosphate
Kif – kinesin family member
K-fibre – kinetochore fibres
KRAS – Kirsten rat sarcoma
L5 – loop 5
LB – Luria broth
LDLa – low-density lipoprotein receptor class A
LIMKs – Lin11, Isl1, Mec3 kinases
MAM – meprin A-5 protein and receptor protein-tyrosine phosphatase mu
MAP – microtubule-associated protein
MCAK – mitotic centrosome-associated kinesin
McTN - microtentacles
MEF – mouse embryonic fibroblast
MET – mesenchymal-epithelial transition
MLC – myosin light chain
mRNA – messenger RNA
MTOC – microtubule organising centre
NaCl – sodium chloride
NaHCO₃ – sodium bicarbonate
Na₂HPO₄ – disodium phosphate
NaOH – sodium hydroxide
NEDD1 – neural precursor cell expressed, developmentally down-regulated 1
NEK – NIMA-related kinase
NHS – National Health Service (UK)

NIMA – Never In Mitosis A
NLRP3 – NLR family pyrin domain containing 3
NLS – nuclear localisation signal
NPM – nucleophosmin
NSCLC – Non-small cell lung cancer
PAK – p21-activated kinases
PBS – phosphate buffered saline
PCM – pericentriolar material
PEST – proline-glutamic acid-serine-threonine
PFS – progression free survival
PI3K – phosphoinositide 3-kinases
PLK1 – polo like kinase 1
PTM – post-translational modification
RCC1 – regulator of chromosome condensation 1
RGS2 – regulator of G-protein signalling 2
ROCKs – Rho-associated coiled-coil containing kinases
r.o.i – region of interest
rpm – revolutions per minute
RPMI – Roswell Park Memorial Institute
RTK – receptor tyrosine kinase
SAC – spindle assembly checkpoint
SCLC – Small cell lung cancer
SDS – sodium dodecyl sulphate
siRNA – small interfering RNA
SIRT2 – sirtuin 2
STAT – signal transducer and activator of transcription proteins
STLC – S-Trityl-L-Cysteine
SVBP – small vasohibin binding protein
TACC3 – transforming acidic coiled-coil-containing protein 3

TAPE – tandem atypical β -propeller in EML protein

TD – trimerization domain

TE – Tris-EDTA

TEMED - tetramethylethylenediamine

TPX2 – microtubule nucleation factor

TTF-1 – thyroid transcription factor 1

TTL – tubulin tyrosine ligase

V1 – Variant 1

V2 – Variant 2

V3 – Variant 3

V4 – Variant 4

V5 – Variant 5

VASH – vasohibin

WASP – Wiskott-Aldrich syndrome protein

WD – tryptophan-aspartic acid

WT – wild type

YFP – yellow fluorescent protein

+TIP - +end tracking protein

CHAPTER 1

Introduction

1.1. Lung cancer

1.1.1. Incidence, classification and diagnosis

Lung cancer remains the leading cause of cancer related death worldwide, accounting for around a quarter of these deaths (cancer.org, 2022). In the UK, 21% of cancer-related deaths are the result of lung cancer (Cancer Research UK, nd). According to the American Cancer Society, more people die from lung cancer each year than breast, colon and prostate cancers combined (cancer.org, 2022). Lung cancers are classified as either small cell lung cancer (SCLC) or non-small cell lung cancer (NSCLC) with around 85% of lung cancers being NSCLC (Figure 1.1) (cancer.org, 2022). NSCLC is further divided into three categories: adenocarcinomas, squamous cell carcinomas and large cell carcinomas, with adenocarcinomas being the most common type, accounting for around 40% of all NSCLC cases (Figure 1.1) (National Cancer Institute, 2022; Zappa and Mousa, 2016).

Adenocarcinomas arise in alveolar cells that secrete mucus usually in the periphery of the lung. In contrast, squamous cell carcinomas arise from epithelial cells that line the airways and extend into the centre of the lungs (Zappa and Mousa, 2016). Large cell carcinomas are often diagnosed as a tumour that fails to fit into adenocarcinoma or squamous cell carcinoma categories, but also usually tend to begin in the centre of the lung (Zappa and Mousa, 2016). This classification of lung cancer is usually determined using immunohistochemical (IHC) analysis of tissue samples taken from a patient's tumour. Adenocarcinomas and squamous cell carcinomas both have distinct diagnostic markers, Thyroid Transcription Factor-1 (TTF-1) for adenocarcinoma and p40 or p63 for squamous cell carcinoma (Fletcher, 2019; Stenhouse *et al.*, 2004; Nobre, Albergaria and Schmitt, 2013). Large cell carcinoma is usually diagnosed if none of these diagnostic markers are found (Fletcher, 2019).

1.1.2. Oncogenic drivers of lung adenocarcinoma

Many lung adenocarcinomas share common genetic alterations. Three of the most frequently seen oncogenic drivers are *KRAS* mutations, *EGFR* mutations and *ALK*

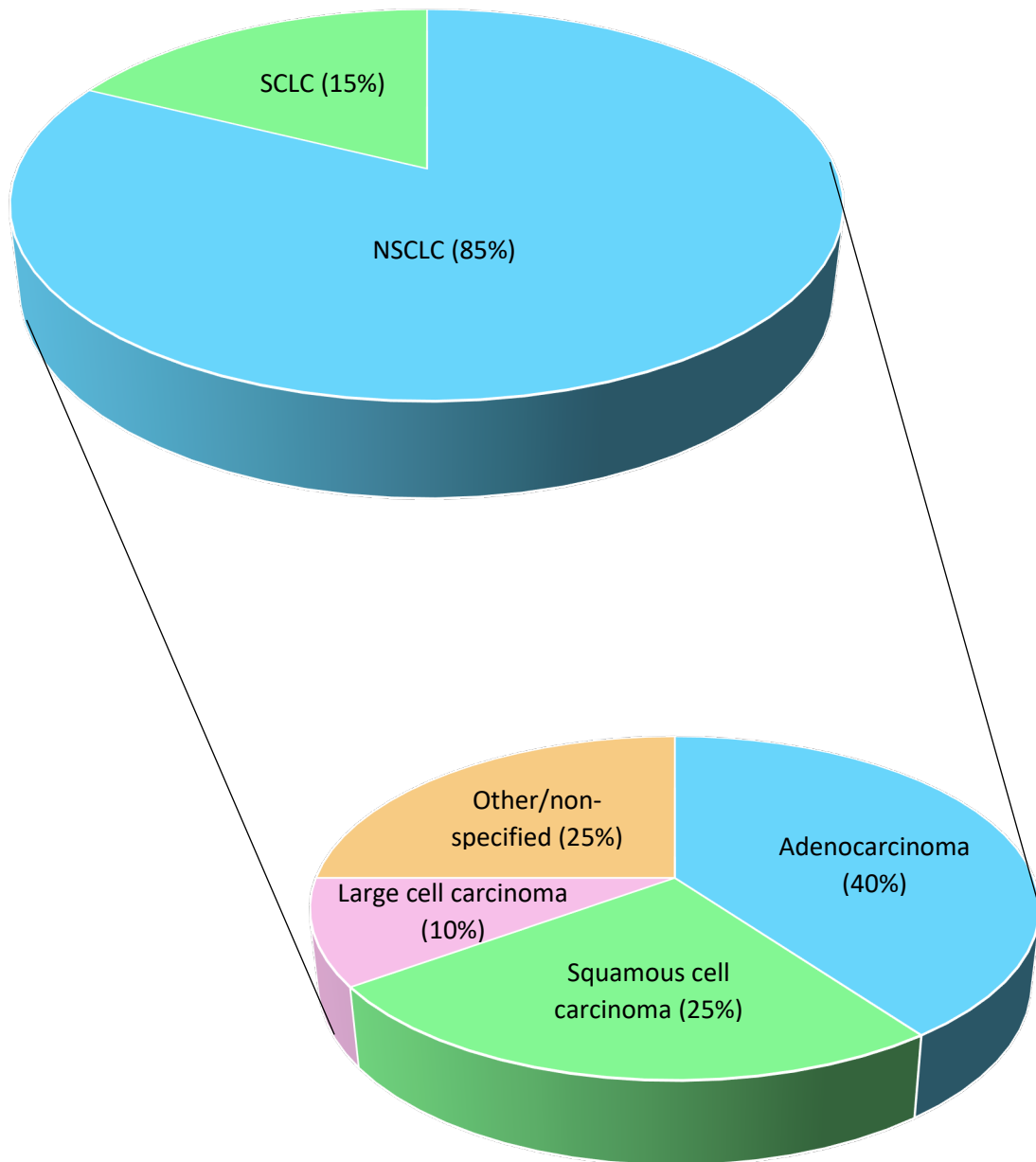


Figure 1.1. Histological classification of lung cancer. Lung cancers are categorised as either SCLC or NSCLC (top). NSCLC are then further subcategorised into adenocarcinoma, squamous cell carcinoma or large cell carcinoma based on IHC analysis (bottom). Figure adapted from Targeted Oncology (2017).

rearrangements (Figure 1.2) (Luo and Lam, 2013; Grosse *et al.*, 2019). Many other genetic alterations have been identified, such as mutations in *BRAF* or *MET* or fusions of *ROS1* or *RET*, albeit these occur less frequently and will not be discussed further in this thesis (Chevallier *et al.*, 2021).

Mutations in the *Kirsten rat sarcoma (KRAS) gene* occur in approximately 30% of lung adenocarcinomas, making these the most common oncogenic driver of this cancer type (Chevallier *et al.*, 2021; Grosse *et al.*, 2019). As KRAS is a small GTPase, some mutations lead to its constitutive activation and subsequently the activation of signalling cascades which result in cancer cell proliferation (Chevallier *et al.*, 2021). Interestingly, the mutation of residue G12 is frequently seen in multiple cancer types and is thought to account for as many as 89% of *KRAS* mutations (Liu, Kang and Tang, 2022). Most commonly mutated to G12C in NSCLC, inhibitors that target this mutant protein have been developed: sotorasib and adagrasib (Liu, Kang and Tang, 2022). Excitingly, sotorasib was approved for the treatment of NSCLC by the FDA in 2021 and was made available to patients in the UK via the NHS a year later (Jaber, 2021; NHS England, 2022). Previously, patients that presented with mutant *KRAS* would have been treated with chemotherapy and, more recently, immunotherapy (Chevallier *et al.*, 2021).

The second most frequently occurring genetic alteration in lung adenocarcinoma is mutation of the *Epidermal Growth Factor receptor (EGFR)*, with approximately 19% of these cancers possessing a mutation in this gene (Chevallier *et al.*, 2021; Grosse *et al.*, 2019). EGFR belongs to the ErbB family of receptors and consists of an extracellular ligand binding domain, a transmembrane domain and an intracellular tyrosine kinase domain (Díaz-Serrano *et al.*, 2018). Ligand binding to EGFR results in its dimerization, either with itself or other members of the ErbB receptor family, and activation of the tyrosine kinase domain. Activation of EGFR results in activation of multiple downstream signalling pathways including JAK/STAT, PI3K/Akt and RAS/RAF/MAPK, which ultimately lead to cell proliferation, survival and migration (Díaz-Serrano *et al.*, 2018). In lung cancers, deletion of exon 19 or

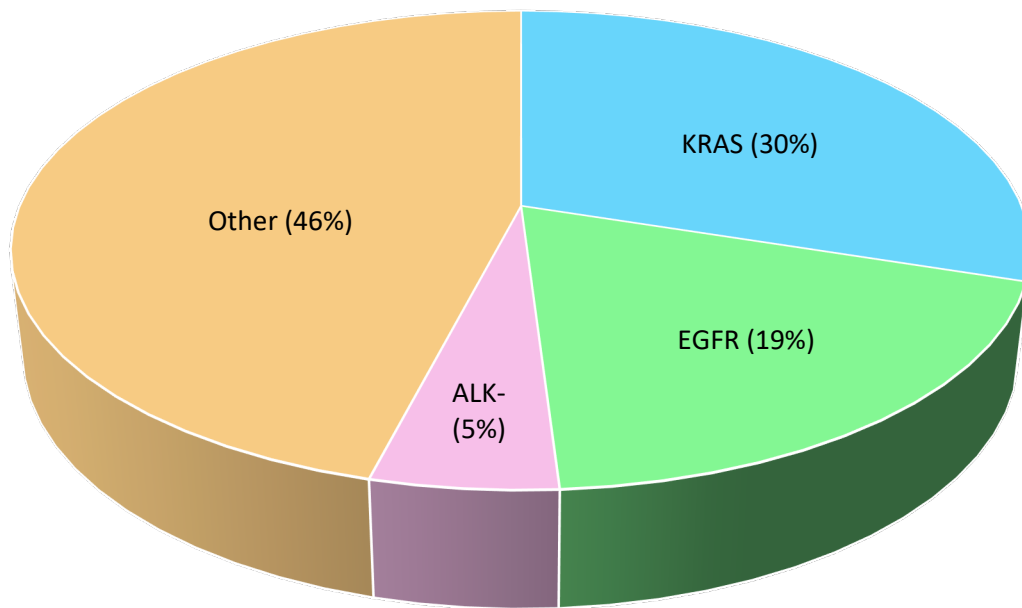


Figure 1.2. Incidence of oncogenic drivers of lung adenocarcinoma. The three most common oncogenic drivers of lung adenocarcinoma are proportionally shown in the pie chart – KRAS (blue), EGFR (green) and ALK (pink). Other (orange) represents all other known oncogenic drivers of these cancers as well as samples where no oncogenic driver is identified.

L858R substitution in exon 21, both found in the tyrosine kinase domain, collectively account for around 90% of oncogenic genetic alterations present in EGFR (Díaz-Serrano *et al.*, 2018; Chevallier *et al.*, 2021). These alterations result in ligand-independent activation of EGFR and drive cell proliferation through activation of the downstream signalling pathways (Chevallier *et al.*, 2021). Interestingly, EGFR mutations frequently occur in patients with limited smoking history (Díaz-Serrano *et al.*, 2018). To date, three generations of EGFR inhibitors have been approved for use in the clinic, although acquired resistance is a significant problem and forms the basis of further research into future generations of EGFR inhibitors (Díaz-Serrano *et al.*, 2018).

The third most common genetic alteration found in lung adenocarcinomas is fusion of the *Anaplastic Lymphoma Kinase (ALK)* gene, which exists in approximately 5% of lung adenocarcinomas (Grosse *et al.*, 2019; Chevallier *et al.*, 2021). Multiple ALK fusion partners have been identified. However, the most common fusion partner in NSCLC is *EML4* (Du *et al.*, 2018; Liu *et al.*, 2020). EML4-ALK fusions are thoroughly discussed in section 1.2. and form the basis for this study.

1.1.3. Current treatments of lung cancer

Current treatments for lung cancer include surgery, radiotherapy, chemotherapy and immunotherapy and are very much assessed on a case-by-case basis. Factors that determine which treatment is most suitable for each patient include whether the cancer is in one lung or both, whether the cancer has spread further than the lungs and a patient's general health (nhs.uk, 2019). If the cancer is just in one lung and the patient is in good health generally, surgery is usually recommended. The procedure recommended depends on the number, size and positioning of the tumour(s) and will either involve removing one small piece of the lung (small tumours in one position in the lung); a large piece of the lung (larger tumour in one position) or the entire lung (if the tumour is located in the middle of the lung or there are multiple tumours throughout the lung). This may then be followed by chemotherapy to ensure any cancerous cells left behind after surgery are killed (NHS, 2019; Zappa and Mousa, 2016).

If surgery is deemed unsuitable for a patient, radiotherapy can be offered as an alternative (Lemjabbar-Alaoui *et al.*, 2015; NHS, 2019). This can either be used alone or in combination with chemotherapy. Radiotherapy can be given in different ways – either externally (conventional or stereotactic) or internally where a radioactive material delivered by a catheter is pressed up against the tumour. External radiotherapy is more commonly used in the treatment of lung cancer and internal radiotherapy is more often used in palliative care (NHS, 2019).

If the cancer has spread beyond the lungs, chemotherapy or immunotherapy are recommended (Lemjabbar-Alaoui *et al.*, 2015; NHS, 2019). Chemotherapy provides a combination of toxic drugs such as platinum compounds (cisplatin/carboplatin), taxanes (docetaxel/paclitaxel), vinca alkaloids (vinblastine), usually administered via an intravenous drip and given repeatedly over multiple sessions (Zappa and Mousa, 2016). The number of chemotherapy sessions needed depend on the type and grade of the cancer. Alternatively, immunotherapy aims to stimulate the immune system to attack cancer cells. Common immunotherapeutic drugs used in the treatment of lung cancer are pembrolizumab and atezolizumab (NHS, 2019).

Finally, if the cancer contains specific mutations such as the ones described in section 1.1.2., targeted therapies may be offered either as an alternative to chemotherapy, or after a course of chemotherapy has been given. Targeted therapies include sotorasib for KRAS mutations, EGFR inhibitors, such as erlotinib or gefinitib, and ALK inhibitors which are discussed further in section 1.2.5. (NHS, 2019; Lemjabbar-Alaoui *et al.*, 2015; Jaber, 2021).

1.2. EML4-ALK fusions

1.2.1. Discovery and occurrence in cancer

EML4-ALK fusions were first identified in 2007 through screening of cDNA libraries produced from a specimen taken from a Japanese NSCLC patient (Soda *et al.*, 2007). In the same study, transfection of EML4-ALK constructs into mouse 3T3 fibroblasts confirmed the

transformative activity of EML4-ALK and injection of these fibroblasts into nude mice led to the development of tumours (Soda *et al.*, 2007). Further screening of a larger cohort of patients revealed that EML4-ALK fusions are found in approximately 5% of NSCLCs (Soda *et al.*, 2007). These fusions have since been identified in a variety of other cancers, including but not limited to: breast, colorectal and pancreatic cancers (Lin *et al.*, 2009; Ou *et al.*, 2021; Singhi *et al.*, 2017).

EML4-ALK fusions are the result of a chromosome inversion event of chromosome 2p (Soda *et al.*, 2007). Since the initial discovery, over fifteen different variants of EML4-ALK have been identified, further described in section 1.2.4 (Sabir *et al.*, 2017). Interestingly, EML4-ALK fusions are most commonly identified in younger patients who have no or light smoking history (Sasaki *et al.*, 2010). Importantly, EML4-ALK fusions are mutually exclusive to other common oncogenic drivers of NSCLC, including mutations in EGFR and KRAS, and are now routinely screened for in lung cancer patients (Gainor *et al.*, 2013; Lei *et al.*, 2022).

1.2.2. Echinoderm microtubule-associated protein-Like (EML) proteins

The founding member of the Echinoderm Microtubule Associated Protein (EMAP) family was initially discovered in extracts from unfertilised sea urchin eggs and was found to co-purify with microtubules and decorate microtubules both in interphase and mitotic cells (Suprenant *et al.*, 1993). EMAP orthologs were later identified in other species including worms and humans (termed EMAP-like proteins (ELP or EML)) and are relatively well conserved, with most EMLs having a basic N-terminal domain and a C-terminal domain containing WD repeats (Suprenant *et al.*, 2000; Hueston *et al.*, 2008).

Humans express six EML proteins termed EML1-EML6 (Fry *et al.*, 2016). Structurally, EML1-EML4 are highly similar, whereas EML5 and EML6 diverge from the typical EMAP structure. EML1-EML4 possess a relatively unstructured N-terminus consisting of a coiled coil and basic linker region and a highly structured C-terminus containing WD repeats and a hydrophobic EML protein (HELP) motif. Collectively, the structure formed by the WD repeats and HELP

motif is referred to as the Tandem Atypical β -Propeller in EML protein (TAPE) domain (Fry *et al.*, 2016; Richards *et al.*, 2014). Interestingly, EML5 and EML6 contain no N-terminal coiled coil and encompass three contiguous TAPE domains (Figure 1.3) (Fry *et al.*, 2016).

A crystal structure of the TAPE domain from EML1 was solved that revealed a pair of β -propellers formed from the WD repeats with the HELP domain forming a hydrophobic core between the two propellers (Richards *et al.*, 2014). Interestingly, one of the β -propellers was found to deviate from the canonical structure typical of seven bladed β -propellers (Richards *et al.*, 2014). Usually, each blade of a seven bladed β -propeller consists of antiparallel β -sheets which twist to form four strands and this is true of the N-terminal β -propeller of the EML1 TAPE domain (Richards *et al.*, 2014). The C-terminal β -propeller on the other hand, consists of six canonical blades and one non-canonical blade, where two individual subdomains form blade 12 rather than the continuous four stranded β -sheet structure previously described (Richards *et al.*, 2014). Overall, the structural integrity of the TAPE domain is maintained despite the non-canonical blade in the C-terminal β -propeller, however the secondary structure is different to typical seven bladed β -propeller proteins (Richards *et al.*, 2014).

Crystal structures of the EML2 and EML4 N-terminal coiled coil regions were also solved which revealed the coiled coil is necessary for trimerization of EML proteins leading to this region being called the trimerization domain (TD) (Richards *et al.*, 2015). Moreover, EML proteins contain a conserved ALAD (alanine, leucine, alanine, aspartic acid) motif within the TD, consisting of 17 amino acids which facilitates self-association. Intriguingly, EML proteins not only self-associate but, in some cases, heterotrimers can be formed (Richards *et al.*, 2015). Specifically, where the ALAD motif sequence is reasonably conserved between EML proteins, as is the case between EML2 and EML3 but not EML1 and EML3, co-immunoprecipitation experiments revealed hetero-association of the different EML proteins (Richards *et al.*, 2015). In addition to trimerization, the TD was also shown to be required for microtubule binding. However, the TD alone was not sufficient to confer microtubule association but the N-terminal domain as a whole could associate suggesting other

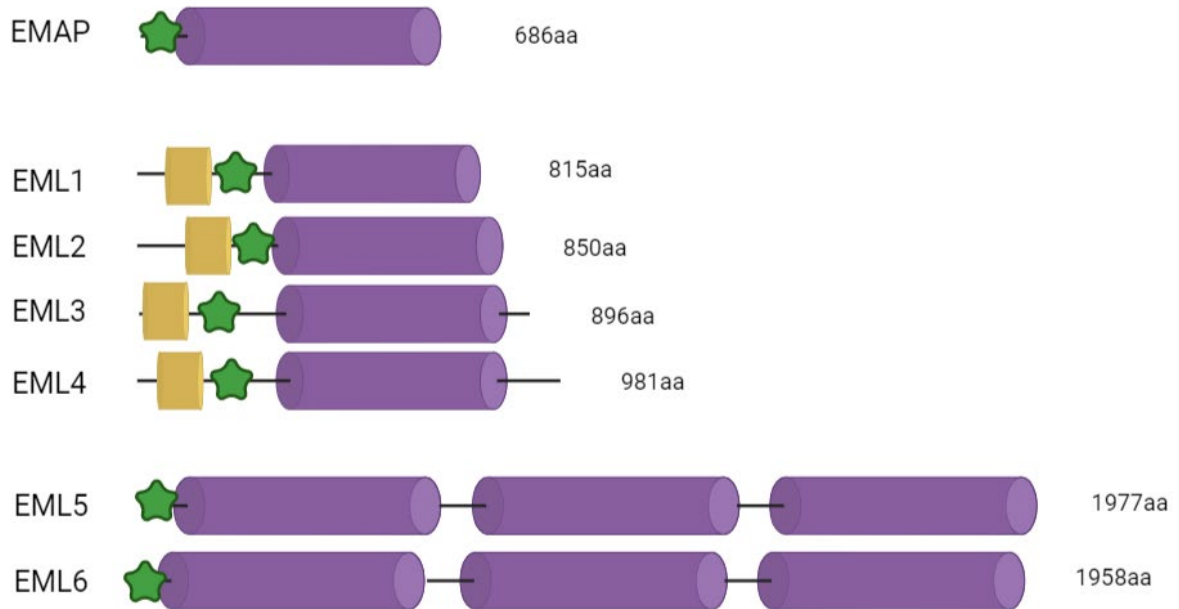


Figure 1.3. EML proteins. Schematic diagram showing the sea urchin Echinoderm Microtubule Associated Protein (EMAP) and the six human orthologs (EML1-EML6). All EMLs (and EMAP) contain a basic N-terminus (green) and at least one TAPE domain (purple). In addition, EML1-EML4 contain an N-terminal coiled coil (yellow) which facilitates trimerization. Figure adapted from Fry *et al.* (2016).

residues in the N-terminal basic linker region are required in addition to the TD (Richards *et al.*, 2015). Interestingly, the TAPE domain was shown to be capable of binding soluble α/β tubulin heterodimers (Richards *et al.*, 2014).

EML1-EML4 have all been shown capable of binding interphase microtubules (Richards *et al.*, 2015; Eichenmüller *et al.*, 2002; Tegha-Dunghu *et al.*, 2008; Pollmann *et al.*, 2006; Houtman *et al.*, 2007). In contrast, it has recently been shown in our lab using YFP/FLAG tagged constructs that EML5 and EML6 do not associate with interphase microtubules, consistent with these two EMLs lacking the N-terminal coiled coil domain (Hafiyani, 2022). Interestingly, EML6 was seen to localise at the spindle poles late in mitosis and around the contractile ring at cytokinesis, suggesting that EML6 may have a unique role towards the end stages of cell division, although this remains to be elucidated (Hafiyani, 2022).

In addition to binding interphase microtubules, EML1-EML4 have all previously been found to localise to the mitotic spindle (Eichenmüller *et al.*, 2002; Tegha-Dunghu *et al.*, 2008; Pollmann *et al.*, 2006). However, studies in our lab revealed that both EML3 and EML4 dissociate from microtubules of the mitotic spindle (Fry *et al.*, 2016; Adib *et al.*, 2019). Interestingly, it was shown that the mitotic kinases NEK6 and NEK7 (discussed in section 1.3.2.2) phosphorylate the N-terminal domain of EML4 at residues S144 and S146 and this phosphorylation perturbed EML4-microtubule interaction (Adib *et al.*, 2019). Mutation of these two residues to alanine resulted in EML4 still being present on the mitotic spindle, increasing the stability of the spindle microtubules and disturbing chromosome congression (Adib *et al.*, 2019).

It is clear from previous studies that the binding of EMLs to microtubules affects their dynamics. However, these studies present contrasting views on whether EMLs stabilise or destabilise microtubules (Houtman *et al.*, 2007; Eichenmüller *et al.*, 2002). These studies were performed on different EML proteins, so it is possible that distinct EMLs alter microtubule dynamics in a different manner. In addition, there is evidence of alternative

splicing of EML proteins so it could also be that different splice variants regulate microtubules in contrasting ways (Lepley, Palange and Suprenant, 1999). Indeed, a recent study provided some evidence for this where it was found that the short isoform of EML2 (EML2-S) preferentially binds tyrosinated microtubules whereas full length EML2 (EML2-L) had no preference for tyrosinated or detyrosinated microtubules (Hotta *et al.*, 2022). Hence, at the current time, the role of different EMLs in regulating microtubule dynamics remains unclear and further research is needed.

There is also evidence of EML proteins being associated with human disease. For example, EML1 has previously been linked to Usher's syndrome where patients suffer from deafness and blindness (Eudy *et al.*, 1997). Furthermore, EML1 mutations have been attributed to neuronal heterotopia in mice and humans, a defect in neuronal cell migration (Kielar *et al.*, 2014). Similarly, upregulation of EML5 expression in neurons and glial cells has been linked to epilepsy (Sun *et al.*, 2015). These diseases are all consistent with the expression of EML proteins in the nervous system and their suspected roles in development and mechano-transmission (Houtman *et al.*, 2007; Kielar *et al.*, 2014; O'Connor *et al.*, 2004; Hueston *et al.*, 2008).

Importantly, EML proteins have been associated with cancer where they are commonly fused to other genes forming oncogenic fusion proteins. These fusion genes are arguably more studied than the EML proteins themselves. A fusion between EML1-ABL1 was the first oncogenic fusion involving an EML protein to be identified in 2005 in T cell acute lymphoblastic leukaemia (De Keersmaecker *et al.*, 2005). Subsequently, EML4-ALK fusions were identified in NSCLC (discussed in depth in section 1.2.4) (Soda *et al.*, 2007). More recently, a double fusion involving the fusion of EML6 to ALK and FBXO11-ALK has also been identified in a tumour from a lung adenocarcinoma patient, although this fusion is currently poorly characterised (Lin, Ren and Liang, 2018). It will be interesting to see if other fusions involving EML proteins come to light in the future.

1.2.3. Anaplastic Lymphoma Kinase (ALK)

The Anaplastic Lymphoma Kinase (ALK) was first discovered in 1994 as part of an oncogenic fusion protein formed with nucleophosmin (NPM) in anaplastic large cell lymphoma (ALCL) (Morris *et al.*, 1994). Strikingly, around a third of tumours of this type have an NPM-ALK fusion in which the C-terminal kinase domain of ALK is fused to the N-terminus of NPM (Morris *et al.*, 1994). After the identification of NPM-ALK in ALCL, research began investigating the normal role of ALK in cell biology. It was later discovered by two groups that ALK was a receptor tyrosine kinase (RTK) consisting of an extracellular ligand binding domain, a transmembrane domain and an intracellular tyrosine kinase domain (Figure 1.4) (Morris *et al.*, 1997; Iwahara *et al.*, 1997). Both of these studies reported the exclusive expression of ALK in the nervous system where it is believed to be important for the normal development and function of the nervous system (Morris *et al.*, 1997; Iwahara *et al.*, 1997). However, the physiological role of ALK remains poorly understood.

The kinase domain of ALK has striking similarity to that of the insulin receptor and for this reason ALK is included in a subfamily of the insulin receptor superfamily (Morris *et al.*, 1997; Hallberg and Palmer, 2016). However, the extracellular ligand binding domain shows more divergence from other RTKs and includes a low-density lipoprotein receptor class A domain (LDL_A), meprin A-5 protein and receptor protein-tyrosine phosphatase mu (MAM) domains and a glycine-rich region (Lorén *et al.*, 2001).

The ligands capable of activating ALK were discovered much later. FAM150A and FAM150B were both found to bind to the ALK extracellular domain and activate ALK signalling (Guan *et al.*, 2015; Reshetnyak *et al.*, 2015; Reshetnyak *et al.*, 2021; De Munck *et al.*, 2021). These ligands were found to be highly expressed in the thyroid and adrenal glands respectively (Zhang *et al.*, 2014), although studies of these ligands remain scarce. Upon ligand binding, ALK dimerises and autophosphorylation results in release of an autoinhibitory confirmation and thus activates ALK (Figure 1.4) (Bossi *et al.*, 2010; Lee *et al.*, 2010; Della-Corte *et al.*, 2018). ALK signalling activates a plethora of downstream signalling pathways, including MEK/ERK, JAK/STAT and PI3K/Akt, making it easy to see how the deregulation of ALK can

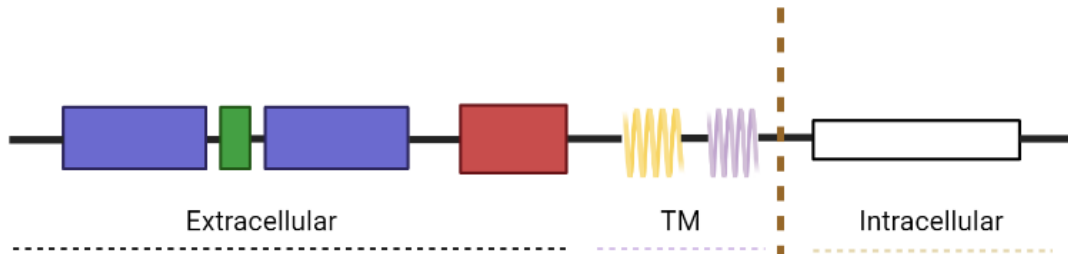
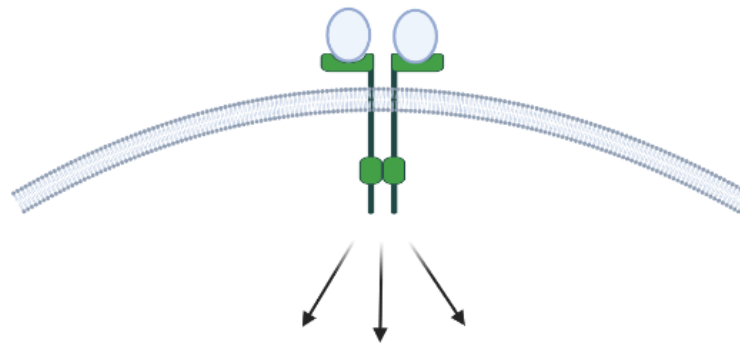
A**B**

Figure 1.4. The ALK tyrosine kinase receptor. (A) The ALK kinase consists of an intracellular tyrosine kinase domain (white) and transmembrane and juxtamembrane domains (yellow and lilac) typical of the insulin receptor superfamily. The extracellular domain is less reminiscent of the insulin receptor superfamily and consists of MAM domains (blue), an LDLa domain (green) and a glycine rich region (red). The dotted brown line represents the breakpoint in ALK, the intracellular portion of which forms fusion proteins such as EML4-ALK or NPM-ALK. (B) The ALK receptor (green) is a transmembrane receptor (cell membrane shown). Ligands (blue) bind the extracellular domain of ALK resulting in its dimerization and activation. Once active, ALK activates multiple signalling pathways (black arrows). Adapted from Sabir *et al.* (2017).

contribute to oncogenic progression (Hallberg and Palmer, 2016).

In the case of cancer, ALK activation is achieved independently of ligand binding. This can be achieved in one of two ways: (i) activating mutation of ALK or (ii) ALK dimerization mediated by a fusion partner (Hallberg and Palmer, 2016). A number of ALK activating mutations have been identified in neuroblastoma, a common and often fatal childhood cancer (George *et al.*, 2008). For example, ALK mutation was found in 8% of primary neuroblastoma patient samples and the most frequently seen mutation, F1174L, was subsequently found in three neuroblastoma cell lines (George *et al.*, 2008). These mutations were shown to activate ALK leading to the phosphorylation of downstream substrates, such as STAT3 and Akt, and the ability of these mutants to transform cytokine dependent Ba/F3 cells (George *et al.*, 2008). Alternatively, the fusion of ALK to proteins such as NPM or EML4 results in dimerization of the fusion proteins and subsequent autophosphorylation of ALK, resulting in constitutive activation of the ALK kinase domain (Hallberg and Palmer, 2016). Although these are the most commonly reported ALK fusions, a vast array of other fusions involving ALK do exist, some of which are also found in ALCL or NSCLC (Hallberg and Palmer, 2016; Xiang *et al.*, 2022).

1.2.4. EML4-ALK fusion proteins

EML4-ALK fusions consist of the N-terminal region of EML4 fused to the C-terminal tyrosine kinase domain of ALK (Soda *et al.*, 2007). The amount of EML4 incorporated into the fusion differs between variants, due to there being different breakpoints in the *EML4* gene, although all EML4-ALK variants contain the same portion of the ALK kinase (Sabir *et al.*, 2017). Soda *et al.* (2007) initially discovered two variants of EML4-ALK, variant 1 and 2 (V1 and V2), where introns 13 and 20 of *EML4* were fused to intron 20 of *ALK*, respectively. Variants 3a and 3b (V3a/V3b) were discovered shortly afterwards, both of which consist of the first six exons of *EML4* fused to exon 20 of *ALK*; V3b contains an extra eleven amino acids not present in V3a as a result of alternative splicing (Choi *et al.*, 2008). Interestingly, V1, V2 and V3 collectively account for approximately 90% of EML4-ALK fusions detected in lung cancer patients (Sabir *et al.*, 2017). Other less common variants of EML4-ALK have also

been discovered, with as many as fifteen EML4-ALK variants currently described (Sabir *et al.*, 2017).

The alternative breakpoints in the *EML4* gene mean that EML4-ALK variants diverge in the functional domains of EML4 that they possess. Importantly, all EML4-ALK variants contain the trimerization domain (TD) of EML4 which results in the trimerization of EML4-ALK variants. This facilitates ALK autophosphorylation and constitutive activation of the ALK kinase (Richards *et al.*, 2015). Constitutive activation of ALK results in oncogenic signalling downstream of EML4-ALK variants, including through the PI3K/Akt, Ras/Raf/MEK/ERK and JAK/STAT pathways contributing to cell proliferation, survival and migration (Hallberg and Palmer, 2016; Sabir *et al.*, 2017; Papageorgiou *et al.*, 2022). Moreover, EML4-ALK variants can be incorporated into phase separated foci which act as signalling hubs promoting oncogenic progression (Sampson *et al.*, 2021; Tulpule *et al.*, 2021; Qin *et al.*, 2021).

EML4-ALK variants can be categorised into long variants, which contain a partial TAPE domain (V1, V2 and V4) and short variants, which contain no TAPE domain (V3 and V5) (Figure 1.5). As described in section 1.2.2, the TAPE domain is a highly structured region and the inclusion of a disrupted TAPE domain in longer EML4-ALK variants renders these fusion proteins unstable. Moreover, the longer EML4-ALK variants rely on interaction with molecular chaperone HSP90 for stability (Heuckmann *et al.*, 2012; Richards *et al.*, 2014). Interestingly, the differences in protein stability exhibited by EML4-ALK variants has previously been linked to sensitivity to ALK inhibitors, with patients with V3 or V5 showing greater resistance to targeted ALK inhibition (Woo *et al.*, 2017; Heuckmann *et al.*, 2012). This is consistent with findings that patients with EML4-ALK V3 have shorter progression-free survival and worse overall survival than patients with longer EML4-ALK variants (Christopoulos *et al.*, 2018; Woo *et al.*, 2017).

The intracellular localisation of EML4-ALK variants also varies greatly. Whilst longer variants predominantly form aggregates in the cytoplasm, EML4-ALK V3 is recruited to interphase

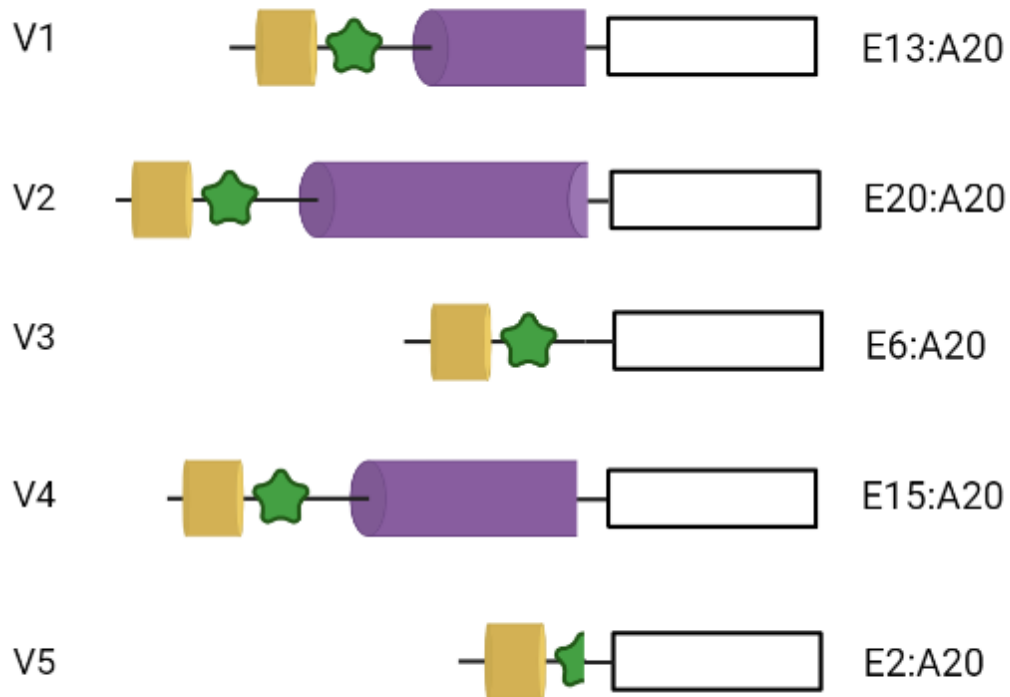


Figure 1.5. EML4-ALK variants. A schematic view of the first five EML4-ALK variants discovered are shown. They all contain the C-terminal ALK tyrosine kinase domain (white). Shorter variants (V3 and V5) contain only the coiled coil (yellow) and some of the basic region (green) of EML4. In addition to this, longer variants contain part of the EML4 TAPE domain (purple). Text on the right-hand side indicates which exons of EML4 (E) are fused with ALK exon 20 (A20). Adapted from Sabir *et al.* (2017).

microtubules (Richards *et al.*, 2015; O'Regan *et al.*, 2020). It has been shown that the N-terminal portion of EML4, including the TD and basic linker region, is required for microtubule binding (Richards *et al.*, 2015). Although all EML4-ALK variants contain the TD and at least part of the linker region, it is possible that the interaction of longer variants with HSP90 may sterically block the interaction of longer variants with microtubules (Richards *et al.*, 2015). However, a recent study has shown that an EML4-ALK V1 mutant with deletion of the 12N blade from the EML4 TAPE domain was able to localise to microtubules, suggesting that a misfolded 12N blade may block the interaction of longer EML4-ALK variants with microtubules (Sampson *et al.*, 2021).

EML4-ALK V3 not only binds interphase microtubules but also remains bound to spindle microtubules during mitosis. This is in contrast to wild type EML4, which is removed from microtubules upon mitotic entry (Lucken *et al.*, 2022; Adib *et al.*, 2019). Interestingly, cells expressing V3 exhibit hyperstabilised K-fibers and exhibit more mitotic errors, including misaligned and lagging chromosomes, than cells expressing EML4-ALK V1 (Lucken *et al.*, 2022). In addition, EML4-ALK V3 expressing cells also exhibit centrosome amplification and an enhanced microtubule nucleation capacity compared to V1 expressing cells, suggesting EML4-ALK V3 may affect centrosome biology (Lucken *et al.*, 2022; Sampson *et al.*, 2022).

The ability of EML4-ALK V3 to bind to interphase microtubules may well be responsible for some of the more aggressive properties of tumours with this variant. In support of this hypothesis, cultured cells expressing EML4-ALK V3 appear more mesenchymal in shape compared to cells expressing the longer EML4-ALK variants, such as V1. Specifically, they appear more elongated and form long cytoplasmic protrusions that contain microtubules and actin filaments (O'Regan *et al.*, 2020). V3 expressing cells also exhibit accelerated and less directional migration as demonstrated using wound healing, single cell tracking and Boyden chamber-style directional migration assays (O'Regan *et al.*, 2020). Cells expressing V3 also contain more stable microtubules compared to cells expressing longer EML4-ALK variants. This was demonstrated by the detection of elevated acetylated tubulin levels by both Western blotting and immunofluorescence microscopy (O'Regan *et al.*, 2020; Sampson

et al., 2022). Consistent with this, microtubules in cells expressing EML4-ALK V3 were more resistant to the microtubule destabilizing drug, vincristine, compared to cells expressing EML4-ALK V1 (Sampson *et al.*, 2022). Thus, it is plausible that microtubule stabilisation in EML4-ALK V3 cells may be responsible for the mesenchymal morphology and accelerated migration phenotypes and contribute to treatment failure in NSCLC patients.

The mesenchymal-like changes in cells expressing EML4-ALK V3 were found to depend on the NEK9 and NEK7 kinases (described in section 1.3) (O'Regan *et al.*, 2020). EML4-ALK V3, NEK9 and NEK7 are believed to form a complex. A physical interaction between EML4-ALK V3 and the NEK9 kinase was demonstrated by co-immunoprecipitation, whilst a direct interaction between NEK9 and NEK7 has also been confirmed by biochemical and structural biology approaches (O'Regan *et al.*, 2020; Haq *et al.*, 2015; Belham *et al.*, 2003). Persuasive evidence also suggests that the catalytic activity of both NEK9 and NEK7 are required for the formation of protrusions, the increased migration and the stabilisation of microtubules in V3 cells (O'Regan *et al.*, 2020). When NEK9 or NEK7 were depleted from cells expressing V3, cell length and migration were reduced while migration became more directional. Furthermore, cell lines expressing constitutively active mutants of NEK9 or NEK7 developed similar morphologies to cells expressing EML4-ALK V3, whereas no morphology changes were seen in cells expressing kinase inactive NEK9 or NEK7. Cells expressing activated NEK9 or NEK7 also migrated further, faster and less directionally than their respective parental cell lines. In addition, acetylated tubulin expression was significantly higher in the activated NEK9 cell line compared to cells expressing WT or kinase inactive NEK9. Importantly, chemical inhibition of ALK or expression of a catalytically-inactive EML4-ALK V3 induced neither morphology changes or increased migration. Together, these data suggest that the NEK9 and NEK7, but not ALK, kinases must be active in order for microtubule stabilisation, cell morphology and migration changes to occur (O'Regan *et al.*, 2020).

Therefore, our current working model is that EML4-ALK V3 recruits NEK9 to interphase microtubules where it becomes locally activated and this in turn recruits and activates NEK7 (Figure 1.6) (O'Regan *et al.*, 2020). Whilst it is clear that the NEK9 and NEK7 kinases act

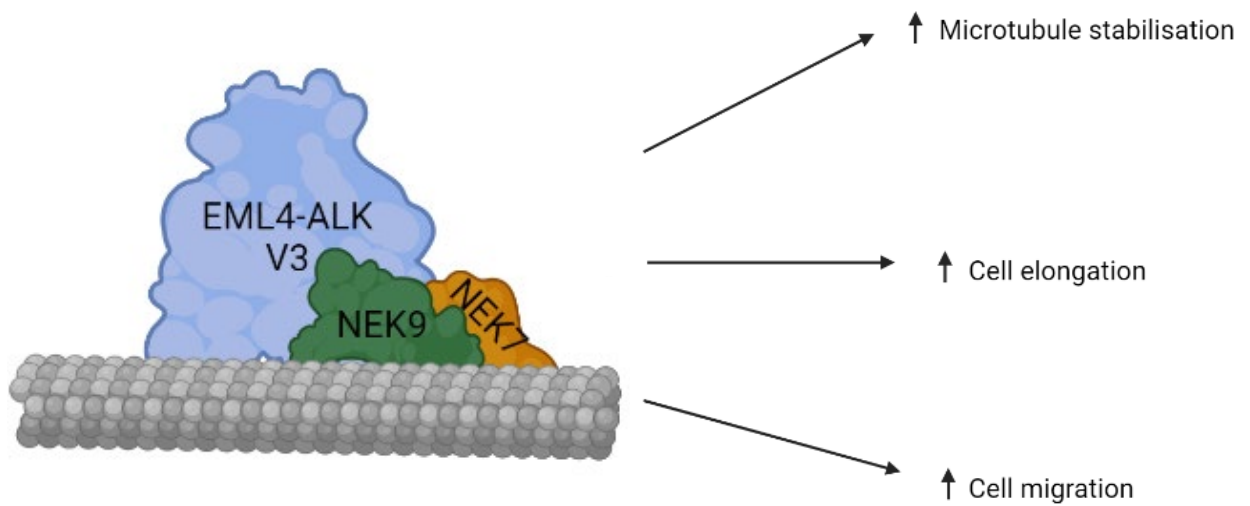


Figure 1.6. Current working model of EML4-ALK V3:NEK9:NEK7 pathway. EML4-ALK V3 (blue) is capable of binding microtubules through the N-terminal domain of EML4. EML4 physically interacts with NEK9 (green) which in turn directly interacts with NEK7 (orange). Together, this leads to increased microtubule stabilisation, cell elongation and accelerated cell migration.

downstream of EML4-ALK V3 to promote changes in morphology and migration, the downstream substrates and mechanisms remain unclear. Nevertheless, these observations offer a potential explanation for the increased metastatic spread and ALK inhibitor resistance characteristic of patients with EML4-ALK V3 driven cancers (Christopoulos *et al.*, 2018).

1.2.5. ALK inhibitors in current therapies

The current standard of care treatment for patients with ALK-positive NSCLC are targeted ALK inhibitors (Woo *et al.*, 2017). Following identification of EML4-ALK as an oncogenic driver, attention immediately turned to the possible use of drugs that had already been developed that inhibited the catalytic activity of ALK, such as crizotinib. Initially, studies confirmed the treatment of NSCLC with crizotinib was superior to standard chemotherapy approaches using drugs such as pemetrexed or docetaxel, with progression free survival (PFS) significantly longer in patients treated with crizotinib (Kwak *et al.*, 2010; Shaw *et al.*, 2013; Solomon *et al.*, 2014). This led to the fast-track approval of crizotinib by the FDA for treatment of ALK+ NSCLC in 2011 (Kazandjian *et al.*, 2014). However, it quickly became apparent that these cancers acquire resistance to these inhibitors (Rolfo *et al.*, 2014). Common mutations in the ALK catalytic domain that confer resistance include L1196M, C1156Y and G1202R (Choi *et al.*, 2010; Heuckmann *et al.*, 2011; Gainor and Shaw, 2013; Elshatlawy *et al.*, 2023). In an attempt to combat this, later generations of ALK inhibitors have been developed, with ceretinib, alectinib and brigatinib being approved for clinical use as second-generation inhibitors and lorlatinib as a third-generation inhibitor (Wu *et al.*, 2016; Elshatlawy *et al.*, 2023).

However, it has also become clear that not all variants of EML4-ALK respond equally to the ALK inhibitors. Studies using cultured cells have shown that cells expressing EML4-ALK V3 are broadly resistant to crizotinib, ceretinib and alectinib (Woo *et al.*, 2017; Noh *et al.*, 2017). Indeed, these findings are mirrored in the clinic where NSCLC patients with V3 showed poorer progression-free survival with first- and second-line ALK inhibitor treatment (Christopoulos *et al.*, 2018; Woo *et al.*, 2017; Noh *et al.*, 2017).

The most recent advance in the ALK inhibitor field is the development of fourth-generation ALK inhibitors, including those which are “double-mutant active”, meaning they are effective at treating ALK+ cancers with multiple common ALK mutations such as G1202R+L1196M, that confer resistance to previous generations of ALK inhibitors (Peng *et al.*, 2022; Ou *et al.*, 2021). Two fourth-generation inhibitors have been developed, TPX-0131 and NVL-655, which are currently in phase I/II clinical trials (identifier: NCT04849273 and NCT05384626 respectively). Pre-clinical studies have found that both drugs are active against common mutations in ALK, such as G1202R and L1196M, and are also central-nervous system (CNS) penetrant (Murray *et al.*, 2021; Pelish *et al.*, 2021). These studies are particularly promising for patients whose cancers have developed resistance to current approved ALK inhibitors due to secondary ALK mutations and for patients who have brain metastases.

In addition to the development of fourth generation ALK inhibitors, experimental approaches are being explored in cultured cells using combinations of ALK inhibitors and microtubule poisons. While combinations of ceretinib or alectinib with the microtubule stabilising drug, paclitaxel, were found to be synergistic in EML4-ALK V3 expressing cells, combinations of crizotinib or ceretinib with the microtubule destabilising drug, vincristine, were effective in reducing viability of cells expressing EML4-ALK V1 (Lucken *et al.*, 2022; Sampson *et al.*, 2022). These results suggest that microtubule dynamics are an important factor to consider when selecting combination treatments. Combination of ALK inhibitors with HSP90 inhibitors has also been investigated in the context of ALK+ NSCLC in light of the finding that the long variants require HSP90 for protein stability. Initially, crizotinib and 17-DMAG, a HSP90 inhibitor, were shown to display synergy in cells with EML4-ALK variants (Heuckmann *et al.*, 2012). However, for reasons that remain unclear, HSP90 inhibitors have shown limited success in the clinic to date (Pillai and Ramalingam, 2018).

In addition to the combination of ALK inhibitors with other chemotherapeutic agents, combining ALK inhibitors with radiotherapy or immunotherapy has also been explored (Papageorgiou *et al.*, 2022). Administration with crizotinib was found to be synergistic with

radiotherapy treatment in H3122 cells derived from an NSCLC patient that expresses EML4-ALK V1. Indeed, this combination was more effective at treating H3122 xenografts in mice than either treatment alone (Dai *et al.*, 2015). Unfortunately, the combination of ALK inhibitors with immunotherapy has not proven to be as promising so far, with one clinical trial being terminated early due to severe adverse side effects (Spigel *et al.*, 2018). Nevertheless, combination treatments of ALK inhibitors with either chemotherapeutic agents, radiotherapy or immunotherapy are a worthwhile avenue to continue to explore in the hope of improving current treatment of patients with ALK rearranged NSCLC.

1.3. Mammalian NEK kinases

1.3.1. Never In Mitosis A (NIMA) protein

The mammalian NEK kinase family are orthologs of the Never In Mitosis A (NIMA) protein. NIMA was discovered in *Aspergillus nidulans* in 1975 and was found to be a regulator of mitotic progression (Morris, 1975). Using temperature sensitive mutants of *Aspergillus nidulans*, NIMA was found to be required for transition from G2 to prophase (Oakley and Morris, 1983). NIMA was later identified as a kinase (Osmani *et al.*, 1988) and related proteins have since been identified in other species, including unicellular fungi such as yeast, lower eukaryotes such as *Chlamydomonas*, *Drosophila* and *Plasmodium* as well as humans (Bachus *et al.*, 2022; Fry, Bayliss and Roig, 2017; Moniz *et al.*, 2011; Meirelles *et al.*, 2014; Quarmby and Mahjoub, 2005; Mahjoub, Qasim Rasi and Quarmby, 2004; Reininger *et al.*, 2009).

1.3.2. The NEK kinase family

The mammalian NIMA Related Kinase (NEK) family is a specific group of eleven serine-threonine kinases (NEK1-NEK11). The kinases were sequentially named in the order of identification and all contain a relatively well-conserved kinase domain. Most of the NEKs, apart from NEK3, NEK5 and NEK11, contain an inhibitory tyrosine residue within the catalytic site that blocks activity and allows regulation in an allosteric manner (Bachus *et al.*, 2022). The NEK kinases can be grouped into three clades based on phylogenetic analysis,

with NEK4, NEK6, NEK7, NEK8, NEK9 and NEK10 forming clade 1, NEK11 being the sole member of clade 2, and NEK1, NEK2, NEK3 and NEK5 belonging to clade 3 (Bachus *et al.*, 2022).

Despite belonging to the same family, the NEK kinases are diverse in their size, structure and protein domain content as a result of major differences in their non-catalytic regions (Figure 1.7). This is reflective of the multitude of diverse roles these proteins have within the cell. The smallest members of the NEK kinase family, NEK6 and NEK7, consist only of their kinase domains and a short N-terminal extension (Moniz *et al.*, 2011). The longer NEK kinases contain additional domains, most notably coiled-coil motifs, PEST sequences that are commonly found in proteins with short half-lives, Regulator of Chromosome Condensation 1 (RCC1)-like domains, deadbox domains and armadillo repeats. The RCC1 domains are homologous to the major structural element within RCC1, a Ran GEF, although no evidence exists to suggest that the NEK kinases containing an RCC1 domain (NEK8 and NEK9) have GEF activity (Moniz *et al.*, 2011). Deadbox domains are involved in a plethora of cellular processes, including gene expression, assembly of complexes such as ribosomes and nuclear export of mRNA (Jarmoskaite and Russell, 2011; Meirelles *et al.*, 2014). The only NEK kinase in possession of a deadbox domain is NEK5 (Moniz *et al.*, 2011). Similarly, NEK10 has its own unique domain, distinct from the other NEKs, with armadillo repeats, which may be involved in protein-protein interactions (Huber *et al.*, 1997; Meirelles *et al.*, 2014; Moniz *et al.*, 2011). The incorporation of these different domains into the various NEK kinases may offer some explanation of their diverse activities.

1.3.2.1. NEK9

NEK9 (also known as Nercc1) consists of an N-terminal kinase domain in addition to other regulatory domains such as RCC1 domains and a coiled coil that are important for NEK9 function. Importantly, RCC1 acts as an autoinhibitory domain through a yet undefined mechanism and its deletion results in a constitutively active kinase (Roig *et al.*, 2002; Fry, Bayliss and Roig, 2017). Interestingly, the coiled coil promotes dimerization and is also required for auto-activation (Roig *et al.*, 2002). Intriguingly, between the RCC1 domains and

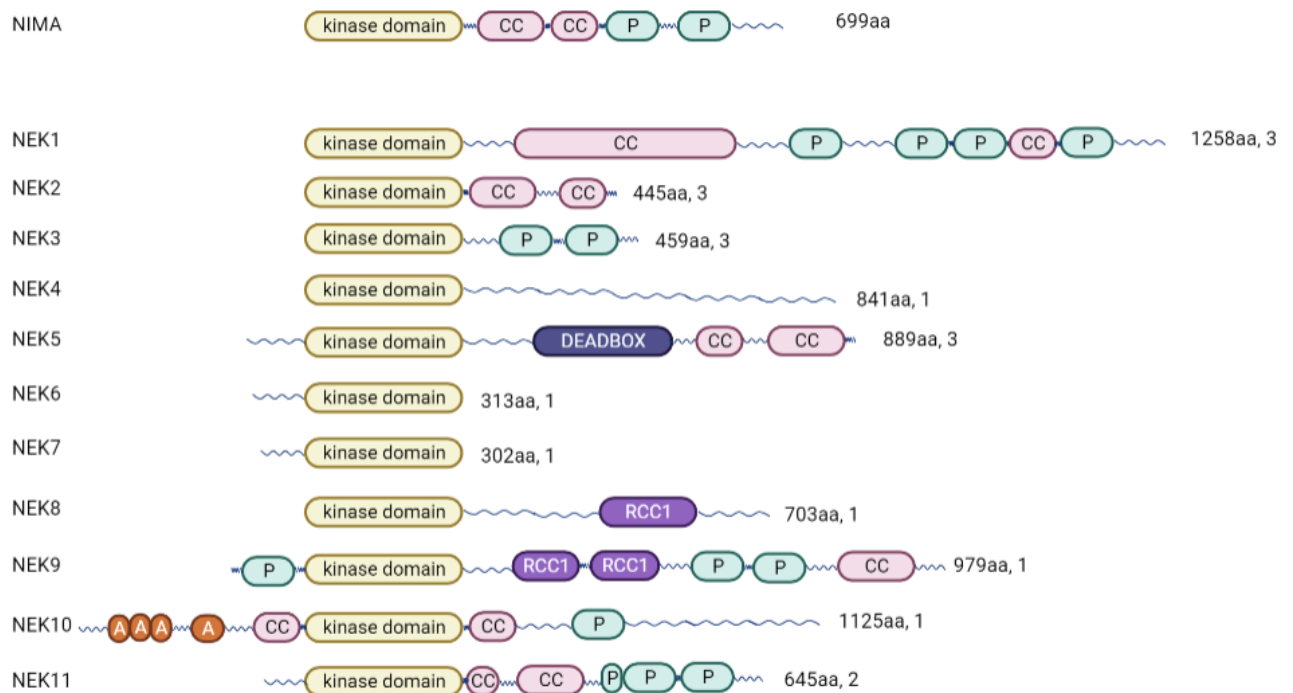


Figure 1.7. Comparison of *Aspergillus* NIMA and human NEK kinase domain organisation.

Schematic diagram of the eleven human NEK kinases, as well as the founding member of this family, NIMA from *Aspergillus nidulans*. All eleven human NEKs contain a kinase domain (aligned in the schematic) plus other functional domains, some of which exist in NIMA. CC = Coiled coil; P = PEST; A= Armadillo. Amino acid sequence length and phylogenetic clade are written on the right-hand side of each kinase. Figure adapted from Moniz *et al.* (2011).

coiled coil lies a stretch of S/TP and PXXP motifs where NEK6 and NEK7 are known to bind NEK9 (this interaction is described further in section 1.3.3). Moreover, dynein light chain LC8, also binds to inactive NEK9 within this region and blocks interaction with NEK6 and NEK7, therefore only active NEK9 is capable of interaction with NEK6 and NEK7 (Regué *et al.*, 2011).

NEK9 is heavily involved in the control of mitosis, as well as having roles in ciliogenesis and gene regulation (Bachus *et al.*, 2022). At mitotic onset, NEK9 is phosphorylated by CDK1 and PLK1 resulting in its activation (Roig *et al.*, 2002; Sdelci *et al.*, 2012). Once activated, NEK9 promotes chromosome alignment and segregation and interference with NEK9 in cells results in spindle abnormalities, chromosome misalignment and prometaphase arrest (Roig *et al.*, 2002).

In addition to this, it has been shown that NEK9 also has roles at the spindle poles in mitosis. Activated NEK9 localises to the spindle poles where physical interaction with γ -tubulin was demonstrated by co-immunoprecipitation experiments (Roig *et al.*, 2005). Furthermore, the deletion of *Xenopus* XNercc (NEK9 ortholog) from *Xenopus* egg extracts caused delayed spindle assembly and a reduction in bipolar spindle formation (Roig *et al.*, 2005). It was later uncovered that NEK9 phosphorylates an adaptor protein, NEDD1, which also interacts with γ -tubulin and this phosphorylation event results in the recruitment of NEDD1- γ -tubulin to the centrosome (Sdelci *et al.*, 2012). Further evidence for the role of NEK9 in mitosis comes from the identification of the mitotic signalling modules, comprised of NEK9-NEK6-Kif20A and NEK9-NEK7-Kif14 (described in section 1.3.2.2), and the NEK9-NEK6/NEK7-Eg5 signalling module which drives bipolar spindle formation (described in section 1.3.3 and 1.5.2) (Cullati *et al.*, 2017; Rapley *et al.*, 2008; Bertran *et al.*, 2011).

Together, NEK8 and NEK9 are the only NEK kinases to incorporate an RCC1 domain (Moniz *et al.*, 2011). Interestingly, there are strong links between mutations in the RCC1 domain of NEK8 and ciliopathies (Liu *et al.*, 2002; Otto *et al.*, 2008). Similarly, human skeletal dysplasia

has also been attributed to a mutation resulting in a premature stop codon in the *NEK9* RCC1 domain (Casey *et al.*, 2016). Genetic screening of patients with skeletal dysplasia revealed a premature stop codon in the *NEK9* gene which results in a truncated *NEK9* protein, missing a large portion of the RCC1 domain (Casey *et al.*, 2016). Intriguingly, fibroblasts taken from these patients displayed a decrease in cilia number and length. Additionally, expression analysis of the *NEK9* ortholog, *nekl-1* in *C. elegans*, revealed almost exclusive expression in ciliated cells (Casey *et al.*, 2016). Together, these findings provide evidence that *NEK9* is involved in ciliogenesis.

A link between *NEK9* and gene regulation came from studies which explored the interaction between *NEK9* and adenovirus E1A protein (Jung, Radko and Pelka, 2016). Upon adenovirus infection of a cell, the virus must deactivate host defence mechanisms in order to prosper and it appears E1A interaction with *NEK9* is an example of a mechanism used to achieve this. This study demonstrated that *NEK9* could bind to promoters of the viral genome as well as the host cell's genome and act as a transcriptional repressor (Jung, Radko and Pelka, 2016). Of note, the *NEK9*-E1A complex was able to silence *GADD54A*, a p53 inducible gene (Jung, Radko and Pelka, 2016). Similarly, studies in cancer cells have shown that *NEK9* is crucial for cancer cell proliferation in p53 inactive cells and repression of *NEK9* resulted in changes to expression of genes that encode cell cycle regulators and mRNA processing factors (Kurioka *et al.*, 2014). Together, these studies provide evidence of a role for *NEK9* in gene regulation.

1.3.2.2. NEK6 and NEK7

NEK6 and *NEK7* are the smallest members of the NEK kinase family and share 77% sequence identity (Bachus *et al.*, 2022). Interestingly, the catalytic domains exhibit 86% sequence conservation and the diversity arises from the short N-terminal extensions which confer substrate specificity (de Souza *et al.*, 2014). Indeed, a study which produced a *NEK7* interactome using yeast-2-hybrid and immunoprecipitation with mass spectrometry approaches, found many *NEK7* interacting proteins distinct to those which interact with *NEK6*. This suggests that despite being relatively well conserved, these two NEKs are likely

to have some distinct functions (de Souza *et al.*, 2014). Similar to other members of the NEK family, NEK6 and NEK7 have been found to play diverse roles in cell cycle control and microtubule regulation.

NEK6 and NEK7 are activated by NEK9 at the onset of mitosis, where NEK9 phosphorylates specific serine residues present in their activation loops (Belham *et al.*, 2003). The activation of each component of this signalling cascade is described further in section 1.3.3. In addition, siRNA depletion or expression of kinase inactive mutants of NEK6 or NEK7 caused metaphase arrest and apoptosis, highlighting the significance of these two kinases in mitotic control (O'Regan and Fry, 2009). Furthermore, treatment of these cells with a SAC inhibitor allowed the cells to progress through metaphase, but they later arrested in cytokinesis (O'Regan and Fry, 2009). These data suggest NEK6 and NEK7 have two independent functions at both metaphase and cytokinesis.

Indeed, subsequent research identified two signalling modules involving kinesins consisting of NEK9-NEK6-Kif20A and NEK9-NEK7-Kif14 that regulate late mitotic progression and cytokinesis, respectively (Cullati *et al.*, 2017). The NEK9-NEK6-Kif20A signalling module was shown to become active in prometaphase and allows the timely recruitment of Kif20A to the central spindle by anaphase where it facilitates microtubule bundling (Cullati *et al.*, 2017). Similarly, Kif14 is also recruited to the central spindle in anaphase by the NEK9-NEK7-Kif14 signalling module where it transports the citron kinase, which is necessary for the completion of cytokinesis (Cullati *et al.*, 2017). Intriguingly, Kif20A and Kif14 are not the only kinesins NEK6 and NEK7 can interact with. NEK6 and NEK7 also phosphorylate Eg5 (Kif11), which is essential for the formation of a bipolar spindle in early mitosis (Rapley *et al.*, 2008; Bertran *et al.*, 2011). This will be discussed in more depth in sections 1.3.3 and 1.5.2.

Similar to certain other members of the NEK family, NEK6 has also been linked to the DNA damage response. Indeed, NEK6 has been shown to be directly phosphorylated by CHK1 and CHK2 kinases in response to DNA damage (Lee *et al.*, 2008). This phosphorylation inhibits

NEK6 activity and promotes effective G2/M arrest, again highlighting the necessity of NEK6 for mitotic progression (Lee *et al.*, 2008).

NEK6 and NEK7 perform multiple roles which are essential for bipolar spindle formation. For example, NEK6 phosphorylates the chaperone protein, HSP72, which results in its recruitment to the mitotic spindle (O'Regan *et al.*, 2015). Here, HSP72 facilitates the assembly of K-fibres through the recruitment of microtubule-binding proteins, ch-TOG and TACC3 (O'Regan *et al.*, 2015). Interestingly, NEK6 phosphorylation of HSP72 has also been linked to the clustering of supernumerary centrosomes (Sampson *et al.*, 2017). NEK7 is equally necessary for spindle formation. A study found that NEK7 interacts with and recruits Regulator of G-protein signaling 2 (RGS2) to the mitotic spindle and depletion of either of these proteins was seen to result in reduction of γ -tubulin at the spindle poles and chromosome alignment and congression errors (de Souza *et al.*, 2015). Furthermore, in RGS2 depleted cells, the spindle was mis-orientated suggesting that these proteins are necessary for the correct organisation of the mitotic spindle (de Souza *et al.*, 2015). Additionally, NEK6 and NEK7 were also shown to phosphorylate EML4 resulting in its removal from spindle microtubules; this was necessary to allow accurate chromosome congression presumably by modulating microtubule dynamics (Adib *et al.*, 2019). These studies all provide evidence for NEK6 and NEK7 performing regulatory roles in relation to the microtubule cytoskeleton. Indeed, NEK7 has previously been found to promote microtubule dynamic instability (Cohen *et al.*, 2013). This study measured microtubule dynamics using a fluorescent EB3 protein (+ end tracking protein) to track the plus ends of microtubules. Cells depleted of NEK7 were found to have less dynamic microtubules as shown by lower growth/shrinkage speeds, suggesting that NEK7 promotes dynamic instability (Cohen *et al.*, 2013).

In addition to these roles in bipolar spindle organization, another study suggested a role for NEK6 and NEK7 in centriole duplication. Here, expression of recombinant versions of NEK6 or NEK7 that carried a tag directing these kinases to the centrosome resulted in extra centriole formation (Kim, Kim and Rhee, 2011). Meanwhile, depletion of NEK7 resulted in

failure to duplicate centrioles and a loss of recruitment of PCM proteins to the centrosome (Kim, Kim and Rhee, 2011).

Finally, in what appears to be a quite distinct function, NEK7 has a role in activating the NLR Family Pyrin Domain Containing 3 (NLRP3) inflammasome in macrophages, which results in the release of interleukins in response to pathogens and other stimuli (Sun *et al.*, 2020). The NLRP3 inflammasome is a multi-protein complex containing NLRP3 as well as pro-caspase-1 and has been associated with a variety of inflammatory diseases, such as Alzheimer's disease, inflammatory bowel disease (IBD) and type II diabetes (Sun *et al.*, 2020). NEK7 has been found to directly bind to NLRP3 and promote the assembly of the inflammasome complex in a manner that is independent of NEK7 catalytic activity (Sharif *et al.*, 2019).

1.3.3. The NEK9-NEK6/NEK7 signalling cascade

The exact mechanism of NEK9 activation is still unclear, although NEK9 is capable of autophosphorylation and autoactivation (Roig *et al.*, 2002). However, it has been shown that both CDK1 and PLK1 can phosphorylate NEK9 at the onset of mitosis, when NEK9 becomes active (Roig *et al.*, 2002; Bertran *et al.*, 2011; Sdelci *et al.*, 2012). CDK1 phosphorylates NEK9 in its C-terminal domain creating a binding site for PLK1. Moreover, PLK1 was found to phosphorylate T210 in the activation loop of NEK9, which is essential for NEK9 activation (Bertran *et al.*, 2011; Roig *et al.*, 2005). It is therefore proposed that CDK1 phosphorylation of NEK9 permits the binding and subsequent phosphorylation of NEK9 by PLK1, which results in NEK9 activation (Bertran *et al.*, 2011).

Initial evidence that a signalling cascade of NEK kinases exists surfaced in 2003 when it became clear that NEK9 could phosphorylate and activate NEK6 and NEK7 (Belham *et al.*, 2003). Here, NEK9 was found to bind and phosphorylate S206 in the activation loop of NEK6 and the corresponding residue, S195, in NEK7 and the use of phosphomutants supported the importance of phosphorylation at these residues for the activation of these kinases (Belham *et al.*, 2003; O'Regan & Fry, 2009). Later studies aimed to better elucidate the

mechanism of NEK6/NEK7 activation using structural biology. The crystal structure of NEK7 revealed an autoinhibitory tyrosine residue (Y97) which interacts with the activation loop resulting in an inactive conformation (Richards *et al.*, 2009). Moreover, a Y97A mutant of NEK7 and an equivalent Y108A mutant of NEK6 are constitutively active, highlighting the importance of these residues in regulating the kinase activation status (Richards *et al.*, 2009). In addition, incubation of the C-terminal non-catalytic domain of NEK9 with NEK6 or NEK7 was seen to increase the activity of the kinases, but failed to increase the activity of the phosphonull NEK6 or NEK7 mutants, suggesting that interaction with the NEK9 non-catalytic domain somehow relieves the inhibitory tyrosine from the active site (Figure 1.8) (Richards *et al.*, 2009).

Further biochemical studies revealed that residues 810-828 of NEK9 are the minimum requirement for physical interaction with NEK7 (Haq *et al.*, 2015). Moreover, a crystal structure obtained of a NEK7-Y97F mutant in complex with residues 810-828 of NEK9, revealed that NEK7 was present as a back-to-back dimer, where the residue at position 97 was shifted due to interactions formed through dimerization (Haq *et al.*, 2015). In addition, activation of NEK7 was shown to rely on NEK9 dimerization and the authors therefore proposed that dimeric NEK9 promotes the dimerization of NEK7, which in turn releases the autoinhibitory Y97 residue thereby activating NEK7 in an allosteric manner (Haq *et al.*, 2015).

An example of a cellular function that utilises this NEK kinase signalling cascade is centrosome separation at prophase. Here, PLK1 activates the NEK9-NEK6/NEK7 cascade which in turn results in Eg5 recruitment to centrosomes where it facilitates their separation (Bertran *et al.*, 2011). In line with this, Eg5 had previously been found to be a target of NEK6, where its phosphorylation on S1033 is essential for mitotic progression (Rapley *et al.*, 2008). Together, these studies identify a downstream target of the NEK9-NEK6/NEK7 signalling cascade and demonstrate a functional application of this pathway in mitosis.

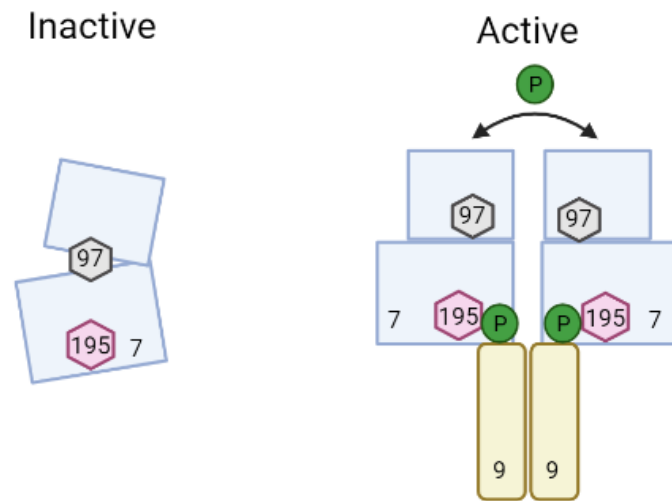


Figure 1.8. Mechanism of NEK7 activation. Left - NEK7 (blue) in its inactive form contains an inhibitory tyrosine residue, Y97 (grey). Right - NEK9 (yellow) dimers promote the dimerization of NEK7 which somehow relieves the inhibitory Y97 residue and allows for NEK7 autophosphorylation (arrow across top). NEK9 also directly phosphorylates NEK7 on S195 (pink). Figure adapted from Fry, Bayliss and Roig (2017).

This signalling pathway is just one example where the NEK9-NEK6/NEK7 cascade is present. Other examples with roles in mitosis have been described such as the NEK9-NEK6-Kif20A or NEK9-NEK7-Kif14 pathways (described in section 1.3.2.2) (Cullati *et al.*, 2017). Another example where the NEK9-NEK7 signalling cascade exists was identified in EML4-ALK V3 expressing cells. As described in section 1.2.4, cells expressing EML4-ALK V3 develop an elongated morphology and become more migratory and these changes were found to depend on NEK9 and NEK7 activity (O'Regan *et al.*, 2020). Furthermore, the NEK9-Eg5 signalling axis has been linked with increased metastatic potential in colon cancer samples, where expression of both these proteins was elevated in the majority of cancer samples (Kim *et al.*, 2023). Consistent with this, NEK9, NEK6 and NEK7 have all been found to be upregulated in a variety of cancers (O'Regan *et al.*, 2020; He *et al.*, 2018; Zhou *et al.*, 2016). This highlights the significance of the NEK9-NEK6/NEK7 signalling cascade in mitotic control and the consequence of its deregulation in cancer.

1.4. Microtubules

1.4.1. Microtubule structure, organisation and function

Together with actin filaments and intermediate filaments, microtubules constitute a component of the cellular cytoskeleton (Hohmann and Dehghani, 2019). Microtubules consist of α/β -tubulin heterodimers which, in the presence of GTP, polymerise to form a protofilament and assemble laterally to form a hollow tube, usually comprising 13 protofilaments, with a width of 25 nm (Desai and Mitchison, 1997). Microtubules consisting of fewer or more than 13 protofilaments do exist across different species of plants, animals and microorganisms and have been observed *in vitro*, however microtubules *in vivo* usually consist of 13 protofilaments (Chaaban and Brouhard, 2017). Importantly, microtubules are polar structures where the slow growing minus end (-) is usually located at a microtubule organising centre (MTOC) and the fast growing plus end (+) extends towards the cell periphery (Baas and Lin, 2011). Notably, the polarity exists not only for the microtubule as a whole but also along the length of the lattice which is crucial for the movement of microtubule motors (discussed in section 1.4.2) (Baas and Lin, 2011).

Microtubules are dynamic structures and frequently undergo growth (polymerisation) and shrinkage (depolymerisation). The switch from growth to shrinkage is known as catastrophe, while the switch from shrinkage to growth is known as rescue. The stochastic nature of these four processes means that microtubules exhibit a property known as dynamic instability (Figure 1.9) (Gardner, Zanic and Howard 2013; Mitchison and Kirschner, 1984). The process of dynamic instability relies on GTP, which binds to both the α - and β -tubulin subunit. The presence of GTP-bound tubulin subunits at microtubule plus ends creates a GTP-cap that stabilises the plus end and allows polymerisation to take place (Mitchison and Kirschner, 1984). Upon GTP hydrolysis by the β -tubulin subunit, a conformational change takes place in the α/β -tubulin heterodimer that causes the bending of protofilaments. This in turn destabilises the microtubule lattice and depolymerisation occurs (Mitchison and Kirschner, 1984). Moreover, dynamic instability is regulated by microtubule-associated proteins (MAPs), such as plus-end tip tracking proteins (+TIPs), which can alter the frequency and rate of the different parameters of microtubule dynamics (Zhang *et al.*, 2015; Akhmanova and Steinmetz, 2010).

Dynamic instability allows for the rapid re-organisation of the microtubule cytoskeleton, something which is crucial for a number of its functions. Indeed, rapid re-organisation of microtubules is needed at the onset of mitosis, when microtubules and their associated proteins cooperate to form the mitotic spindle (Prosser and Pelletier, 2017). At this time, interphase microtubules are almost completely depolymerised and reassemble to form the mitotic spindle (Petry, 2016). Importantly, dynamic instability of microtubules contributes to the 'search and capture' of chromosomes during prometaphase (Kirschner and Mitchison, 1986). In this model, microtubules polymerise and search the cytoplasmic space. Once attached to a kinetochore, these microtubules become capped and stabilised, whereas those that are not attached will depolymerise (Kirschner and Mitchison, 1986).

Another important function of microtubules is the transport of intracellular cargos. Microtubules act as tracks for motor proteins, such as dyneins and kinesins (discussed in section 1.4.2), which are responsible for the transport of vesicles and organelles (Barlan and

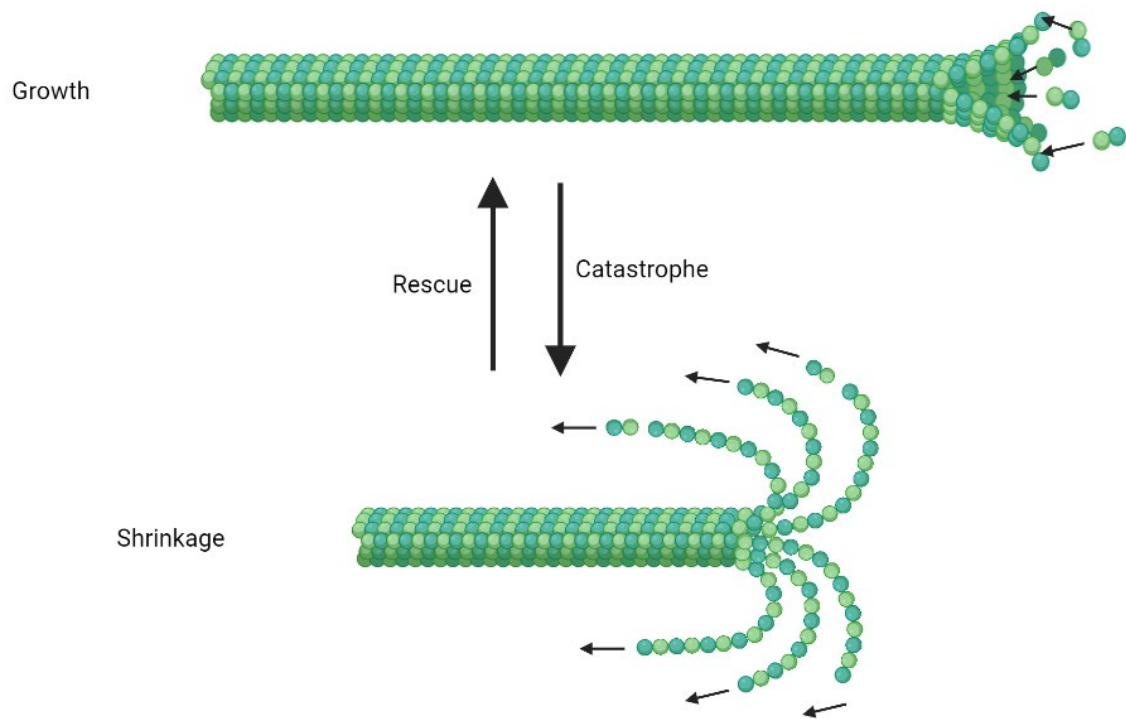


Figure 1.9. Dynamic instability of microtubules. Microtubules undergo phases of growth (polymerisation) and shrinkage (depolymerisation) and are able to rapidly switch between the two. Catastrophe is the switch from growth to shrinkage and rescue is the switch from shrinkage to growth. These processes give microtubules the property of dynamic instability. Figure adapted from Bowne-Anderson *et al.* (2013).

Gelfand, 2017). This is particularly important in neuronal cells where the transport of cargos is imperative for synaptic activity and general neuronal function (Barlan and Gelfand, 2017).

In addition to their roles in mitosis and intracellular transport, microtubules also have roles in maintaining cell shape, polarity and migration (discussed further in section 1.6.3) (Jolly *et al.*, 2010; Tomasek and Hay, 1984; Etienne-Manneville, 2013). Lastly, microtubules are a key component of eukaryotic cilia and flagella (Satir and Christensen, 2007).

1.4.2. Microtubule motors

As described in the previous section, microtubules act as tracks for the transport of cargos and organelles. The microtubules alone are not enough to facilitate intracellular transport but require motor proteins that are capable of both interacting with the cargo and processivity along microtubules. Microtubule motor proteins typically fall into one of two major superfamilies: kinesins and dyneins (Caviston and Holzbaur, 2006).

Kinesins (also known as KIFs) generally consist of three domains: motor, stalk and tail. All kinesins possess a relatively well-conserved catalytic motor domain where ATP is hydrolysed and energy released for processive movement. The microtubule binding site also exists within the motor domain (Miki, Okada and Hirokawa, 2005). Interestingly, kinesins show more variance in their stalk and tail domains which reflects the variety of cargos kinesins can interact with and the diverse processes kinesins are involved with in the cell (Miki, Okada and Hirokawa, 2005). Considering specific kinesins are conserved between species but multiple superfamilies exist within a single species, it has been proposed that evolution resulted in the divergence of kinesins, which now perform distinct functions (Miki, Okada and Hirokawa, 2005).

Mammalian kinesins can be categorised into fifteen superfamilies, each of which can contain multiple individual proteins, based on phylogenetic analysis (Figure 1.10). These

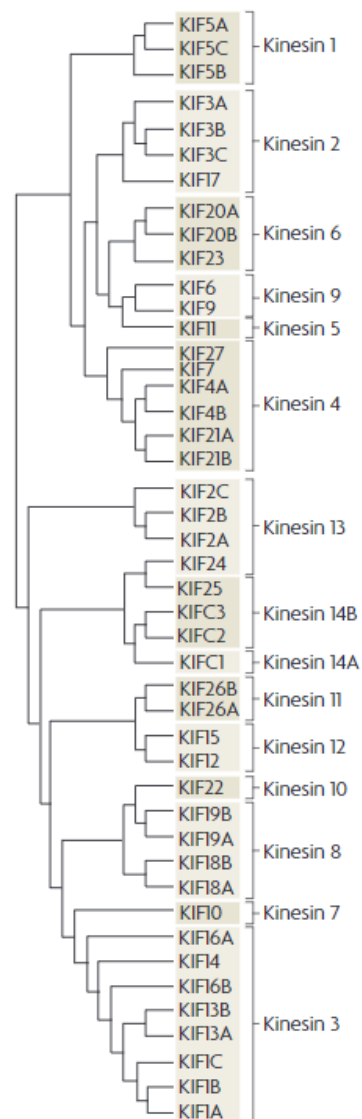


Figure 1.10. Phylogenetic tree of the mouse kinesin superfamily. Mammals have 45 genes encoding kinesins, all of which are included in this phylogenetic tree. These kinesins are grouped into 15 families (Kinesin 1-Kinesin 14B). Figure taken from Hirokawa *et al.* (2009).

superfamilies can be further grouped into three categories depending on the position of the motor domain (Hirokawa *et al.*, 2009). N-kinesins, which make up the majority of kinesins, have an N-terminal motor domain and are plus-end directed whereas C-kinesins, such as KIFC2 and KIFC3, have a motor domain at the C-terminus and are minus-end directed. The third category is M-kinesins which have a motor domain in the centre of the protein sequence and these depolymerise microtubules, an example of an M-kinesin being KIF2A (Hirokawa *et al.*, 2009). Although minus-end directed kinesins do exist, they are rare and the majority of well-researched kinesins are plus-end directed, therefore kinesins generally are described as plus-end directed motors.

Most kinesins assemble into homodimers and are believed to move along microtubules in a “hand-over-hand” fashion where each motor domain sequentially takes a step in the direction of motion (Shao and Gao, 2006). Excitingly, direct observation of kinesin-1 “walking” along microtubules in living cells confirmed a 16 nm length hand-over-hand movement recently, using a super-resolution imaging technique called MINFLUX (Deguchi *et al.*, 2023). Here, kinesin-1 was expressed in living cells and single motor domains labelled with fluorescent dyes. MINFLUX was able to spatially and temporally track the movement of the motor domains (Deguchi *et al.*, 2023).

In contrast to kinesins, dyneins are minus-end directed motors with roles in intracellular transport, cell division and ciliary beating (Roberts *et al.*, 2013). Dyneins are large multi-subunit proteins, each dynein containing two heavy chains and multiple smaller subunits, including intermediate chains, light intermediate chains and light chains (Vallee *et al.*, 2004). The motor domain exists within the dynein heavy chain, along with diverse tail domains, which facilitate subunit association necessary for interaction with cargo (Roberts *et al.*, 2013).

Similar to kinesins, nine major subfamilies of dynein heavy chain exist, with cytoplasmic dynein 1 being the major transporter in human cells, involved in almost all minus-end

directed transport (Roberts *et al.*, 2013). Cytoplasmic dynein 2 is involved with the transport of cargos along cilia and flagella and the other seven dyneins form part of the ciliary axoneme, where they are required for cilia beating (Roberts *et al.*, 2013). Crucially, dynein often relies on a co-factor, dynactin, to allow it to perform its role in intracellular transport (Schroer and Sheetz, 1991; Gill *et al.*, 1991). Dynactin forms a complex with dynein, where it increases dynein processivity as well as facilitates the interaction of dynein with cargoes (King and Schroer, 2000; Waterman-Storer *et al.*, 1997).

1.4.3. The centrosome and microtubule nucleation

The centrosome is the major microtubule organising centre (MTOC) of the human cell, and the site from where microtubules are nucleated and attached by their minus ends. At the onset of mitosis, a cell usually has two centrosomes which separate to form the poles of the mitotic spindle. This process is essential for the formation of a bipolar spindle and accurate chromosome segregation (Fukasawa, 2005). Following cytokinesis, each daughter cell will receive only one centrosome, highlighting the need for centrosome duplication to occur in the subsequent round of the cell cycle in preparation for the next mitosis (Fukasawa, 2005).

The centrosome consists of a pair of centrioles (mother and daughter) surrounded by pericentriolar material (PCM). Interestingly, centrioles display an evolutionary conserved 9-fold radial symmetry and are barrel-shaped structures approximately 500 nm in length and 200 nm in diameter (Nigg and Holland, 2018; Jana, 2021). Indeed, the first step in centrosome duplication is the disengagement of the mother and daughter centriole, where the tight link between them is severed although a distinct loose tether remains (Nigg and Holland, 2018). This is followed by the assembly of new procentrioles at the proximal ends of the mother and daughter centrioles, a step which occurs during S phase (Nigg and Holland, 2018; Jana, 2021). During G₂, the procentrioles gain length and mature by recruiting PCM proteins. The original daughter centriole acquires appendages that are required for microtubule nucleation and is thus now also known as a mother centriole (Nigg and Holland, 2018). Meanwhile, the two fully grown procentrioles are now daughter centrioles. Together, the duplicated centrioles have now formed two centrosomes. Upon

mitotic entry, the loose tether between the two new centrosomes is severed (this involves a member of the NEK kinase family - NEK2 (Fry *et al.*, 1998)) and the centrosomes separate to form the two opposing spindle poles (involving Eg5 – see section 1.5.2). Upon cytokinesis, each centrosome consisting of two centrioles is separated into two new daughter cells (Figure 1.11) (Nigg and Holland, 2018; Jana, 2021).

The centrosome cycle is coupled to DNA replication in S phase and must only occur once per cell cycle. Deregulation of the centrosome cycle can result in centrosome amplification, where cells have more than two centrosomes (Fukasawa, 2005; Godinho and Pellman, 2014). During mitosis, these cells may form multipolar spindles that can lead to problems in equal segregation of chromosomes resulting in daughter cells that may be aneuploid (Fukasawa, 2005; Godinho and Pellman, 2014). In an attempt to progress through mitosis, cells may employ mechanisms that cluster supernumerary centrosomes so that a pseudo-bipolar spindle is formed (Brinkley, 2001). However, merotelic kinetochore-microtubule attachments can still occur in cells with pseudo-bipolar spindles, which will lead to chromosome segregation errors and contribute to aneuploidy (Godinho and Pellman, 2014). Indeed, deregulation of the centrosome cycle is one factor that leads to diseases such as cancer (Nigg and Holland, 2018).

The primary function of the centrosome in cells is to nucleate microtubules. Although the precise mechanism remains unclear, microtubule nucleation occurs primarily within the PCM and crucially requires the γ -tubulin ring complex (γ -TuRC) (Woodruff, Wueseke and Hyman, 2014; Job, Valiron and Oakley, 2003). The core of the γ -TuRC consists of γ -tubulin and γ -tubulin complex proteins (GCP2-6) and is used to overcome a kinetic barrier which would otherwise hinder microtubule nucleation (Kollman *et al.*, 2011; Thawani and Petry, 2021). Initially, it was believed that the γ -TuRC acts as a seed from which microtubules assemble (Job, Valiron and Oakley, 2003). Indeed, later studies confirmed that the γ -TuRC acts as a microtubule template with 13 γ -tubulins per turn of the complex, consistent with microtubules typically consisting of 13 protofilaments (Kollman *et al.*, 2010).

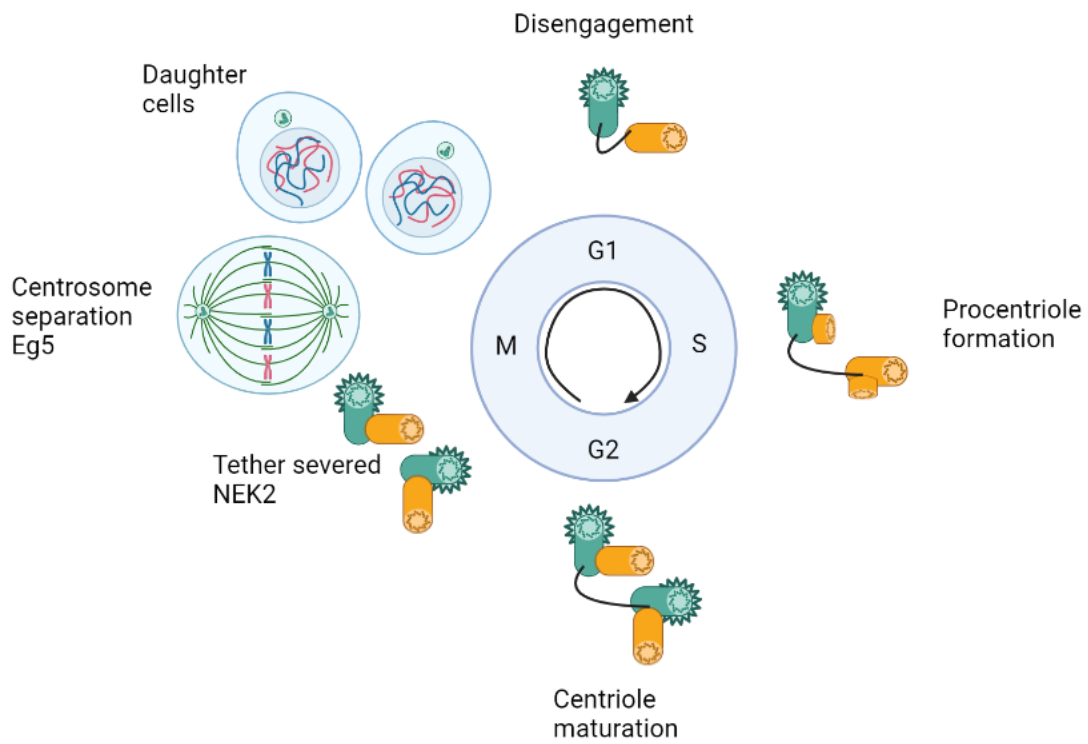


Figure 1.11. The centrosome duplication cycle. A cell begins the cell cycle in G1 having only one centrosome consisting of a mother (green) and daughter (yellow) centriole. The tight link is severed in G1 (disengagement) but the centrioles remained tethered. By S phase, new procentrioles begin to form. In G2, the new procentrioles mature and gain PCM proteins and the original daughter centriole gains appendages and becomes a mother centriole. At mitotic entry, the tether is severed as a result of NEK2 kinase activity and Eg5 facilitates centrosome separation to form the mitotic spindle poles. After abscission, each new daughter cell receives one centrosome, consisting of two centrioles, and the centrosome cycle begins again. Figure adapted from Wang, Jiang and Zhang (2014).

In addition to its role in nucleating microtubules, the centrosome can also act as a signalling hub to coordinate signalling pathways involved in cell cycle control (Arquint, Gabryjonczyk and Nigg, 2014; Lin, Xie and Chan, 2022). Intriguingly, CDK1/cyclin B, PLK1 and Aurora A kinases have all been seen to localise to the centrosome (Bailly *et al.*, 1989; Golsteyn *et al.*, 1995; Dutertre *et al.*, 2004). Thus, it is thought that mitotic progression relies on activation of CDK1/cyclin B complexes at the centrosome, where the centrosome clusters all the necessary regulators of the complex in close proximity for efficient signalling to take place (Arquint, Gabryjonczyk and Nigg, 2014). Similarly, proteins of the DNA damage checkpoint such as CHK1 have also been found at the centrosome during interphase (Krämer *et al.*, 2004). Moreover, centrosomal CHK1 regulates the activity of CDC25B, which activates CDK1 at the centrosome, suggesting that CHK1 prevents untimely activation of CDK1, important for correct cell cycle progression (Krämer *et al.*, 2004). Interestingly, other tyrosine kinases have been found to localise to the centrosome such as Src family kinases (Ley *et al.*, 1994). Hence, the concentration of multiple kinases/phosphatases at the centrosome suggests the centrosome may spatially organise cell signalling (Arquint, Gabryjonczyk and Nigg, 2014).

1.4.4. Microtubule post-translational modifications

Tubulins, the core component of microtubules, undergo a range of post-translational modifications (PTMs) which can impact microtubule dynamics and function. Tubulin PTMs can either occur on the highly structured tubulin body or the unstructured C-terminal tubulin tails (Janke and Magiera, 2020). A vast array of tubulin PTMs exist which may modify either α -tubulin or β -tubulin or both. Examples of PTMs include acetylation, detyrosination/tyrosination, glutamylation/polyglutamylation, methylation, phosphorylation and glycylation/polyglycylation, amongst others (Janke and Magiera, 2020). For the purpose of this thesis, only PTMs that are associated with microtubule stabilisation will be described, namely acetylation and detyrosination/tyrosination (Bär *et al.*, 2022).

A well characterised PTM of the tubulin body is the acetylation of α -tubulin at lysine 40 (K40). Intriguingly, this is the only known tubulin PTM that is found inside the lumen of the microtubule (Janke and Montagnac, 2017). Moreover, α -tubulin K40 is only found to be

acetylated within the microtubule lattice and not in α/β -tubulin heterodimers meaning that the enzyme that catalyses K40 acetylation (α -tubulin acetyltransferase 1 (α TAT1)), must somehow gain access to the narrow microtubule lumen. How α TAT1 gains access to the microtubule lumen still remains puzzling to researchers, but a number of hypotheses exist including entry via the open microtubule end or localised entry through defective sites within the microtubule lattice (Janke and Montagnac, 2017). Notably, the acetylation of K40 is a reversible process and the deacetylation of α -tubulin is performed by histone deacetylase 6 (HDAC6) and sirtuin 2 (SIRT2) (Janke and Montagnac, 2017).

Microtubule stabilisation is associated with K40 acetylation, although whether stabilisation occurs because of K40 acetylation or whether K40 acetylation occurs as a result of microtubule stabilisation is still unclear. Nevertheless, antibodies that detect acetylated K40 in α -tubulin are commonly used as a marker for microtubule stabilisation in cell-based studies (Janke and Montagnac, 2017). However, recent studies have shown that K40 acetylation increases the flexibility of microtubules making them more resistant to mechanical stress, thus contributing to the life span of long-lived microtubules (Portran *et al.*, 2017; Xu *et al.*, 2017).

Tubulin acetylation is not the only PTM that can affect microtubule stability. Indeed, tyrosination/detyrosination also indirectly affect microtubule dynamics by modulating the binding of specific motor proteins (Bär *et al.*, 2022). Detyrosination involves the stripping of the C-terminal tyrosine residue on α -tubulin by tyrosine carboxypeptidases, such as vasohibin (VASH) when in complex with small vasohibin binding protein (SVBP). Interestingly, detyrosination is also a reversible process and the reverse reaction, tyrosination, involves the re-addition of the C-terminal tyrosine residue by tubulin-tyrosine ligase (TTL) (Bär *et al.*, 2022).

Intriguingly, studies have shown that the mitotic centrosome associated kinesin (MCAK), which promotes microtubule depolymerisation, and CLIP-170, which promotes microtubule

polymerisation, both preferentially bind tyrosinated microtubules (Peris *et al.*, 2009; Peris *et al.*, 2006). Here, they are thought to contribute to the dynamic instability of tyrosinated microtubules and these proteins are lost upon detyrosination of microtubules which subsequently become more stable (Peris *et al.*, 2009; Peris *et al.*, 2006; Bär *et al.*, 2022).

1.5. The Eg5 kinesin

1.5.1. Eg5 structure and function

Eg5 (also known as KIF11 or Kinesin Spindle Protein (KSP)) is a plus-end directed kinesin belonging to the Kinesin-5 family, with a major role in mitosis (Sawin *et al.*, 1992). Early studies revealed that Eg5 co-localised with spindle microtubules in *Xenopus* egg extracts, with particular enrichment at the spindle poles (Sawin *et al.*, 1992). Notably, Eg5 does not associate with interphase microtubules in animal cells and requires phosphorylation by CDK1 for recruitment to the mitotic spindle (Sawin and Mitchison, 1995; Blangy *et al.*, 1995; Cahu *et al.*, 2008). Intriguingly, plant cells are an exception to this where Eg5 localises along microtubules throughout the cell cycle, including in interphase (Liu, Ran and Zhou, 2018). Despite this, sequence analysis of the Eg5 motor domain revealed that this domain is conserved across multiple species of the plant and animal kingdoms suggesting the overall conservation of Eg5 function throughout evolution (Liu, Ran and Zhou, 2018).

Immunodepletion of Eg5 from *Xenopus* egg extracts or microinjection of anti-Eg5 antibodies into human cells inhibited mitotic spindle formation and caused cell cycle arrest highlighting its essential role for bipolar spindle formation and efficient mitosis (Sawin *et al.*, 1992; Blangy *et al.*, 1995). Eg5 was later identified to be a bipolar tetrameric molecule (a pair of dimers) that has the ability to cross-link anti-parallel microtubules (Kashina *et al.*, 1996; Acar *et al.*, 2013; Kapitein *et al.*, 2005; Mann and Wadsworth, 2019). Moreover, Eg5 can 'walk' on the microtubules it cross-links causing antiparallel spindle microtubules to slide past one another, a property that is essential for spindle pole separation and formation of a bipolar spindle (Kapitein *et al.*, 2005; McIntosh, Molodtsov and Ataullakhanov, 2012).

Typical of kinesins, Eg5 monomers consist of three domains: a motor domain, stalk domain and tail domain (Figure 1.12) (Waitzman and Rice, 2014; Liu, Ran and Zhou, 2018). Whilst microtubule binding and the ATPase activity of Eg5 are facilitated by the motor domain, the stalk and tail domains each have their own functions (Liu, Ran and Zhou, 2018). The stalk domain is required to cross-link and slide antiparallel microtubules as it is known to orientate the motor domains relative to each other. Furthermore, only the N-terminal half of the stalk domain is required for Eg5 dimers to be formed, whereas the C-terminal portion of the stalk contains a bipolar assembly (BASS) domain which is necessary for the formation of tetramers from two sets of dimers (Figure 1.12) (Acar *et al.*, 2013; Waitzman and Rice, 2014). The tail domain on the other hand regulates microtubule localisation of the Eg5 protein. Indeed, previous studies have shown that CDK1 phosphorylation of residues in the tail domain (T926 in humans and T937 in *Xenopus*) is necessary for spindle localisation of Eg5 (Blangy *et al.*, 1995; Sawin and Mitchison, 1995).

1.5.2. Eg5 in centrosome separation and spindle formation

Evidence of Eg5 having a role in centrosome separation was first seen in 1995 when micro-injection of anti-Eg5 antibodies was observed to arrest cells in mitosis with monoastrial microtubule arrays (Blangy *et al.*, 1995). Analysis of the spindles in these cells revealed that centrosomes were still very close together and surrounded by condensed chromosomes which had failed to align for metaphase (Blangy *et al.*, 1995). The mitotic arrest was the result of activation of the spindle assembly checkpoint due to condensed chromosomes that were not attached in a bi-oriented manner. It was later discovered that NEK6 (section 1.3.2.2/1.3.3) can also phosphorylate Eg5 during mitosis with the key site identified as S1033, which is also in the tail domain (Rapley *et al.*, 2008). This phosphorylation event did not prevent the binding of Eg5 to spindle microtubules. However, expression of a phosphonull Eg5-S1033A mutant resulted in a large percentage of cells with monopolar spindles, suggesting that NEK6 regulation of Eg5 is necessary for centrosome separation (Rapley *et al.*, 2008).

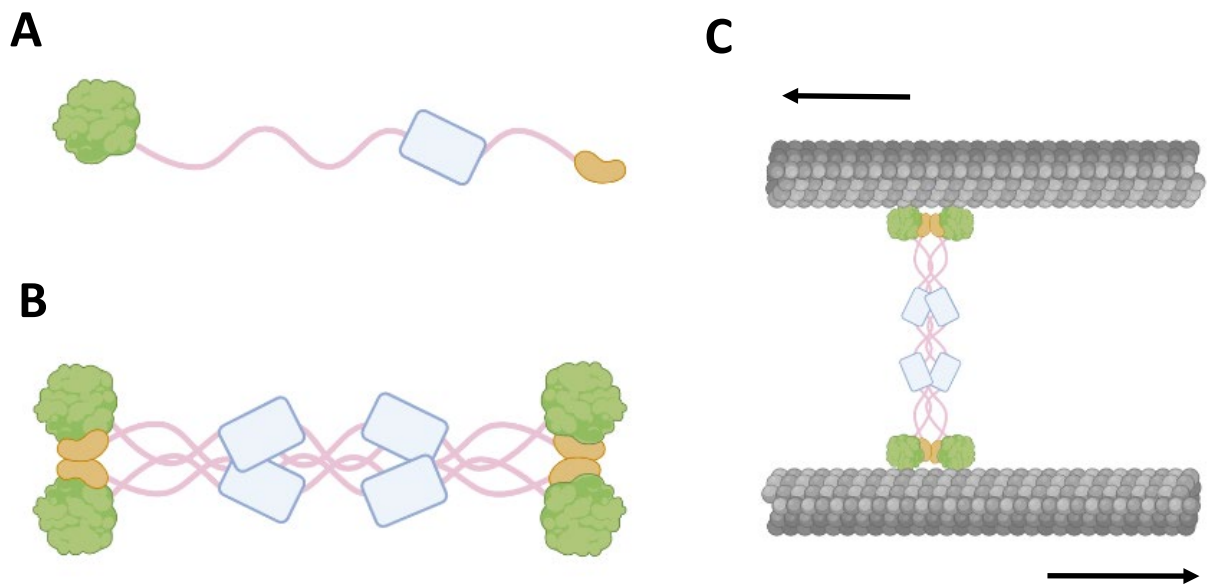


Figure 1.12. Schematic diagram of Eg5 domain structure. (A) Eg5 monomers contain a motor domain (green), stalk (pink) and tail domain (yellow). The C-terminus of the stalk contains a BASS domain (blue) that is required for the formation of homotetramers (B). (C) Eg5 tetramers cross-link antiparallel microtubules where two motor heads walk on each microtubule allowing them to slide past each other. Arrows indicate direction of movement. Adapted from Liu, Ran and Zhou (2018).

A later study provided evidence of a kinase-dependent signalling cascade consisting of PLK1-NEK9-NEK6/NEK7-Eg5 that was shown to control centrosome separation (Bertran *et al.*, 2011). Individual depletion of each component of this signalling cascade was shown to abrogate centrosome separation. Moreover, depletion of PLK1, NEK9, NEK6 or NEK7 in cells perturbed the recruitment of Eg5 to mitotic centrosomes, when compared to mock depleted control cells. The recruitment of Eg5 to mitotic centrosomes in PLK1 depleted cells, as well as centrosome separation, could be rescued by an activated mutant of NEK9 or overexpression of NEK6 which has previously been shown to stimulate NEK6 activity (Bertran *et al.*, 2011; Belham *et al.*, 2003). Additionally, failure to phosphorylate S1033 of Eg5 - as shown by expression of an Eg5 phosphonull (S1033A) mutant - resulted in loss of recruitment of Eg5 to prophase centrosomes and unseparated spindle poles (Bertran *et al.*, 2011). Together, these data show that the NEK9-NEK6/NEK7 signalling module acts downstream of PLK1 to phosphorylate Eg5, resulting in its recruitment to the centrosomes where its microtubule cross-linking and kinesin activity drive centrosomes apart (Bertran *et al.*, 2011).

An additional interaction has been described which may also be necessary for centrosome separation. Eg5 was shown to interact with the mitotic spindle assembly factor, TPX2 (Ma *et al.*, 2011). This interaction was necessary for K-fibre formation and for the spindle microtubule localisation of Eg5 (Ma *et al.*, 2011). Furthermore, TPX2 contains a nuclear localisation signal (NLS), which can be phosphorylated by NEK9, preventing its import to the nucleus (Eibes *et al.*, 2018). It was proposed that NEK9 phosphorylation of TPX2 results in a pool of TPX2 being retained around centrosomes, where it interacts with and anchors Eg5. This interaction is thought to permit Eg5 activity to drive centrosome separation (Eibes *et al.*, 2018).

1.5.3. Eg5 in neurons

Although primarily studied in the context of mitotic spindle assembly, Eg5 has also been implicated in the control of axon length in neuronal cells. Exposure of cultured sensory neurons to the Eg5 inhibitor, monastrol, led to an increase in axonal number and length.

This led the authors to propose that Eg5 acts to oppose axonal growth in post-mitotic neurons (Haque *et al.*, 2004). Consistent with this, Eg5 depletion was also found to stimulate axon growth of cultured neurons and increase axon branching (Myers and Baas, 2007).

In addition to regulating axonal growth, Eg5 is believed to have a role in controlling the migration of neurons. Eg5 was found to be phosphorylated in one side of the growth cone, opposite to the side microtubules invaded to drive growth cone turning, suggesting that Eg5 phosphorylation blocks entry of microtubules on one side of the growth cone (Nadar *et al.*, 2008). The authors proposed that Eg5 has a direct role in controlling the direction of migration in neurons by controlling the side of the growth cone that microtubules can invade (Nadar *et al.*, 2008). Furthermore, a separate study showed that inhibiting Eg5 resulted in faster but less directional migration in cultured neurons (Falnikar, Tole and Baas, 2011). Interestingly, these neurons were also found to have shorter leading processes after Eg5 inhibition (Falnikar, Tole and Baas, 2011).

Of particular interest to this study, Eg5 was shown to be phosphorylated by NEK7 in differentiating neurons where it contributes to the extension of dendrites (Freixo *et al.*, 2018). Firstly, NEK7 expression was found to increase in mouse hippocampal neurons 15 days after induction of differentiation. Secondly, depleting NEK7 from these neurons resulted in a significant reduction in dendrite length, a phenotype that was mirrored by inhibition of Eg5. Thirdly, NEK7 was found to phosphorylate Eg5 on S1033 in neurons resulting in its recruitment to distal dendrites. Finally, expression of an Eg5-S1033D phosphomimetic mutant was able to rescue dendrite length after NEK7 depletion, whereas wild-type Eg5 and a phosphonull Eg5-S1033A mutant both failed to do so (Figure 1.13) (Freixo *et al.*, 2018). An earlier study performed in cultured rodent primary neurons reported that inhibition of Eg5 resulted in shorter and thinner dendrites (Kahn *et al.*, 2015). Together, these studies suggest that Eg5 performs contrasting roles in dendrites and axons consistent with the different orientations of microtubules in dendrites and axons (Stone, Roegiers and Rolls, 2008). Axons contain microtubules in a plus-end-out orientation (distal

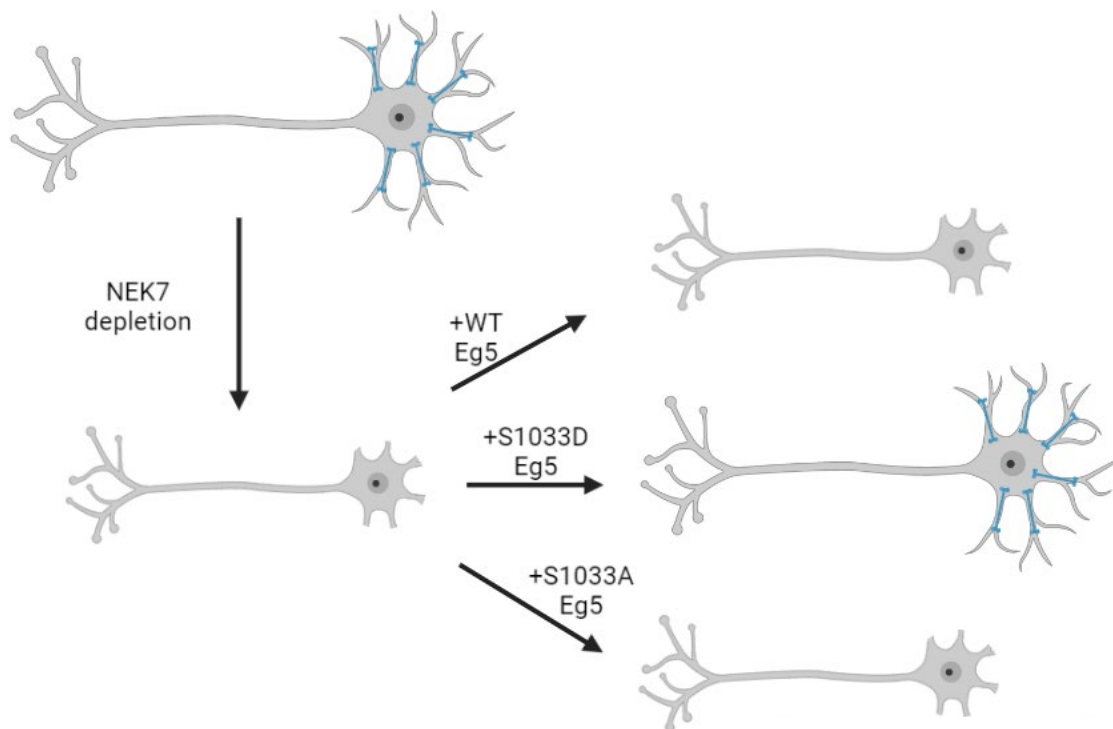


Figure 1.13. NEK7 phosphorylation of Eg5 at S1033 promotes dendrite extension in neurons. NEK7 depletion reduced the length of differentiating neurons. Transfection of an Eg5-S1033D phosphomimetic mutant could rescue dendrite length but not WT Eg5 or Eg5-S1033A. Phosphorylation of Eg5 at S1033 (blue) promotes its recruitment to microtubules in dendrites. Based on findings from Freixo *et al.* (2018).

to the cell body), whereas dendrites have the majority of microtubules oriented minus-end-out (Stone, Roegiers and Rolls, 2008).

1.5.4. Eg5 as a microtubule polymerase

A relatively recent study investigating the motor properties of Eg5 unexpectedly revealed that Eg5 does in fact have microtubule polymerase activity (Chen and Hancock, 2015). Incubating an Eg5 dimer with microtubules *in vitro* was demonstrated to increase the growth rate whilst reducing the catastrophe frequency of the microtubules when compared to control microtubules in the absence of Eg5. Subsequently, a later study proposed that Eg5 can promote a curved-to-straight transition in tubulin which promotes lateral bond formation necessary for microtubule growth (Chen *et al.*, 2019). This hypothesis was based on findings that Eg5 reduces the affinity of so-called 'wedge' microtubule inhibitors, such as colchicine, vinblastine and nocodazole, which promote microtubule shrinkage by stabilising the kinked conformation of tubulin, meaning lateral bonds are no longer able to form (Chen *et al.*, 2019).

Intriguingly, single molecule fluorescence experiments revealed that Eg5 could track the plus-ends of microtubules where Eg5 paused for 7 seconds (Chen and Hancock, 2015). Furthermore, it was demonstrated that the Eg5 motor domain preferentially binds microtubules over free tubulin, consistent with Eg5 being a polymerase rather than a depolymerase (Chen *et al.*, 2019). Taking these experiments together, the authors proposed that Eg5 stabilises the interactions between newly added tubulin dimers with the pre-existing protofilament by stepping on to the tubulin dimer and straightening it therefore enhancing microtubule polymerisation (Chen and Hancock, 2015; Chen *et al.*, 2019).

1.5.5. Eg5 in cancer

Eg5 expression is frequently upregulated in a variety of cancers, including colorectal, breast, liver and NSCLC (Kim *et al.*, 2023; Jin *et al.*, 2017; Shao *et al.*, 2021; Saijo *et al.*, 2006).

Interestingly, overexpression of Eg5 *in vivo* can contribute to spindle defects leading to

aneuploidy, genomic instability and tumour formation (Castillo *et al.*, 2007). This study generated transgenic mice which were designed to overexpress Eg5. These mice were found to develop a variety of malignancies after an average of 21 months which included hematopoietic neoplasias, pulmonary and mammary adenocarcinomas, and ovarian neoplasms (Castillo *et al.*, 2007). In addition to this, mouse embryonic fibroblasts (MEFs) isolated from these transgenic mice revealed a significant proportion of monopolar or multipolar spindles in mitotic cells. Analysis of the DNA content of these cells by flow cytometry revealed a substantial number of cells overexpressing Eg5 to be tetraploid or even octoploid (Castillo *et al.*, 2007). Together, these findings demonstrate that Eg5 overexpression can contribute to many of the pre-requisites of cancer formation, namely aneuploidy, genomic instability and cellular transformation. In line with this, multiple studies have also highlighted the use of Eg5 as a prognostic marker, where patients with higher Eg5 expression are seen to have distant metastases and lower overall survival rates than those with low expression (Kim *et al.*, 2023; Shao *et al.*, 2021; Jin *et al.*, 2017).

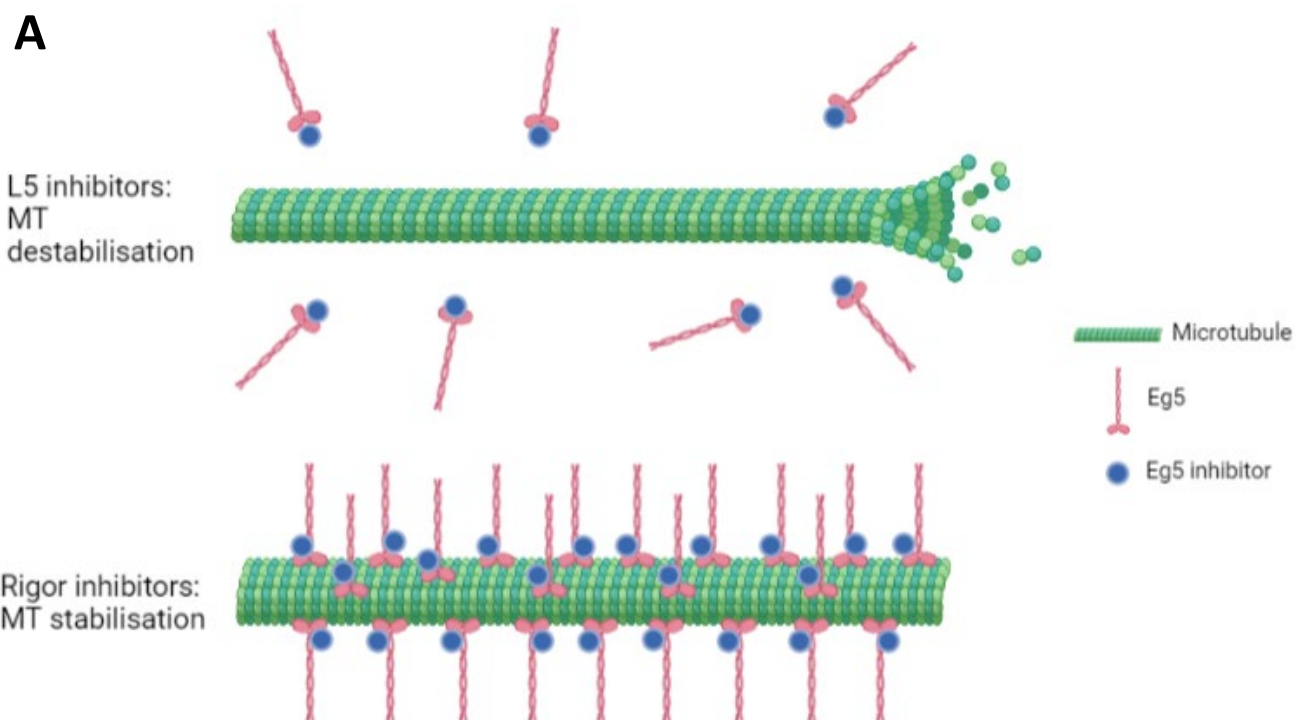
Eg5 has also been linked to cancer cell migration and invasion. A study investigating the effects of an Eg5 inhibitor, dimethylnastron, found this inhibitor reduced the invasion of multiple pancreatic cancer cell lines (Sun *et al.*, 2011). Cells were treated with varying concentrations of dimethylnastron and their ability to invade through Matrigel in a transwell assay system was assessed. Indeed, higher concentrations of dimethylnastron showed a greater effect on reducing cell invasion (Sun *et al.*, 2011). This study also claimed that dimethylnastron reduced migration of pancreatic cancer cells in a wound healing assay (Sun *et al.*, 2011). However, Eg5 inhibitors cause mitotic arrest, which brings into question whether these assays are appropriate to use when cells are treated with such inhibitors. Nonetheless, a similar study which investigated the effect of Eg5 inhibitors on migration of gastric adenocarcinoma cells obtained similar results, this time from a transwell migration assay in the presence or absence of chemoattractant (Marconi *et al.*, 2019). In this study, the Eg5 inhibitor, K858, and two similar novel inhibitors developed by the authors were used and all three inhibitors markedly reduced cell migration (Marconi *et al.*, 2019).

Eg5 is also believed to have a role in angiogenesis. A study demonstrated that upon stimulation of angiogenesis in vivo, Eg5 expression was upregulated in chick chorio-allantoic membrane (Exertier *et al.*, 2013). Similar results were produced in human umbilical vein endothelial cells (HUVECs) cultured in vitro. Immunohistochemical staining of glioblastoma or renal cell carcinoma samples revealed Eg5 was localised within endothelial cells and capillaries, respectively (Exertier *et al.*, 2013). Interestingly, HUVEC proliferation, adherence, spreading and migration could be suppressed with Eg5 inhibitors. Eg5 inhibition was also found to hinder angiogenesis in vivo in both a mouse aortic ring assay and upon injection of Eg5 inhibitors into chick or zebrafish embryos (Exertier *et al.*, 2013). Taken together, these findings provide intriguing evidence that Eg5 is necessary for establishment of vascular systems.

1.5.6. Eg5 inhibitors

The crucial role of Eg5 in dividing cells makes Eg5 an attractive target for chemotherapeutic intervention. A variety of Eg5 inhibitors have been developed which have different mechanisms of action. Eg5 inhibitors can be divided into two categories: loop 5 (L5) inhibitors, which destabilise microtubules, and rigor inhibitors, which stabilise microtubules (Chen *et al.*, 2017). Examples of L5 inhibitors include monastrol, S-trityl-L-cysteine (STLC), ispinesib and filanesib, whereas rigor inhibitors include 2-[1-(4-fluorophenyl)cyclopropyl]-4-(pyridin-4-yl)thiazole (FCPT) and BRD9876 (Figure 1.14) (Chen *et al.*, 2017; Skoufias *et al.*, 2006).

Specifically described as ATP uncompetitive inhibitors, L5 inhibitors bind in or near the L5 loop and inhibit the ATPase activity, preventing an essential conformational change from happening in the Eg5 motor which would permit association with microtubules. Hence, these inhibitors weaken Eg5 interaction with microtubules and makes them prone to depolymerisation (Larson *et al.*, 2010; Chen *et al.*, 2017). The addition of these kind of inhibitors to cells prevents the separation of centrosomes and formation of a bipolar spindle, meaning that cells will arrest in mitosis with a monopolar spindle (Skoufias *et al.*, 2006; Chen *et al.*, 2017). These drugs are attractive candidates for chemotherapy as they



B

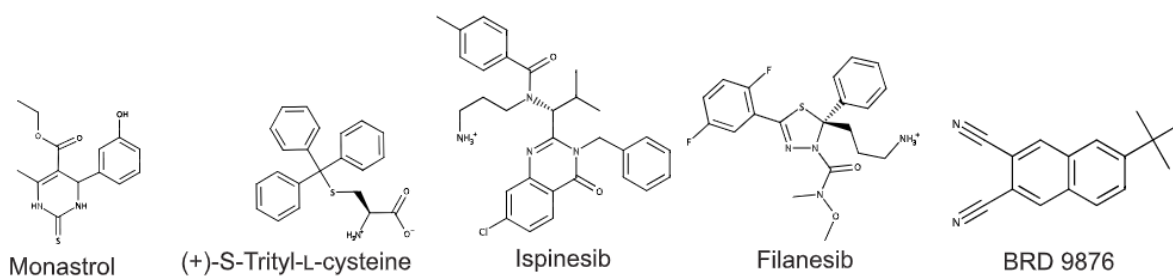


Figure 1.14. Mechanisms of Eg5 inhibitors. (A) Eg5 inhibitors can be classified as either loop 5 or rigor inhibitors. Loop 5 inhibitors weaken the interaction between Eg5 and the microtubules resulting in microtubules destabilisation. Rigor inhibitors on the other hand strengthen the Eg5-microtubule interaction resulting in microtubule stabilisation. (B) The chemical structures of five well-used Eg5 inhibitors. Monastrol, STLC, ispinesib and filanesib are all loop 5 inhibitors, whereas BRD9876 is a rigor inhibitor (adapted from Chen *et al.* (2017)).

will, in theory, selectively target dividing cells without causing toxic side-effects on non-proliferating cells, such as neurons, which is a drawback of microtubule poisons (Shi and Mitchison, 2017). However, many of these L5 inhibitors have given disappointing results in clinical trials (Shi and Mitchison, 2017; Garcia-Saez and Skoufias, 2021). Nevertheless, one inhibitor, filanesib (also known as Arry-520) has now reached phase III clinical trials after showing promising results in the treatment of multiple myeloma (Owens, 2013; Indorato *et al.*, 2019).

Eg5 rigor inhibitors stabilise microtubules and can be ATP-competitive or non-competitive (Chen *et al.*, 2017). FCPT is an example of an ATP-competitive rigor inhibitor that binds in the ATP binding site of L5; BRD9876 binds to the α 4- α 6 interface but there are contrasting views of whether BRD9876 is an ATP-competitive or non-competitive inhibitor (Groen *et al.*, 2008; Chattopadhyay *et al.*, 2015; Chen *et al.*, 2017). Treatment of cells with either of these rigor inhibitors prevents bipolar spindle formation unless cells are already in mitosis at the time of treatment. Cells already in mitosis maintain spindle integrity when treated with these inhibitors. However, it has been reported that treating cells with FCPT results in less microtubules at spindle poles and the mis-localisation of TPX2 and γ -tubulin to the spindle equator rather than the spindle poles (Chen *et al.*, 2017; Groen *et al.*, 2008).

1.6. Cell migration

1.6.1. Mesenchymal cell migration

Cell migration is essential for many biological processes, including embryonic development, wound healing and immune responses. It is also necessary for pathological events, such as cancer cell dissemination and metastasis. Two general methods of cell migration have been described: mesenchymal migration and amoeboid migration. Whilst amoeboid migration relies heavily on acto-myosin contraction where cells appear blebbed and lack adhesions, mesenchymal migration is characterised by cells adopting a particular type of morphology with a distinct leading and trailing edge with force generated on adhesion sites (Graziani *et al.*, 2022; Etienne-Manneville, 2013). Due to the mesenchymal-like morphologies of cells used in this study, amoeboid migration will not be discussed further.

Mesenchymal migration can be broken down into four key events that must take place in order for efficient cell movement: protrusion, adhesion, contraction and retraction (Figure 1.15) (Etienne-Manneville, 2013). Different types of protrusion are required at the front of the cell which drive cell migration and are largely comprised of highly branched actin filaments (Rottner and Schaks, 2019). The first of these essential protrusions is a lamellipodium. Lamellipodia are dynamic structures formed from the assembly of branched actin filaments which physically push the cell membrane forward in the direction of migration (Innocenti, 2018; Rottner and Schaks, 2019). Lamellipodia are established due to the activity of the Rho GTPases Rac1 and Cdc42 and activation of their downstream targets, the WAVE complex (target of Rac1), WASP/N-WASP (target of Cdc42), which in turn activate the Arp2/3 complex that promotes actin branching (Rottner and Schaks, 2019; Etienne-Manneville and Hall, 2002; Mattila and Lappalainen, 2008). Another type of protrusion formed by migrating cells are filopodia. Filopodia are thin hair-like structures formed from bundled actin filaments that are capable of sensing the extracellular environment (Mattila and Lappalainen, 2008; Etienne-Manneville and Hall, 2002). In contrast to lamellipodia, filopodia are formed due to the activity of Cdc42 which can activate formins, such as mDia2, that also control actin organization (Peng *et al.*, 2003; Rottner and Schaks, 2019).

A third specialised type of actin-based protrusion, termed invadopodia, are formed by cancer cells and contribute to the degradation of the basement membrane through co-ordination of extracellular proteolytic activity (Paterson and Courtneidge, 2018). Once the basement membrane is degraded, cancer cells can invade into the extracellular matrix (ECM) and thus begin the process of metastasis. These specialised protrusions are also thought to form downstream of Cdc42 activity, mediated by N-WASP and the Arp2/3 complex (Paterson and Courtneidge, 2018; Rottner and Schaks, 2019). A number of proteins are associated with invadopodia, including proteases from the matrix metalloprotease family (MT1-MMP, MMP2 and MMP9) and serine protease family (e.g. separase and urokinase-type plasminogen activator (uPA)), which facilitate the breakdown of the basement membrane (Paterson and Courtneidge, 2018). It is worth noting that some normal cell types such as osteoclasts and immune cells are also capable of forming protrusions

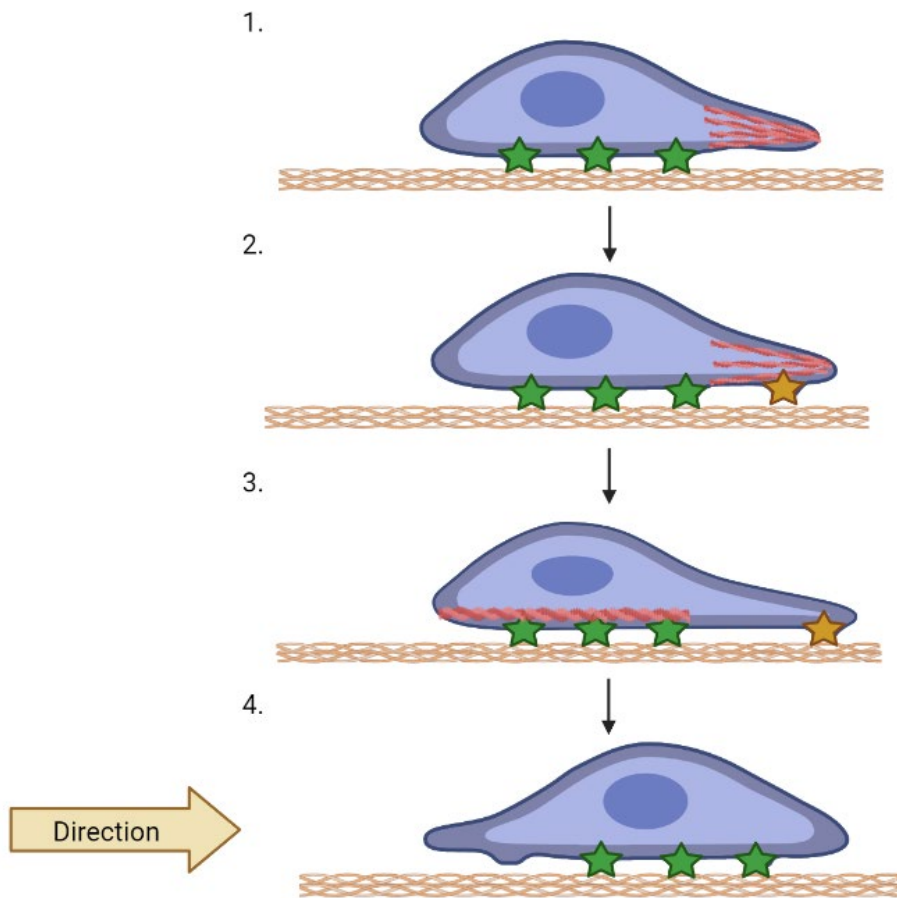


Figure 1.15. Four steps of mesenchymal cell migration. 1. The first step of mesenchymal cell migration is protrusion. Actin (red) polymerisation occurs at the front of the cell and pushes the cell membrane forward. 2. The second stage is the formation of new focal adhesions (yellow star) behind the leading edge of the cell. Focal adhesions provide points of contact between the cell and the extracellular matrix (orange). 3. The third stage is contraction. Acto-myosin contraction generates force over mature focal adhesions (green) which allows the cell to pull itself forward. 4. The final stage is retraction of the cell rear. Focal adhesions are disassembled at the cell rear. Yellow arrow indicates direction of migration. Figure adapted from Ananthakrishnan and Ehrlicher, 2007.

capable of proteolytic activity. Here, these invasive protrusions are known as podosomes (Paterson and Courtneidge, 2018).

The second essential step of mesenchymal migration is adhesion. Focal adhesions form underneath protrusions at the leading edge and attach the actin cytoskeleton to the extracellular matrix (ECM), providing points of contact for the cell to generate traction (Parsons, Horwitz and Schwartz, 2010). The initial link between the cell and the ECM is formed by the extracellular portion of integrins, transmembrane proteins that bind to specific recognition sequences in ECM components such as collagen and fibronectin. Once a physical link has been established, a conformational change occurs in the intracellular portion of the integrins, which exposes its cytoplasmic tail where focal adhesion proteins such as talin and vinculin are recruited to the nascent adhesion site (Parsons, Horwitz and Schwartz, 2010). The recruitment of focal adhesion proteins to the nascent adhesion site relies on tyrosine phosphorylation events predominately performed by the focal adhesion kinase (FAK) and Src (Maziveyi and Alahari, 2017).

Once assembled, focal adhesions can mature and eventually disassemble at the rear of the cell. Mature focal adhesions are linked to actin filaments and it is here that the cell generates the force required to pull itself over the adhesion (Maziveyi and Alahari, 2017). The maturation of focal adhesions into focal complexes is thought to be in part due to acto-myosin contractility (Parsons, Horwitz and Schwartz, 2010). The tension generated by acto-myosin causes stretching of focal adhesion proteins, such as talin, which exposes binding sites for other focal adhesion proteins, namely vinculin, resulting in further recruitment of these proteins to form larger complexes (del Rio *et al.*, 2009). Although less well understood than focal adhesion assembly, it is clear that focal adhesion disassembly is coupled to cell retraction. Disassembly is also thought to occur as a result of acto-myosin contractility and Rho GTPase activity, as well as calpain mediated cleavage of talin and integrin β subunits (Parsons, Horwitz and Schwartz, 2010; Franco *et al.*, 2004; Flevaris *et al.*, 2007).

Acto-myosin contractility is required not only for the turnover of focal adhesions, but also for the contraction of the cell as a whole (Haga and Ridley, 2016). The main regulators of acto-myosin contractility are the Rho GTPase, RhoA, and its downstream effectors, Rho-associated coiled-coil containing kinases (ROCKs). Upon activation, ROCKs can phosphorylate and activate LIM-kinases (LIMKs), which subsequently phosphorylate and inactivate cofilin, an actin severing protein (Ohashi *et al.*, 2000). This increases the stability of actin filaments. In addition to this, ROCKs also phosphorylate and inactivate myosin light chain (MLC) phosphatase. The result of this is an increase in cellular levels of phosphorylated MLC which promotes the cross-linking of actin filaments by myosin II and therefore the production of contractile forces (Narumiya, Tanji and Ishizaki, 2009; Haga and Ridley, 2016). RhoA signalling via the formin, mDia, is also responsible for the formation of actin stress fibres, a subset of which associate with mature focal adhesions (Narumiya, Tanji and Ishizaki, 2009; Haga and Ridley, 2016).

The final stage of mesenchymal cell migration is retraction, which also largely relies on acto-myosin contractility (Etienne-Manneville, 2013). Crucially, focal adhesions must be disassembled at the rear of the cell and failure to do so will inhibit the movement of cells. The turnover of focal adhesions also relies on microtubules (Etienne-Manneville, 2013; Ezratty, Partridge and Gundersen, 2005) and this will be discussed further in section 1.6.3.

Finally, it is worth noting that for efficient mesenchymal migration, it is essential that cells maintain a distinct front-to-rear polarity. The Rho GTPase, Cdc42, is known to have direct roles in this (Etienne-Manneville, 2004; Cau and Hall, 2005). Cdc42 participates in signalling pathways that act on the microtubules and actin cytoskeleton, resulting in cell polarisation. The first of these signalling pathways involves a physical interaction between Cdc42 and Par6 which inactivates aPKC. This pathway is known to reorientate the centrosome which may lead to the capture of microtubule plus ends at the leading edge (Cau and Hall, 2005; Etienne-Manneville, 2004). Moreover, Cdc42 can also interact with IQGAP1 which associates with CLIP-170, a microtubule plus-end associated protein. This pathway also results in the capture of microtubules and interfering with these interactions leads to a loss of

polarisation in cells (Fukata *et al.*, 2002). Another pathway involves an interaction between Cdc42 and PAK kinases which results in PAK activation. Once active, PAKs can localise β -pix and Rac1 at the leading edge where actin polymerisation takes place (Cau and Hall, 2005).

In summary, mesenchymal cell migration is a complex process that relies on the establishment of a distinct cell front and rear. Multiple signalling pathways exist which act principally on the actin cytoskeleton but also on microtubules in order to form a protrusive front and a retracting rear and these pathways must be tightly controlled in both space and time to allow for efficient migration.

1.6.2. Epithelial to mesenchymal transition

Epithelial-to-mesenchymal transition (EMT) is a process by which epithelial cells alter their phenotype and gain migratory and invasive potential (Roche, 2018). Furthermore, EMT is characterised by a loss of cell-cell adhesion and cell-matrix adhesion, a change in cell-surface proteins, a loss of apical-basal polarity and gain of front-rear polarity; remodelling of the cytoskeleton underlies many of these morphology changes (Roche, 2018). Mesenchymal cells also exhibit more resistance to senescence and apoptosis and can display stem-cell like properties (Thiery *et al.*, 2009). Again, EMT is a normal process essential in embryonic development and body patterning (Thiery, 2002). Importantly, EMT is a reversible process, with transitions between EMT and mesenchymal-to-epithelial transition (MET) being necessary in organ development (Thiery, 2002; Kalluri and Weinberg, 2009). Interestingly, cancer cells will often undergo a partial EMT where they maintain the cell-cell adhesive properties of epithelial cells but benefit from the migratory potential of mesenchymal cells. Moreover, these cells can collectively migrate as clusters (Jolly *et al.*, 2015).

A key marker of EMT is the loss of E-cadherin expression. E-cadherin is a cell surface protein essential for mediating cell-cell adhesion where it facilitates the formation of adherens junctions through interaction with α/β -catenins, which in turn bind the actin cytoskeleton (Thiery, 2002). Desmosomes can also be formed through E-cadherin interaction between

neighbouring cells, where cells are anchored together through indirect interaction with intermediate filaments (Thiery, 2002). Coupled with the loss of E-cadherin expression in mesenchymal cells is an increase in N-cadherin expression (Mrozik *et al.*, 2018). Interestingly, the expression of N-cadherin promotes cell clustering, albeit with weaker interactions and therefore assists collective cell migration (Klymenko *et al.*, 2017). Expression of N-cadherin at the rear of “leader” cells results in the formation of actin-based protrusions at the front of the “leader” cell. This is achieved through the activation of Rac1 and Cdc42 GTPases at the cell front, whereas an N-cadherin-p120 catenin complex excludes α 5-integrin at the rear, where junctions with “follower” cells are formed. The exclusion of α 5-integrin at the cell rear inhibits Rac1 and Cdc42 activity at the rear, thus N-cadherin directly participates in the establishment of front-rear polarity of mesenchymal cells and to cytoskeleton reorganisation mediated by Rho GTPases (Ouyang *et al.*, 2013).

The loss of E-cadherin can be triggered by transcription factors which bind to the promoter region of the E-cadherin gene (*CDH1*) and repress its transcription. Transcription factors known to do this include SNAI1 (Snail), SNAI2 (Slug), Twist, Zeb1 and Zeb2 (Loh *et al.*, 2019; Roche, 2018). These transcription factors can cooperate with enzymes, such as DNA methylases, which keep the promotor of *CDH1* hypermethylated, resulting in its epigenetic silencing (Serrano-Gomez, Maziveyi and Alahari, 2016). Growth factors, such as fibroblast growth factor (FGF), or signalling pathways such as the Wnt pathway are known to regulate the expression of these EMT-promoting transcription factors (Loh *et al.*, 2019).

In summary, the key events mediating EMT are the loss of E-cadherin expression and its replacement with N-cadherin. This cadherin switch can directly alter cellular properties such as adhesion, polarity, cytoskeleton organisation and cell morphology which promote the migration and invasion of mesenchymal cells.

1.6.3. The role of microtubules in cell migration

The role of actin filaments in cell migration is extremely well characterised. However, it has become clear that microtubules also have multiple roles in the cell migration process above and beyond dictating cell polarity through centrosome positioning (Wadsworth, 1999).

Whilst the assembly of actin filaments drives the formation of membrane protrusions, such as lamellipodia, microtubules play more subtle roles in this process. Microtubules are largely excluded from lamellipodial protrusions, but a few microtubules (termed pioneer microtubules) are permitted access where they contribute to trafficking of components required at the leading edge, as well as for mechanical support and signalling (Wadsworth, 1999; Etienne-Manneville, 2013; Garcin and Straube, 2019).

Microtubule-mediated trafficking of membrane components, mRNAs and signalling molecules to the leading edge is necessary for efficient directional migration. Crucially, cell membrane tension must be balanced with the forces of actin polymerisation at the cell front. To that end, the cell membrane must be extended and microtubules transport newly synthesised lipids and other necessary components to the leading edge for this purpose (Raucher and Sheetz, 2000; Garcin and Straube, 2019). Microtubules also transport mRNAs of proteins that are directly involved with actin polymerisation, such as the Arp2/3 complex, profilin and β -actin (Mingle *et al.*, 2005; Johnsson and Karlsson, 2010; Hill, Schedlich and Gunning, 1994). The localised translation of these proteins is thought to contribute to limiting actin polymerisation to the leading edge (Garcin and Straube, 2019). In addition to membrane components and mRNAs, the Rho GTPases Rac1 and Cdc42 and one of their activators β -pix are also delivered to the leading edge via microtubule transport (Osmani *et al.*, 2010; Palamidessi *et al.*, 2008).

The pushing force behind membrane protrusion is predominantly generated by actin polymerisation, although some evidence exists that suggests microtubules may also contribute to force generation (Etienne-Manneville, 2013). In neurons, microtubule sliding facilitated by kinesin-1 has been shown to be sufficient for initial neurite extension (Lu *et al.*, 2013). Indeed, this study showed neither actin nor microtubule polymerisation was required

to generate neurite outgrowth (Lu *et al.*, 2013). Additionally, microtubules are required for the migration and invasion of mesenchymal cells in 3D culture models, where they promote the generation of long protrusions necessary to form adhesion sites needed for the cell to pull itself along (Bouchet *et al.*, 2016). This was shown to be dependent on microtubule plus-end binding proteins, SLAIN2 and CLASP1, which prevent catastrophes from occurring. It was shown that pseudopods were unable to lengthen upon microtubule catastrophes at the pseudopod tip (Bouchet *et al.*, 2016).

Microtubule polymerisation or depolymerisation acts as a signal that activates different Rho GTPases. Microtubule polymerisation was first found to activate Rac1 at the leading edge in 1999, where lamellipodia were seen to form in cells after nocodazole washout (Waterman-Storer *et al.*, 1999). Furthermore, treatment of cells with taxol was also found to stimulate lamellipodia formation (Waterman-Storer *et al.*, 1999). Later research found that microtubules can in fact interact with guanine nucleotide exchange factors (GEFs), which activate the Rho GTPases. One study found the GEF Tiam2 (also known as STEF) was required for Rac1 activation during microtubule growth (Rooney *et al.*, 2010). In contrast to this, microtubule depolymerisation activates RhoA at the cell rear (Krendel, Zenke and Bokoch, 2002). Here, the RhoA GEF, GEFH1, physically interacts with microtubules where it is kept in an inactive state. Microtubule depolymerisation facilitates the release of GEFH1 when it can then activate RhoA at the cell rear (Krendel, Zenke and Bokoch, 2002).

Microtubules are also involved in the regulation of focal adhesions, where they are thought to be involved in focal adhesion assembly, maturation and turnover. In fact, dynamic microtubules repeatedly associate with focal adhesion sites (Kaverina, Rottner and Small, 1998). The role of microtubules in focal adhesion dynamics is likely to be mediated in part by the ability of microtubules to regulate Rho GTPases (Stehbens and Wittmann, 2012; Etienne-Manneville, 2013). Indeed, microtubule depolymerisation has been shown to activate RhoA, which has previously been shown to facilitate focal adhesion assembly (Krendel, Zenke and Bokoch, 2002; Ridley and Hall, 1992). Furthermore, the increase in actomyosin contractility stimulated by RhoA also results in adhesion maturation (Krendel, Zenke

and Bokoch, 2002). Similarly, Rac1 and its activator Tiam2 are thought to be required for focal adhesion disassembly, where Tiam2 has been shown to target microtubules to focal adhesions (Rooney *et al.*, 2010).

Microtubule-mediated transport of proteins is also thought to be involved in the focal adhesion life cycle. For example, microtubules are necessary to deliver integrins to the cell surface which form the building blocks of focal adhesions (Theisen, Straube and Straube, 2012). Similarly, microtubules also transport Adenomatous Polyposis Coli (APC) to their plus-ends in proximity to nascent focal adhesion sites where it is proposed APC stimulates focal adhesion dynamics (Fang and Svitkina, 2022). One study has shown that APC interacts with FAK and paxillin at the leading edge of the cell, therefore APC may have a role in focal adhesion assembly (Matsumoto *et al.*, 2010). Conversely, studies have shown that APC nucleates actin filaments at focal adhesions where microtubule growth along actin stress fibres is required for microtubule capture at focal adhesions and their dissolution (Juanes *et al.*, 2017; Kaverina, Rottner and Small, 1998).

Lastly, microtubule stabilisation has been linked to cell migration and metastasis in multiple studies (Boggs *et al.*, 2015; Bance *et al.*, 2019; Kim *et al.*, 2023). The first of these studies found that breast cancer cells formed long protrusions that contained acetylated microtubules, termed microtentacles (McTN), which are believed to play a role in the reattachment of suspended tumour cells (Boggs *et al.*, 2015). Furthermore, mutation of the α -tubulin acetylation site, K40, to arginine reduced chemotactic cell migration, suggesting that tubulin acetylation somehow promotes a metastatic phenotype (Boggs *et al.*, 2015). Similarly, another study showed that siRNA depletion of α TAT1 reduced the rate of migration in astrocytes (Bance *et al.*, 2019). Moreover, α TAT1 was found to localise to focal adhesion sites where it is believed to locally stabilise microtubules and have an involvement in focal adhesion dynamics (Bance *et al.*, 2019). Finally, acetylated tubulin expression has been found to be elevated in a number of cancer types. For example, one study found elevated acetylated tubulin in 74% of samples from a cohort of colon cancer patients and this was linked to increased metastatic potential (Kim *et al.*, 2023).

1.7. Aims and objectives

The mechanisms by which EML4-ALK V3 enables cancer cells to become more mesenchymal in morphology and migratory remain elusive. By understanding the pathways these cancer cells are using to promote cell migration, invasion and metastasis, there is potential for novel drug targets to be identified that could block these pathways and perhaps slow the spread of these cancer cells to secondary sites in the body. In addition to morphology and migration changes, research has also revealed significant alterations to the microtubule cytoskeleton in cells that express EML4-ALK V3, although how these alterations occur is still unclear. As it is known that these phenotypic changes are dependent on NEK9 and NEK7, and that a NEK7-Eg5 pathway exists in neurons that promotes dendrite extension, we were interested to see if this pathway was responsible for the phenotypic changes observed in EML4-ALK V3 cancer cells. In addition, some evidence suggesting that EML4-ALK V3 may have a role at the centrosome has recently emerged with cells expressing EML4-ALK V3 exhibiting centrosome amplification and increased microtubule nucleation capacity (see section 1.2.4). This could promote genomic instability in these cancer cells. Therefore, we also sought to further investigate whether EML4-ALK V3 might localise to the centrosome along with the potential downstream components, NEK7 and Eg5.

The aims of this project were therefore:

- (i) to investigate whether Eg5 regulates interphase microtubule stability, cell morphology and migration in EML4-ALK V3 cancer cells;
- (ii) to determine whether Eg5 is a downstream substrate of NEK7 in EML4-ALK V3 cancer cells;
- (iii) to determine whether EML4-ALK V3 and downstream substrates localise to the centrosome and alter its behaviour.

The specific experimental objectives to investigate these aims were as follows:

- (i) compare the expression and intracellular localisation of Eg5 in isogenic BEAS-2B and NSCLC cell lines expressing EML4-ALK V3 to parental or EML4-ALK V1 cell lines;
- (ii) determine whether cell morphology and migration are altered in EML4-ALK V3 cells upon chemical inhibition of Eg5 with STLC, filanesib and BRD9876;
- (iii) determine whether Eg5 is regulated by NEK7 in EML4-ALK V3 cell lines using siRNA depletion of NEK7;
- (iv) explore the localisation of Eg5 S1033 phosphomutants in EML4-ALK V1 and V3 cell lines and determine whether phosphorylation of S1033 increases microtubule stability and cell length;
- (v) investigate whether EML4-ALK V3 and downstream components of the NEK9-NEK7 pathway localise to the centrosome;
- (vi) explore whether microtubule nucleation from the centrosome is increased in cells expressing EML4-ALK V3.

CHAPTER 2

Materials and methods

2.1. Materials and reagents

Table 2.1.1. Reagents and materials

Reagent/material	Supplier
Ammonium persulfate (APS)	Sigma Aldrich
Bacteriological agar	Sigma Aldrich
β -mercaptoethanol	Sigma Aldrich
Boric acid	Fisher
Bovine Serum Albumin (BSA)	Fisher Scientific
Butanol	Fisher
Coverslips (22 mm/13 mm)	Scientific Laboratory Supplies
Dimethyl Sulfoxide (DMSO)	Sigma Aldrich
DTT	Melford
EDTA	Fisher
Enhanced chemiluminescence (ECL) Western blotting substrate	Pierce
Ethanol	Fisher Scientific
GeneRuler 1 kb plus DNA ladder	ThermoFisher
Glycerol	Fisher Scientific
Glycine	Melford
HCl	Fluka
HEPES	Melford
Hoechst 33258	Invitrogen
KCl	Acros organics
KH_2PO_4	Fisher
Luria Broth (LB) pellets	Melford
Methanol	Fisher Scientific
Microscope slides	VWR
Midi prep kit	Zymo research
NaCl	Melford
NaHCO_3	Sigma Aldrich

Na ₂ HPO ₄	Melford
NaOH	Organics
Nescofilm	Nesco
Nitrocellulose (0.45 µm pores)	Amersham
Nonidet P-40	Fluka BioChemika
N-propyl gallate	Sigma Aldrich
pH indicator paper	VWR
Precision Plus Protein Dual Colour Standard protein ladder	BioRad
Protein assay dye	BioRad
Protein inhibitor cocktail (PIC)	Proteoloc
ProtoGel (30% w/v acrylamide)	Geneflow national diagnostics
RNase A	Invitrogen
RNase Away	Invitrogen
Skimmed milk powder	VWR
Sodium deoxycholate	Sigma Aldrich
SDS	Sigma Aldrich
SYBR-Safe	Invitrogen
TEMED	Santa Cruz
Tris base	Fluorochem
Triton X-100	Sigma Aldrich
Tween-20	MP Chemicals
Whatman paper	Scientific Laboratory Supplies
XL-10 GOLD bacteria	Agilent Technologies
X-ray films	Scientific Laboratory Supplies
0.2 µm filter	Pall Corporation
1 ml/50 ml syringe	BD Plastipak
27G needles	BD Bioscience

Table 2.1.2. Plasmids

Plasmid	Received From	Antibiotic resistance
pCS2 FLAG-Eg5 WT	Dr. Joan Roig, Barcelona	Amp
pCS2 FLAG-Eg5 S1033A	Dr. Joan Roig, Barcelona	Amp
pCS2 FLAG-Eg5 S1033D	Dr. Joan Roig, Barcelona	Amp

Table 2.1.3. Sequencing primers

Primer name	Sequence (5' – 3')
Eg5 Fwd1	CAGCCAAATTCGTCTGCGAAG
Eg5 Fwd2	GCATACTCTAGTCGTTCCCAC
Eg5 Fwd3	CTCAAGACTGATCTTCTAAGT
Eg5 Rev1	GATCTGGGCTCGCAGAGGTAA
Eg5 Rev2	CTTCGCAGACGAATTTGGCTG

Table 2.1.4. Cell lines

Cell line (Source/supplier)	Cell origin	Media	Supplemented with
BEAS-2B Parental (Dr Jene Choi, Seoul Korea)	Bronchial epithelia	RPMI 1640	10% FBS (v/v), 1% Penicillin- Streptomycin (v/v), 1% G418 (w/v)
BEAS-2B EML4- ALK V1/V3 (Dr Jene Choi, Seoul, Korea)	Bronchial epithelia	RPMI 1640	10% FBS (v/v), 1% Penicillin- Streptomycin (v/v), 1% G418 (w/v), 0.25µg/ml puromycin
H3122 (ATCC)	Lung adenocarcinoma	RPMI 1640	10% FBS (v/v), 1% Penicillin- Streptomycin (v/v)

H2228 (ATCC)	Lung adenocarcinoma	RPMI 1640	10% FBS (v/v), 1% Penicillin- Streptomycin (v/v)
-----------------	------------------------	-----------	---

Table 2.1.5. Cell culture reagents

Cell culture reagent	Supplier
Collagen Type I, rat tail	Corning
DMEM Powder	Gibco
Doxycycline	Invitrogen
FBS	Gibco
FuGENE HD (E2311)	Promega
G418	Sigma
Oligofectamine 2000 (12252011)	Invitrogen
OptiMEM	Gibco
Penicillin-Streptomycin (100U/ml)	Gibco
Puromycin	Invitrogen
RPMI	Gibco
Trypsin	Gibco

Table 2.1.6. Cell culture materials

Plastic	Supplier
6 cm dish	TPP
10 cm dish	TPP
T75 flask	TPP
6 well plate	TPP
8 well chamber slide	LabTek
Cryogenic tubes	TPP

Table 2.1.7. Drugs

Drug (Catalogue number)	Supplier	Final concentration
BRD9876 (HY-110208)	Generon	10 μ M
Filanesib (HY-15187)	Generon	100 nM
Nocodazole (M1404)	Sigma	500 nM
STLC (2799-07-7)	Sigma	5 μ M

Table 2.1.8. siRNAs

siRNA (Catalogue number)	Supplier	Final concentration
GAPDH (AM4631)	Ambion	50 nM
NEK7_a (J-003795-12-0050)	Dharmacon	50 nM
NEK7_b (J-003795-14-0050)	Dharmacon	50 nM

Table 2.1.9. Primary antibodies

Antibody (Catalogue number)	Supplier	Species	WB dilution	IF dilution
α -tubulin (PA5-19489)	Invitrogen	Rabbit	1:5000	1:1000
α -tubulin (T5168)	Sigma	Mouse		1:1000
Acetylated tubulin (T6793)	Sigma	Mouse		1:1000
ALK (D5F3)	Cell Signalling	Rabbit	1:1000	1:500
ALK (4C588)	Invitrogen	Mouse		1:500
Eg5 (23333-1-AP)	Proteintech	Rabbit	1:1000	1:200
FLAG (F7425)	Sigma	Rabbit	1:1000	1:500

γ -tubulin (T6557)	Sigma	Mouse		1:1000
γ -tubulin (T3559)	Sigma	Rabbit		1:1000
GAPDH (14C10)	Cell Signalling	Rabbit	1:500	
NEK7 (SAB2501398)	Sigma	Goat	1:500	1:500

Table 2.1.10. Secondary antibodies

Antibody (Catalogue number)	Supplier	Species	WB dilution	IF dilution
Anti-mouse HRP (A90-116P)	Bethyl Laboratories		1:2000	
Anti-rabbit HRP (A120-101P)	Bethyl Laboratories		1:2000	
Anti-goat HRP (SAB3700295)	Sigma		1:1000	
Alexa Fluor 488 (A11008)	Invitrogen	Rabbit		1:200
Alexa Fluor 488 (A11001)	Invitrogen	Mouse		1:200
Alexa Fluor 594 (A11012)	Invitrogen	Rabbit		1:200
Alexa Fluor 594 (A11005)	Invitrogen	Mouse		1:200
Alexa Fluor 647 (A31571)	Invitrogen	Mouse		1:200

2.2. Methods

2.2.1. Cell culture

2.2.1.1. Cell maintenance

Cells were grown in plastic flasks or on plates and kept in a 37°C, 5% CO₂ incubator. When ~80% confluent, cells were washed in PBS and incubated with trypsin at 37°C for 10 minutes to detach the cells. Cells were then collected using 2-8 ml of pre-warmed media, depending on the cell line and re-plated into new flasks or the relevant plates containing 2-10 ml pre-warmed media.

2.2.1.2. Cell storage

Cells were stored in liquid nitrogen. To freeze down cells from culture, cells were washed in PBS and trypsin was added to detach cells. Cells were collected into falcon tubes with 2 ml of pre-warmed media then centrifuged at 1200 rpm for 5 minutes. Media was aspirated off and cells were resuspended in 4.5 ml FBS and 500 µl DMSO. Cells were then transferred into cryogenic tubes for storage. Cells were frozen in a -80°C freezer overnight before being transferred into liquid nitrogen.

To get cells out of liquid nitrogen and into culture, cells were quickly defrosted in a 37°C water bath and 1 ml of pre-warmed media added to the tube. Cells were then added dropwise to a dish containing pre-warmed media.

2.2.1.3. Induction of proteins in inducible cell lines

In inducible cell lines, expression of proteins of interest was induced by adding 1 µg/ml doxycycline into the media for 72 hours (unless otherwise stated).

2.2.1.4. FuGENE transfection

Cells were seeded into a 6 well plate in the relevant culture media 24-48 hours before transfection and allowed to reach 50-80% confluency. FuGENE was warmed to room temperature and vortexed before use. Serum and antibiotic free OptiMEM media was added to a tube followed by 2 µg plasmid DNA (at concentration 1 µg/ml) and 3 µl FuGENE in a 2:3 v/v ratio, giving a total volume of 200 µl. The transfection mix was then incubated at room temperature for 20 minutes. Meanwhile, cells were washed with antibiotic-free OptiMEM media twice before 1.8 ml of antibiotic-free OptiMEM was added to each well. Transfection mix was then added dropwise to cells and cells incubated at 37°C for 24 hours. Transfection efficiency was approximately 10% based on immunofluorescence microscopy staining.

2.2.1.5. siRNA depletion

Cells were seeded into a 6 well plate containing OptiMEM supplemented with 10% FBS at a confluency of approximately 30% the day before transfection. On the day of transfection, the cell culture hood and equipment used were thoroughly cleaned with RNase away spray. OptiMEM was warmed to 37°C and oligofectamine was warmed to room temperature. 5 µl of the siRNA oligos were mixed with 180 µl OptiMEM in an Eppendorf tube and 12 µl of OptiMEM and 3 µl of oligofectamine were mixed in a separate tube and incubated at room temperature for 5 minutes. The tubes containing the oligofectamine and siRNA oligos were then mixed and incubated at room temperature for a further 20 minutes. Cells were washed in OptiMEM containing no FBS or antibiotics 3 times before 800 µl of OptiMEM was added and the oligofectamine mixture added to each well dropwise. Cells were then incubated for 4 hours at 37°C before adding 500 µl of OptiMEM media containing 30% FBS into the wells. Cells were then incubated for 72 hours. The significant loss of protein observed by Western blot demonstrates that the protein has been substantially reduced in most cells.

2.2.1.6. Embedding in collagen for 3D cell culture

To embed cells in a collagen matrix, protocols were based on those published by Artym and Matsumoto (2010). Briefly, rat tail type I collagen was neutralised using 10X DMEM (made from powder), then 10X reconstitution buffer was added (2.2 g sodium bicarbonate, 4.8 g HEPES dissolved in 100 ml deionised H₂O) followed by 1X PBS. 2N HCl and 2N NaOH were used to give a final pH of 7.1-7.4. Next, a layer of the neutralised collagen was spread over the bottom of wells in a chamber slide and incubated at 37°C with 5% CO₂ for 25 minutes to allow the collagen to polymerise. After the collagen had polymerised, a cell suspension was added on top of the collagen layer and again incubated for 30 minutes to allow cells to attach to the collagen. Attachment was checked using a standard tissue culture microscope and by gently moving the chamber slides to check cells moved with the collagen matrix. Media was then aspirated off and another layer of collagen added on top of the cells to form a sandwich. The chamber slide was again placed back into the incubator for 30 minutes to allow the top layer of collagen to polymerise. After the top layer of collagen had polymerised, 400 µl of the relevant cell culture media for the cell line was added to the chamber slide. The chamber slide was then incubated for 24 hours to allow cells to spread and begin to migrate through the collagen matrix.

2.2.1.7. Collagen-coated coverslips

Coverslips were coated with collagen where indicated. For this, 300 µl of 1 mg/ml rat tail type I collagen was pipetted directly on top of a coverslip placed in a 6 well plate. The coverslip was incubated at room temperature for 1 hour before being washed three times in PBS. The coverslips were then left to dry for 10 minutes before cells were seeded.

2.2.1.8. Microtubule depolymerisation and regrowth assay

To depolymerise microtubules, cells in a 6 well plate were treated with 500 nM nocodazole on ice for 30 minutes. To then enable microtubule regrowth, cells were quickly washed with pre-warmed media twice to remove residual nocodazole before being incubated with pre-warmed media at 37°C for the indicated time periods.

2.2.2. Preparation of Eg5 constructs

The WT, S1033A and S1033D Eg5 plasmids were kindly provided by Dr. Joan Roig, Barcelona. The plasmids were delivered on filter paper. To remove the plasmids from filter paper, filter paper was cut with sterile scissors around the area of each construct. The small pieces of filter paper were placed into Eppendorf tubes containing 100 µl TE buffer, mixed gently and incubated at room temperature for 10 minutes. The tubes were then centrifuged for a few seconds and the supernatant used for bacterial transformation. The plasmids were transformed into XL-10 Gold bacteria and grown on LB-ampicillin agar plates overnight. The following day, a colony was selected and placed into a tube containing 5 ml LB media and 5 µl ampicillin. The culture was then amplified in 50 ml and a midi prep was performed according to manufacturer's instructions to isolate the plasmid. Plasmids were then analysed on 1% agarose gels at 80 V for 45 minutes to confirm plasmid size. Plasmids were then sent to Source BioScience Cambridge to be sequenced.

2.2.3. Cell lysis, SDS-PAGE and Western blotting

Cells were washed with ice cold PBS before being scraped into RIPA buffer (50 mM Tris-HCl pH 8, 150 mM NaCl, 1% SDS, 0.5% sodium deoxycholate, 0.5% Nonidet P-40, 0.5% Triton-X-100, supplemented with 1:100 RNase A, 1:1000 DNase, 1:100 DTT and 1:1000 Protease Inhibitor Cocktail). Lysates were then incubated on ice for 30 minutes before being passed through a 27G needle attached to a 1 ml syringe and then centrifuged at 13300 rpm for 20 minutes. The protein concentration of clarified lysates was determined using the Bradford assay, where absorbance at 650 nm was measured and compared to a set of BSA standards. Samples were then mixed with an appropriate volume of sample buffer (62.5 mM Tris-HCl pH 6.8, 10% v/v glycerol, 2% w/v SDS, 5% v/v β-mercaptoethanol, 0.01% w/v bromophenol blue) to normalise protein concentration before being heated to 100°C for 10 minutes to denature samples.

Lysates were loaded onto 10% SDS-PAGE gels (10% resolving gel: 4 ml protogel, 5 ml H₂O, 3 ml lower Tris pH 8.8, 150 µl of 10% APS and 10 µl TEMED; stacking gel: 650 µl protogel, 3 ml

H₂O, 1.25 ml upper Tris pH 6.8, 75 µl of 10 % APS and 5 µl TEMED) and separated at 180 V for 1 hour. The gels were transferred onto nitrocellulose membranes using a semi-dry transfer unit (Amersham) at 70 mA per gel for 1 hour in the presence of Blotting buffer (6.06 g Tris base, 28.8 g glycine, made up to 2 L with deionised water and supplemented with 10% methanol when needed). Nitrocellulose membranes were blocked in 5% w/v milk with PBST (1X PBS, 0.1% v/v Tween-20) for 1 hour at room temperature and then incubated with the relevant primary antibody in milk overnight at 4°C. Membranes were then washed three times in PBST, 10 minutes per wash and then incubated with the relevant secondary antibody in milk for 1 hour at room temperature. Membranes were again washed in PBST three times, 10 minutes per wash. ECL solution was added according to manufacturer's instructions. Blots were then exposed to X-ray film and developed using a hyperprocessor in a dark room.

2.2.4. Fixed and live cell microscopy

2.2.4.1. Immunofluorescence staining

Cells were plated on acid-etched glass coverslips before treatment and/or induction. Cells were fixed in ice cold methanol for a minimum of 20 minutes at -20°C. Cells were then washed 3 times in PBS before being blocked and permeabilised in 3% BSA containing 0.2% Triton X-100 for 1 hour at room temperature. Coverslips were then inverted onto parafilm containing droplets of the relevant primary antibodies diluted into 3% BSA containing 0.2% Triton X-100 for 2 hours. Coverslips were placed back into the 6 well plate and washed 3 times in PBS for 5 minutes per wash. Coverslips were then inverted onto parafilm containing droplets of the relevant secondary antibodies diluted in 3% BSA containing 0.2% Triton X-100 for 1 hour. Coverslips were washed 3 times in PBS for 5 minutes per wash before being mounted onto glass slides using mounting media (16 ml glycerol, 0.6 g N-propyl gallate, 4 ml H₂O).

2.2.4.2. Confocal microscopy

For lower resolution imaging, a VisiTech Infinity 3 confocal microscope was used fitted with a Hamamatsu C11440 -22CU Flash 4.0 V2 sCMOS camera and 60x Plan Apo (NA = 1.4) and 20x Plan Apo (NA = 0.75) objectives.

2.2.4.3. Super-resolution imaging

A Zeiss Airyscan 2 microscope was used for super-resolution imaging fitted with a Plan-Apochromat 63X objective (NA = 1.4). Airyscan calculation was used to improve resolution of images.

2.2.4.4. Live cell imaging

For live cell imaging, cells were embedded into collagen as described in section 2.2.1.6 in 8 well chamber slides. Cells were imaged using a PhaseFocus Livecyte 2 imaging system fitted with a 37°C, 5% CO₂ incubator. A PLN 10X objective (NA=0.25) was used to capture images every 15 minutes for 24 hours from three non-overlapping regions per well.

2.2.5. Quantitative analyses

2.2.5.1. Imaris co-localisation analysis

Co-localisation analysis was performed using Imaris software where two channel images were captured and a mask, drawn in Fiji, was applied over an area of interest. Areas of interest were selected where the microtubules were clearest in each image and excluding the nucleus to get a more accurate measurement of the co-localisation of Eg5 with microtubules. The area inside the mask was then thresholded using the Costes method, which allowed for automatic threshold detection (Costes *et al.*, 2004). Next, a co-localisation channel was built in Imaris which identified co-localised pixels within the area of interest. From the co-localisation channel, channel statistics were calculated which included a measurement of the percentage of channel B (Eg5) co-localised with channel A

(microtubules). The measurements were recorded in GraphPad Prism and presented in graphical format.

2.2.5.2. Fiji co-localisation analysis

In experiments where co-localisation analysis was required of specific areas, e.g. centrosomes, the PlotMultiColor4.3. Fiji macro developed by Dr. Kees Straatman was used. Briefly, a line was drawn through the relevant area of a two-channel image. The macro plots the intensity profiles of each channel along the length of the line drawn. Intensity values were copied from Fiji and put into Excel where the Pearson's Correlation Coefficient was calculated. The closer the calculated Pearson's value is to 1, the more co-localised the two channels are. A value close to 0 indicates a more random distribution of proteins in the two-channel image, whereas negative Pearson's values indicate anti-correlation so where one protein is localised the other is not.

2.2.5.3. Fluorescence intensity analysis

For fluorescence intensity analysis, images were captured on the VisiTech Infinity 3 confocal microscope with 40 section Z-stacks per image. In Fiji, images were processed using the sum slice function (Image → Z-stacks → Sum slices) which adds the intensity values throughout the Z-stack together. Next, the perimeter of the cell was drawn using the freehand tool so that the intensity values taken were from within the cell. Measurements were taken using Analyse → Measure and the measurements taken were cell area, mean intensity and integrated density. A background measurement was also taken from every image from a small square drawn in an area surrounding the cell with no apparent fluorescence signal. To calculate a corrected intensity value, the following formula was used:

$$\begin{aligned} & \textit{corrected intensity} \\ & = \textit{integrated density} - (\textit{cell area} * \textit{mean intensity of background}) \end{aligned}$$

where the integrated density is the total fluorescence intensity from the entire cell (The Open Lab Book, n.d). Corrected measurements for the control treatment were averaged and the average made to equal 1. Individual measurements for the control and treated cells

were then made relative to this average. These values were plotted on a graph and statistical analysis performed.

2.2.5.4. Cell length analysis

Cell lengths were measured in Fiji where a line was drawn over the longest length of the cell, through the nucleus. The length of the line was then recorded in GraphPad Prism and presented in graphical format. Nucleation sites were measured in the same way where the diameter of the nucleation site was measured from the centre of the microtubule aster along the longest emanating microtubule.

2.2.5.5. Single cell migration analysis

Imaris software was used to track individual cells and measurements were taken for mean speed, average distance travelled between time points and straightness. Briefly, Imaris takes a time series of images and a spot is placed on each cell. The spot moves with the cell throughout the time series and the path taken by the cell is tracked. Data collated from Imaris was pasted into Microsoft Excel and sorted according to track duration. Any tracks shorter than 20 images (either because the cell had moved beyond the field of view or because a cell had entered mitosis) were not included in the final representation of data. Average distance between time points (total distance/number of time points), mean speed and straightness measurements were copied into GraphPad Prism to be presented in graphical format and statistical analysis performed.

2.2.5.6. Western blot quantification

Western blots were quantified in Fiji. A box was drawn around each band of the Western blot and an intensity profile obtained for each band. The area underneath the curves produced from the intensity profiles were recorded. Bands of interest were determined relative to the bands for the α -tubulin loading control for the relevant sample to allow

correction for loading errors. The values for the protein of interest in the control sample were made equal to 1 and the test samples made relative to the control.

2.2.5.7. Statistical analysis

All graphs were produced in GraphPad Prism Version 8.0/9.0 and are representative of three independent experiments unless otherwise stated. Statistical analysis was also performed using this software. Statistical tests performed were one-tailed unpaired Student's *t*-test assuming unequal standard deviations when comparing two unrelated groups and one way ANOVA with post-hoc testing when comparing three or more groups. Statistical significance is defined by: $P < 0.05$ *; $P < 0.01$ **; $P < 0.001$ ***; $P < 0.0001$ ****; ns – not significant.

CHAPTER 3

EML4-ALK V3 promotes recruitment of Eg5 to interphase microtubules downstream of NEK7

3.1. INTRODUCTION

EML4-ALK fusions are found in around 5% of NSCLC and arise due to a chromosome inversion event on chromosome 2 (Soda *et al.*, 2007). Multiple variants of the EML4-ALK fusion exist due to different breakpoints in the *EML4* gene. All variants contain the same intracellular portion of ALK that includes its tyrosine kinase domain, but differ in the amount of EML4 they contain. All of the variants contain the N-terminal trimerization domain of EML4 and either none or some of the highly structured TAPE domain (Sabir *et al.*, 2017). The disruption of the TAPE domain in longer EML4-ALK variants such as V1 and V2, renders these fusion proteins unstable. V3 and V5 on the other hand contain none of the EML4 TAPE domain and as a consequence these fusions are more stable (Richards *et al.*, 2014; Heuckmann *et al.*, 2012).

Recently, it has been uncovered that NSCLC patients with EML4-ALK V3 are much more likely to have metastatic disease, less likely to respond to current therapies and are less likely to survive than patients with other EML4-ALK variants (Christopoulos *et al.*, 2018; Woo *et al.*, 2017). Strikingly, EML4-ALK V3 has been found to bind interphase microtubules *in vitro*, whereas other EML4-ALK variants were distributed throughout the cytoplasm (O'Regan *et al.*, 2020). Furthermore, the cell cycle kinases, NEK9 and NEK7 were recruited to microtubules, downstream of EML4-ALK V3, while microtubule stabilisation was also observed. Cells expressing EML4-ALK V3 appear more mesenchymal in morphology, becoming less cobblestone-like and more elongated. They also exhibit an increased rate of migration as measured in wound healing, single cell tracking and chemotactic-dependent directional migration assays (O'Regan *et al.*, 2020). These findings begin to offer a potential explanation as to why patients fare so badly with EML4-ALK V3. However, how these phenotypes are caused by the EML4-ALK V3:NEK9:NEK7 signalling cascade is unknown.

Given the localisation of EML4-ALK V3 to interphase microtubules and the changes in microtubule dynamics exhibited by EML4-ALK V3 expressing cells, we hypothesised that a microtubule regulator could be a downstream target of the signalling pathway. One such microtubule-associated protein that potentially fits this hypothesis is the mitotic kinesin,

Eg5. Eg5 crosslinks anti-parallel microtubules and allows them to slide past one another, a function which is indispensable for bipolar spindle assembly in mitosis (McIntosh, Molodtsov and Ataulakhanov, 2012). However, Eg5 usually only associates with microtubules during mitosis and not in interphase (Sawin and Mitchison, 1995). Phosphorylation of T926 by the mitotic kinase, CDK1, has been shown to recruit Eg5 to the mitotic spindle at the onset of prophase where it remains until the end of telophase (Cahu *et al.*, 2008; Sawin and Mitchison, 1995).

Interestingly, Eg5 localisation is also regulated by NEK7. NEK7 phosphorylation of Eg5 at S1033 also facilitates its recruitment to centrosomes, leading to centrosome separation (Bertran *et al.*, 2011; Rapley *et al.*, 2008). Intriguingly, NEK7 can also phosphorylate Eg5 during interphase in specialised cell types, notably to promote dendrite extension in neurons (Freixo *et al.*, 2018). Fascinatingly, Eg5 is overexpressed in a variety of cancers and has been shown to contribute to tumour formation in mice (Garcia-Saez and Skoufias 2021; Castillo *et al.*, 2007).

In this chapter, I describe experiments that begin to investigate whether Eg5 could be recruited to interphase microtubules downstream of the EML4-ALK:NEK9:NEK7 signalling pathway. Specifically, using a commercial Eg5 antibody, the expression and localisation of Eg5 is explored and compared between different EML4-ALK expressing cell lines. In addition, the relationship between NEK7 and Eg5 is explored in the context of EML4-ALK V3.

3.2. RESULTS

3.2.1. Characterisation of EML4-ALK variant expression in cell lines used in this study

Before starting to analyse Eg5 expression and localisation, it was important to confirm expression of the appropriate EML4-ALK proteins in the cell lines used in this study. For this purpose, lysates were prepared from BEAS-2B parental cells, BEAS-2B cells that express EML4-ALK V1 or V3 upon induction with doxycycline, and NSCLC patient cell lines, H3122 and H2228, which endogenously express EML4-ALK V1 and V3, respectively. BEAS-2B cell lines were induced for 72 hours before being lysed and analysed by Western blot using an antibody raised against the C-terminal tyrosine kinase domain of ALK. Uninduced samples were also analysed. Western blots confirmed expression at the expected molecular weight of both EML4-ALK variants in the induced samples with EML4-ALK V3 at ~90 kDa and EML4-ALK V1 at ~130 kDa (Figure 3.1A). These proteins were induced to approximately the same levels. Interestingly, higher molecular weight versions of both EML4-ALK variants were detected, which has previously been shown to be the result of ALK-mediated autophosphorylation. Bands were also detected below the expected molecular weights of both EML4-ALK variants which are suspected to be degradation products. Western blotting revealed expression was slightly leaky as weak bands were also detected in uninduced samples. No bands for ALK were detected in the parental BEAS-2B cell line, with or without doxycycline, consistent with ALK not being expressed in these bronchial epithelial cells. An antibody against α -tubulin was used as a loading control and showed equal expression in all samples.

Lysates were also prepared from untreated NSCLC patient cell lines, H3122 (V1) and H2228 (V3) and Western blot analysis undertaken with the same antibodies as indicated above. The blots confirmed expression of EML4-ALK V1 at 130 kDa and EML4-ALK V3 at 90 kDa (Figure 3.1B). Again, these proteins showed a similar level of expression.

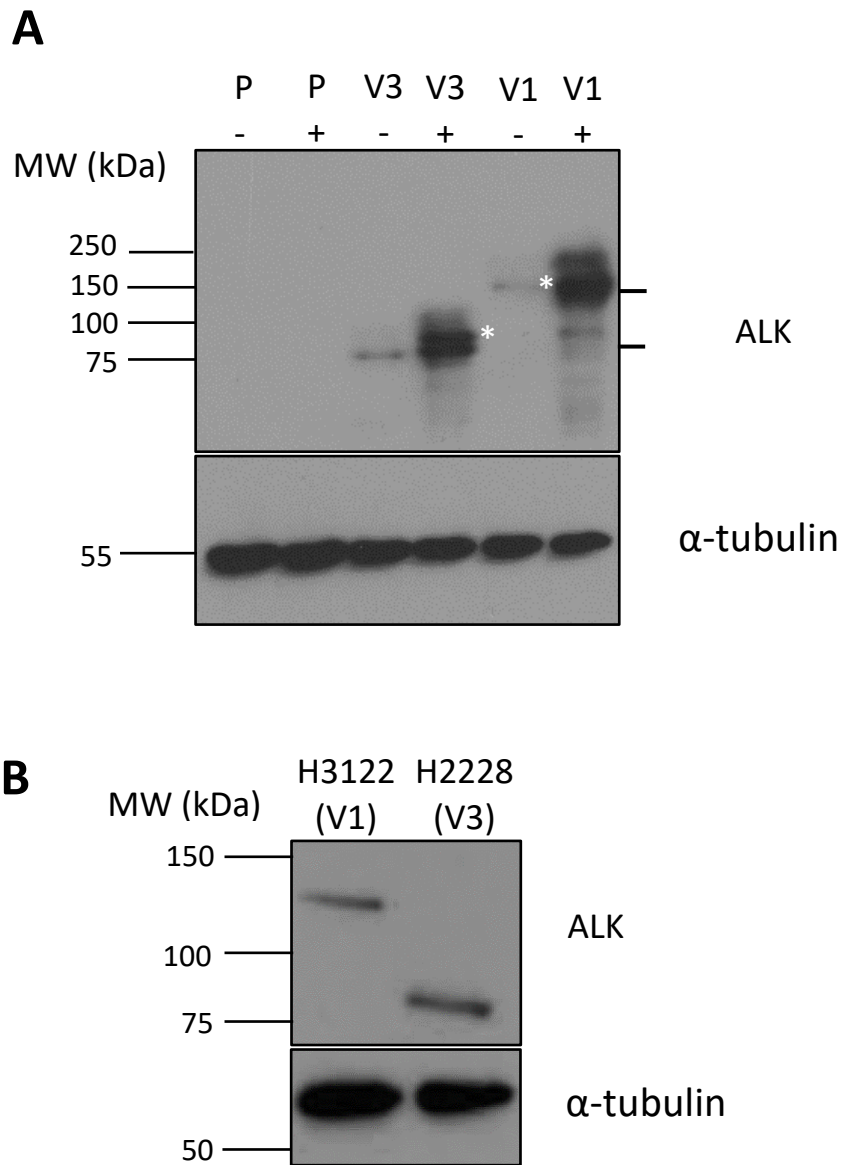


Figure 3.1. Expression of EML4-ALK variants in cell lines used in this study. (A) Lysates from BEAS-2B cells were analysed by Western blot with ALK and α -tubulin antibodies as indicated. P = parental; V3 = variant 3; V1 = variant 1; + = induced with doxycycline; - = uninduced. * = phosphorylated ALK. (B) Lysates from NSCLC patient cell lines, H3122 and H2228 were analysed as described in A. Blots are representative of at least three independent experiments. Molecular weights are indicated on the left of blots.

3.2.2. Analysis of Eg5 expression in EML4-ALK cell lines

In order to study the expression and localisation of Eg5, a commercially available antibody was purchased from Proteintech, which was raised against amino acids 707-1052, located in the tail domain of Eg5. To determine the level of Eg5 expression in cells expressing different EML4-ALK variants, Western blots of whole cell lysates were probed with the Eg5 antibody. Here, only induced samples were used from the three BEAS-2B cell lines. A band was detected at 120 kDa, the predicted molecular weight of Eg5, in each cell lysate (Figure 3.2A). The intensity of the Eg5 bands on these Western blots was measured in Fiji and normalised relative to the α -tubulin expression. This revealed that there was no significant alteration in Eg5 expression upon expression of either EML4-ALK V1 or V3 (Figure 3.2B).

Eg5 expression was then analysed by Western blot in lysates prepared from the H3122 and H2228 cell lines. Interestingly, while Eg5 was clearly detected at the expected size of 120 kDa in H3122 (V1) cells, it was barely visible in H2228 (V3) cells (Figure 3.2C). Bands were quantified as described above confirming a significantly reduced level of Eg5 expression in the H2228 (V3) cell line compared to the H3122 cell line (Figure 3.2D). However, analysis of the COSMIC database indicated that the H2228 cell line had a missense mutation in the *KIF11* gene, which encodes Eg5, resulting in an amino acid substitution, A282V (Cancer.sanger.ac.uk, nd). This amino acid is positioned in the Eg5 motor domain (Figure 3.2E). This may cause either the mRNA or protein for Eg5 to be less stable than the wild-type, explaining the reduction in Eg5 expression seen in this cell line.

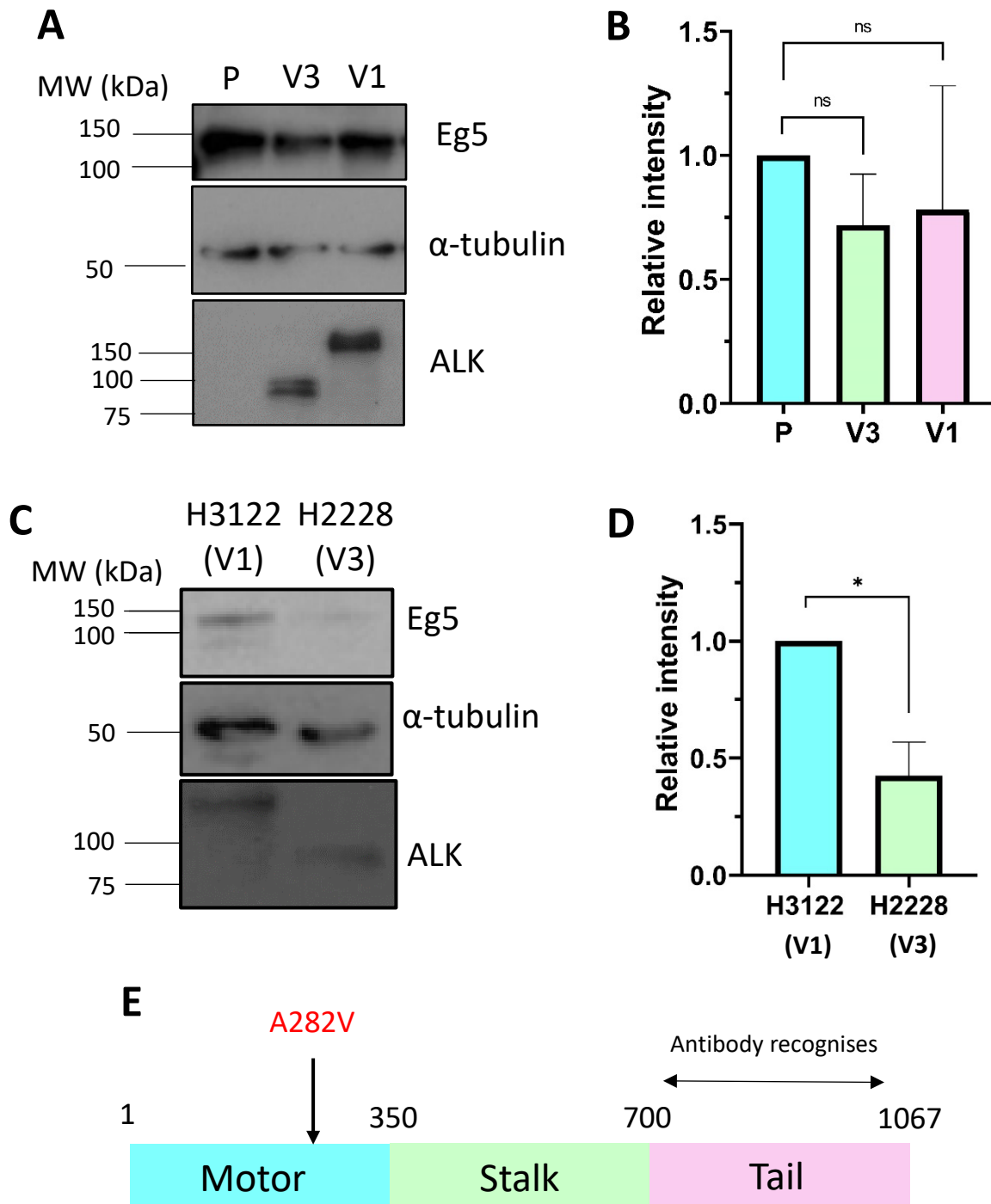


Figure 3.2. Eg5 expression in EML4-ALK cell lines. (A) Lysates from BEAS-2B cell lines were analysed by Western blot using antibodies against Eg5, α -tubulin and ALK as indicated. P = parental. (B) Eg5 expression was quantified from blot represented in A. (C) Lysates from NSCLC patient cell lines were analysed as in A. (D) Eg5 expression was quantified for blot represented in C. (E) Schematic diagram of Eg5 protein showing A282V mutation site and antibody recognition site. Graphs are representative of three independent experiments and show means and standard deviation of each group.

3.2.3. Localisation of Eg5 to the mitotic spindle in cells expressing EML4-ALK variants

We next examined Eg5 localisation in the three induced BEAS-2B cell lines and NSCLC patient cell lines by immunofluorescence microscopy. Staining with antibodies against Eg5 and α -tubulin demonstrated the expected localisation of Eg5 to the mitotic spindle in all cell lines, confirming that Eg5 was correctly localised during mitosis in cells expressing the EML4-ALK variants. Super-resolution imaging revealed Eg5 was present on spindle microtubules with a higher intensity at spindle poles, consistent with the role of Eg5 in centrosome separation. Furthermore, no Eg5 staining was detected on astral microtubules (Figure 3.3A&B).

3.2.4. Comparison of methods for measuring co-localisation

A number of different co-localisation based experiments were undertaken in this project. There are many different ways to approach measuring co-localisation from images and indeed two different methods have been used in this study: an Imaris algorithm and the Fiji PlotMultiColor 4.3. macro, both of which can be used to calculate a Pearson's correlation coefficient. The Imaris software takes a two-channel image and builds a separate channel of co-localised pixels. For these studies, a cytoplasmic region of interest (r.o.i.) was selected where distinct microtubules were observed and which used as much of the cell as this allowed, and a mask drawn in Fiji was placed over the r.o.i. in Imaris. The area within the mask was then thresholded and pixels that showed co-localisation between the two channels were highlighted in a separate channel. Channel statistics were then taken for the co-localisation channel, which included a measurement of the percentage of the protein of interest (in this case Eg5) that co-localised with microtubules (Figure 3.4).

On the other hand, the PlotMultiColor Fiji macro was used to measure co-localisation from two channel images in specific areas of the cell, for example phase separated foci or the centrosomes. Here, a 10 μ m line was drawn through the structures of interest, as well as the surrounding cytoplasm. Intensity profiles were obtained from both channels of the image along the 10 μ m line and the values from these profiles were used to calculate the Pearson's

correlation coefficient. The Pearson's value can be interpreted as +1 = complete co-localisation; 0 = random localisation; -1 = anti-co-localisation i.e. where one protein is, the other is not.

The Imaris method was deemed more appropriate for examining punctate staining patterns throughout large areas of the cell. For this type of staining, the PlotMultiColor macro gave a range of Pearson's values, which didn't really reflect what was seen in the images. Specifically, when measuring co-localisation of Eg5 with microtubules using this macro, lines were drawn through microtubules with the Eg5 channel switched off in order to avoid bias. As a result, lines sometimes intersected Eg5 punctae on every microtubule the line crossed but in other cases Eg5 punctae were only present on some microtubules the line crossed, which is why a range of Pearson's values were produced that were less representative of what was seen in the images (Figure 3.5).

The Imaris method did however have its own limitations. Firstly, the software was unable to automatically detect a threshold on very thin protrusions, so only wider areas of the cell could be used for this analysis. Secondly, this analysis is very dependent on the density of microtubules within the cell. For example, a cell with more microtubules packed together will show a higher percentage of co-localisation compared to a cell with microtubules that are more separated. It was for this reason that a mask was drawn over cells to set a region of interest where individual microtubules were more distinct and separate. This did still however allow the majority of the cell to be used in most images making the final percentages more representative of the whole cell as compared to the PlotMultiColor method.

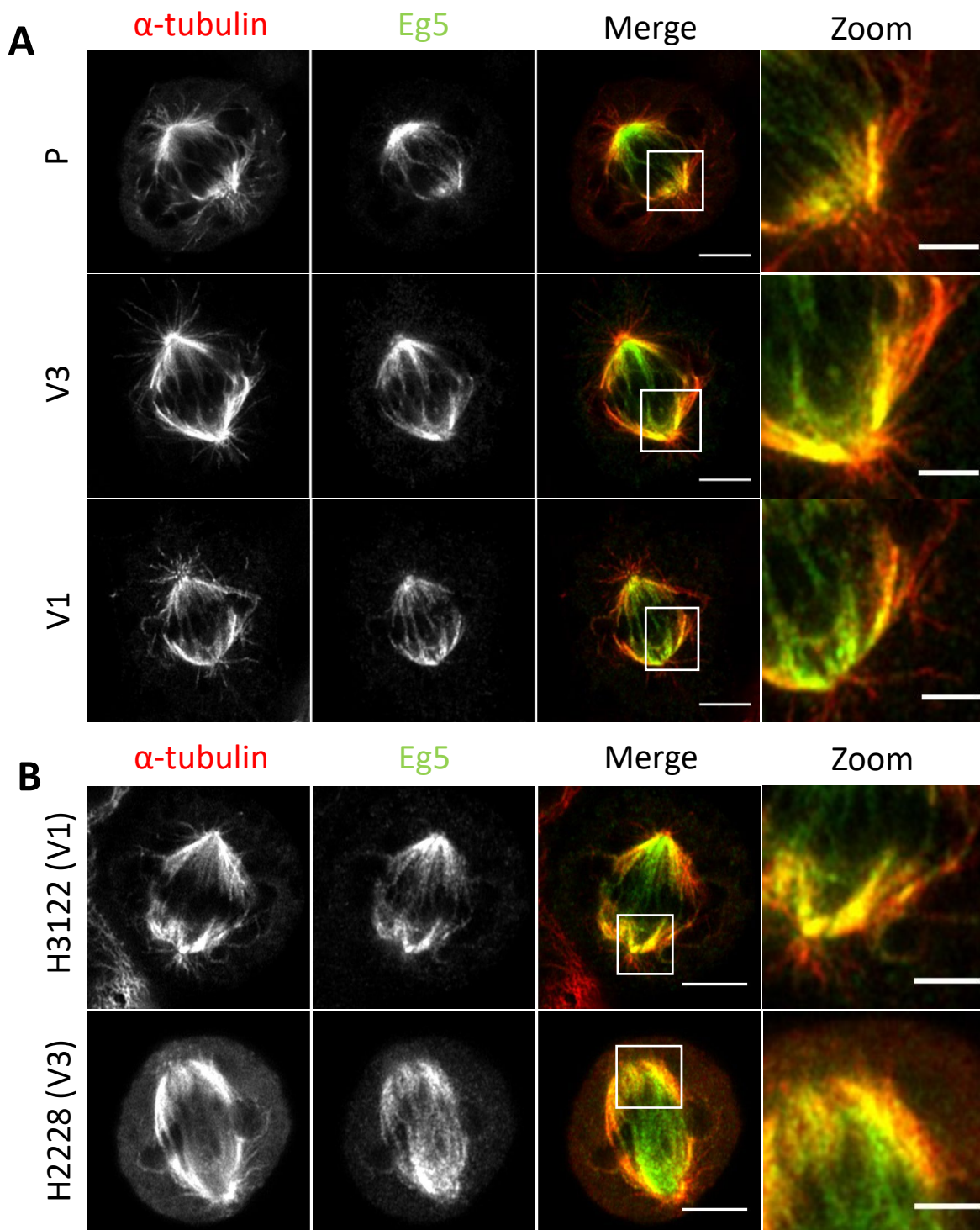


Figure 3.3. Eg5 localises to the mitotic spindle in cells expressing EML4-ALK variants. (A) Induced BEAS-2B cell lines were stained with Eg5 (green) and α -tubulin (red) antibodies and spindles were imaged. P = parental. (B) NSCLC patient cell lines were stained as described in A. White boxes show zoom regions. Scale bars in merge images = 5 μ m and zooms = 2 μ m. Images representative of a minimum of three independent experiments.

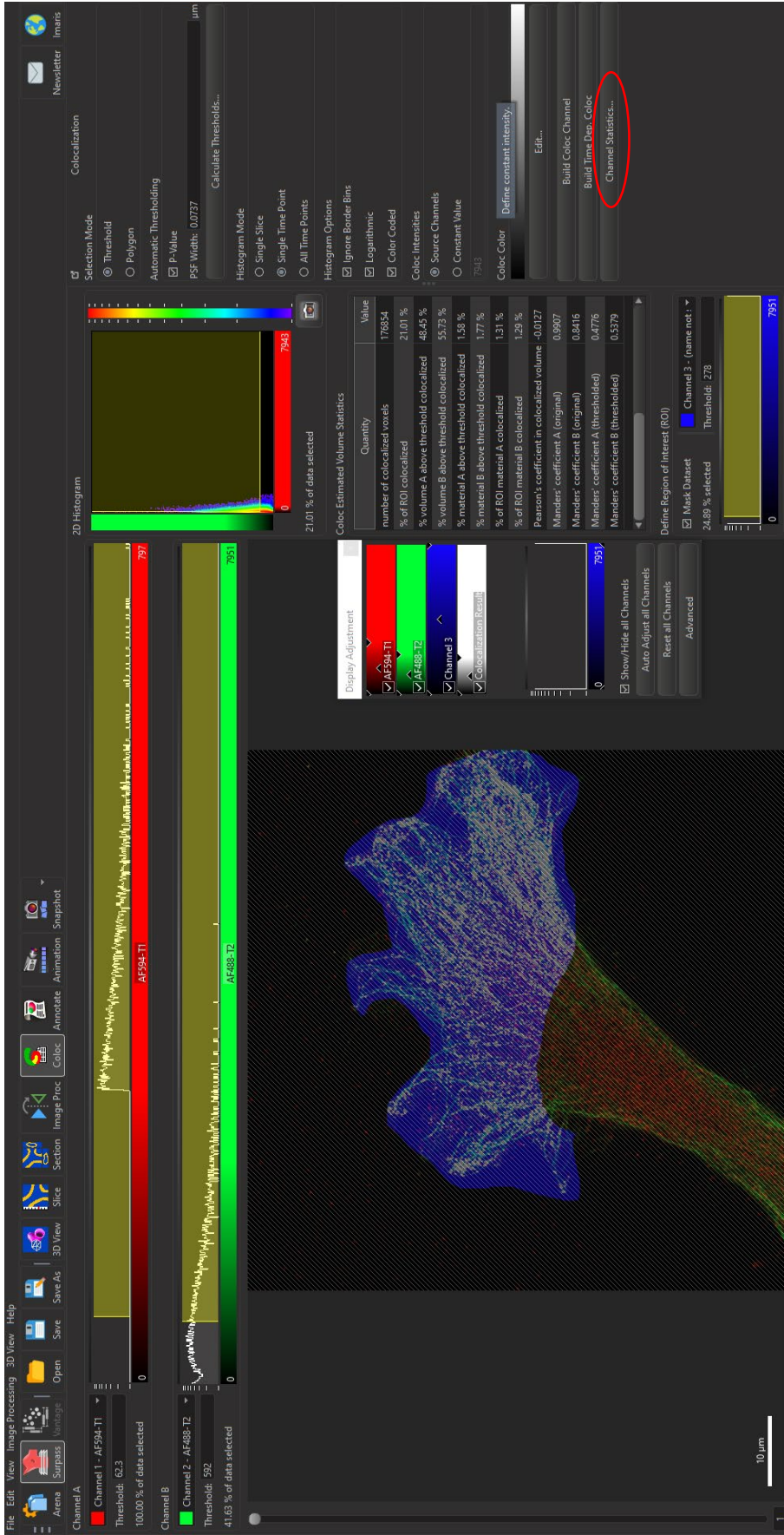


Figure 3.4. – Imaparis software was used for co-localisation analysis. Two channel images (Eg5 (red) and α -tubulin (green)) were masked (blue) and thresholded using the Costes method in Imaparis and a co-localisation channel was built (white). Channel statistics (red circle) such as percentage of channel A co-localised with channel B were taken from the co-localisation channel.

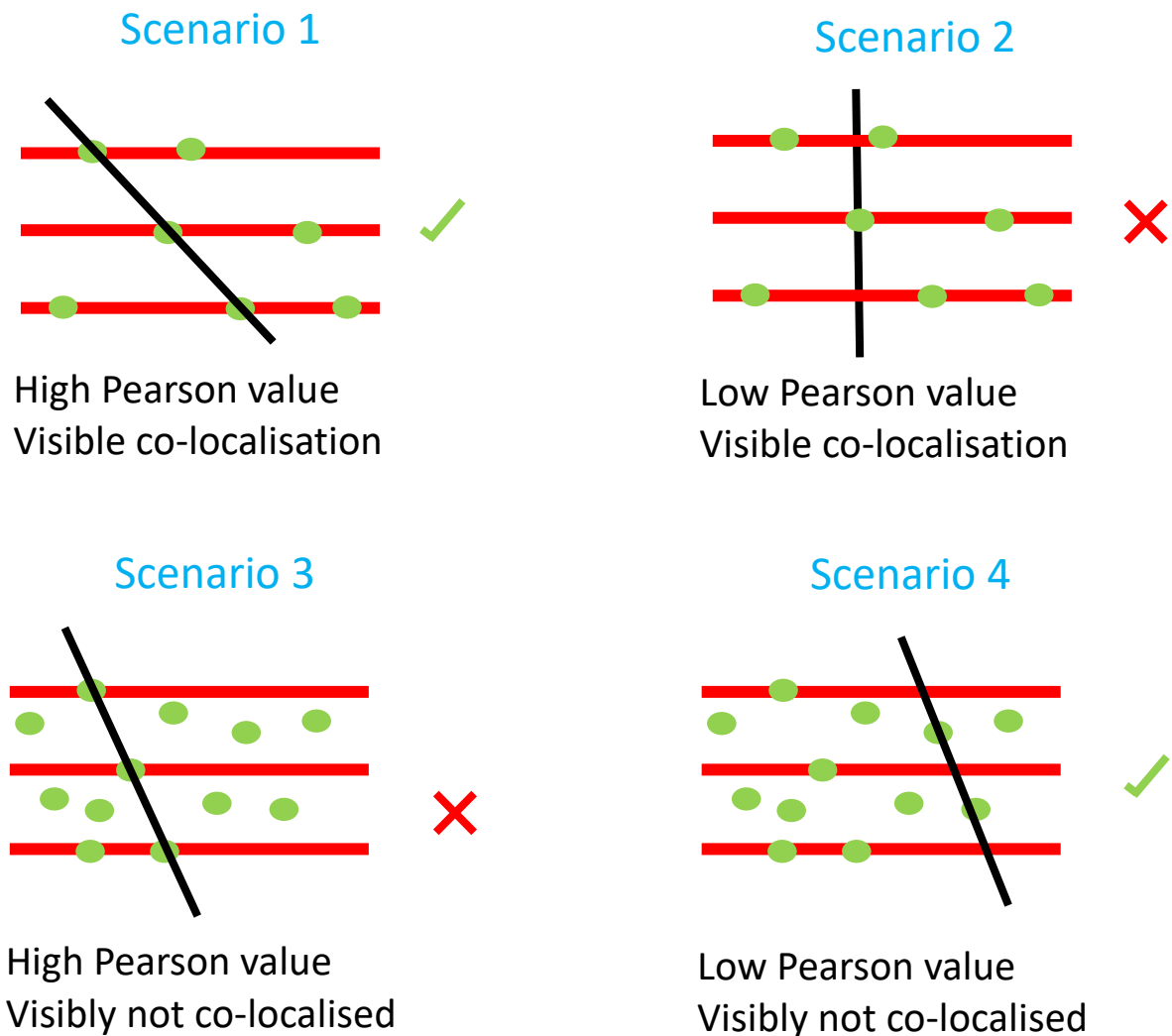


Figure 3.5. Schematic diagram showing why the PlotMultiColor macro is not appropriate for measuring co-localisation of punctate staining patterns. Diagram shows four scenarios with microtubules (red) and a protein of interest (green) where the staining pattern is punctate. Black lines represent the line that is drawn by the macro user in order to obtain intensity profiles. Ticks represent scenarios where the Pearson's values obtained reflect what is seen in the image; crosses represent scenarios where the Pearson's value does not reflect what is seen in the image.

3.2.5. Eg5 is recruited to interphase microtubules in EML4-ALK V3 expressing cells

Having established that Eg5 is found on the spindles of mitotic cells in our cell lines, we were interested to check its localisation in interphase cells. For this, BEAS-2B cell lines were induced for 72 hours before being fixed and stained for immunofluorescence microscopy using Eg5 and α -tubulin antibodies. Super-resolution images of interphase cells were captured and percentage co-localisation of Eg5 with the microtubules was measured using Imaris software (Figure 3.4). Eg5 staining appeared as discrete punctae throughout the cells in all three cell lines (Figure 3.6A). For this reason, the Imaris co-localisation method was selected as more appropriate for measuring co-localisation of Eg5 with the microtubules in these cells. Strikingly, around 20% more Eg5 was seen to co-localise with interphase microtubules in cells expressing EML4-ALK V3, than in the parental or EML4-ALK V1 cell lines (Figure 3.6B).

We also examined whether Eg5 was recruited to interphase microtubules in the H2228 and H3122 cell lines. Cells were stained using Eg5 and α -tubulin antibodies, imaged and quantified as previously described. The H2228 (V3) cells showed a two-fold higher percentage of Eg5 that co-localised with interphase microtubules as compared with the H3122 (V1) cell line, consistent with the data observed in BEAS-2B cells. Again, the Eg5 protein appeared as discrete punctae throughout the cells in both cell lines (Figure 3.7A&B).

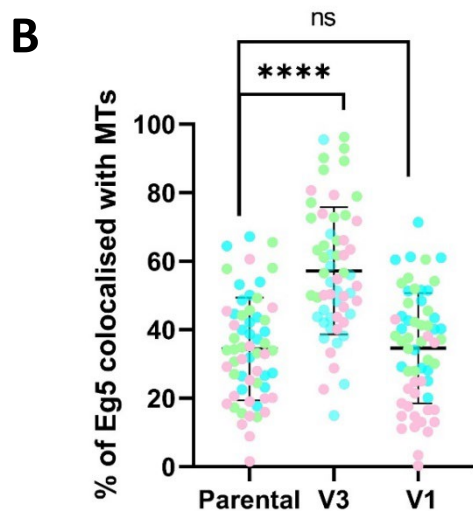
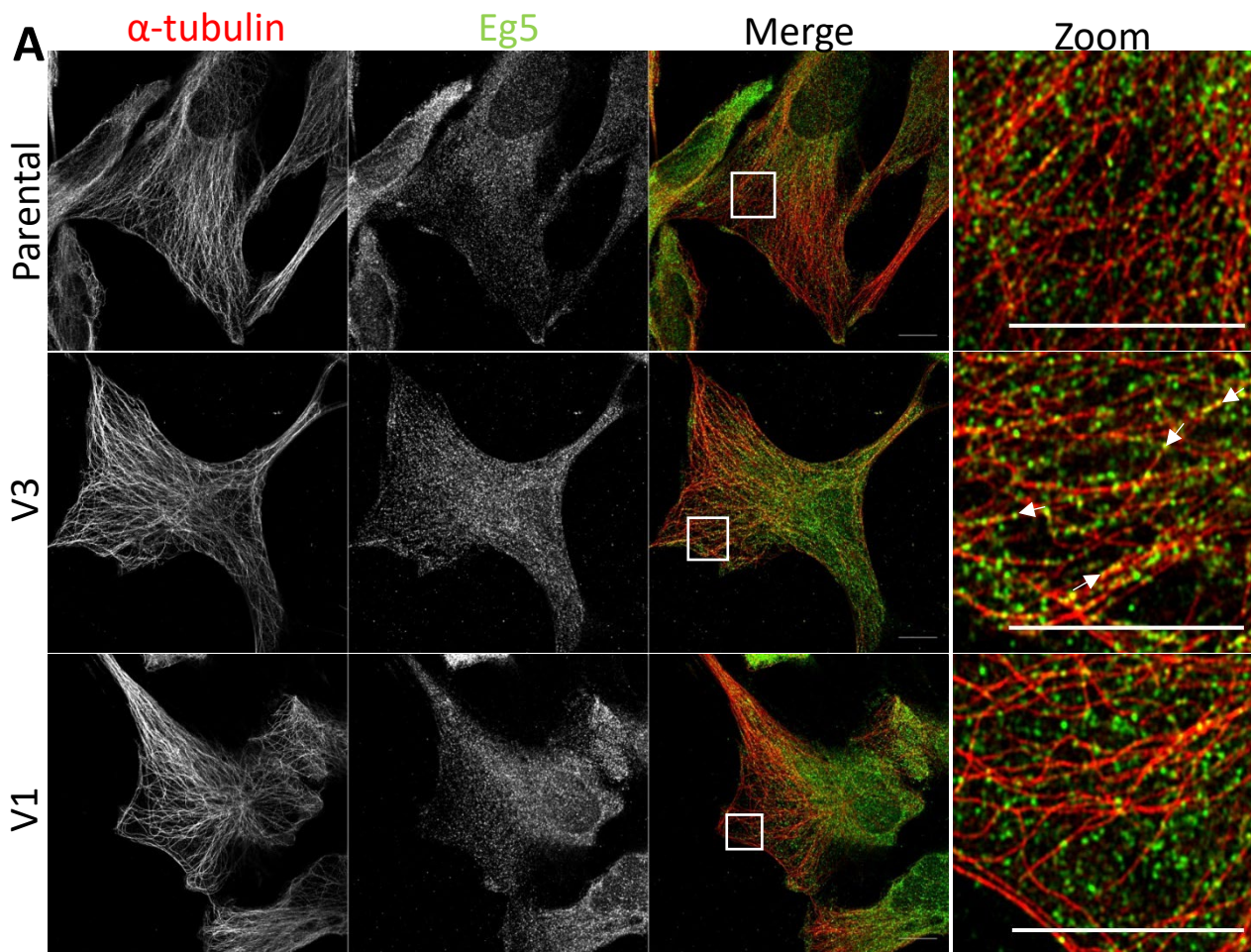


Figure 3.6. Eg5 co-localises with interphase microtubules in BEAS-2B cells expressing EML4-ALK V3.

(A) Induced BEAS-2B cells were stained with Eg5 (green) and α -tubulin (red) antibodies. White arrows indicate visible co-localisation. White boxes show zoom region. Scale bars = 10 μ m. (B) Co-localisation was measured using Imaris software. Measurements were taken from a total of 60 cells from 3 independent experiments. Graph shows individual data points (one colour per repeat), means and standard deviations.

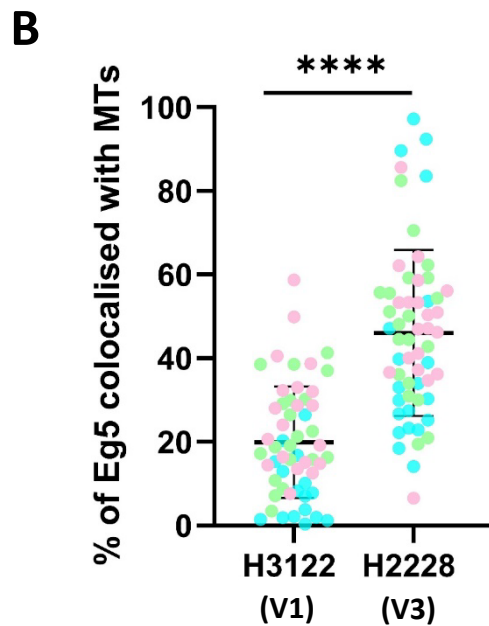
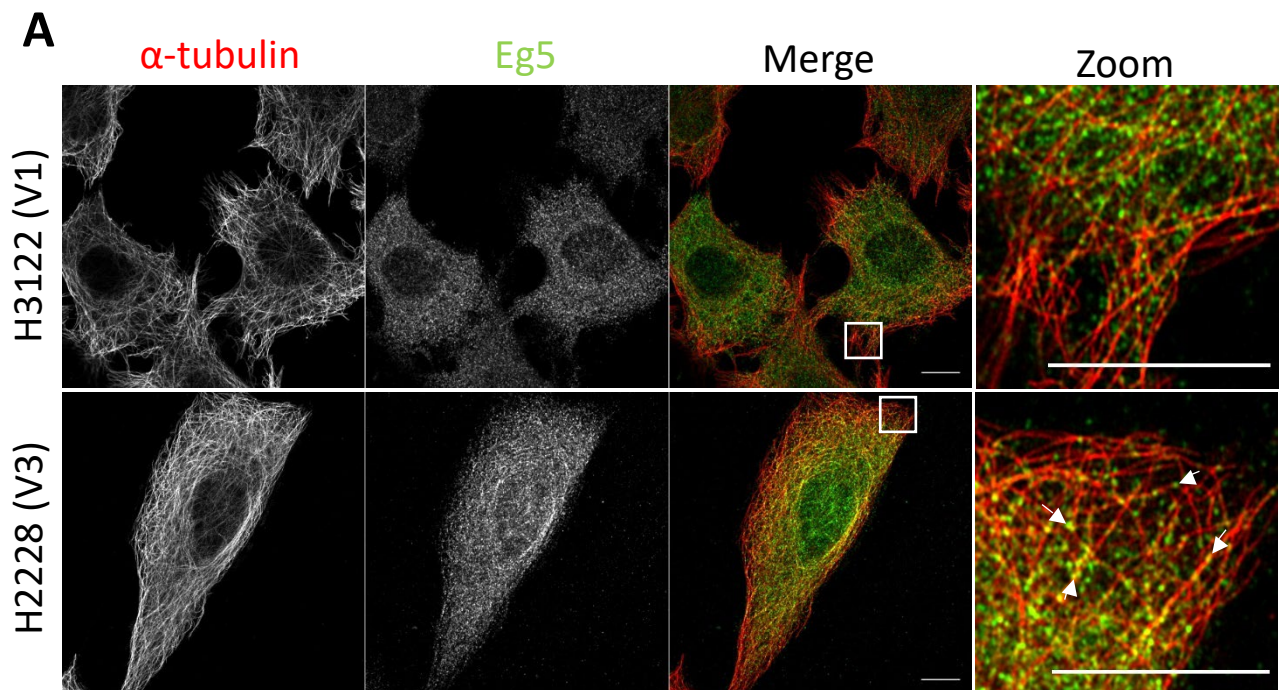
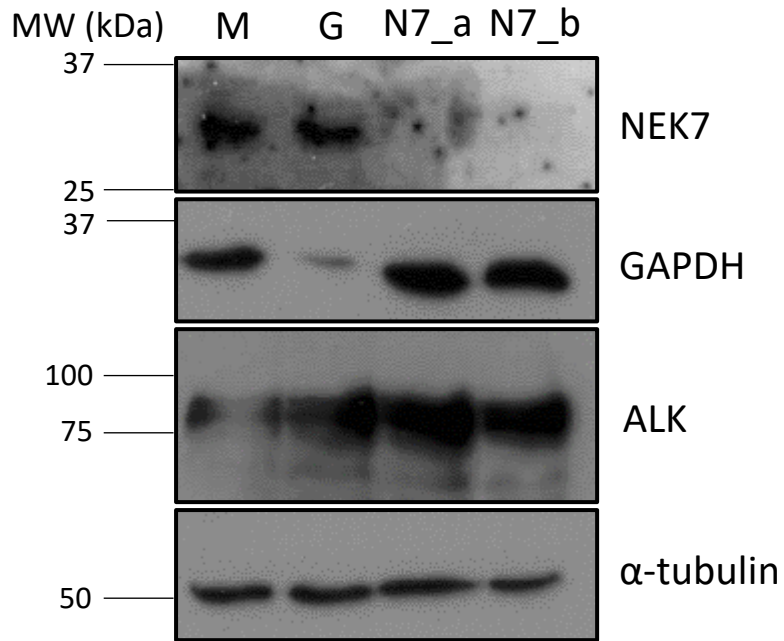
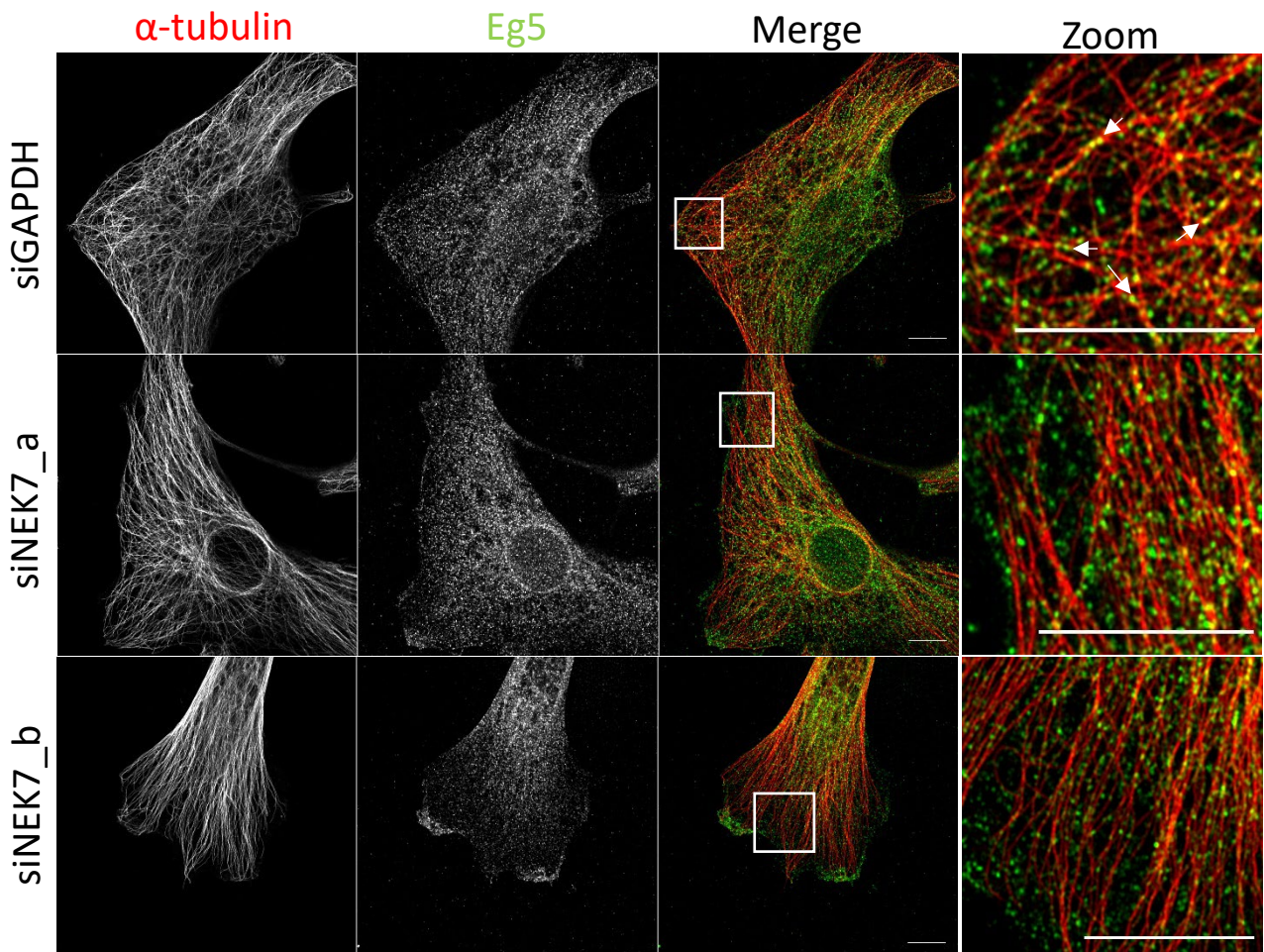


Figure 3.7. Eg5 co-localises with interphase microtubules in H2228 cells. (A) NSCLC patient cells were stained with Eg5 (green) and α -tubulin (red) antibodies. White arrows indicate visible co-localisation. White boxes show zoom region. Scale bars = 10 μ m. (B) Imaris software was used to measure co-localisation. Measurements were taken from 60 cells from three independent experiments (one repeat per colour). Graph shows individual data points, means and standard deviations.

3.2.6. NEK7 depletion reduces Eg5 localisation to interphase microtubules in V3 expressing cells

Previous research from our lab has shown that EML4-ALK V3 binds interphase microtubules and recruits the mitotic kinases, NEK9 and NEK7. Furthermore, the morphology and migration phenotypes exhibited by EML4-ALK V3 expressing cells were shown to be dependent on these kinases (O'Regan *et al.*, 2020). Given that Eg5 is a known substrate of NEK7 (Bertran *et al.*, 2011; Rapley *et al.*, 2008) and has been shown to act downstream of NEK7 in the extension of dendrites in non-dividing neuronal cells (Freixo *et al.*, 2018), we were curious to investigate if NEK7 was responsible for recruiting Eg5 to interphase microtubules in the EML4-ALK V3 cell lines. To test this hypothesis, two siRNAs against NEK7, previously optimised in our lab, were used to deplete NEK7 from BEAS-2B:EML4-ALK V3 cells; a GAPDH siRNA was used as a control. Cells were induced for 24 hours before being transfected with siRNAs for 72 hours. Western blotting using an antibody against endogenous NEK7 confirmed successful depletion of the NEK7 protein by both siRNA oligos. Successful depletion of GAPDH in the control sample was shown using a GAPDH antibody (Figure 3.8A). A mock sample with no depletion was also included to show normal expression of both the NEK7 and GAPDH proteins, while EML4-ALK V3 expression was confirmed using an ALK antibody (Figure 3.8A).

Depleted cells were then stained for immunofluorescence microscopy analysis using antibodies against Eg5 and α -tubulin, and images analysed using the Imaris method to determine co-localisation (Figure 3.8B). The results revealed loss of recruitment of Eg5 to interphase microtubules in cells depleted of NEK7 with both NEK7 siRNAs showing significant reduction compared to the siGAPDH control sample (Figure 3.8B & C). Interestingly, the siGAPDH control sample showed a somewhat lower percentage of Eg5 localising with the microtubules than previously seen in the non-depleted BEAS-2B:EML4-ALK V3 cell line (Figure 3.6B), suggesting that the process of transfection itself may have a modest effect on microtubule localisation.

A**B**

C

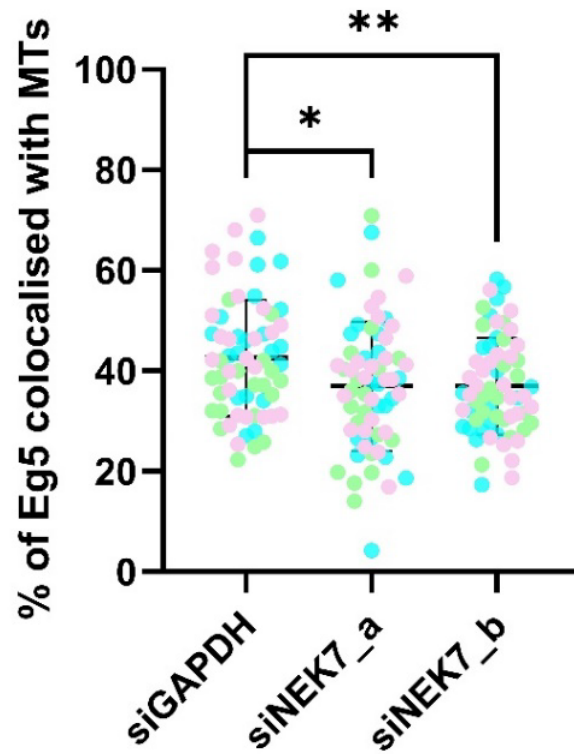


Figure 3.8. NEK7 depletion reduces Eg5 recruitment to interphase microtubules in BEAS-2B:EML4-ALK V3 cells. (A) Cells were depleted of NEK7 or GAPDH as indicated. Lysates from these cells were analysed by Western blot using antibodies against NEK7, GAPDH, ALK and α -tubulin as indicated. Molecular weights are shown on the left of the blots. M = mock; G = siGAPDH; N7_a = siNEK7_a; N7_b = siNEK7_b. (B) Depleted cells were stained with Eg5 (green) and α -tubulin (red) antibodies. White arrows indicate visible co-localisation. White boxes show zoom region. Scale bars = 10 μ m. (C) Co-localisation was measured in Imaris. Measurements were taken from a total of 65 cells from three independent experiments. Graphs show individual data points (one colour per repeat), means and standard deviations of each group.

We then sought to determine if a similar reduction in microtubule localisation of Eg5 would be observed in the H2228 cell line upon depletion of NEK7. Cells were depleted with the two NEK7 siRNAs and the GAPDH control siRNA for 72 hours before being lysed for Western blotting or fixed for immunofluorescence staining. Some difficulties were experienced transfecting siNEK7_a into this cell line; however, siNEK7_b was consistently successful in depleting NEK7 (Figure 3.9A). Sufficient depletion was achieved once using siNEK7_a in this cell line, although the Western blots produced for the controls of this repeat were not of high quality and have not been shown. Depleted cells were fixed and stained using antibodies against Eg5 and α -tubulin, imaged and the percentage of co-localisation measured in Imaris. Consistent with data obtained from the BEAS-2B:EML4-ALK V3 cells, a significant reduction in the percentage of Eg5 recruited to microtubules was seen after NEK7 depletion compared to the siGAPDH control sample (Figure 3.9B & C).

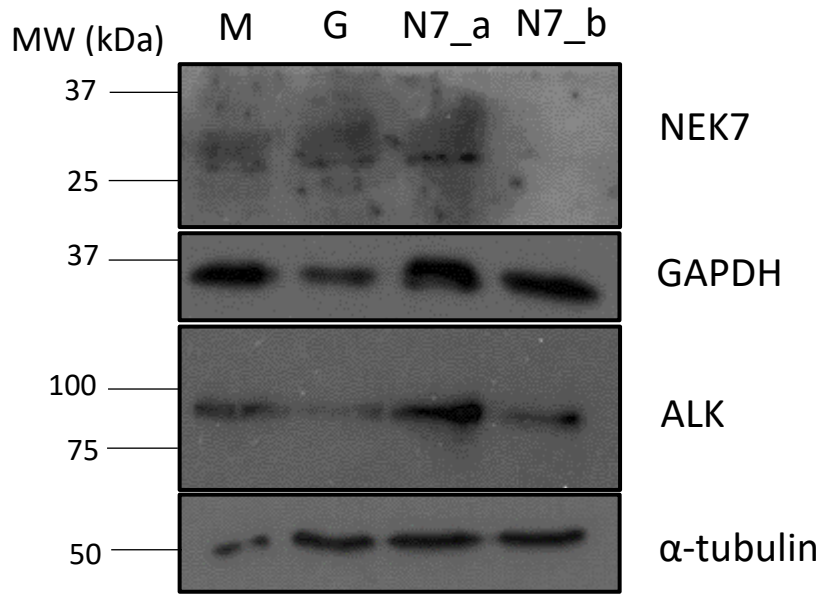
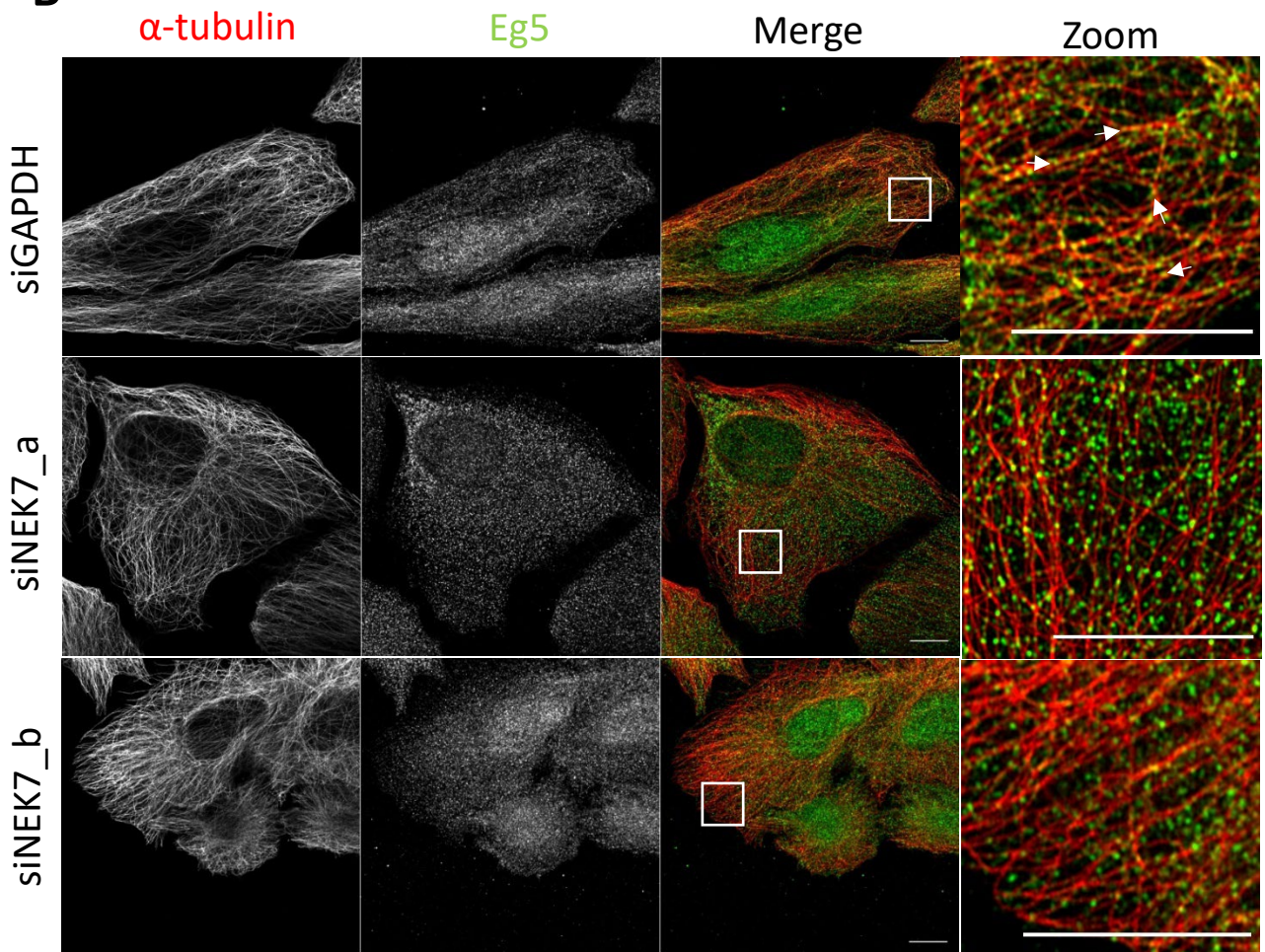
3.2.7. Phosphomimetic Eg5 localises to interphase microtubules in cells expressing EML4-ALK V1

Previous research has shown that NEK7 phosphorylates Eg5 on S1033, which results in its recruitment to centrosomes where it is crucial for centrosome separation and efficient mitotic progression (Bertran *et al.*, 2011; Rapley *et al.*, 2008). Furthermore, NEK7 mediated phosphorylation of this residue has been shown to regulate the extension of dendrites in neurons (Freixo *et al.*, 2018). We therefore investigated whether phosphorylation of this residue might be important for recruitment of Eg5 to interphase microtubules in EML4-ALK V3 expressing cells. For this purpose, FLAG-tagged phosphomimetic (S1033D) and phosphonull (S1033A) mutants of Eg5, as well as a FLAG-tagged wild-type (WT) Eg5 construct, were kindly provided by Dr. Joan Roig (Molecular Biology Institute of Barcelona).

We hypothesised that a phosphomimetic Eg5 mutant protein might localise to interphase microtubules in EML4-ALK V1 cells that lack activation of NEK7, while the phosphonull Eg5 mutant protein would fail to localise to interphase microtubules in the EML4-ALK V3 cells. Therefore, the WT and S1033D Eg5 constructs were transfected into BEAS-2B:EML4-ALK V1 cells, while WT and S1033A Eg5 were transfected into BEAS-2B:EML4-ALK V3 cells. The cell

lines were induced for 48 hours before being transfected with the relevant constructs; cells were lysed for Western blot or fixed for immunofluorescence microscopy after an additional 24 hours.

Western blotting using a FLAG antibody confirmed successful transfection of the WT and specific phosphomutant constructs in the appropriate cell lines with a band detected at the predicted size of 120 kDa in the relevant cells (Figure 3.10A). Strikingly, when these cells were then analysed by immunofluorescence microscopy, an increased proportion of the phosphomimetic Eg5-S1033D mutant protein was seen to co-localise with interphase microtubules than the WT Eg5 protein in V1 cells (Figure 3.10B & C). Interestingly though, no significant difference was detected in the amount of the WT and phosphonull S1033A Eg5 localised to microtubules in V3 cells (Figure 3.10D & E). This could be because the endogenous Eg5 protein was still present in these cells and this may have been phosphorylated by NEK7 and then assembled with the phosphonull Eg5 mutant into tetramers that localised to the microtubules. However, there was no difference in the percentage of recombinant FLAG-tagged WT Eg5 co-localising with interphase microtubules between the V1 and V3 cells, although this could be due to substantially higher expression of the transfected protein in both cell lines.

A**B**

C

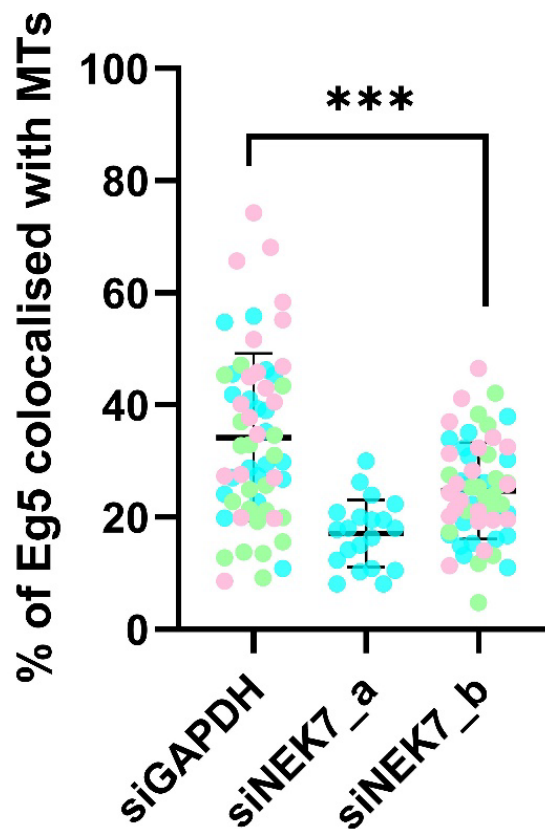
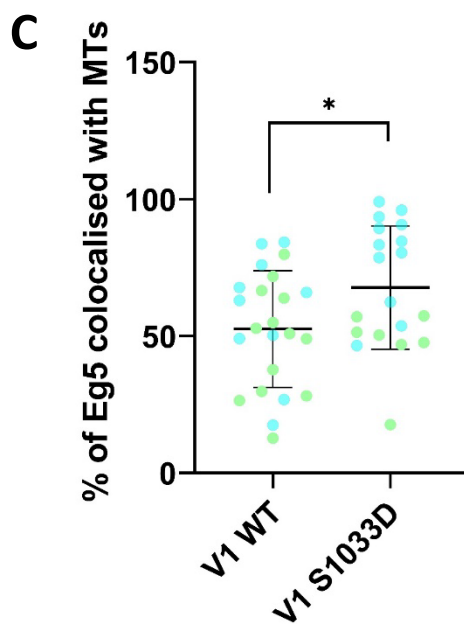
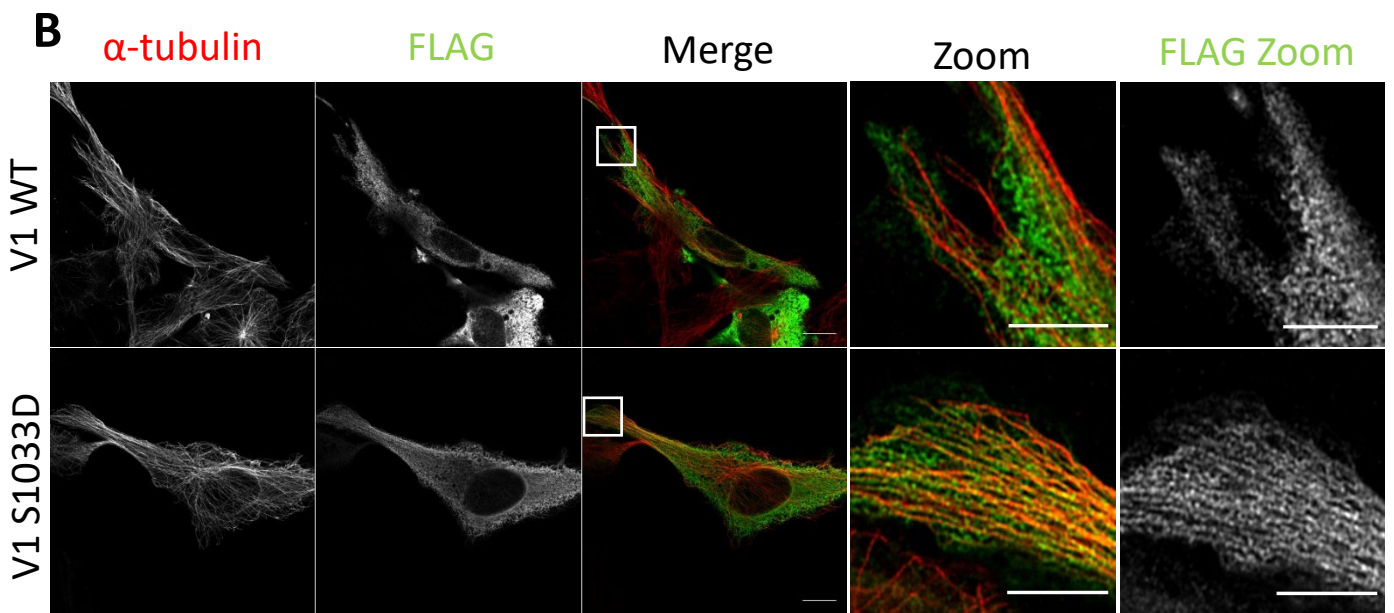
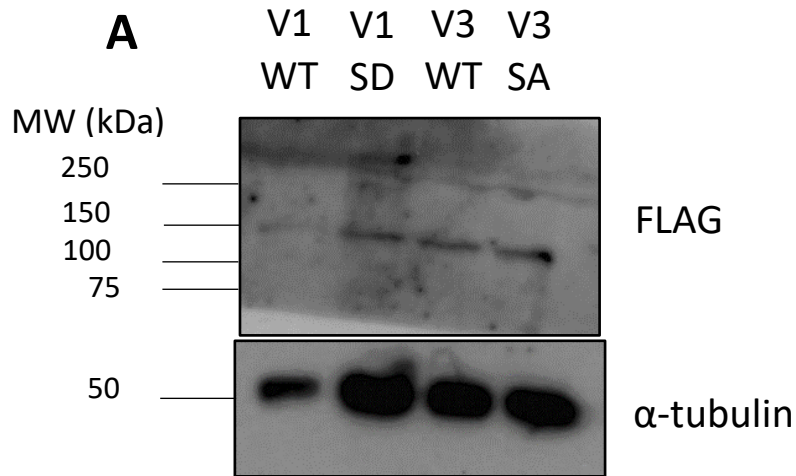


Figure 3.9. NEK7 depletion reduces Eg5 recruitment to interphase microtubules in H2228 cells. (A) H2228 cells were depleted of NEK7 or GAPDH and lysed for Western blot analysis. Analysis was performed with NEK7, GAPDH, ALK and α -tubulin antibodies as indicated. Molecular weights are shown on the left of the blots. M = mock; G = siGAPDH; N7_a = siNEK7_a; N7_b = siNEK7_b. (B) Depleted cells were stained with Eg5 (green) and α -tubulin (red) antibodies. White arrows indicate visible co-localisation. White boxes show zoom regions. Scale bars = 10 μ m. (C) Co-localisation was measured in Imaris. A total of 60 cells were measured for the siGAPDH and siNEK7_b conditions from three independent experiments (one repeat per colour). 20 cells were measured for siNEK7_a from one repeat. Graph shows individual data points, means and standard deviations of each group. Statistical analysis was not performed to compare siGAPDH and siNEK7_a due to the data being from one repeat for siNEK7_a.



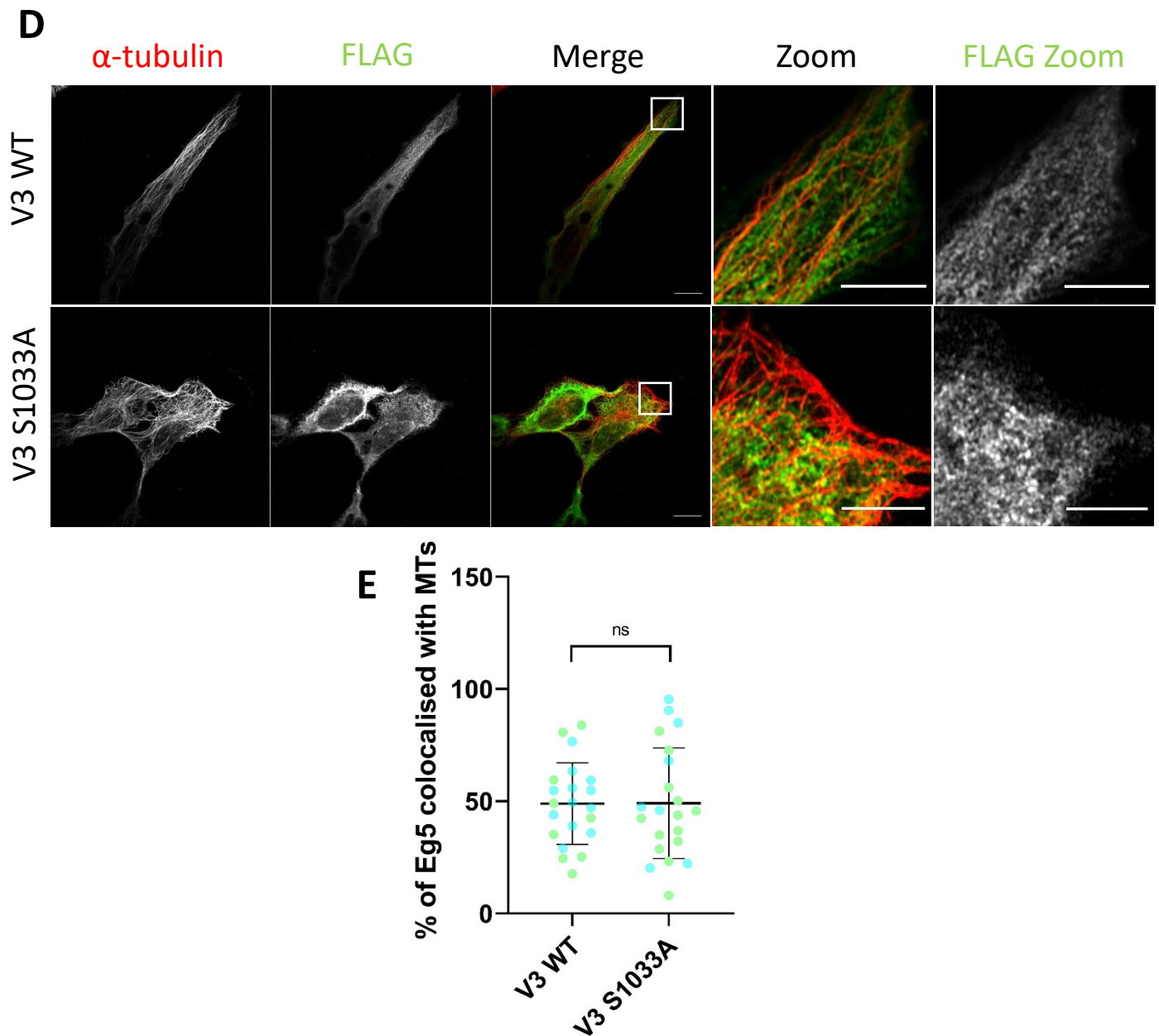


Figure 3.10. More S1033D Eg5 localises with interphase microtubules in BEAS-2B:EML4-ALK V1 cells than WT Eg5. (A) FLAG-tagged Eg5 constructs were transfected into the indicated cell lines. Lysates from these cells were analysed with FLAG and α -tubulin antibodies as indicated. Molecular weights are shown on the left of the blots. (B) V1 cells were stained with FLAG and α -tubulin antibodies. White boxes show zoom regions. Scale bars = 10 μ m in merge; 5 μ m in zooms. (C) Imaris co-localisation analysis was performed for cells represented in B. A total of 23 and 19 cells were measured respective to order of groups on the graph. (D) V3 cells were stained as described in B. White boxes and scale bars as before. (E) Co-localisation analysis was performed in Imaris for cells represented in D. A total of 21 cells were measured for each group. Graphs show individual data points from two independent experiments (one colour per repeat), means and standard deviations.

3.2.8. Eg5 is not recruited to phase separated foci formed by EML4-ALK variants

Three papers have recently reported the incorporation of EML4-ALK variants into liquid-liquid phase separated foci that form in the cytoplasm of cells (Tulpule *et al.*, 2021; Sampson *et al.*, 2021; Qin *et al.*, 2021). These foci have been shown to contain not only the EML4-ALK proteins but also downstream components of signalling pathways activated by ALK that are capable of co-ordinating oncogenic signalling (Sampson *et al.*, 2021). Following our observation that Eg5 is recruited to interphase microtubules in EML4-ALK V3 expressing cells, we were curious to see whether Eg5 can be incorporated into phase separated foci formed by either the EML4-ALK V1 or V3 proteins. For this purpose, induced BEAS-2B: EML4-ALK V1 and V3 cell lines were stained with ALK and Eg5 antibodies and processed for immunofluorescence microscopy. A small number of phase separated foci were found to be present in both cell lines and were identified throughout the cytoplasm as relatively large bright punctae (Figure 3.11A).

To determine whether Eg5 was recruited to these punctae, the PlotMultiColor method was selected for measuring co-localisation in the phase separated foci, as we were only interested in a small number of foci in the cell. As previously described, a 10 μm line was drawn on images using Fiji software that, where possible, cut through a minimum of two large ALK punctae per cell. Analysing images in this way revealed only weak correlation between the ALK punctae and Eg5 in both the V1 ($R= 0.1224$) and V3 ($R= 0.08949$) cell lines, with no significant difference between the two. This suggests no significant recruitment of Eg5 to ALK punctae in either cell line (Figure 3.11B).

A similar investigation was undertaken using the NSCLC patient cell lines to determine whether Eg5 was recruited to phase separated EML4-ALK foci in these cell lines. Cells were again stained with ALK and Eg5 antibodies and analysed by immunofluorescence microscopy (Figure 3.12A). The Pearson's correlation values were calculated for the phase separated foci and again revealed a weak correlation between Eg5 and ALK signals in both cell lines ($R=0.08821$ in H3122 cells and $R=0.1248$ in H2228 cells), suggesting no significant co-localisation to these phase-separated foci (Figure 3.12B).

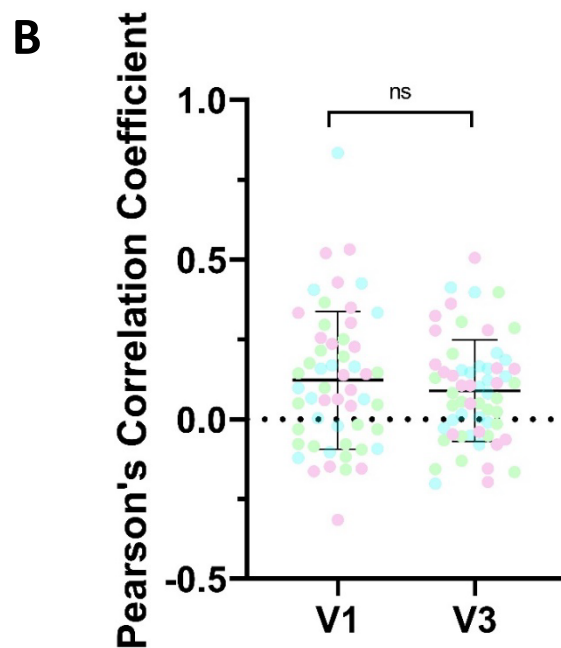
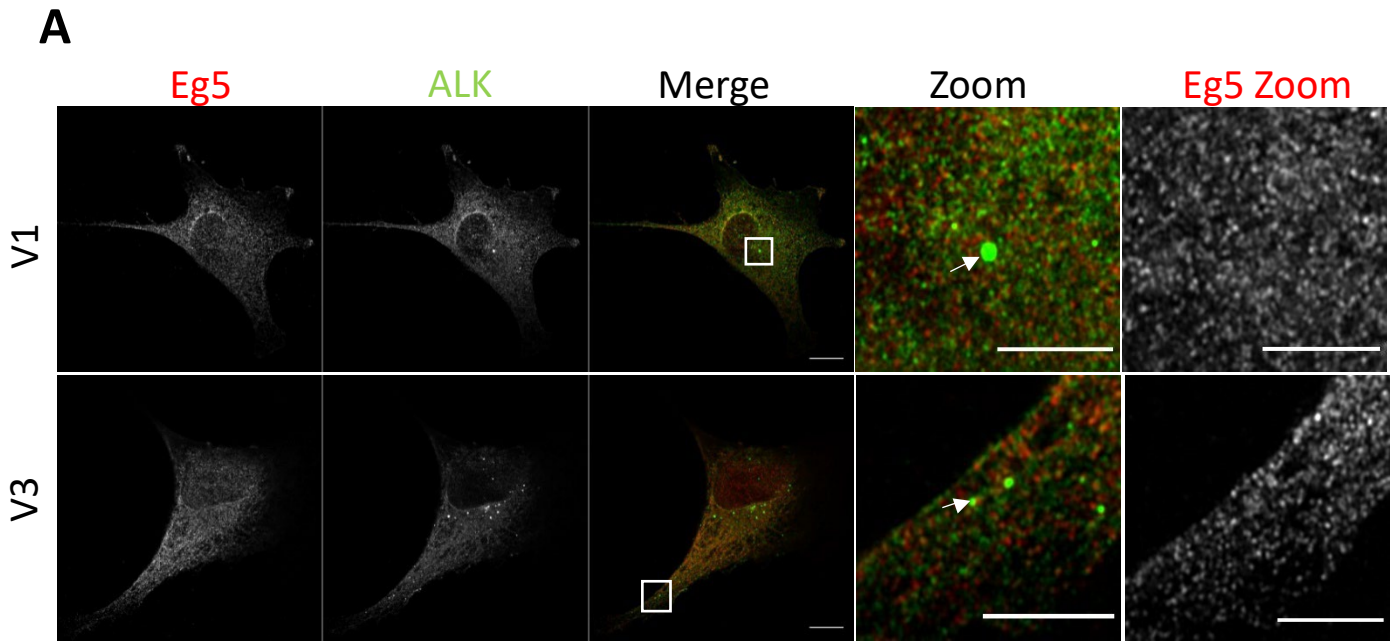


Figure 3.11. Eg5 is not recruited to phase separated foci in BEAS-2B:EML4-ALK cell lines. (A)

Induced cells were fixed and stained with Eg5 (red) and ALK (green) antibodies. White boxes show zoom regions. White arrows indicate where Pearson's correlation measurements were taken from red and green channels. Scale bars = 10 μm in merge; 5 μm in zooms. (B) The PlotMultiColor 4.3

macro was used for co-localisation analysis from images represented in A. Data is representative of three independent experiments. Graph shows individual data points (one colour per repeat), means and standard deviations. N= 54 for V1 cells and N=60 for V3 cells.

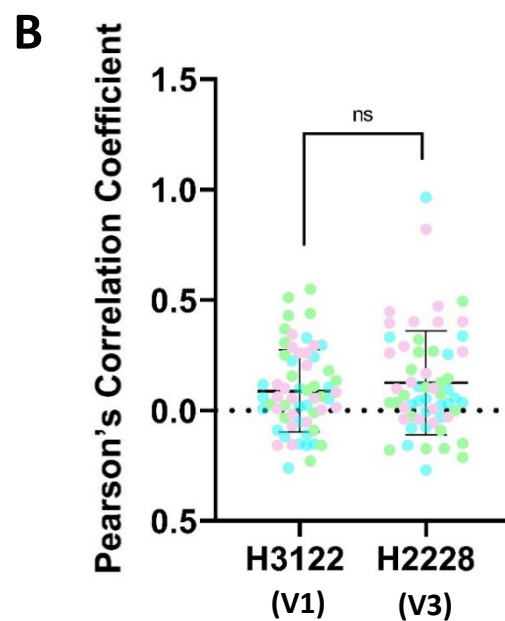
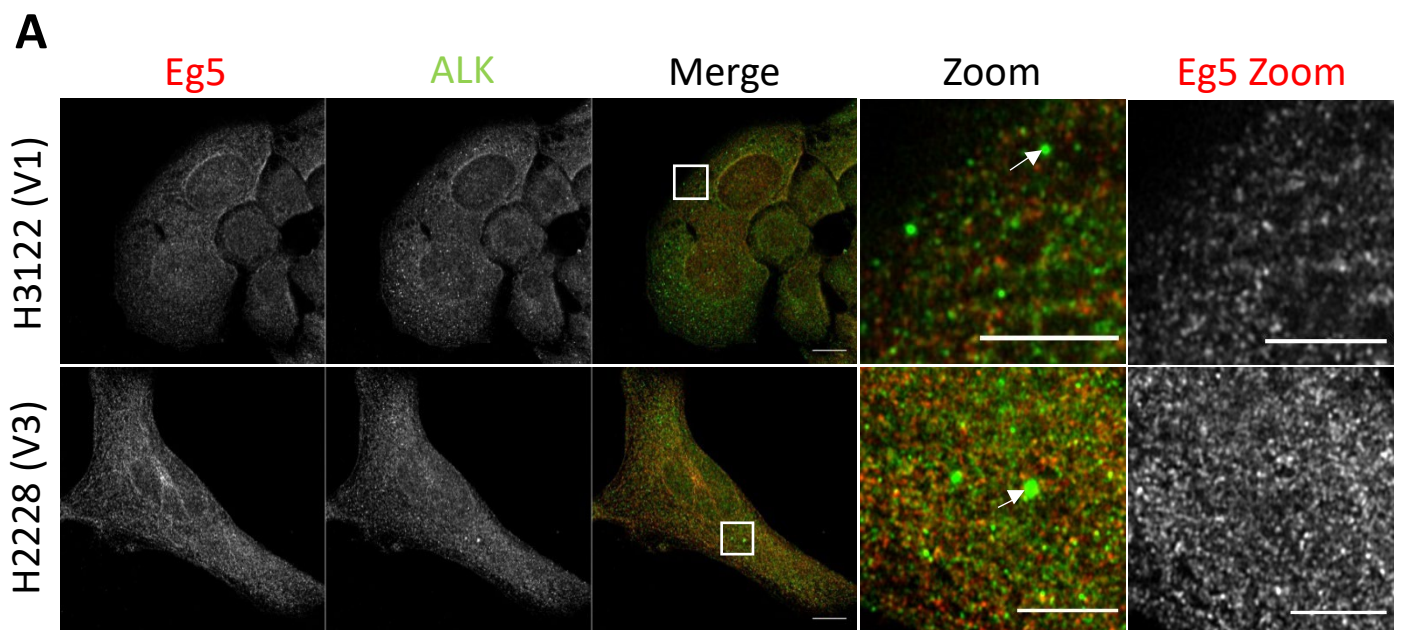


Figure 3.12. Eg5 is not recruited to phase separated foci in NSCLC patient cell lines. (A) Cells were stained with antibodies against Eg5 (red) and ALK (green). White boxes show zoom regions. White arrows indicate where Pearson's correlation measurements were taken from red and green channels. Scale bars = 10 μ m in merge; 5 μ m in zooms. (B) Co-localisation was measured using the Plot MultiColor Fiji macro for images represented in A. Data is representative of three independent experiments. Graph shows individual data points (one repeat per colour), means and standard deviations. 60 data points were obtained from H3122 cells and 59 from H2228 cells.

3.3. DISCUSSION

Recent studies undertaken in our lab revealed a signalling pathway downstream of EML4-ALK V3 that was not present in cells expressing the other major EML4-ALK variants, notably V1 and V2. EML4-ALK V3 was discovered to bind interphase microtubules and these microtubules exhibited excessive stabilisation (O'Regan *et al.*, 2020). Furthermore, a physical interaction was found between EML4-ALK V3 and two cell cycle-dependent serine/threonine kinases, NEK9 and NEK7, which resulted in their activation and translocation to microtubules (O'Regan *et al.*, 2020). However, it remains unclear what the downstream substrates of these kinases in this signalling pathway are and how they may contribute to the observed phenotypic changes.

This chapter set out to test the hypothesis that the microtubule-associated kinesin motor protein, Eg5, is a downstream substrate of the EML4-ALK V3:NEK9:NEK7 pathway. Our reasoning for this was that Eg5 is a microtubule associated protein that is a known substrate of NEK7 (Bertran *et al.*, 2011; Rapley *et al.*, 2008) and that phosphorylation of Eg5 by NEK7 has previously been shown to result in similar phenotypic alterations in neurons to those observed in cells expressing EML4-ALK V3 or activated NEK7 (Freixo *et al.*, 2018).

To conduct these investigations, two sets of cell lines were used: NSCLC patient cell lines that endogenously express either EML4-ALK V1 or V3 (H3122 and H2228) and BEAS-2B cell lines that had been engineered to inducibly express these EML4-ALK variants. It is worth noting that while the patient-derived cell lines express the two different EML4-ALK variants, they also harbour many other genetic alterations that could affect their biology. This is the reason why a second model system was employed for these experiments. The parental BEAS-2B cell line is derived from bronchial epithelial cells and hence established from a non-cancerous tissue relevant to lung cancer. Stable inducible cell lines were derived from the parental cell line that expressed EML4-ALK V1 or V3. Other than the EML4-ALK variant, the BEAS-2B cell lines are isogenic meaning that they are genetically identical making them an ideal model for these studies.

Given the importance of Eg5 in enabling formation of a bipolar mitotic spindle, it is unsurprising that Eg5 expression is upregulated in many cancers that are composed of rapidly dividing cells (Castillo *et al.*, 2007; Saijo *et al.*, 2006; Garcia-Saez and Skoufias, 2021). However, upon investigation in our BEAS-2B cell lines, no difference in Eg5 expression was found upon induction of EML4-ALK variants. Interestingly, expression was significantly higher in the H3122 cell line when compared to the H2228 cell line. This could be explained by the presence of a mutation in the *KIF11* gene that encodes the Eg5 protein. Hence, H2228 cells express a mutant Eg5 protein and it is possible that either the mRNA or protein are less stable resulting in a reduction in the expression of Eg5. However, it remains feasible that this is also a consequence of the different EML4-ALK proteins present in these cells as these oncogenic fusion proteins are known to impact on gene expression.

Intriguingly, Eg5 was found to be recruited to interphase microtubules in cells expressing EML4-ALK V3 but not EML4-ALK V1. In cycling cells, Eg5 is normally only recruited to microtubules in mitosis as a result of phosphorylation by CDK1 (Sawin and Mitchison, 1995; Liu, Ran and Zhou, 2018). Here, Eg5 appeared as discrete punctae that in V3 cells were largely dotted along interphase microtubules. Co-localisation analysis revealed around 20% more Eg5 was co-localising with interphase microtubules in both BEAS-2B:EML4-ALK V3 cells and H2228 cells as compared to the corresponding parental or V1 cell lines. Interestingly, in differentiated neurons, a recent study has found that by locking Eg5 on to microtubules using a chemical inhibitor, microtubule stabilisation is increased (Freixo *et al.*, 2018). This observation was also reported using isolated microtubules attached to coverslips (Chen *et al.*, 2017). Therefore, it is a possibility that Eg5 binding to interphase microtubules in EML4-ALK V3 expressing cells could contribute to their stabilisation. This will be explored further in the next chapter.

During mitotic entry in dividing cells, Eg5 is phosphorylated not only by CDK1 but also by NEK7, an event that supports centrosome separation and formation of a bipolar spindle (Bertran *et al.*, 2011; Rapley *et al.*, 2008). We therefore investigated whether it was NEK7 that was responsible for the recruitment of Eg5 to interphase microtubules downstream of

EML4-ALK V3. Depletion of NEK7 with two different siRNA oligonucleotides led to a decrease in the percentage of Eg5 co-localising with interphase microtubules in EML4-ALK V3 expressing cells. This supports the hypothesis that NEK7 is indeed required for this untimely recruitment of Eg5 to interphase microtubules. It was likely that this is the outcome of a phosphorylation event rather than a physical interaction between NEK7 and Eg5. However, to provide further evidence for this and in the absence of a potent chemical inhibitor of NEK7, a catalytically inactive mutant of NEK7 could be transfected into EML4-ALK V3 cells depleted of endogenous NEK7 and the percentage of Eg5 localising to microtubules measured.

NEK7 was demonstrated to specifically phosphorylate S1033 in the tail domain of Eg5. Hence, as an additional approach to test the role of NEK7-dependent phosphorylation, we examined the consequences on Eg5 recruitment to interphase microtubules of expression of S1033 phosphomutants of Eg5. An S1033D mutant mimics the phosphorylation of this residue (phosphomimetic), while an S1033A mutant represents a non-phosphorylatable (phosphonull) protein (Bertran *et al.*, 2011; Rapley *et al.*, 2008; Freixo *et al.*, 2018). Interestingly, when the phosphomimetic mutant was transfected into cells expressing EML4-ALK V1, the percentage of the mutant Eg5 that co-localised with interphase microtubules was significantly higher than that of the WT protein. This suggests that phosphorylation at this site can lead to accumulation of Eg5 on interphase microtubules. However, when the phosphonull (S1033A) mutant was transfected into cells expressing EML4-ALK V3, no significant difference was seen in the localisation of the mutant Eg5 protein to the microtubules compared to the WT protein. As the endogenous Eg5 was still present in these cells, it could be recruited to microtubules upon phosphorylation by NEK7. Hence, as Eg5 is a tetrameric protein, the endogenous protein might assemble with the phosphonull mutant into tetramers that are recruited to microtubules. Thus, future experiments should test localisation of the phosphonull mutant in V3 cells depleted of the endogenous Eg5. It would also be interesting to examine the localisation of these phospho-mutant Eg5 proteins in cells expressing EML4-ALK but which have been depleted of NEK7. We predict that this would not prevent localisation of the phosphomimetic mutant Eg5 to microtubules.

There are several reports that suggest EML4-ALK variants can be incorporated into liquid-liquid phase separated foci that are capable of ALK-dependent oncogenic signalling (Sampson *et al.*, 2021; Tulpule *et al.*, 2021; Qin *et al.*, 2021). However, we found no evidence of a significant recruitment of Eg5 to EML4-ALK-containing phase separated foci in cells expressing either EML4-ALK V1 or V3. As the phase separated foci do not associate with microtubules (Sampson *et al.*, 2021), it follows that microtubule associated proteins, such as Eg5, would not associate with phase separated foci. Importantly though, these data suggest that a strong physical interaction between EML4-ALK V3 and Eg5 is unlikely. However, it will still be worth exploring whether NEK7 is present in these foci or not.

To conclude, whilst EML4-ALK V3 does not affect Eg5 expression, there is a potentially exciting change in Eg5 localisation with Eg5 recruited to interphase microtubules in cells expressing EML4-ALK V3 but not V1. Moreover, our data suggests that this occurs downstream of NEK7. Together, this provides compelling evidence that Eg5 is a downstream effector of the EML4-ALK V3:NEK9:NEK7 signalling module. However, exactly what Eg5 is doing to microtubules in these cells and whether this is important for the cellular phenotypes remains to be elucidated. In the next chapter, I describe experiments that set out to investigate whether Eg5 is contributing to the altered cellular phenotypes exhibited by EML4-ALK V3 cells including microtubule stabilisation, cell elongation and increased cell migration.

CHAPTER 4

The morphology of cells expressing EML4-ALK V3 is dependent on phosphorylation and motor activity of Eg5

4.1. INTRODUCTION

Metastasis is the spread of cancer cells from a primary tumour to secondary sites located in other organs around the body and accounts for 90% of cancer-related deaths (Seyfried and Huysentruyt, 2013). A key event in the process of metastasis is the epithelial-to-mesenchymal transition (EMT) of cells, a normal phenomenon which is crucial for embryonic development of many animals (Thiery, 2002; Kalluri and Weinberg, 2009). EMT is characterised by cells losing their polarity, becoming more elongated (mesenchymal) in morphology as well as more migratory and invasive (Thiery *et al.*, 2009). Cancer cells may use this normal process to their advantage with EMT offering an explanation of how epithelia-derived tumour cells are able to detach from their primary site and invade surrounding tissues (Kalluri and Weinberg, 2009).

In the case of ALK+ NSCLC, patients with EML4-ALK V3 are more likely to have metastatic disease than those with other variants (Christopoulos *et al.*, 2018). This is consistent with findings that cells in culture expressing EML4-ALK V3 develop a mesenchymal morphology with elongated cytoplasmic protrusions that contain both actin and stabilised microtubules (O'Regan *et al.*, 2020). They also exhibit elevated rates of migration, suggesting that these cells may have undergone an EMT-like process, although classical markers of EMT, such as cadherins and β -catenin, have not been explored. Similar changes have been reported in breast cancer cells where elevated levels of acetylated tubulin, a marker of microtubule stabilisation, were shown to promote cell migration and formation of cytoplasmic protrusions, termed microtentacles, containing stable microtubules (Boggs *et al.*, 2015). As well as contributing to invasion of neighbouring tissues, it is thought that these protrusions and the increased migratory potential contributes to reattachment of circulating tumour cells to a secondary site (Boggs *et al.*, 2015). Furthermore, microtubule acetylation has been shown to stimulate cell migration, as well as focal adhesion turnover, in astrocytes (Bance *et al.*, 2019). For this reason, elevated acetylated tubulin levels could be a good prognostic marker to indicate increased metastatic potential (Boggs *et al.*, 2015).

What remains unclear is what causes these phenotypic changes in cells expressing EML4-ALK V3 but not other common EML4-ALK variants. In the previous chapter, it was shown that Eg5, a mitotic kinesin, was recruited to interphase microtubules in V3 expressing cells, downstream of the NEK7 kinase. As previously described, Eg5 normally only associates with microtubules during mitosis and not interphase (Sawin and Mitchison, 1995). Many chemical inhibitors of Eg5 have been developed, some of which weaken the interaction between Eg5 and the microtubule (L5 inhibitors) while others strengthen this interaction (rigor inhibitors). Both kinds of inhibitors result in mitotic arrest with a monopolar spindle when added during interphase. This demonstrates that the kinesin activity of Eg5 is required to form a bipolar spindle through separation of centrosomes (Bertran *et al.*, 2011). However, these two different inhibitor types have different consequences in cells that have first been pre-arrested in mitosis, with spindles being maintained in those subsequently treated with a rigor inhibitor but collapsing with an L5 inhibitor (Chen *et al.*, 2017; Chattopadhyay *et al.*, 2015). This difference in cellular mechanism of action of these two categories of Eg5 inhibitor is consistent with their different consequences on microtubule stability. Cells treated with L5 inhibitors, which block Eg5 interaction with microtubules, have less stable microtubules compared to cells treated with rigor inhibitors, which lock Eg5 onto microtubules (Chen *et al.*, 2017; Freixo *et al.*, 2018). This indicates that Eg5 can play a role in regulating microtubule stability that is potentially independent of its processivity.

Not only does Eg5 play a part in stabilising microtubules, it has also been found to be a microtubule polymerase (Chen and Hancock, 2015; Chen *et al.*, 2019). It was proposed that Eg5 could step from a growing microtubule onto incoming tubulin dimers thereby stabilising the interaction with the growing protofilaments; this is reflected in an increased growth rate and reduced catastrophe frequency (Chen and Hancock, 2015; Chen *et al.*, 2019). This is consistent with data in neuronal cells that show that Eg5 is required for dendrite extension (Freixo *et al.*, 2018). As NEK7 phosphorylation of Eg5 was also shown to regulate dendrite length, it is tempting to speculate that this may be a result of NEK7-dependent regulation of microtubule stability.

Other research has also implicated Eg5 in cell migration. In neurons, Eg5 is believed to act as a brake on migration, as Eg5 inhibitors lead to faster migration (Falnikar *et al.*, 2011). Furthermore, Eg5 has also been shown to guide microtubules into the peripheral region of a growth cone, assisting changes in the direction of migration (Nadar *et al.*, 2008). However, while Eg5 has been shown to inhibit migration of neurons, the opposite has been shown to be true in cancer cells with Eg5 inhibition reducing cell motility and invasion of both pancreatic and gastric cancer cells (Sun *et al.*, 2011; Marconi *et al.*, 2019).

Beyond the studies described above, both the NEK9-Eg5 signalling axis and microtubule acetylation have been linked to increased metastatic potential in colorectal cancer (Kim *et al.*, 2023). Specifically, immunohistochemical analysis of tumour samples from patients with advanced colorectal cancer revealed elevated expression of NEK9 (69%), Eg5 (53%) and acetylated tubulin (74%) and these were associated with presence of distant metastases (Kim *et al.*, 2023). Therefore, the aim of this chapter was to further explore whether Eg5 is contributing to microtubule stabilisation, cell morphology and migration downstream of the EML4-ALK V3:NEK9:NEK7 signalling module. Specifically, Eg5 inhibitors were used to determine if Eg5 is required for morphology and migration changes, while the phosphorylation of Eg5 at S1033 was explored further in the context of microtubule stabilisation and cell morphology.

4.2. RESULTS

4.2.1. Characterising Eg5 inhibitors in EML4-ALK expressing cells

To begin to investigate whether Eg5 recruitment to microtubules in interphase cells expressing EML4-ALK V3 was important for phenotypes such as cell morphology and migration, three Eg5 inhibitors were purchased for studies described in this chapter. These inhibitors were STLC, filanesib and BRD9876. Eg5 inhibitors can work in one of two ways: weakening the interaction between Eg5 and the microtubules (L5 inhibitors) or strengthening this interaction (rigor inhibitors) (Chen *et al.*, 2017). STLC and filanesib are both L5 inhibitors, while BRD9876 is a rigor inhibitor. STLC has been commonly used for experimental studies, while filanesib is the only Eg5 inhibitor to have progressed to phase III clinical trials (Owens, 2013; Indorato *et al.*, 2019). All Eg5 inhibitors should cause cells to arrest in mitosis. To confirm that this was also the case in cells expressing EML4-ALK proteins, live cell imaging was performed in the presence of each of the drugs. BEAS-2B:EML4-ALK V1 and V3 cell lines were induced for 48 hours before then being treated with 5 μ M STLC, 100 nM filanesib, 10 μ M BRD9876 or DMSO. Doses were chosen based on previous studies in the literature or by the suggested dose on the accompanying data sheet received from the supplier of each drug (Skoufias *et al.*, 2006; Stiff *et al.*, 2020). Cells were then immediately placed in the incubation chamber of a PhaseFocus LiveCyte 2 microscope and three 500-750 μ m² areas imaged every 15 minutes for 24 hours per treatment. The final images taken at 24 hours were used for quantification and the percentage of cells in mitosis based on a sustained rounded cell morphology was calculated for each condition. All three Eg5 inhibitors resulted in a significant percentage of cells in mitotic arrest after 24 hours in both the V1 and V3 BEAS-2B cell lines (Figure 4.1A-C). Furthermore, live imaging revealed that some cells also underwent apoptosis consistent with reports that exposure to Eg5 inhibitors can cause cell death (Tao *et al.*, 2005). These cells had previously arrested in mitosis and displayed a rounded morphology for hours before the cells appeared to bleb and disappear.

A similar experiment was conducted with the NSCLC patient cell lines, H3122 (V1) and H2228 (V3), to confirm mitotic arrest after treatment with Eg5 inhibitors. Live cell imaging

was again performed for 24 hours after drug treatments and the final images used for quantification of mitotic arrest. However, due to the more rounded, cobblestone morphology of H3122 cells, it proved not to be possible to quantify mitotic arrest in this cell line using this imaging approach (Figure 4.2A). Mitotic arrest was however quantified in the H2228 cell line, where cell morphology is flatter and more elongated during interphase. All three Eg5 inhibitors caused a substantial mitotic arrest in H2228 cells (Figure 4.2B). However, only cells treated with filanesib reached statistical significance as, due to low seeding densities, not enough cells were present in the images for STLC or BRD9876 treatment ($P=0.2$; $P=0.07$, respectively). We expect that if more cells had been present in the imaging windows these would also have reached statistical significance.

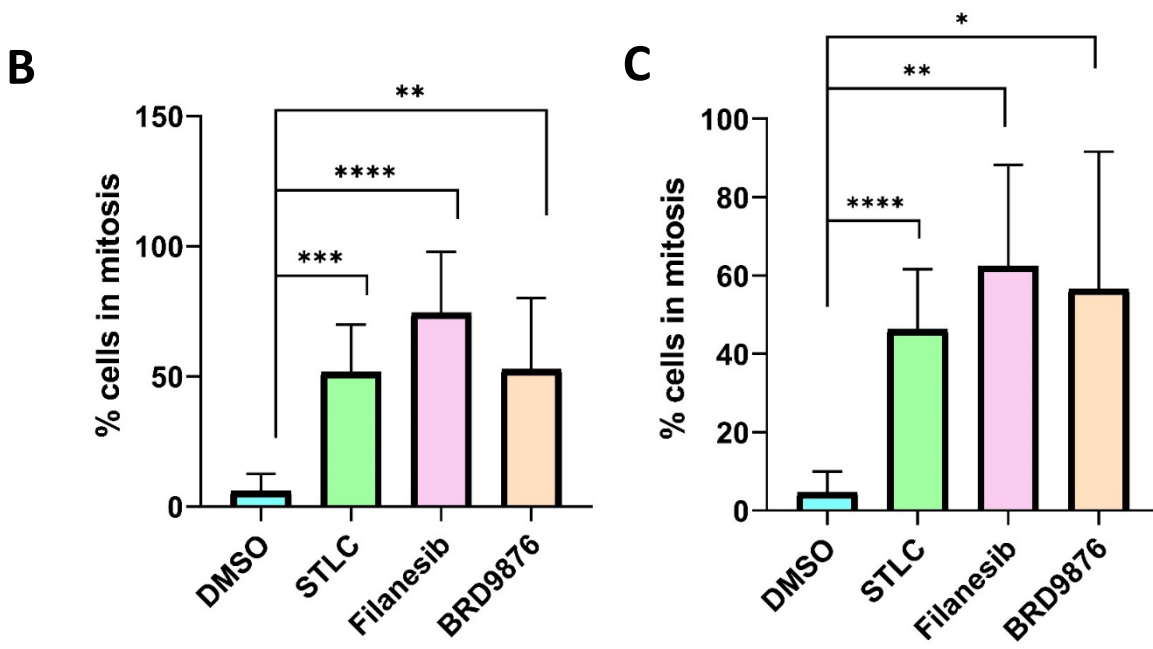
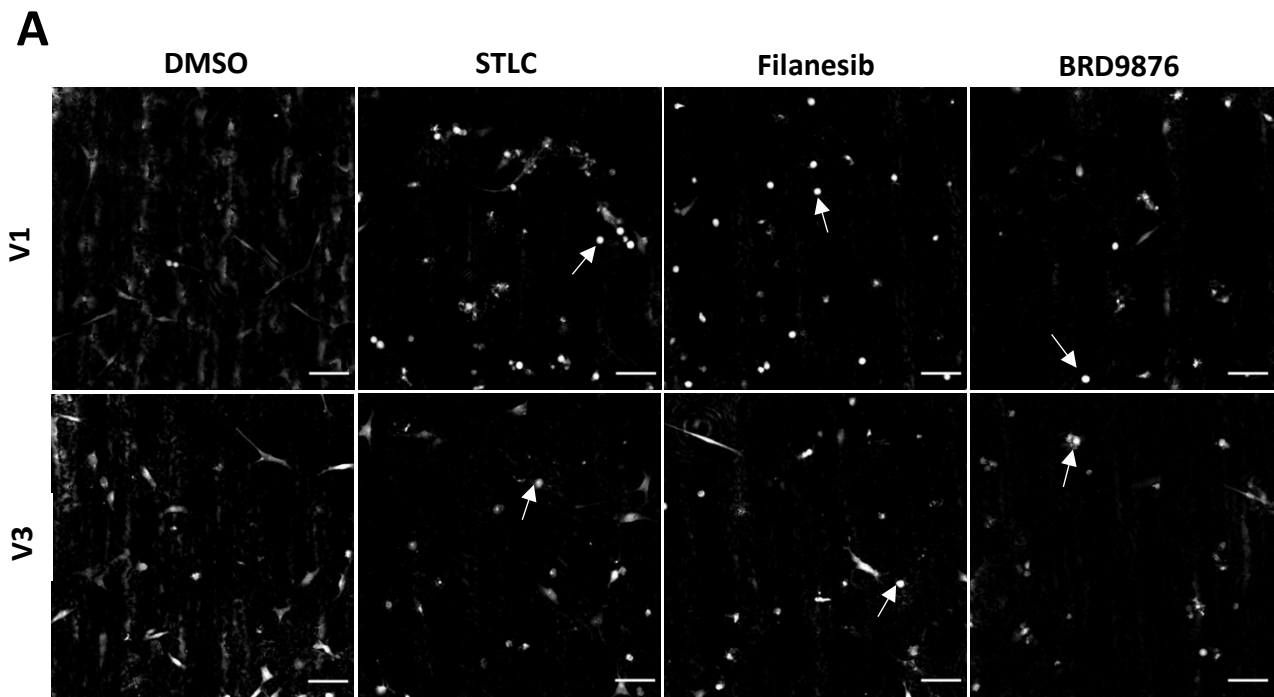


Figure 4.1. Eg5 inhibitors arrest BEAS-2B:EML4-ALK cells in mitosis. (A) Live cell imaging was performed for 24 hours after BEAS-2B cells were treated with Eg5 inhibitors. Mitotic cells indicated by white arrows. Scale bars = 100 μ m. The percentage of BEAS-2B:EML4-ALK V1 (B) and V3 (C) cells that were in mitosis after 24 hours exposure to the labelled drug were calculated from images represented in (A). Three areas were imaged per condition, per repeat. Graphs show means, standard deviations and are representative of three repeats.

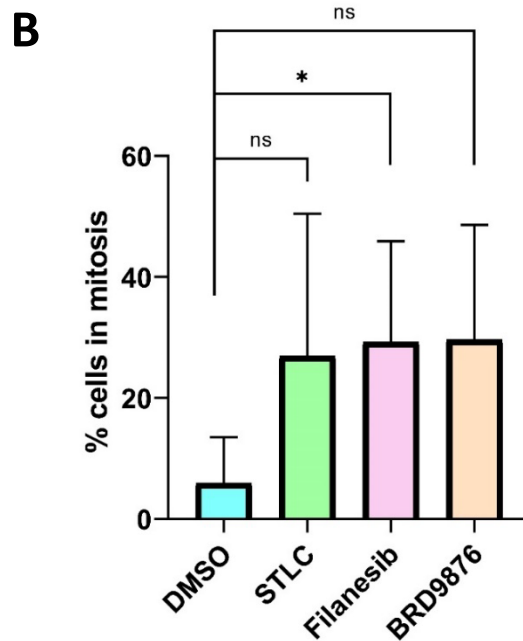
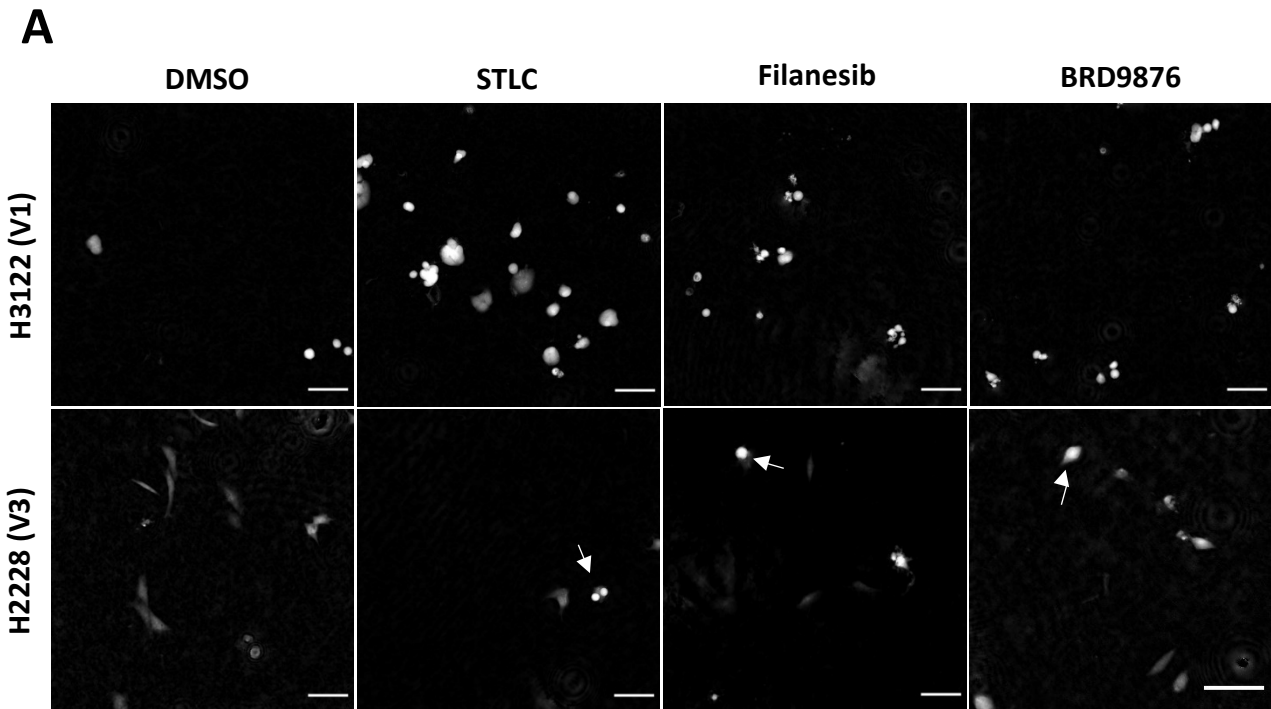


Figure 4.2. Eg5 inhibitors arrest H2228 cells in mitosis. (A) Live cell imaging of H2228 cells was performed for 24 hours after cells were treated with Eg5 inhibitors. Mitotic cells indicated by white arrows. Scale bars = 100 μ m. (B) The percentage of cells in mitosis was calculated for each drug treatment for H2228 cells from live cell imaging after 24 hours - representative images in (A). Three areas were imaged per condition, per repeat. Graph shows means and standard deviations. Graph is representative of three independent experiments.

Eg5 is essential for centrosome separation and the formation of a bipolar spindle (Bertran *et al.*, 2011; Rapley *et al.*, 2008). When cells are treated with Eg5 inhibitors, centrosome separation is no longer achieved and cells form monopolar spindles (Blangy *et al.*, 1995). Therefore, the presence of monopolar spindles was used as an additional marker to confirm the Eg5 inhibitors were working as expected in our cell lines. BEAS-2B:EML4-ALK V3 cells were induced for 48 hours before being treated with the different Eg5 inhibitors for a further 24 hours. The following day, cells were fixed and stained for immunofluorescence microscopy. Cells were stained with antibodies against α -tubulin to detect spindle microtubules and γ -tubulin to identify spindle poles, while DNA was also stained. Monopolar spindles were identified in rounded mitotic cells where condensed chromatin was arranged around a single aster of microtubules with unseparated poles. The vast majority of mitotic cells in samples treated with STLC, filanesib and BRD9876 appeared to have monopolar spindles, in contrast to the control DMSO-treated sample where spindles were bipolar (Figure 4.3A).

Similarly, NSCLC patient H2228 (V3) cells were also treated with the Eg5 inhibitors for 24 hours and stained for immunofluorescence microscopy as previously described to investigate the structure of mitotic spindles. Again, the majority of mitotic cells appeared to have monopolar spindles with all three Eg5 inhibitors (Figure 4.3B). Interestingly, bipolar spindles could also be seen in cells treated with the rigor inhibitor, BRD9876 as compared to the L5 inhibitors (Figure 4.3B). This is consistent with reports in the literature that cells already in mitosis at the time when the drug was added would have already formed bipolar spindles with spindle bipolarity maintained upon mitotic arrest (Chen *et al.*, 2017; Chattopadhyay *et al.*, 2015). This is likely to be the case for other rigor inhibitors that lock Eg5 onto the microtubules, but not for the L5 inhibitors that perturb interaction of Eg5 with microtubules.

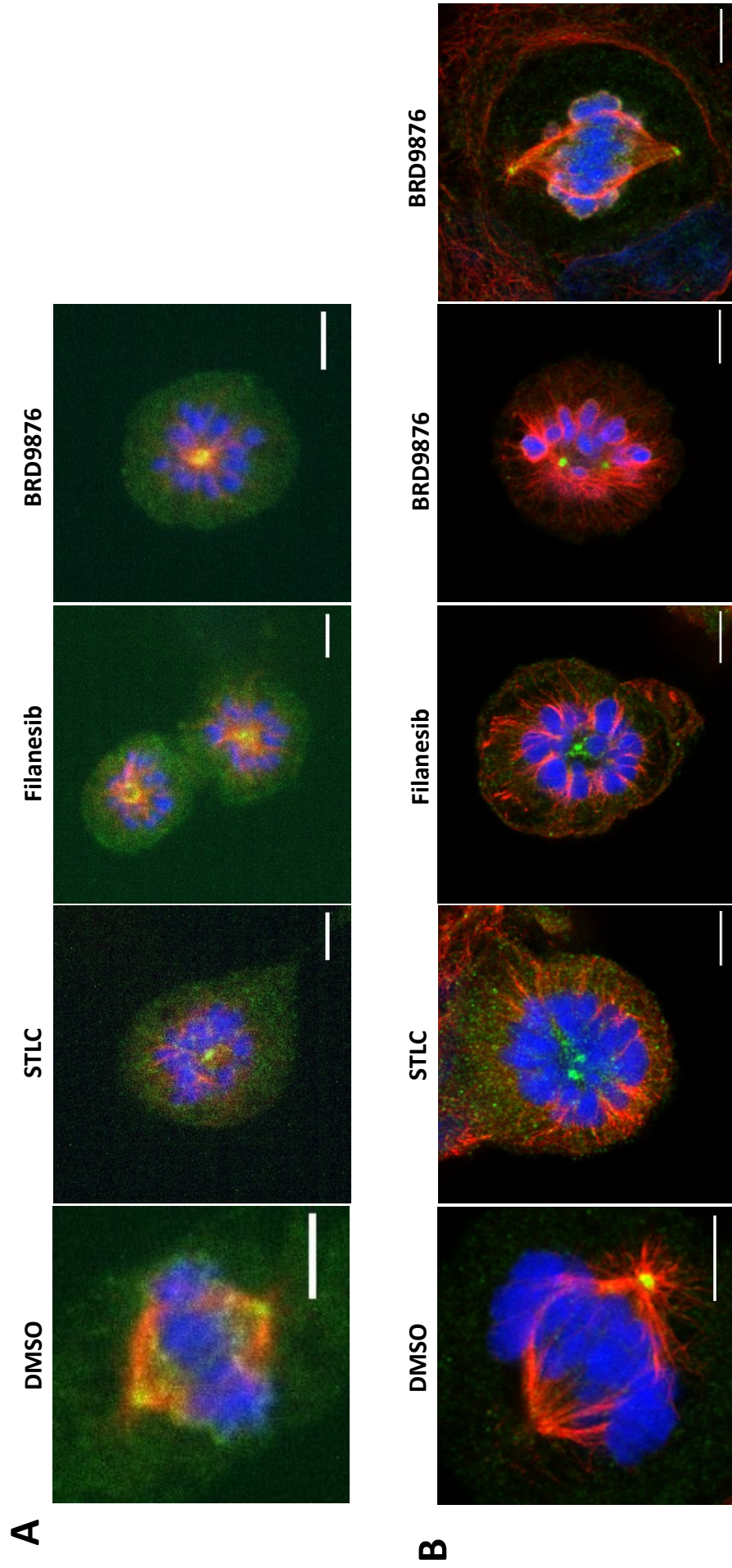


Figure 4.3. Eg5 inhibitors result in the formation of monopolar spindles. (A) BEAS-2B:EML4-ALK V3 cells were treated with the indicated Eg5 inhibitors and immunofluorescence microscopy performed. Cells were stained for α-tubulin (red), γ-tubulin (green) and Hoescht stained DNA (blue). Images representative of three independent experiments. (B) H2228 cells were treated as described for cells in (A). Images are representative of one repeat. Scale bars = 5 μm.

4.2.2. Eg5 inhibitors reduce the length of cells expressing EML4-ALK V3

To determine whether recruitment of Eg5 to interphase microtubules in cells expressing EML4-ALK V3 was contributing to the changes observed in cell morphology, EML4-ALK cell lines were treated with Eg5 inhibitors and cell length measured. BEAS-2B:EML4-ALK V1 and V3 cell lines were induced with doxycycline in a 10 cm dish for 24 hours before being detached and embedded into collagen to give a closer representation of a tumour microenvironment. Once embedded into collagen, cells were left to spread for 24 hours with the addition of more doxycycline to continue induction of the EML4-ALK proteins. The following day, cells were treated with DMSO or the Eg5 inhibitors and, after 1 hour, cells were placed on a PhaseFocus Livecyte 2 imaging system for live imaging. Cell length measurements were made on captured images in Fiji by drawing a line through the cell along the longest length (Figure 4.4A).

The measurements taken using this approach first confirmed that, in the absence of drug treatment, the EML4-ALK V3 cells were significantly longer than the EML4-ALK V1 cells, in line with previous reports (O'Regan *et al.*, 2020). Furthermore, none of the three Eg5 inhibitors had any effect on the cell lengths of BEAS-2B:EML4-ALK V1 cells (Figure 4.4B). Importantly though, filanesib and BRD9876 both significantly reduced V3 cell length. Indeed, BRD9876 completely blocked the phenotype with cells reverting to the same size as untreated V1 cells (Figure 4.4C). The reduction in V3 cell length observed upon treatment with STLC was smaller and did not reach significance although, this could be due to a few outliers at the higher end of the measurements obtained (Figure 4.4C).

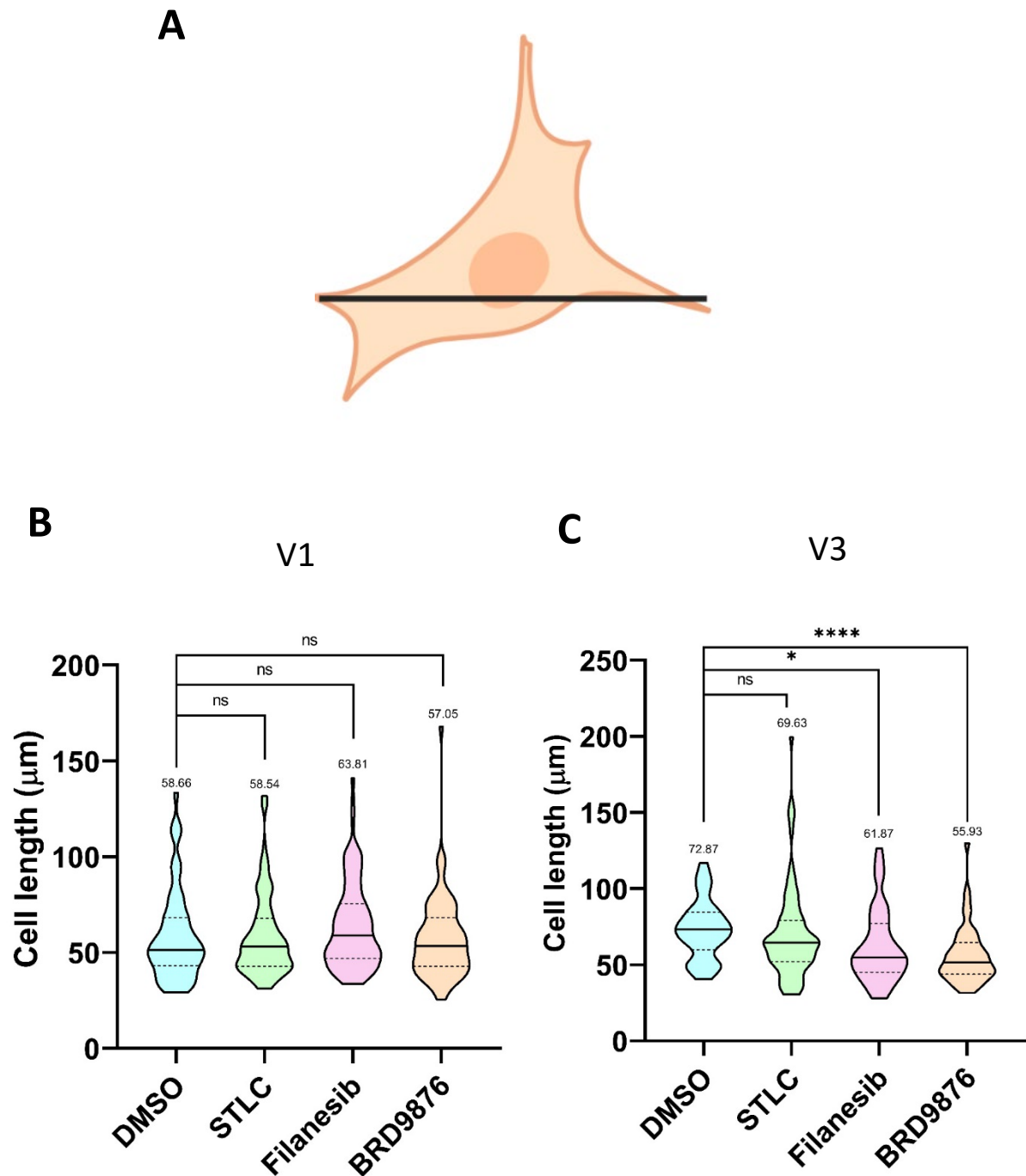


Figure 4.4. The length of BEAS-2B:EML4-ALK V3 cells is significantly reduced by Eg5 inhibitors filanesib and BRD9876. (A) Schematic showing how cell length was measured. Cell length measurements were taken in Fiji from BEAS-2B:EML4-ALK V1 (B) and V3 (C) cells treated with different Eg5 inhibitors or DMSO. Violin plots show spread of data with the median (solid line) and quartiles (dotted lines). Means for each group are written above the violins. N= 55, 93, 95, 76 for EML4-ALK V1 cells and N= 69, 82, 62, 49 for EML4-ALK V3 cells respective to the order of groups on the graphs. Data presented is from three independent experiments.

Previous research has shown that the H2228 (V3) patient cells, which express EML4-ALK V3, are significantly longer than the H3122 (V1) patient cells, which express EML4-ALK V1. Although these cell lines are not isogenic, this difference in morphology was shown to be dependent on the EML4-ALK variant as it was lost upon EML4-ALK depletion (O'Regan *et al.*, 2020). To investigate whether chemical inhibition of Eg5 affected cell length in these cells, they were embedded into collagen, allowed to spread for 24 hours and then treated with DMSO or the Eg5 inhibitors as previously described. After 1 hour, cells were placed on the PhaseFocus Liveocyte 2 system for live cell imaging and cell length measurements taken as described before. Measurements taken confirmed a striking difference between the lengths of H3122 (V1) and H2228 (V3) cells in the absence of drug treatment with the difference between the means for these groups being approximately 60 μm (means = 21.43 μm for H3122 cells and 80.47 μm for H2228 cells). Treatment with each one of the three Eg5 inhibitors had no effect on the length of H3122 (V1) cells (Figure 4.5A). However, consistent with data from BEAS-2B:EML4-ALK V3 cells, treatment with the Eg5 inhibitors, filanesib and BRD9876, significantly reduced the length of H2228 cells by approximately 20 μm (Figure 4.5B). Again, there was a notable reduction in cell length upon treatment of H2228 cells with STLC although this was below the level of significance (Figure 4.5B).

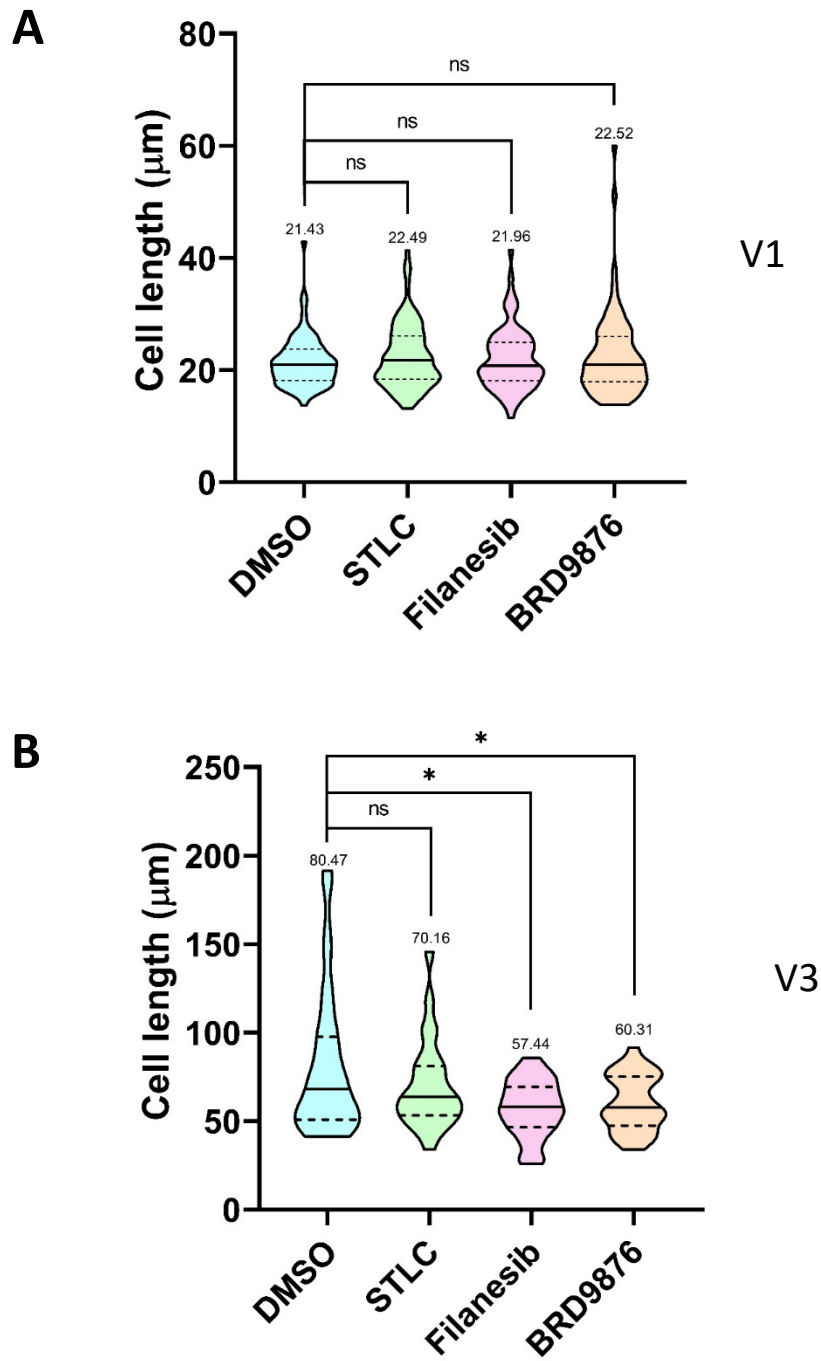


Figure 4.5. The length of H2228 (V3) cells is significantly reduced by Eg5 inhibitors filanesib and BRD9876. Cell length measurements were taken in Fiji from H3122 (A) and H2228 (B) cells treated with different Eg5 inhibitors or DMSO. Violin plots show the median (solid line) and quartiles (dotted lines) for each group. Numbers written above the violins represent the mean for each group. N = 77, 81, 68, 79 for H3122 cells and N = 33, 25, 43 and 30 H2228 cells respective to the order of groups on the graphs. Data presented is from three independent experiments.

4.2.3. Eg5 inhibitors did not alter migration of EML4-ALK V3 cells embedded in collagen

Next, we sought to investigate whether the recruitment of Eg5 to interphase microtubules in cells expressing EML4-ALK V3 was also contributing to changes in their migration using a single cell tracking assay. BEAS-2B:EML4-ALK V1 and V3 cells were induced with doxycycline for 24 hours before being detached and embedded into collagen matrix. Doxycycline was then also added to the matrix for a further 24 hours whilst the cells spread and began to migrate within the collagen to ensure continued production of the EML4-ALK protein. After a further 24 hours, cells were treated with Eg5 inhibitors and live imaging performed on three non-overlapping areas per treatment with images captured every 15 minutes for 24 hours. Images were compiled into videos in Fiji and individual cell tracking analysis performed using Imaris software. Briefly, a spot was placed in the centre of each cell and the movement of the spots tracked throughout the time-course of the video. Data was obtained for average distance travelled between time points, mean speed of movement and directionality. Cells were tracked for 24 hours or until they entered mitosis.

In line with published data, BEAS-2B cells expressing EML4-ALK V3 exhibited enhanced migration using this assay travelling further and faster than BEAS-2B cells expressing EML4-ALK V1 (Figure 4.6A&B) (O'Regan *et al.*, 2020). However, in contrast to previous work, the movement of V3 cells was also seen to be more directional (0.4241) than V1 cells (0.3019) in these experiments (Figure 4.6C). Directionality measurements are obtained by displacement/distance, therefore the closer the value is to 1, the more directional the movement is. In contrast, if the directionality value is closer to 0, the movement of the cell is more random. This finding could be due to these cells being embedded in collagen, whereas in the previous study cells were directly plated into 6 well plates. Interestingly though, none of the Eg5 inhibitors had a significant effect on distance, speed or directionality of BEAS-2B:EML4-ALK V3 cells (Figure 4.7A-C). In contrast, filanesib led to an increase in both distance travelled and speed of migration in BEAS-2B cells expressing EML4-ALK V1 and BRD9876 was seen to decrease distance travelled (Figure 4.7D&E). No differences in distance or speed were seen in cells treated with STLC. The directionality of movement of BEAS-2B cells expressing EML4-ALK V1 was modestly affected by filanesib,

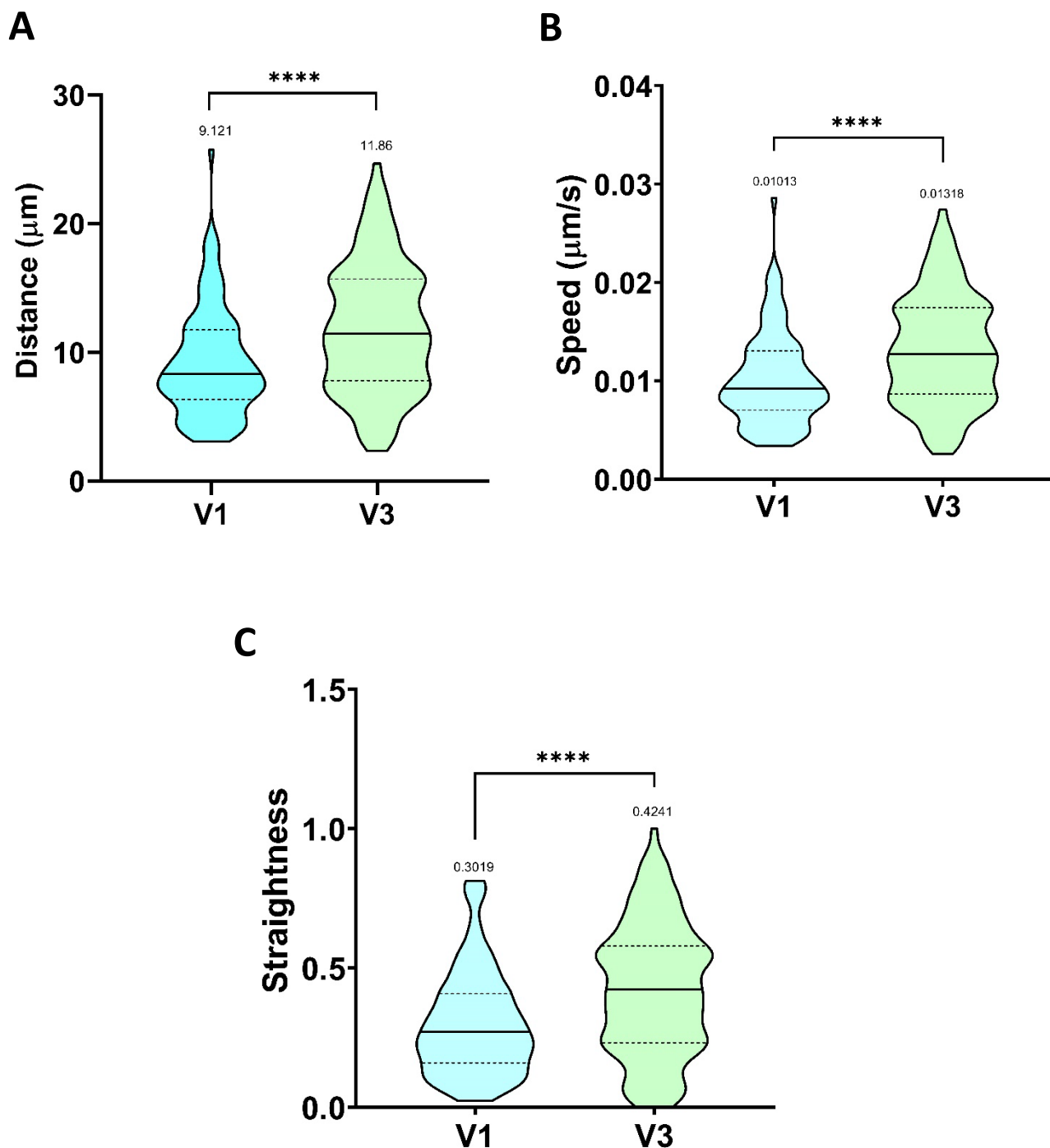
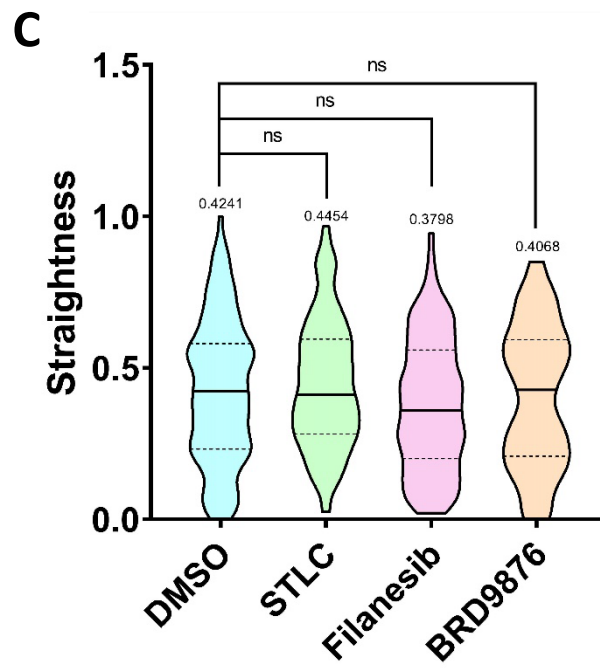
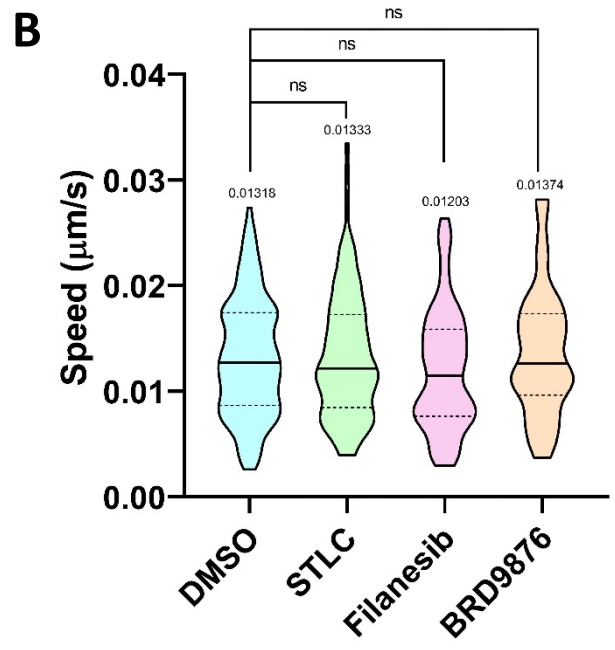
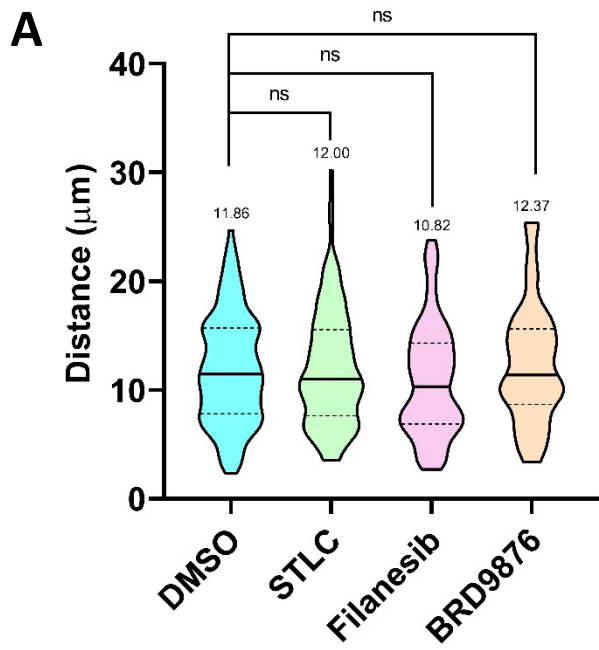


Figure 4.6. BEAS-2B:EML4-ALK V3 cells travel further and faster than V1 cells. Induced cells were embedded into collagen and live cell imaging was performed. Measurements were taken for average distance between time points (A), speed (B) and directionality (C). Graphs represent three independent experiments and show the spread of data, median (solid line), quartiles (dotted lines) and means are written above each violin. N = 100 and 115 cells respective to the order of groups on the graphs.



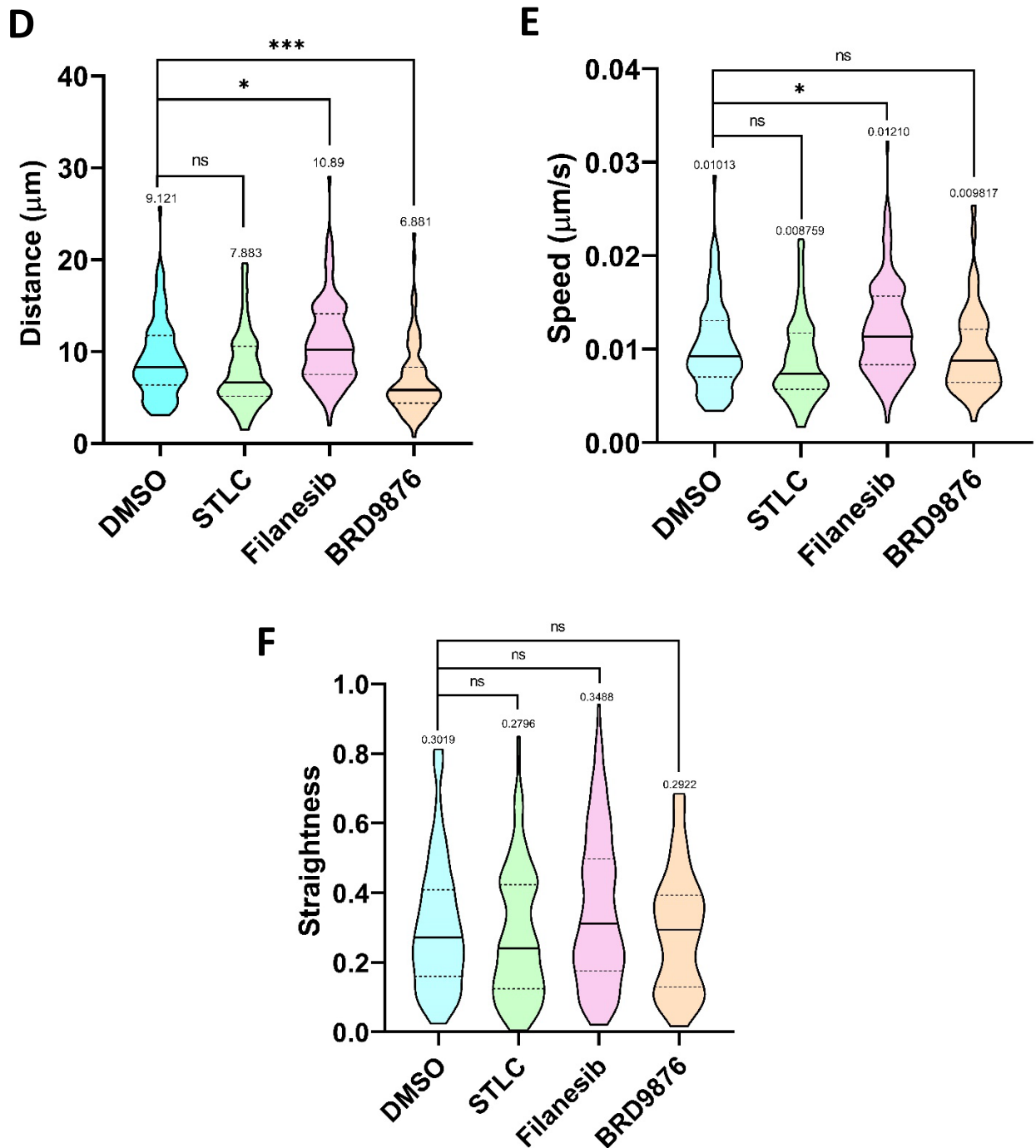


Figure 4.7. Eg5 inhibitors have no effect on migration of BEAS-2B:EML4-ALK V3 cells. Induced cells were treated with the indicated Eg5 inhibitors before live cell imaging was performed for 24 hours. Measurements taken from V3 were average distance travelled between time points (A), speed (B) and directionality (C). The same measurements were also taken from V1 cells (D, E and F respectively). Graphs show the spread of the data, median (solid lines), quartiles (dotted lines) and means for each group are written above each violin. Graphs representative of three independent experiments. N= 115, 111, 92, 62 for V3 cells and N= 100, 128, 125, 52 for V1 cells, respective to the order of groups on the graphs.

albeit not to a level of significance, and was not affected by either of the other Eg5 inhibitors (Figure 4.7F).

To determine whether Eg5 was contributing to differences in cell migration of the NSCLC patient cell lines, H3122 (V1) and H2228 (V3), single cell tracking analysis was performed as described above in the presence of the different Eg5 inhibitors. Specifically, cells were embedded into collagen as before and allowed to spread for 24 hours. Eg5 inhibitors were then added to the embedded cells and three non-overlapping areas per treatment imaged every 15 minutes for 24 hours. Cells were again tracked for 24 hours or until mitotic entry. Unfortunately, due to the cobblestone appearance of H3122 cells, it was difficult to distinguish mitotically arrested cells from interphase cells and for this reason, quantification of migration in the H3122 cell line was not performed. In contrast, it was easy to distinguish the more elongated H2228 cells and tracks for these were quantified. Interestingly, single cell tracking analysis revealed that, while the L5 inhibitors, STLC and filanesib, had no effect on any of the migration parameters, the rigor inhibitor, BRD9876, reduced both the average distance travelled and mean speed of movement of H2228 cells (Figure 4.8A & B). However, BRD9876 did not affect the directionality of movement of H2228 cells (Figure 4.8C).

Taken together, these data suggest that the motor activity of Eg5 is not required for the increased rate of cell migration observed in EML4-ALK V3 expressing cells. The fact that the rigor inhibitor, BRD9876, was seen to reduce migration distance and speed (but not directionality) in H2228 cells may reflect its different role on microtubule properties.

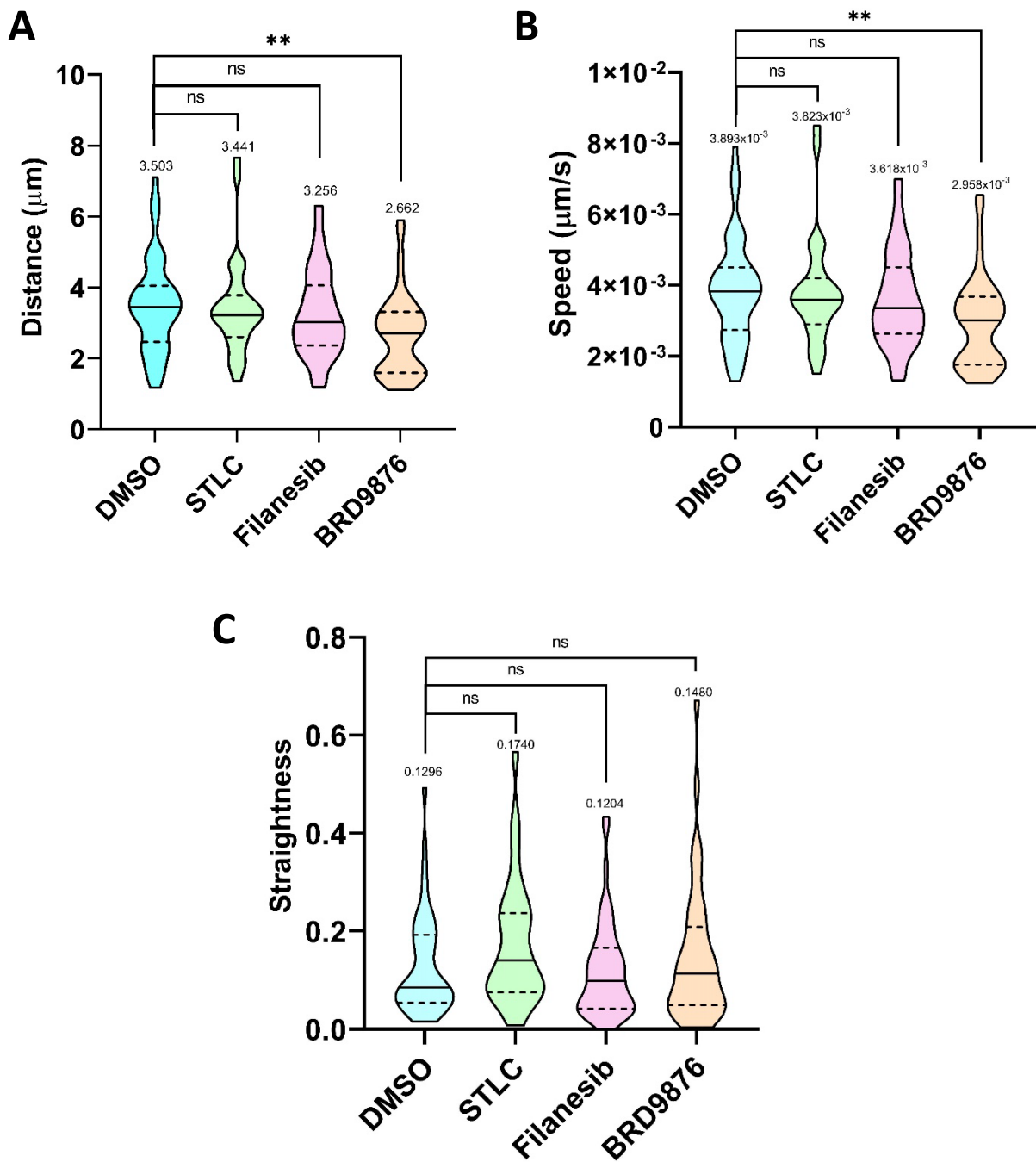


Figure 4.8. BRD9876 reduced distance and speed of migration in H2228 cells. Cells were treated with the indicated Eg5 inhibitors and live cell imaging was performed for 24 hours. Measurements were taken for the average distance travelled between time points (A), mean speed of movement (B) and directionality (C). Graphs represent three independent experiments and show the spread of data, median (solid lines), quartiles (dotted lines) and means for each group are written above each violin. N= 48, 29, 50 and 42 cells respective to the order of groups on the graphs.

4.2.4. NEK7 phosphorylation of Eg5 on S1033 regulates cell length

It has previously been shown that NEK7 phosphorylation of Eg5 on S1033 regulates dendrite length in neurons (Freixo *et al.*, 2018). Given our data indicating that phosphorylation of Eg5 at S1033 regulates its recruitment to microtubules and that Eg5 inhibition reduces the length of cells expressing EML4-ALK V3, we sought to determine if this phosphorylation event also regulated the length of these V3 expressing cells. For this, BEAS-2B:EML4-ALK V1 and V3 cell lines were seeded onto collagen coated coverslips and induced for 48 hours before being transfected with FLAG-tagged Eg5 constructs for 24 hours. Specifically, V1 cells were transfected with WT or the S1033D phosphomimetic mutant, while V3 cells were transfected with WT or the S1033A phosphonull mutant. Transfection into the different cell lines was confirmed by Western blot, which revealed bands at the predicted molecular weight of 120 kDa (Figure 3.10A).

Cells transfected as above were then stained using a FLAG antibody to allow identification of transfected cells and images captured using a VisiTech Infinity 3 confocal microscope. Cell lengths were then measured in Fiji. Strikingly, BEAS-2B cells expressing EML4-ALK V1 were significantly longer when transfected with the phosphomimetic Eg5-S1033D mutant than those transfected with WT Eg5. By contrast, cells expressing EML4-ALK V3 were significantly shorter when transfected with the phosphonull Eg5-S1033A mutant than those transfected with WT Eg5 (Figure 4.9A&B). Hence, we conclude that phosphorylation of Eg5 at S1033 causes an increase in cell length in isogenic cell lines expressing EML4-ALK variants.

To add further evidence that it is NEK7 phosphorylation of Eg5 on S1033 that is regulating cell length in cells expressing EML4-ALK V3, NEK7 was depleted from BEAS-2B:EML4-ALK V3 cells before these cells were transfected with the S1033D or S1033A Eg5 constructs. The intention was to see whether either construct could reverse the decrease in cell length observed upon depletion of NEK7. This would also prevent phosphorylation of the endogenous Eg5 protein by NEK7. For this, BEAS-2B:EML4-ALK V3 cells were seeded onto collagen coated coverslips and induced for 24 hours before being depleted of NEK7 for 48 hours. siNEK7_b was chosen for this transfection as it was deemed the more effective of the

two siRNAs described in chapter 3. After depletion, cells were transfected with the Eg5 constructs for a further 24 hours. Cells were then fixed, stained with FLAG and α -tubulin antibodies and imaged. As expected, NEK7 depletion reduced the length of cells expressing V3 when compared to cells depleted with siGAPDH control oligonucleotides. Strikingly, when these NEK7 depleted cells were transfected with the phosphomimetic Eg5-S1033D protein, the length of cells was restored to a level similar to control depleted cells. However, this was not the case when NEK7 depleted cells were transfected with the phosphonull Eg5-S1033A mutant (Figure 4.10A&B). Many cells transfected with Eg5-S1033D had a very long and thin appearance with some having very long protrusions. On the other hand, cells transfected with S1033A were very short, many cells being notably smaller than untransfected NEK7 depleted cells. Taken together, these experiments provide persuasive evidence that NEK7 phosphorylation of S1033 contributes to the change in morphology of cells expressing EML4-ALK V3 expressing cells.

4.2.5. NEK7 depletion reduces microtubule stability of EML4-ALK V3 cells

Another phenotypic change exhibited by EML4-ALK V3 expressing cells is an increase in microtubule stability, as indicated by an increase in the intensity of acetylated tubulin on the microtubule network (O'Regan *et al.*, 2020; Sampson *et al.*, 2022). To determine whether the NEK9-NEK7 signalling module was contributing to microtubule stabilisation in V3 expressing cells, NEK7 depletions were performed. BEAS-2B:EML4-ALK V3 cells were induced for 24 hours before being depleted of NEK7 or GAPDH for 72 hours. Western blotting confirmed successful depletion of these proteins (Figure 3.8A). Using the same induction and depletion protocol, cells were fixed and stained for immunofluorescence microscopy with an antibody against acetylated tubulin. Images comprising of 40 z-sections were taken. In Fiji, a sum slice projection was performed where the intensity values from each of the 40 z-sections were added together. Cells were analysed as described in section 2.2.5.3. Briefly, measurements were taken for the cell area, mean intensity value and integrated density (total intensity value). The same measurements were also taken for a background area to allow correction for background fluorescence. Acetylated tubulin intensity was significantly reduced in V3 cells depleted of NEK7 with both NEK7 siRNAs as

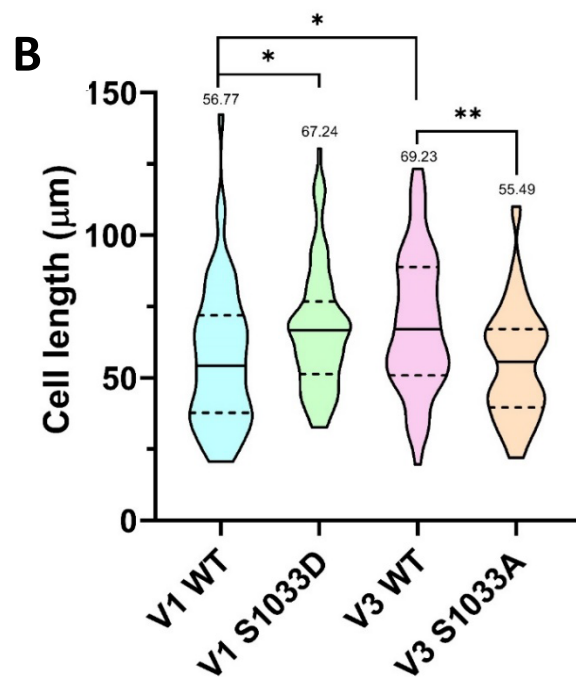
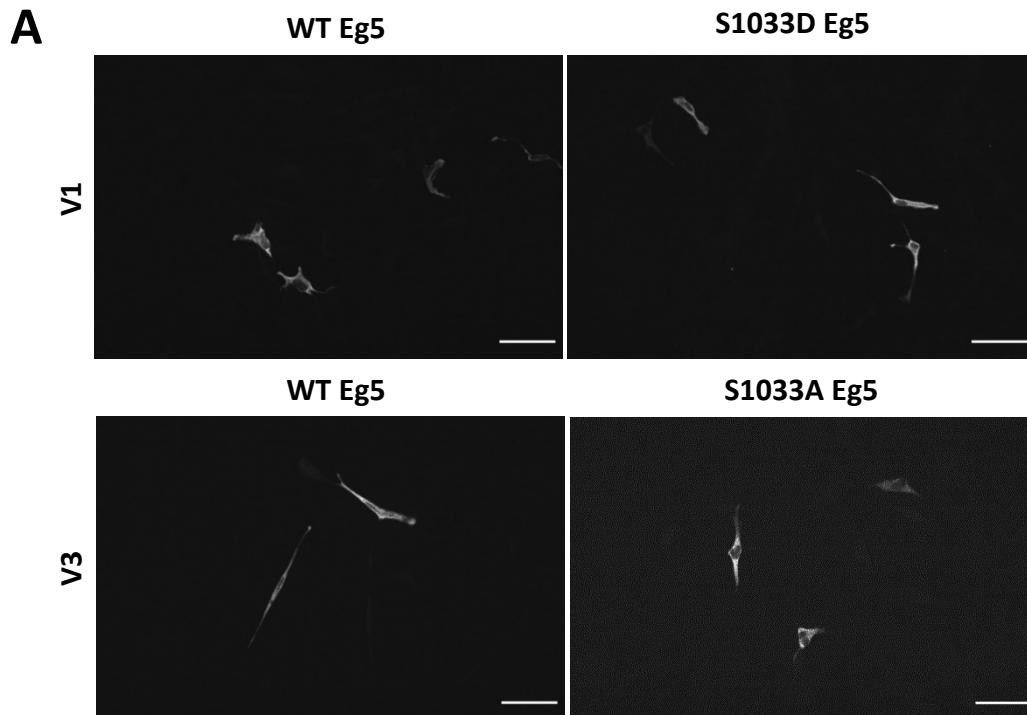


Figure 4.9. Phosphorylation of Eg5 on S1033 regulates cell length of BEAS-2B cells. (A) FLAG-tagged WT or S1033D Eg5 were transiently transfected into BEAS-2B:EML4-ALK V1 cells and WT or S1033A Eg5 transfected into V3 cells. Cells were stained with a FLAG antibody to allow detection of transfected cells. Scale bars = 50 μm . (B) Cell lengths of transfected cells were measured in Fiji. N=60; 79; 60 and 60 cells respective to the order of groups on the graph. Violin plot shows spread of data, median (solid line), quartiles (dotted lines) and means are written above each group. Data presented is representative of three independent experiments.

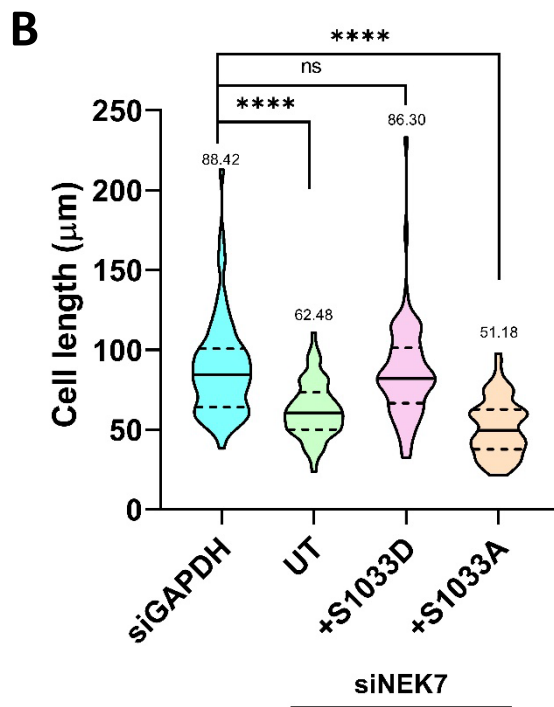
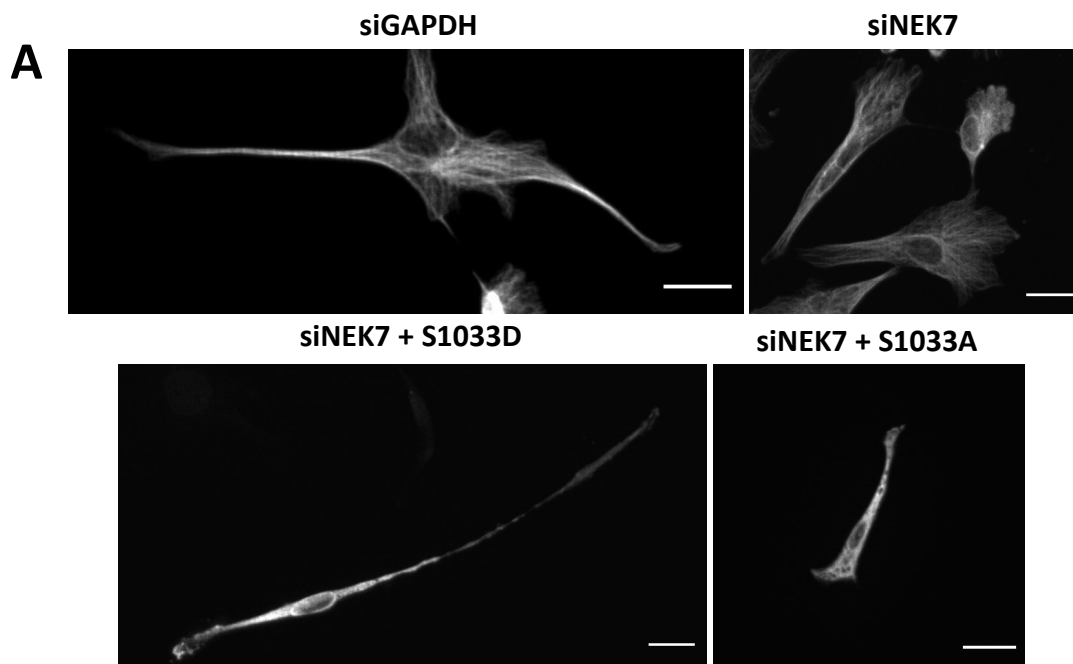


Figure 4.10. S1033D Eg5 rescues the length of BEAS-2B V3 cells after NEK7 depletion. (A) Cells were depleted of NEK7 or GAPDH. S1033D or S1033A Eg5 were transfected into NEK7 depleted cells. FLAG staining allowed detection of transfected cells and α -tubulin staining was used to image non-transfected but depleted cells. Scale bars = 20 μm . (B) Cells lengths were measured for each condition. N = 70, 66, 68 and 70 cells respective to the order of groups on the graph. Violin plot shows spread of data, median (solid line), quartiles (dotted lines) and means are written above each group. Data presented is representative of three independent experiments.

compared to those depleted with the siGAPDH control (Figure 4.11A & B). Images shown in Figure 4.11A are maximum intensity projections representative of the described z stacks where brightness and contrast have not been adjusted.

This experiment was then performed in H2228 (V3) cells. NEK7 depletion was performed with the two NEK7 siRNAs but, as previously described, siNEK7_a proved inconsistent in depleting NEK7 in these cells. Hence, only one sample was analysed as opposed to the three repeats performed with the other siRNAs (Figure 3.9A). Depleted cells were imaged and 40 z-sections per image obtained and analysed as described above. This revealed a reduction in acetylated tubulin intensity in H2228 cells after NEK7 depletion with both NEK7 siRNAs as compared to the siGAPDH control sample (Figure 4.12A&B).

Taken together, the reduction of acetylated tubulin intensity after NEK7 depletion in both BEAS-2B:EML4-ALK V3 cells and H2228 cells strongly suggests that microtubule stabilisation occurs downstream of NEK7.

4.2.6. It is unclear whether microtubule stability is regulated by phosphorylation of Eg5

Following the observation that microtubule stability is increased in cells expressing EML4-ALK V3 downstream of NEK7, we sought to investigate whether Eg5 was contributing to this phenotype. For this, NEK7 was depleted from BEAS-2B:EML4-ALK V3 cells as previously described. The phosphomimetic (S1033D) and phosphonull (S1033A) Eg5 mutants were then transfected into the NEK7 depleted cells before immunofluorescence microscopy analysis with acetylated tubulin and FLAG antibodies. Images were captured as before and fluorescence intensity of acetylated tubulin measured in Fiji.

Consistent with previous data, NEK7 depleted cells were seen to have lower intensities of acetylated tubulin than GAPDH depleted cells. However, transfection with neither the S1033D nor the S1033A Eg5 construct was able to rescue the intensity of acetylated tubulin

in NEK7 depleted cells as measured using the previously described method (Figure 4.13A & B). Cells transfected with the different Eg5 mutants have quite different morphologies though and this led us to question whether measuring fluorescence intensity from images of cells with large morphological differences was appropriate. The formula used to calculate the corrected fluorescence intensity (given in section 2.2.5.3) does take into account cell area when subtracting background fluorescence measurements. Nonetheless, we decided to directly measure cell area and surprisingly found that NEK7 depleted cells transfected with the phosphonull Eg5-S1033A had a significantly reduced mean area compared to either GAPDH depleted cells or NEK7 depleted cells that were untransfected or transfected with Eg5-S1033D (Figure 4.13C). Moreover, no significant difference was found in mean cell area between S1033D transfected cells and siGAPDH or siNEK7 control cells. Whether this has an impact on our measurements of acetylated tubulin intensity is difficult to know. Hence, taken together, these experiments still leave open the question of whether Eg5 is contributing to microtubule stability in EML4-ALK V3 expressing cells.

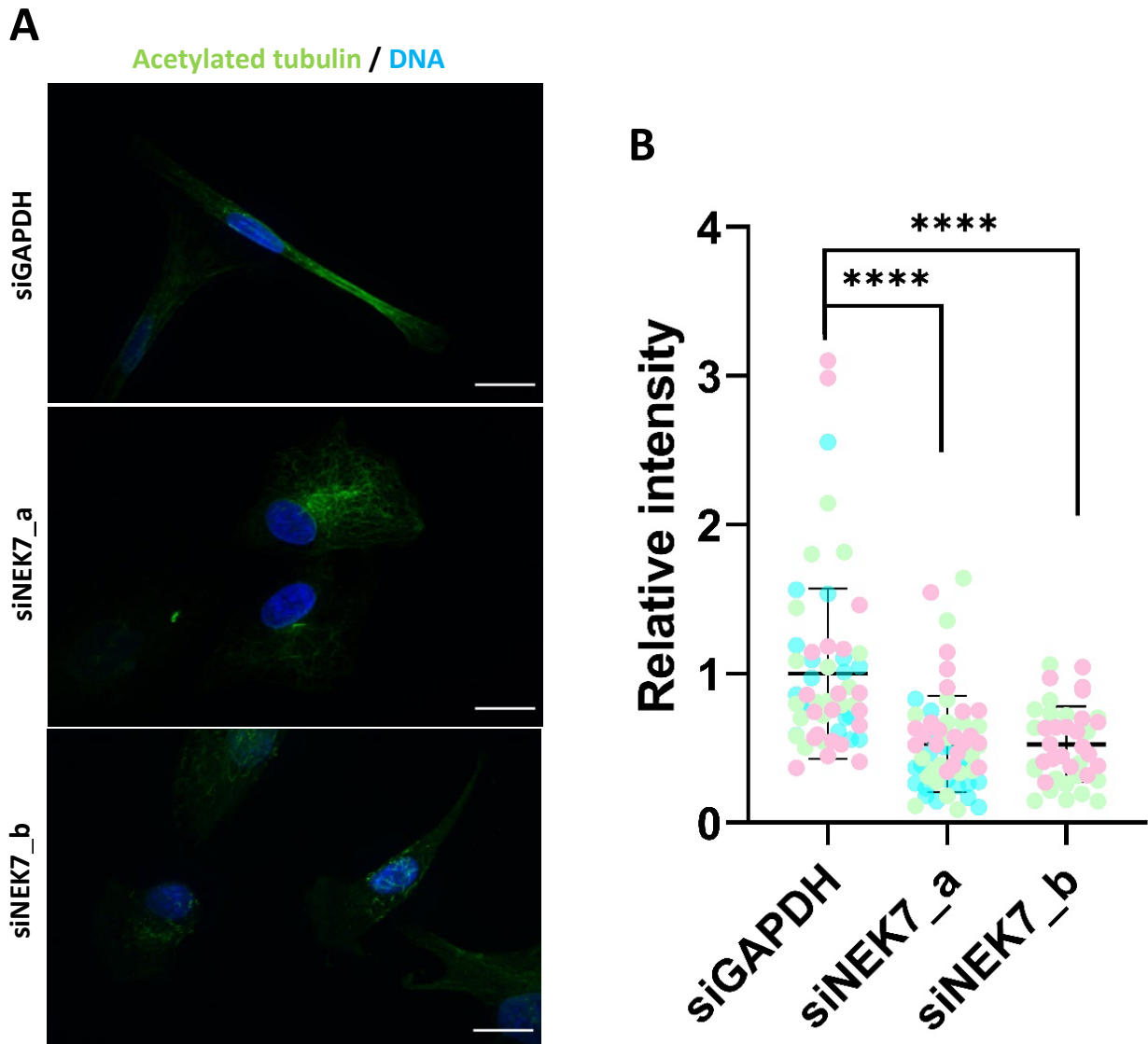


Figure 4.11. NEK7 depletion reduces acetylated tubulin intensity in BEAS-2B:EML4-ALK V3 cells.

(A) Cells were depleted of NEK7 or GAPDH, stained for acetylated tubulin (green) and DNA stained with Hoescht (blue) and imaged. Scale bars = 20 μ m. (B) Fluorescence intensity measurements were taken for the acetylated tubulin channel. Graph shows individual data points (one colour per repeat), means and standard deviations. Data is representative of three independent experiments for siGAPDH and siNEK7_a and two repeats for siNEK7_b. N= 59, 60 and 40 for the groups respective to their order on the graph.

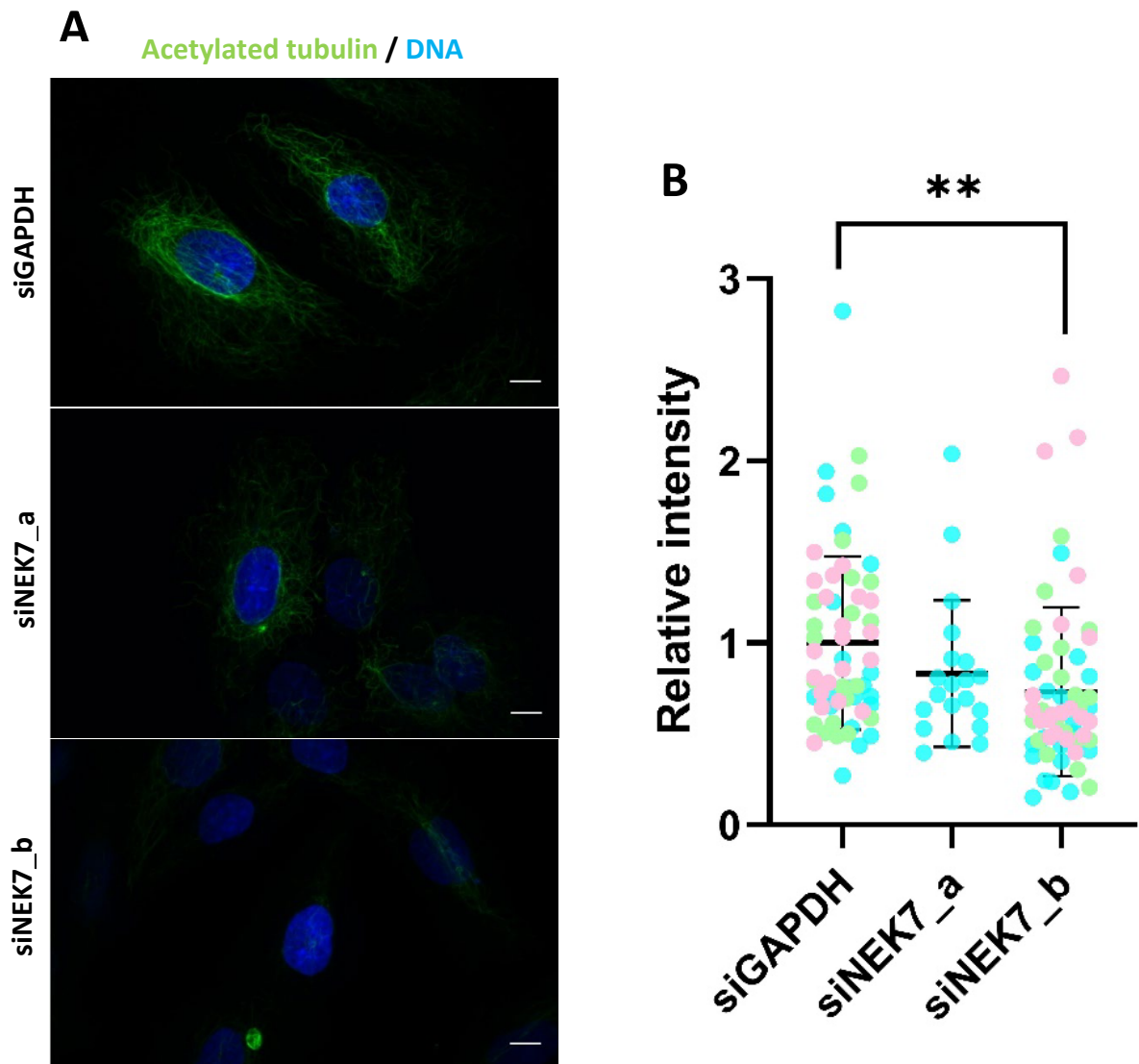
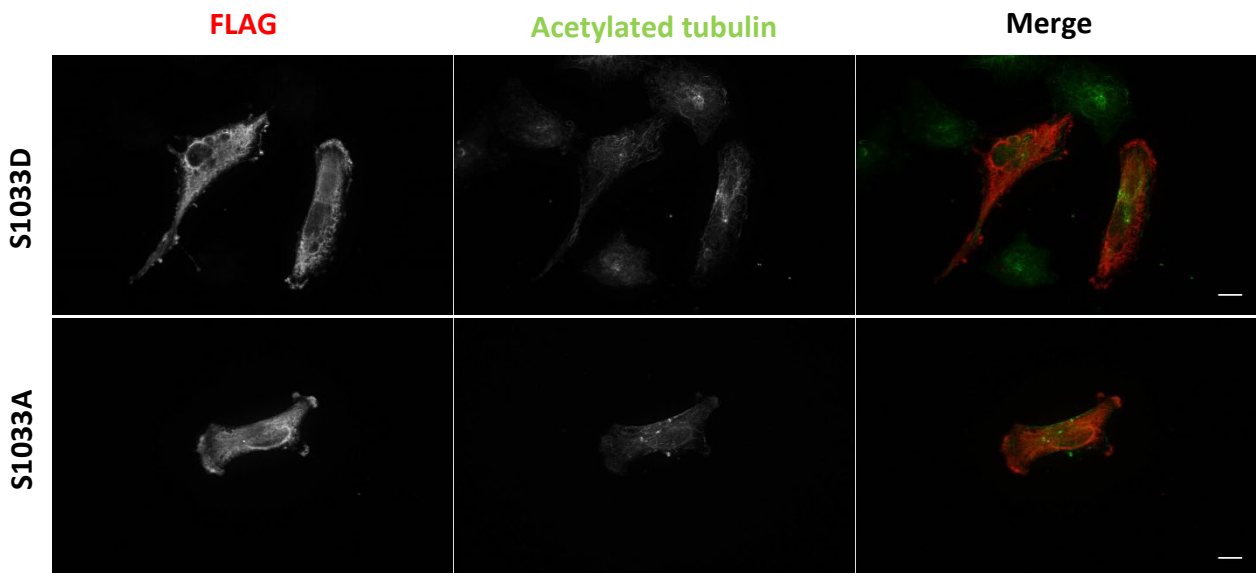
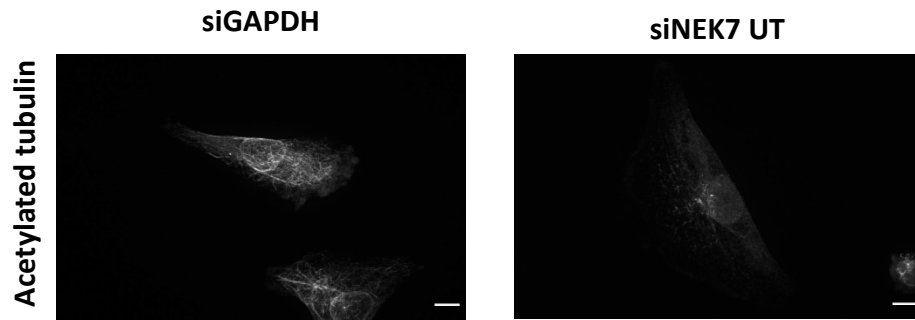


Figure 4.12. NEK7 depletion reduced acetylated tubulin intensity in H2228 (V3) cells. (A) Cells were depleted of either NEK7 or GAPDH and stained with antibodies against acetylated tubulin (green). DNA was stained using Hoescht (blue). Scale bars = 10 μ m. (B) Fiji was used to take fluorescence intensity measurements. Measurements were taken from three independent experiments for siGAPDH and siNEK7_b but only one repeat was achieved with siNEK7_a. Graphs show individual data points (one repeat per colour), means and standard deviations. N = 60, 20 and 60 for the groups respective to their order on the graph. No statistical analysis was performed to compare siGAPDH with siNEK7_a due to there being only one repeat.

A



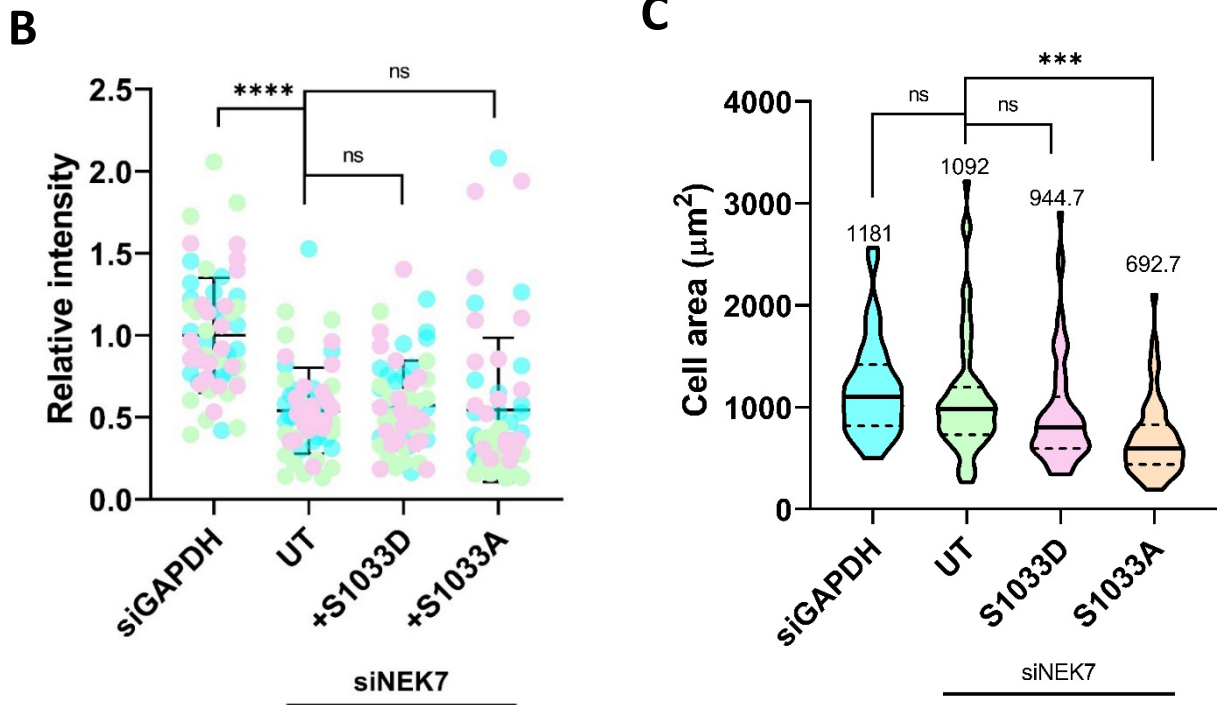


Figure 4.13. Eg5 phospho-mutants do not rescue acetylated tubulin intensity after NEK7 depletion.

(A) BEAS-2B:EML4-ALK V3 cells were depleted of NEK7 and transfected with the indicated constructs. Cells were stained with acetylated tubulin (green) and FLAG (red). siGAPDH and siNEK7 untransfected (UT) images have acetylated tubulin staining. Scale bars = 10 μm . (B) Acetylated tubulin intensity was measured from images represented in A. Graph shows individual data points, means and standard deviations. N= 60, 59, 60 and 58 cells respective to the order of groups on the graph. Data is collected from three independent experiments (one repeat per colour). (C) Cell areas were plotted for cells measured in B. Violin plots show median (solid line), quartiles (dotted lines) and means written above each group.

4.3. DISCUSSION

Clinical research suggests that patients with EML4-ALK V3 have worse outcomes than patients with other variants, including more rapid metastasis, poor response to current targeted treatments and lower survival rates (Christopoulos *et al.*, 2018). This is likely to be explained by EML4-ALK V3 promoting alternative or additional pathological processes in tumour cells. Consistent with this, it was found that in cells expressing EML4-ALK V3, the V3 protein itself as well as NEK9 and NEK7 were recruited to interphase microtubules and this coincided with an increase in microtubule stability, a change to a more mesenchymal-like cell morphology, and increased cell migration (O'Regan *et al.*, 2020). In the previous chapter, it was shown that Eg5, a mitotic kinesin, is also recruited in an untimely manner to microtubules in interphase EML4-ALK V3 cells, and that this was dependent on NEK7. In this chapter, I have used chemical inhibitors and mutant proteins to explore whether Eg5 is required for the three described phenotypic changes exhibited by EML4-ALK V3 cells.

Again, we have used the isogenic BEAS-2B bronchial epithelial cells that can be induced to express EML4-ALK V1 and V3, and NSCLC patient cells that contain the V1 or V3 oncogenic fusions. The patient cell lines have distinct morphologies making them suitable models for our investigations. H3122 cells appear round and cobblestone in appearance, whereas H2228 cells have a more elongated mesenchymal appearance that was shown to be dependent on EML4-ALK V3 expression (O'Regan *et al.*, 2020). The BEAS-2B cells on the other hand, appear mesenchymal in morphology when grown in 2D cultures including parental BEAS-2B cells (even without any EML4-ALK induction) (Han *et al.*, 2020). However, we found that, when induced, BEAS-2B:EML4-ALK V3 cells formed longer cytoplasmic protrusions than the V1 cell line if the cells were embedded in collagen making them suitable for these studies. As collagen embedding is a form of 3D cell culture, it is a step closer to the reality of a tumour microenvironment. All morphology and migration studies described here were therefore performed either with cells embedded into collagen or seeded onto collagen-coated coverslips.

To begin to explore whether Eg5 was having a role in promoting the change in V3 cell morphology, small molecule chemical inhibitors of the 'L5' (STLC and filanesib) and 'rigor' (BRD9876) categories were obtained. While both inhibitors interfere with the catalytic ATPase cycle of the motor domain, L5 inhibitors prevent microtubule binding, while rigor inhibitors lock the motor domain in a microtubule-bound state. Hence, both interfere with Eg5 function although through different molecular mechanisms. We found a significant reduction in the lengths of cells expressing V3 with both types of inhibitor in both of our BEAS-2B and NSCLC cell line models. In contrast, we found no change in the length of cells expressing V1. This indicates that Eg5 is indeed involved in the morphological changes in V3 cells that are observed downstream of the EML4-ALK V3:NEK9:NEK7 signalling module. This is consistent with the discovery that the morphological changes observed in V3 expressing cells are microtubule dependent (O'Regan *et al.*, 2020). The fact that both kinds of inhibitor resulted in a reduction in cell length suggests that the motor activity of Eg5 is required for cell elongation and that its presence on interphase microtubules alone simply is not enough. In mitosis, the Eg5 tetramer crosslinks adjacent microtubules and promotes anti-parallel sliding to enable assembly of a bipolar spindle. However, Eg5 can also act as a microtubule polymerase when Eg5 tetramers that "walk" towards the plus ends stabilise interactions between incoming tubulin dimers and the pre-formed protofilaments (Chen and Hancock, 2015; Chen *et al.*, 2019). Whether it is the microtubule crosslinking or polymerase activity of Eg5 that is responsible for the cell morphology changes remains to be determined, although this could potentially be addressed by measuring the rate of microtubule polymerization in these cells.

Cancer cells often utilise normal cellular mechanisms to their advantage (Thiery, 2002). Indeed, the binding of Eg5 to microtubules in non-mitotic cells has been shown to contribute to the extension of neuronal dendrites and that this requires its phosphorylation by NEK7 on S1033 (Freixo *et al.*, 2018). We therefore investigated whether this mechanism of Eg5 regulation might be important in cells expressing EML4-ALK V3. Strikingly, we found that an Eg5-S1033D - but not Eg5-S1033A - mutant could restore the elongated length of cells expressing V3 but that had been depleted of NEK7. Mutation from serine to aspartic acid mimics phosphorylation of the serine residue as it essentially has a similar charge and

structure, while its mutation to an alanine prevents phosphorylation. The fact that the S1033D 'phosphomimetic' mutant could rescue the cell length but the S1033A 'phosphonull' mutant did not, suggests that phosphorylation of this residue in Eg5 is necessary to regulate cell length. It has been demonstrated that phosphorylation of S1033 by NEK7 supports recruitment of Eg5 to centrosomes in mitosis (Bertran *et al.*, 2011). Hence, based on our demonstration in Chapter 3 that the Eg5-S1033D protein associated with microtubules, we propose that activation of NEK7 in interphase by EML4-ALK V3 leads to phosphorylation of Eg5 at S1033, which in turn promotes not only its microtubule binding but also altered cell morphology.

Eg5 has previously been implicated in regulating the speed and direction of neuronal cell migration (Falnikar *et al.*, 2011; Nadar *et al.*, 2008). Furthermore, Eg5 inhibition has been shown to reduce cell migration of pancreatic cancer cells (Sun *et al.*, 2011). Using single cell tracking, we therefore sought to investigate whether inhibition of Eg5 would block the accelerated rate of migration of V3 cells. Interestingly, a reduction in migration distance and speed was found in H2228 cells that were treated with BRD9876, but not with the L5 inhibitors. However, a significant reduction was not observed when the BEAS-2B:EML4-ALK V3 cell line was treated with BRD9876. On one hand, it is possible that the effect may have simply been smaller in the BEAS-2B V3 cells; equally this result may have been specific to the H2228 cell line. Furthermore, filanesib was seen to increase the distance and speed of migration of BEAS-2B:EML4-ALK V1 cells. These findings suggest that Eg5 is either not involved or at least does not play a central role in the accelerated migration of cells expressing EML4-ALK V3.

Nevertheless, microtubules are well documented to contribute to directional cell migration through intracellular transport of signalling molecules to the leading edge and focal adhesion turnover (Garcin and Straube, 2019; Etienne-Manneville, 2013). Here, we opted to perform single cell tracking assays as Eg5 inhibitors cause mitotic arrest and so tracking could be stopped when cells entered mitosis. It would be interesting to test the Eg5 inhibitors in an alternative cell migration assay, such as a Boyden-chamber style directional

migration assay. In the past, our lab has also performed wound healing assays to measure collective cell migration. However due to the inhibitors causing mitotic arrest, we deemed this approach to be inappropriate as cell confluency is a factor that must be tightly controlled during a wound healing assay. Nonetheless, it could be attempted for short time periods. It is also possible to investigate whether the phosphorylation of Eg5 on S1033 affects the migration of EML4-ALK V3 cells using stable cell lines that express both EML4-ALK V3 and either the S1033D or S1033A Eg5 mutants. As these mutants are not known to induce a strong mitotic arrest, then cell migration could be measured by wound healing or single cell tracking assays where distance, speed and directionality can be measured.

Previous experiments have shown that locking Eg5 onto interphase microtubules using rigor inhibitors increases microtubule stability (Chen *et al.*, 2017; Freixo *et al.*, 2018). Therefore, it was investigated whether phosphorylation of Eg5 on S1033 might also affect microtubule stability. Here, it was first demonstrated that, when NEK7 was depleted from V3 cell lines, microtubule acetylation – a marker of microtubule stability - is indeed reduced. This suggested that an effector downstream of NEK7 is contributing to microtubule stabilisation. We then transfected the Eg5 phosphomutants into NEK7 depleted cells to explore whether either mutant could rescue the phenotype. However, we found that neither S1033D nor S1033A Eg5 could increase microtubule stability. This may suggest that microtubule stabilisation is not solely regulated by recruitment of Eg5 to microtubules. Indeed, previous studies have only shown an increase in microtubule stability when cells are treated with rigor inhibitors. Hence, a measurable change in microtubule stabilisation may only be achieved when Eg5 is locked in an immobile state on microtubules. This could be investigated further in our cell lines by measuring acetylated tubulin intensity in cells treated with L5 or rigor inhibitors.

It should be added that the large differences in cell morphology between cells transfected with the different Eg5 phosphomutants made it difficult to interpret acetylated tubulin intensity data collected from our images. Therefore, future experiments could again make use of stable cell lines in which both EML4-ALK V3 and the Eg5 phosphomutants are

expressed. Acetylated tubulin intensity could then also be assessed by Western blotting to determine whether either phosphomutant rescues the acetylated tubulin intensity after NEK7 depletion, as this approach should not be dependent on cell morphology. An additional experiment that could be performed would be to explore whether acetylated tubulin intensities differed in EML4-ALK V3 cells that were treated with BRD9876 following either mock or NEK7 depletion. As the amount of Eg5 that is on the microtubules is less after NEK7 depletion, we might expect less Eg5 to be locked on by BRD9876. Therefore, it could be hypothesised that less of an increase in acetylated tubulin intensity would be seen in V3 cells depleted of NEK7 but treated with BRD9876 than in cells that were not depleted of NEK7 but still treated with BRD9876. However, this approach could be interpreted as reporting more on the ability of NEK7 to cause Eg5 recruitment to microtubules than on the effect of Eg5 on microtubule stability.

In conclusion, this chapter has shown that NEK7-dependent phosphorylation of Eg5 on S1033 regulates the length of cells expressing EML4-ALK V3. It has also demonstrated that the motor activity of Eg5 is required for cell elongation. It is therefore possible that Eg5 may contribute to metastasis in some ALK+ NSCLC tumours by means of promoting a mesenchymal cell morphology. EMT is a well-established tumour property and contributes not only to invasion but also to reattachment of circulating tumour cells at secondary metastatic sites (Boggs *et al.*, 2015). However, it seems unlikely from our data that Eg5 is solely responsible for the accelerated migration of EML4-ALK V3 cells and this is consistent with other data from our lab demonstrating additional substrates for NEK7 in these cells. Of particular interest, it would be interesting to perform cell viability assays using the different classes of Eg5 inhibitor either alone or in combination with ALK inhibitors to explore whether these could provide an effective treatment option for patients with EML4-ALK V3 cancers.

In the next chapter, further work on how microtubule organization may be altered in cells expressing EML4-ALK V3 will be described with the focus on a potential role of EML4-ALK V3 in microtubule nucleation from the centrosome.

CHAPTER 5

EML4-ALK V3 has a role at the centrosome independent of NEK7 and Eg5

5.1. INTRODUCTION

The centrosome is first and foremost a microtubule organising centre (MTOC) that is found in most animal cells. Responsible for nucleating microtubules, the centrosome is a key component of the mitotic spindle and is required for correct segregation of chromosomes and successful cell division (Fukasawa, 2005). After cytokinesis, each daughter cell only receives one centrosome, making centrosome replication necessary for subsequent cell cycle progression (Fukasawa, 2005). The centrosome normally only duplicates once per cell cycle, usually during S phase. However, in cancer cells, this normal biological process may become deregulated and centrosomes may duplicate more than once per cycle resulting in supernumerary centrosomes, also known as centrosome amplification (Fukasawa, 2005; Godinho and Pellman, 2014). Centrosome amplification may also be a result of cytokinesis failure (Fukasawa, 2005).

Centrosome amplification can be a problem for mitosis and cytokinesis and can result in chromosome segregation errors and aneuploidy through the formation of multipolar spindles (Fukasawa, 2005; Godinho and Pellman, 2014). Alternatively, cancer cells with amplified centrosomes will sometimes cluster centrosomes together to form a pseudo-bipolar spindle (Brinkley, 2001). Often, this results in merotelic attachment of chromosomes to spindle poles, which contributes to aneuploidy (Godinho and Pellman, 2014).

Consequently, centrosome amplification is thought to contribute to chromosome instability, one of the hallmarks of cancer (Fukasawa, 2005; Hanahan and Weinberg, 2011). Indeed, centrosome amplification has been observed in lung cancer-derived cell lines that express EML4-ALK V3, which also show an increase in mitotic errors such as multipolar spindle formation and misaligned chromosomes (Lucken *et al.*, 2022).

As mentioned, the principal purpose of the centrosome is to nucleate microtubules.

Although the process of microtubule nucleation is not completely clear, many studies have highlighted the importance of the γ -tubulin ring complex (γ TuRC) in this process (Job, Valiron and Oakley, 2003; Kollman *et al.*, 2010; Kollman *et al.*, 2011). Indeed, it is believed that the γ -TuRC acts as an anchor for a microtubule seed which is formed by several α/β -

tubulin heterodimeric molecules (Job, Valiron and Oakley, 2003). Interestingly, phosphorylation of the γ -TuRC may result in a conformational change that regulates microtubule nucleation (Thawani and Petry, 2021). Examples of such phosphorylation events include CDK1 mediated phosphorylation of GCP6 which leads to microtubule remodelling and GSK3 β phosphorylation of GCP5 which prohibits the localisation of the γ -TuRC to the centrosome (Oriolo *et al.*, 2007; Izumi *et al.*, 2008). In the case of EML4-ALK driven cancer, it has been shown that H2228 cells, which endogenously express EML4-ALK V3, have a greater microtubule nucleation capacity than H3122 cells that express EML4-ALK V1. Furthermore, the microtubule nucleation capacity of H2228, but not H3122, cells could be reduced with the ALK inhibitor, ceretinib (Sampson *et al.*, 2022). This suggests that ALK activity may promote microtubule nucleation in these cells, but exactly how ALK activity facilitates this is unclear.

Besides their role as an MTOC, centrosomes are recognised as signalling hubs with many components of intracellular signalling pathways, including tyrosine kinases such as Src family kinases, found at the centrosome (Arquint, Gabryjonczyk and Nigg, 2014; Ley *et al.*, 1994). To date, no studies have investigated whether EML4-ALK variants are localised to the centrosome, despite evidence of centrosome amplification and increased microtubule nucleation capacity in cells expressing EML4-ALK V3 (Lucken *et al.*, 2022; Sampson *et al.*, 2022).

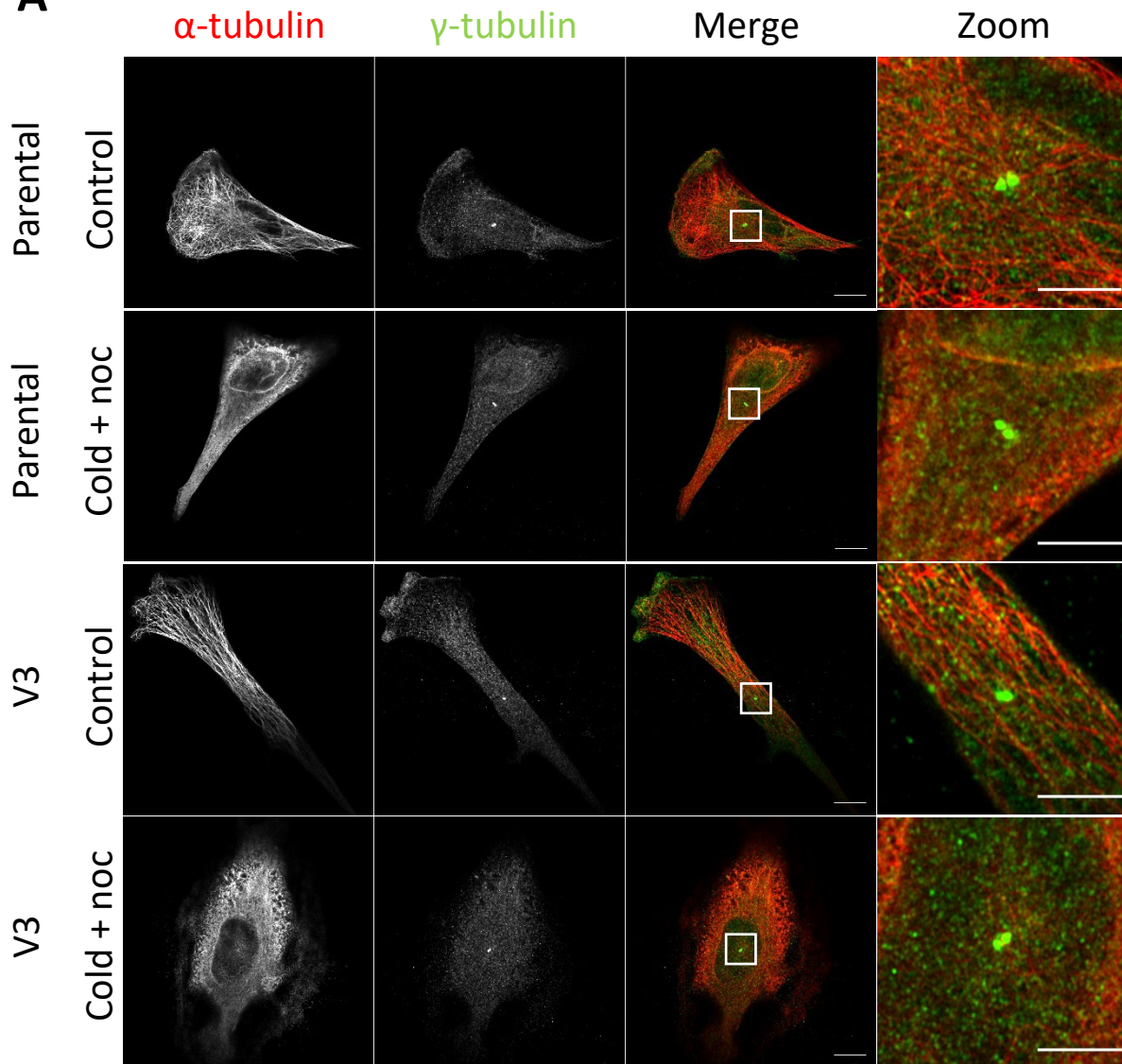
In this chapter, I describe experiments that have explored the localisation of EML4-ALK V3, as well as the downstream components NEK7 and Eg5, with respect to centrosomes, and investigated microtubule nucleation in cells expressing EML4-ALK V3.

5.2. RESULTS

5.2.1. EML4-ALK V3 localises to the centrosome in interphase BEAS-2B cells

Interesting data has recently been published that suggests the lung cancer patient cell line H2228 has an increased microtubule nucleation capacity in comparison to H3122 cells (Sampson *et al.*, 2022). From this, we were interested to deduce whether EML4-ALK V3 itself localises to the centrosome. To investigate this, we used BEAS-2B cells expressing EML4-ALK V3 and the parental BEAS-2B cell line for a control, as well as NSCLC patient cell lines H3122 (V1) and H2228 (V3). In order to accurately visualise whether EML4-ALK V3 localises to the centrosome, it was necessary to firstly depolymerise microtubules due to the known localisation of V3 on interphase microtubules (O'Regan *et al.*, 2020; Richards *et al.*, 2015). To do this, induced BEAS-2B cells and NSCLC cells were treated with 500 nM nocodazole on ice for 30 minutes, before being fixed for immunofluorescence microscopy. Staining with α -tubulin antibodies confirmed complete microtubule depolymerisation throughout the cytoplasm, while staining with γ -tubulin antibodies revealed the position of the centrosome in all cell lines. Clear microtubules were seen in control samples whereas no structures could be seen at all in the treated samples where α -tubulin staining appeared diffuse throughout the cytoplasm (Figure 5.1A&B).

Next, to investigate the localisation of EML4-ALK V3, antibodies against γ -tubulin were used to stain the centrosome and antibodies against ALK were used to stain the induced BEAS-2B cell lines that had been treated with nocodazole on ice. Strikingly, we found EML4-ALK V3 co-localised strongly with the centrosome in the BEAS-2B:EML4-ALK V3 cell line whilst no co-localisation was seen in the BEAS-2B parental cell line (Figure 5.2A). To quantify this finding, the PlotMultiColor4.3 Fiji macro was used as previously described, drawing a 12 μ m line that dissected both centrosomes and some of the surrounding cytoplasm. High Pearson's correlation coefficient values were obtained for the V3 cell line ($R= 0.8084$) suggesting strong co-localisation between the ALK and γ -tubulin channels. Lower Pearson's values ($R= 0.5117$) were obtained for control BEAS-2B parental cells, suggesting less co-localisation in these cells (Figure 5.2B).

A

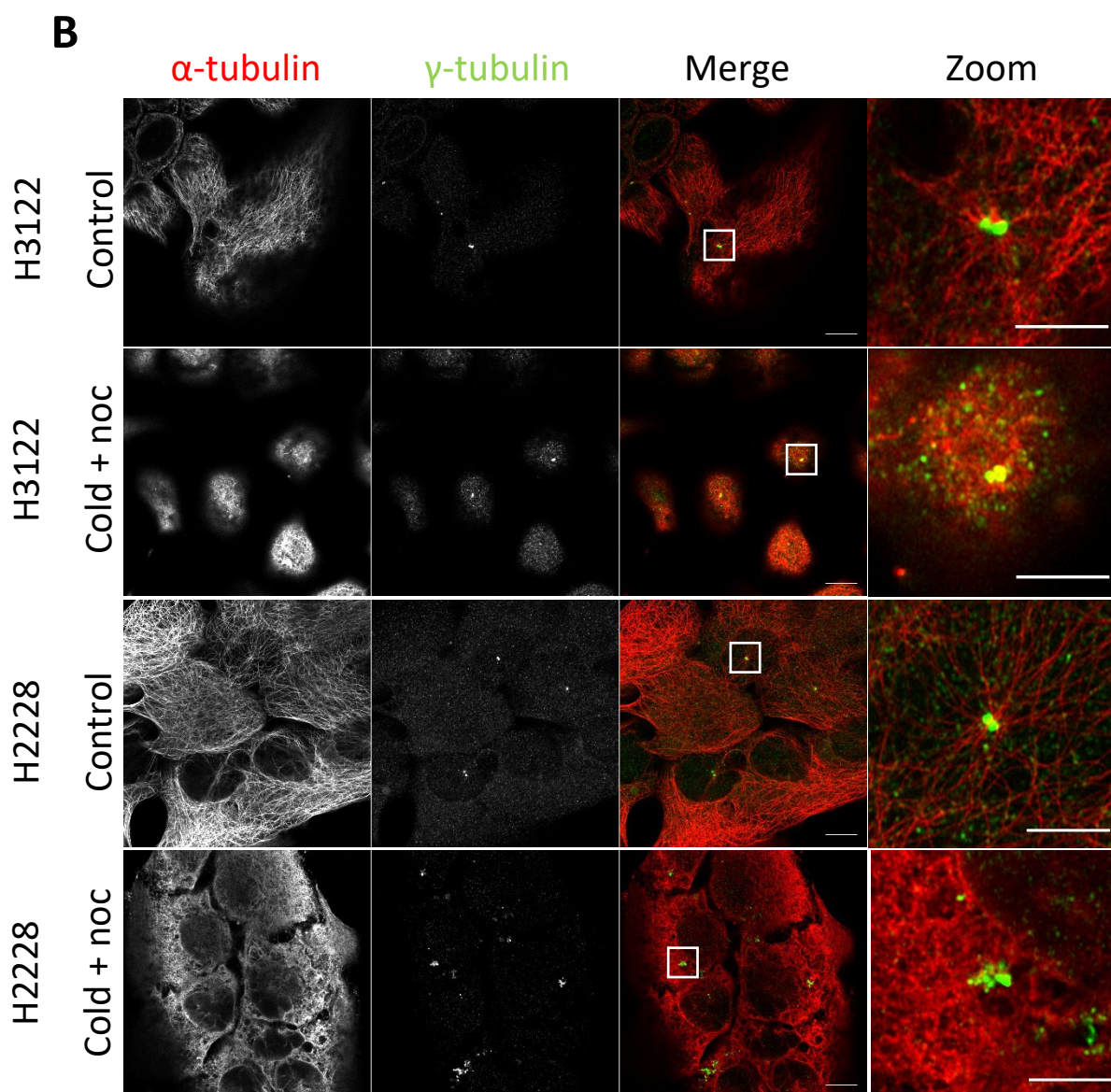


Figure 5.1. A combination nocodazole and cold treatment was performed in BEAS-2B and NSCLC cell lines. (A) Induced BEAS-2B cell lines were treated with nocodazole (noc) on ice for 30 minutes. Cells were stained with α -tubulin (red) and γ -tubulin (green). (B) NSCLC cell lines were treated and stained as described in A. White boxes show zoom region. Scale bars = 10 μ m in merges; 5 μ m in zooms. Images representative of three independent experiments.

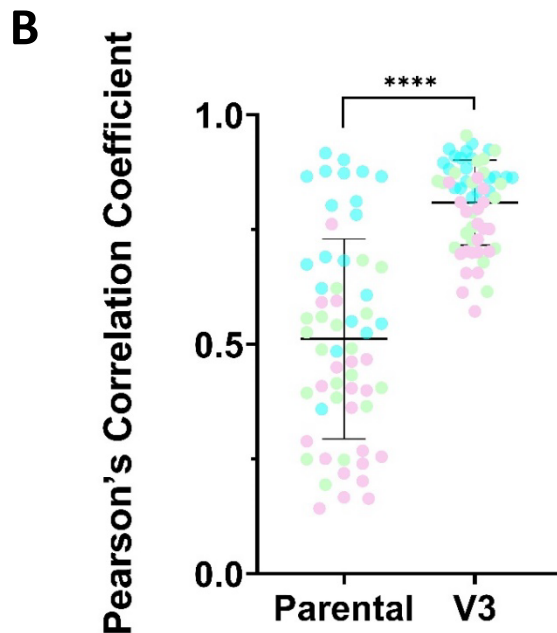
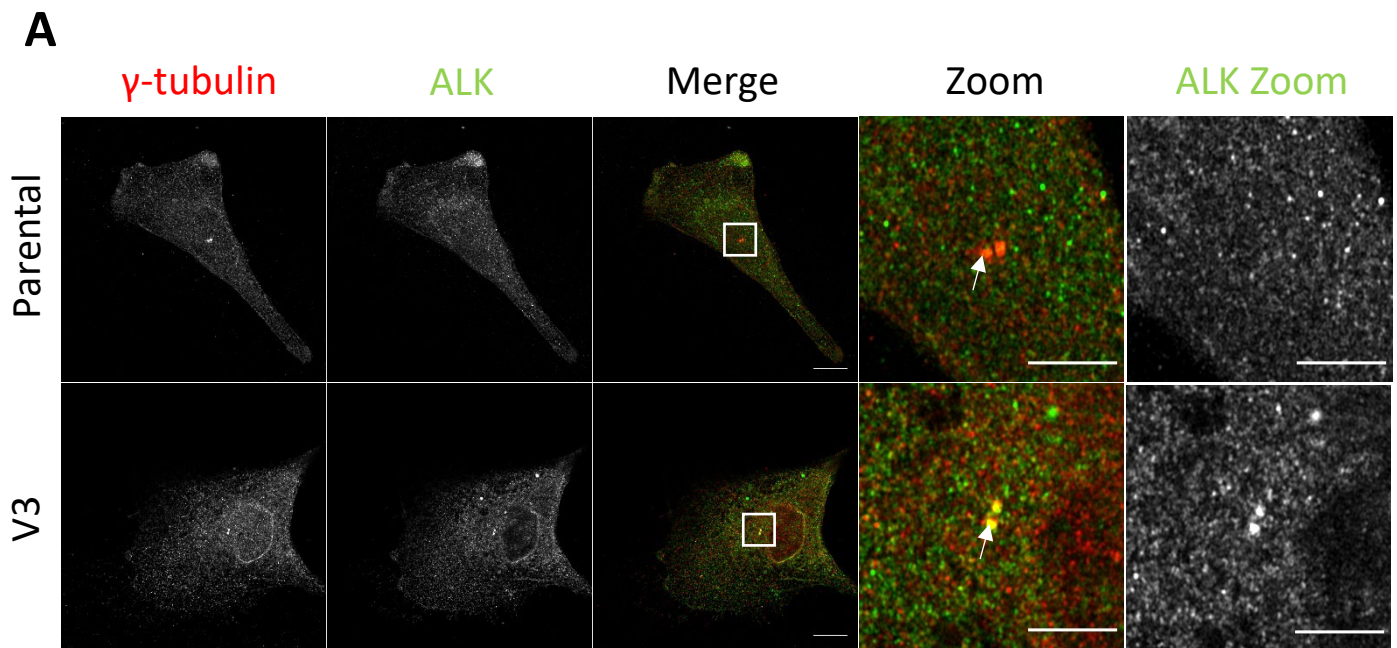


Figure 5.2. EML4-ALK V3 co-localises with the centrosome in BEAS-2B:EML4-ALK V3 cells. (A) Induced cells were treated with nocodazole on ice for 30 minutes before being stained with γ -tubulin (red) and ALK (green) antibodies. White boxes show zoom region. White arrows indicate an example of where Pearson's correlation was measured between the red and green channels. Scale bars = 10 μ m in merge; 5 μ m in zooms. (B) Co-localisation analysis was performed using the Fiji PlotMultiColor 4.3. macro for cells represented in A. Graph shows individual data points (one repeat per colour), means and standard deviations. Graph is representative of three independent experiments. N= 60 cells for both cell lines.

We also sought to investigate whether EML4-ALK V3 co-localised with the centrosome in the NSCLC cell line, H2228. H3122 cells expressing EML4-ALK V1 were used as a control. In order to do this, microtubules were firstly depolymerised as previously described before being fixed for immunofluorescence staining using ALK and γ -tubulin antibodies. In contrast to the induced BEAS-2B cells, we could not detect any major recruitment of either EML4-ALK variant to the centrosome in these cell lines (Figure 5.3A). Indeed, analysis using the PlotMultiColor4.3. Fiji macro revealed only weak correlation as indicated by low Pearson's values in both cell lines ($R= 0.3260$ for H3122 and $R= 0.3837$ for H2228) (Figure 5.3B). However, the Pearson's correlation coefficient was marginally higher in the H2228 than H3122 cell line which could suggest there is a minor increase of centrosome localisation of EML4-ALK V3 protein compared to EML4-ALK V1. This experiment could be repeated using an N-terminal EML4 rather than ALK antibody to stain the EML4-ALK variants to see if this reveals a similar small increase in recruitment of EML4-ALK V3 to the centrosome.

Taken together, these experiments have provided some evidence of EML4-ALK V3 being recruited to the centrosome, consistent with data that suggests EML4-ALK V3 increases microtubule nucleation in cells (Sampson *et al.*, 2022).

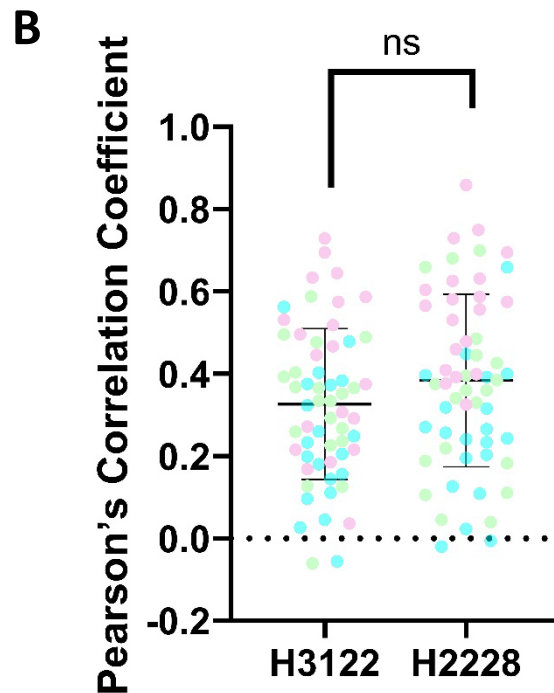
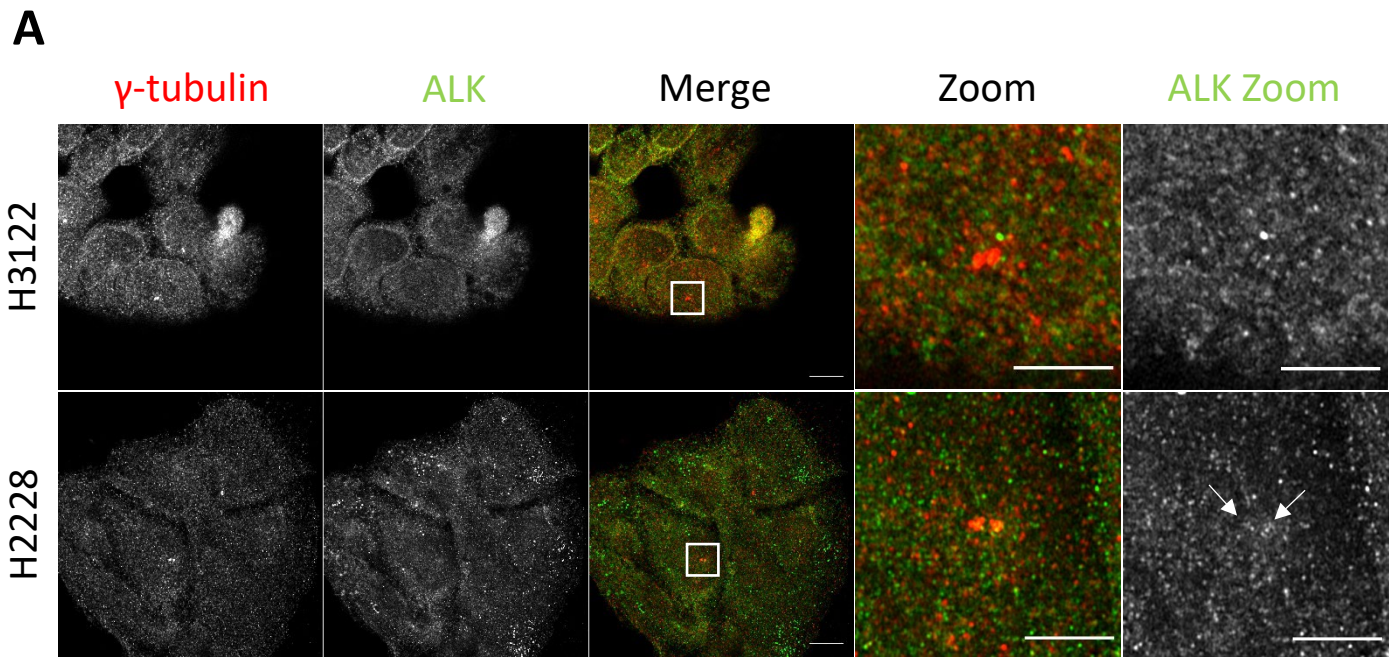


Figure 5.3. There is little recruitment of EML4-ALK variants to the centrosomes in NSCLC cell lines.

(A) Cells were treated with nocodazole on ice for 30 minutes before being fixed and stained with antibodies against γ -tubulin (red) and ALK (green). White boxes show zoom region. White arrows indicate minor recruitment of EML4-ALK V3. Scale bars = 10 μ m in merge; 5 μ m in zooms. (B) Co-localisation was analysed using the Fiji PlotMultiColor4.3. macro for cells represented in A. Graph shows individual data points (one repeat per colour), means and standard deviations. Graph represents three independent experiments. N= 60 cells for both cell lines.

5.2.2. Neither NEK7 nor Eg5 are recruited to centrosomes in BEAS-2B:EML4-ALK V3 cells

From previous published data and data presented in previous chapters of this thesis, our lab have established a novel signalling module: EML4-ALK V3:NEK9:NEK7:Eg5, all of which can be detected on interphase microtubules (O'Regan *et al.*, 2020). As we observed EML4-ALK V3 is recruited to the centrosomes in BEAS-2B cells (Figure 5.2), we also sought to investigate whether other members of this signalling module were present at the centrosomes in these cells.

Here, BEAS-2B:EML4-ALK V3 and parental cells were again treated with nocodazole on ice for 30 minutes to depolymerise microtubules, leaving centrosomes devoid of cytoplasmic microtubules clearly visible. To determine whether NEK7 also co-localised with the centrosome in these cells, antibodies against NEK7 were used to co-stain these cells with γ -tubulin antibodies. Imaging revealed no visible recruitment of NEK7 to interphase cell centrosomes, although staining for NEK7 in these cell lines was very weak, consistent with this protein being in low abundance in these cells (Figure 5.4A). Nevertheless, the Pearson's correlation coefficient was measured from the intensity profiles of images obtained and a weak correlation between NEK7 and γ -tubulin was detected in the EML4-ALK V3 cell line ($R=0.5212$) and a slightly stronger correlation in the parental cells ($R=0.6638$) (Figure 5.4B). Moreover, Pearson's values revealed significantly less NEK7 localised with the centrosomes in BEAS-2B:EML4-ALK V3 cells compared to the parental cell line, suggesting there is no active recruitment of NEK7 to the centrosomes in these cells downstream of EML4-ALK V3 (Figure 5.4B).

Likewise, similar experiments were performed to investigate whether Eg5 was recruited to centrosomes in parental BEAS-2B cells or BEAS-2B cells expressing EML4-ALK V3. Cells were treated as described above and stained with antibodies against Eg5 and γ -tubulin. Imaging revealed no visible recruitment of Eg5 to interphase centrosomes in either cell line (Figure 5.5A). Measuring the Pearson's correlation coefficients from these images revealed weak correlation between Eg5 and γ -tubulin in both cell lines ($R=0.5509$ for parental and $R=0.4470$ for V3), suggesting no significant difference in localisation between the cell lines

(Figure 5.5B). The correlation coefficients measured were significantly higher in the parental cell line compared to the V3 cell line, again suggesting there is no active recruitment of Eg5 to interphase centrosomes in BEAS-2B:EML4-ALK V3 cells.

Together, these findings suggest that any changes to centrosome biology or activity in EML4-ALK V3 expressing cells are most likely independent of the EML4-ALK V3:NEK9:NEK7:Eg5 signalling module. Consistent with this, published data suggests that the increased microtubule nucleation capacity of V3 cells is dependent on ALK activity (Sampson *et al.*, 2022), whereas changes in cell morphology and migration were shown to be independent of ALK activity and dependent on the EML4-ALK V3:NEK9:NEK7 signalling module (O'Regan *et al.*, 2020). Therefore, it is likely that these two pathways (ALK activity and the NEK9:NEK7 module) represent different signalling cascades which have different downstream targets and regulate different cellular processes.

5.2.3. EML4-ALK V3 expressing BEAS-2B cells have increased microtubule nucleation capacity

Research that showed cells expressing EML4-ALK V3 have an increased microtubule nucleation capacity were performed in NSCLC patient cell lines H2228 (V3) and H3122 (V1) (Sampson *et al.*, 2022). As previously discussed, as these are lung cancer cell lines, they also possess other genetic alterations in addition to the EML4-ALK variant they express. For this reason, we sought to determine if similar results on microtubule nucleation would be obtained in our isogenic BEAS-2B cell lines. In order to analyse microtubule nucleation capacity, induced cells firstly had their microtubules depolymerised as previously described. After 30 minutes of nocodazole and cold treatment, cells were quickly washed twice with pre-warmed media, to ensure complete removal of nocodazole. Cells were then incubated with pre-warmed media for either 1, 2, 5 or 10 minutes. The purpose of this time course experiment was to give us an idea of how quickly microtubule regrowth occurred in these cells and to allow us to select an appropriate time point to measure microtubule nucleation site diameter. A sample with no warm media added was included as a control to confirm

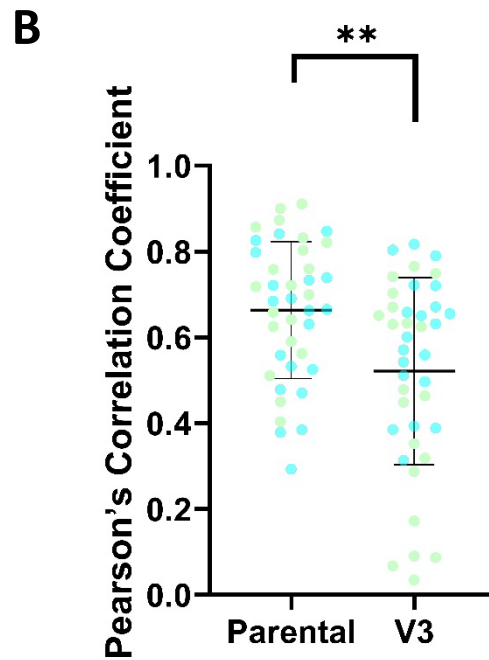
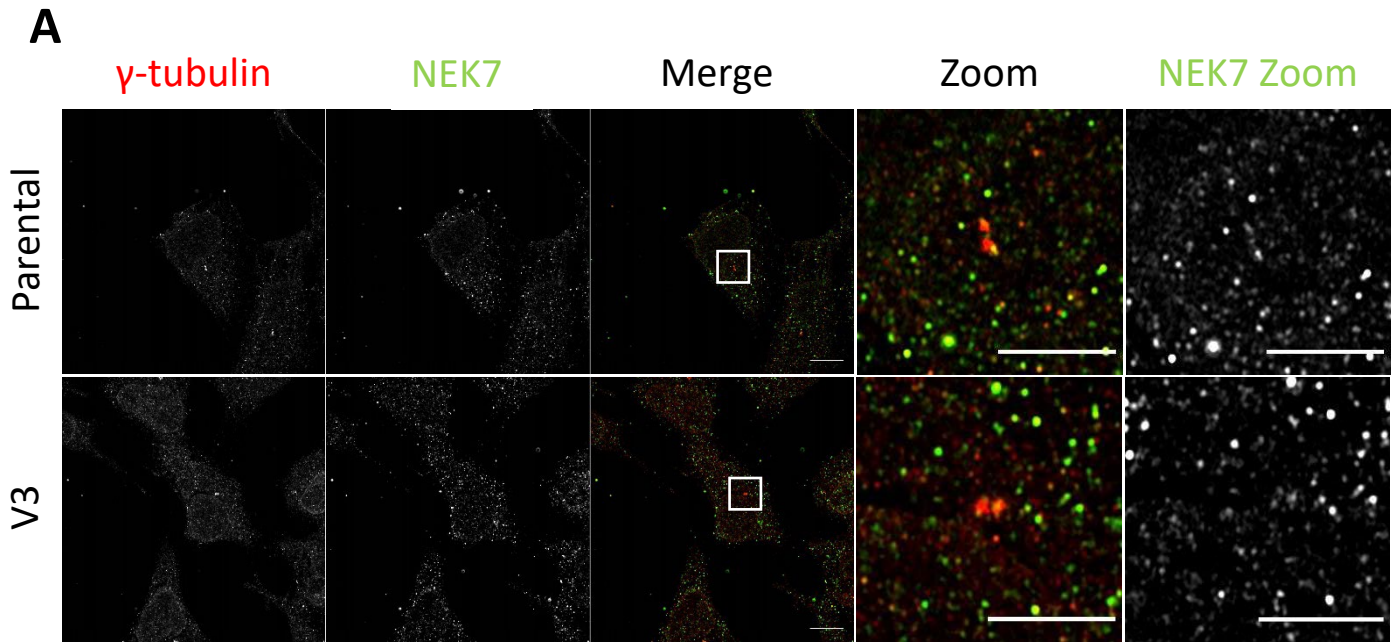


Figure 5.4. NEK7 is not selectively recruited to interphase centrosomes in BEAS-2B:EML4-ALK V3 cells. (A) Induced cells were treated with nocodazole on ice for 30 minutes before being fixed and stained with γ -tubulin (red) and NEK7 (green) antibodies. White boxes show zoom regions. Scale bars = 10 μ m in merge; 5 μ m in zooms. (B) Co-localisation was analysed in Fiji using the PlotMultiColor 4.3. macro for images represented in A. Graph shows individual data points (one colour per repeat), means and standard deviations. Graph represents two independent experiments. N= 40 cells for both cell lines.

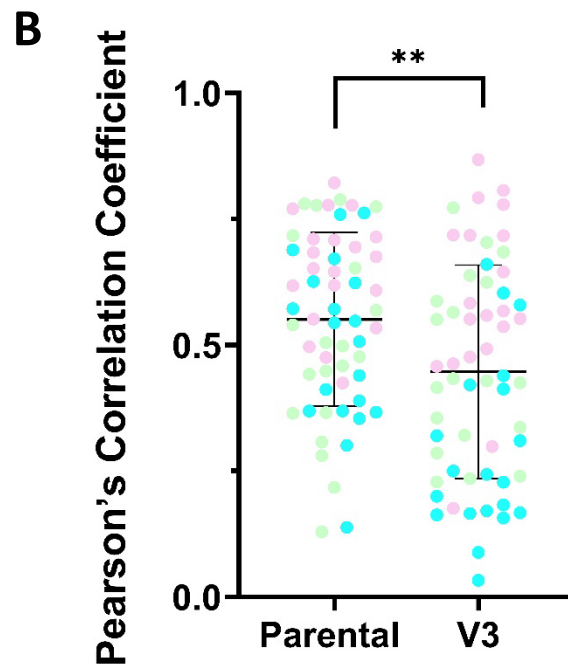
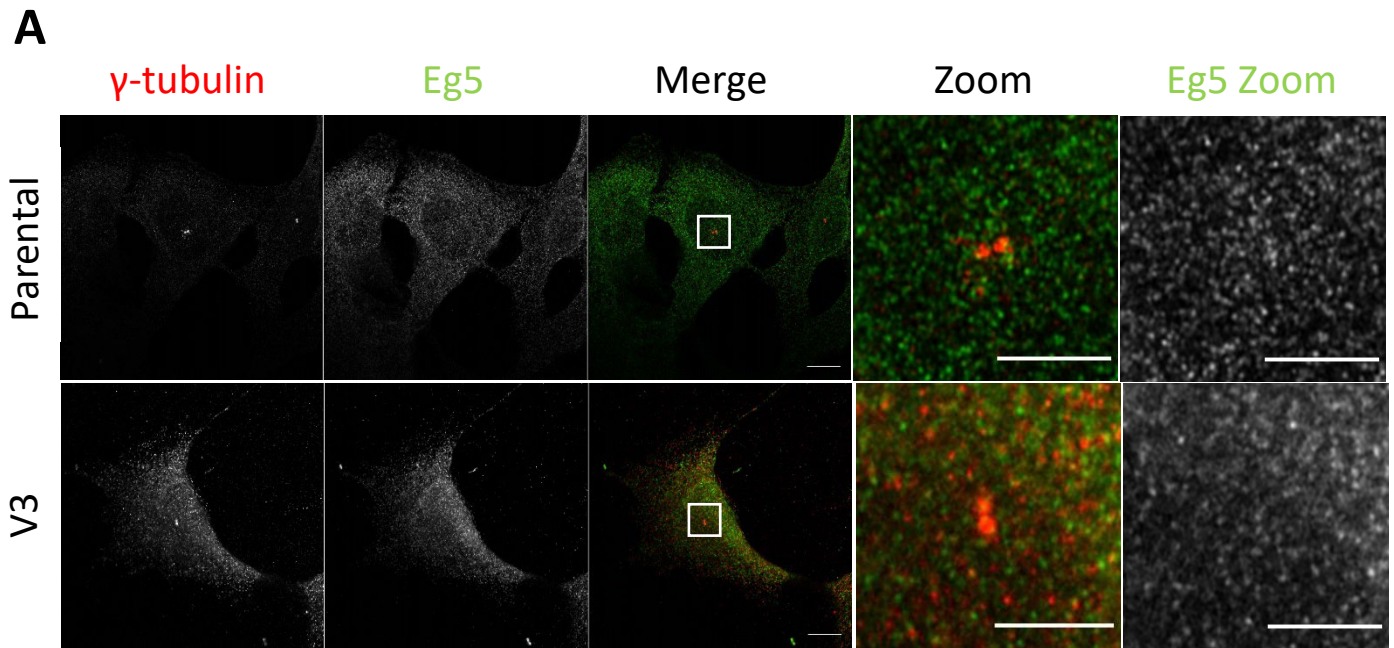


Figure 5.5. Eg5 is not selectively recruited to interphase centrosomes in BEAS-2B:EML4-ALK V3 cells. (A) Induced cells were treated with nocodazole on ice for 30 minutes before being fixed and stained with antibodies against γ -tubulin (red) and Eg5 (green). White boxes show zoom regions. Scale bars = 10 μ m in merge; 5 μ m in zooms. (B) Co-localisation was analysed by the Fiji PlotMultiColor 4.3. macro for cells represented in A. Graph shows individual data points (one repeat per colour), means and standard deviations. Graph represents three independent experiments. N= 60 for parental cells and 59 for V3 cells.

efficient microtubule depolymerisation. Cells were then fixed and stained for immunofluorescence microscopy using antibodies against α -tubulin and γ -tubulin. Imaging revealed complete microtubule depolymerisation in the 0 minute sample. Microtubules were largely repolymerised in many cells after 2 minutes of regrowth, as was the case in the 5 minute and 10 minute samples (Figure 5.6). This led us to select the 1 minute regrowth time point for our future experiments to obtain measurements of the nucleation sites, as regrowth had begun but had not reached a stage where it would be difficult to accurately measure the nucleation site (Figure 5.6).

Having decided to obtain measurements of nucleation site diameter after 1 minute of regrowth, cells were treated as previously described and nucleation sites were imaged revealing larger nucleation sites in V3 BEAS-2B cells compared to parental BEAS-2B cells (Figure 5.7B). From images, the diameter of the nucleation site was measured in Fiji by drawing a line from the central point between the centrosomes along the longest emanating microtubule (Figure 5.7A). Quantification revealed nucleation sites were approximately 5 μm larger in V3 cells than parental cells (Figure 5.7C). We also found a small number of cells had no obvious nucleation site after 1 minute of regrowth. To get an idea of how many cells had a clear nucleation site, 100 cells were counted and the percentage of cells that had a nucleation site was calculated. In parallel to diameter measurements, we found that $\sim 20\%$ more V3 cells had a nucleation site after 1 minute of regrowth compared to parental cells (Figure 5.7D). This difference did not quite reach statistical significance ($P=0.15$), but statistical analysis was completed from two repeats only so potentially would have reached significance with the third repeat.

We also performed these experiments in the NSCLC cell lines, H2228 and H3122. Cells were treated with nocodazole on ice for 30 minutes as before to depolymerise microtubules and a time course experiment was again performed to allow us to decide the most appropriate time point to take measurements from. Cells were fixed and stained as before with α -tubulin and γ -tubulin antibodies. Imaging again confirmed complete microtubule depolymerisation in the control 0 minute samples. We also found that the majority of

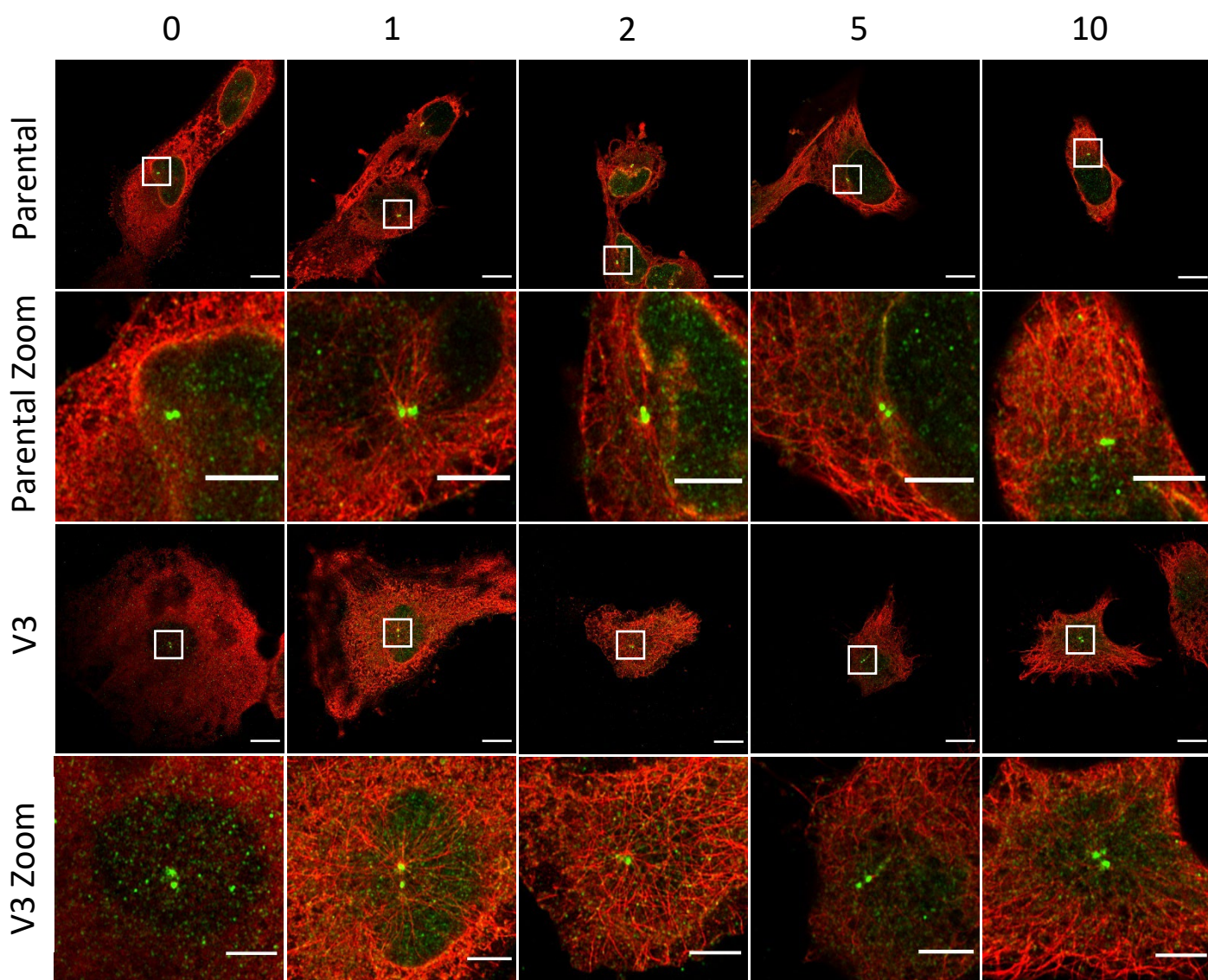


Figure 5.6. Time course of microtubule repolymerisation in BEAS-2B cells. Microtubules were depolymerised in induced BEAS-2B cells using nocodazole and cold treatment. Cells were then exposed to warm media for the times indicated (in minutes). Cells were stained with α -tubulin (red) and γ -tubulin (green). White boxes show zoom region. Scale bars = 10 μ m in whole cell images; 5 μ m in zooms. Images representative of two independent experiments.

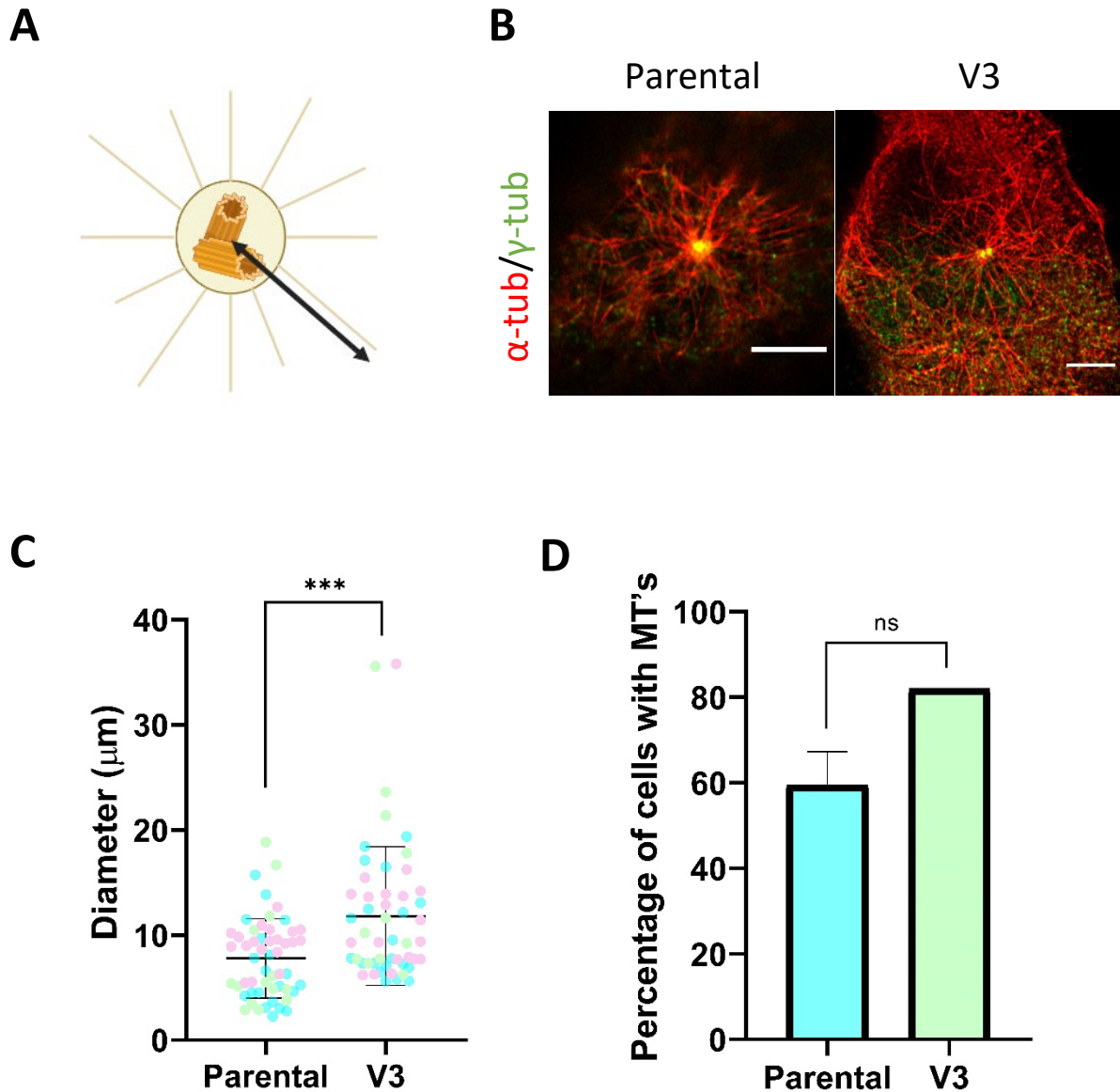


Figure 5.7. BEAS-2B V3 cells have larger nucleation sites than parental cells. (A) Schematic showing how nucleation site diameter was measured. Black line indicates line of measurement. (B) Induced cells were treated with nocodazole on ice for 30 minutes. Cells were washed twice with warm media and then incubated with warm media for 1 minute. Cells were then fixed and stained with α -tubulin (red) and γ -tubulin (green) antibodies. Scale bars = 5 μm . (C) Nucleation site diameter was measured from images represented in A. Graph shows individual measurements (one repeat per colour), means and standard deviations. Representative of three independent experiments. N= 54 cells for parental and N = 51 for V3. (D) Percentage of cells with a distinct nucleation site was calculated. Graph shows means and standard deviations and is representative of two independent experiments.

H2228 cells had completely regrown microtubules after 5 minutes. Nucleation sites were not very distinct after the 1 minute time point in the H3122 cell line; hence, the 2 minute time point was selected to measure nucleation site diameters (Figure 5.8). Imaging nucleation sites in NSCLC cells after 2 minutes of regrowth revealed that H2228 cells had larger nucleation sites than H3122 cells (Figure 5.9A). Measuring the diameter of the microtubule aster confirmed this with asters being approximately 1.5 μm larger in H2228 than H3122 cells (Figure 5.9B). We also quantified the percentage of cells with a clear nucleation site and found almost all of the cells measured had an obvious nucleation site (84% in H3122 and 99% in H2228) (Figure 5.9C).

Together, these findings suggest that the increased microtubule nucleation capacity previously seen in H2228 cells (Sampson *et al.*, 2022) is indeed a consequence of EML4-ALK V3 expression. Not only did measurements of the diameter of microtubule asters at a given time-point confirm that cells expressing V3 have a greater microtubule nucleation capacity, but also counting the percentage of cells that had a clear nucleation site after the relevant time point also showed faster microtubule regrowth in V3 cells compared to parental or V1 cell lines. This potentially could be a result of EML4-ALK V3 localising to the centrosome, although exactly how microtubule nucleation is increased remains unknown.

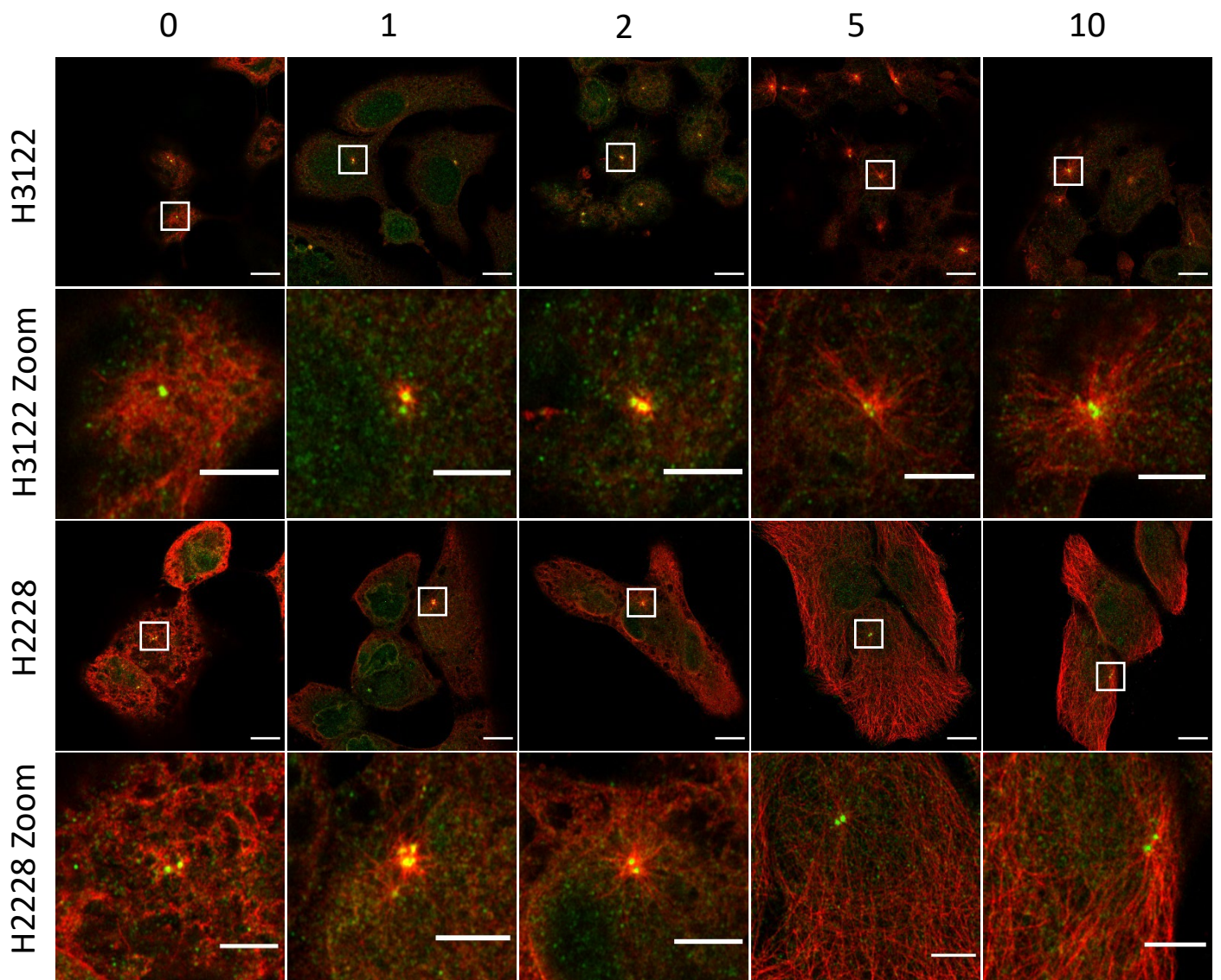


Figure 5.8. Time course of microtubule regrowth in NSCLC cell lines. Cells were treated with nocodazole on ice for 30 minutes before being washed twice with warm media and incubated with warm media for the indicated time points (in minutes). Cells were then fixed and stained with α -tubulin (red) and γ -tubulin (green) antibodies. White boxes show zoom regions. Scale bars = 10 μ m in whole cell; 5 μ m in zooms. Images representative of one experiment.

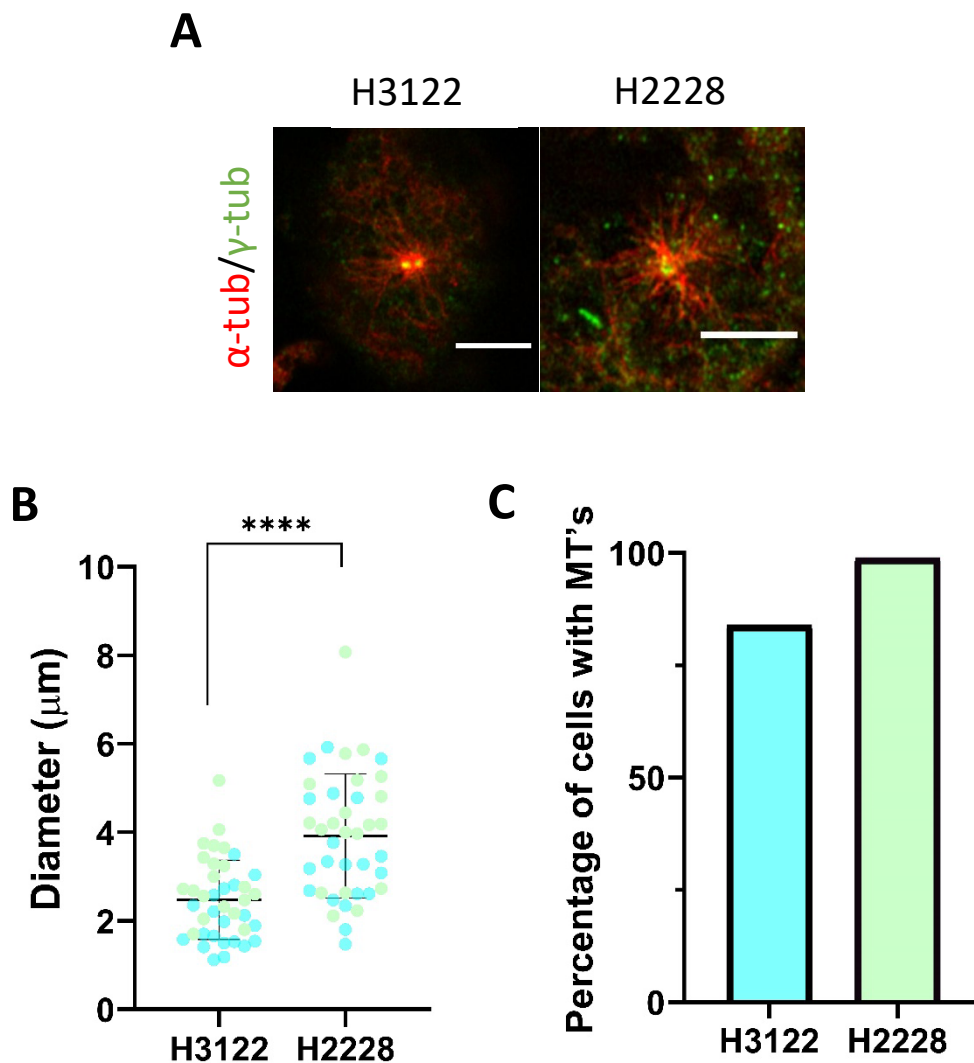


Figure 5.9. H2228 (V3) cells have a higher microtubule nucleation capacity than H3122 (V1) cells.

(A) Cells were treated with nocodazole on ice for 30 minutes before being washed with warm media twice and incubated with warm media for 2 minutes. Cells were then fixed and stained with antibodies against α -tubulin (red) and γ -tubulin (green). Scale bars = 5 μm . (B) Measurements were taken of nucleation site diameter from images represented in A. Graphs show individual data points (one repeat per colour), means and standard deviations. Graph is representative of two independent experiments. N= 40 cells for both cell lines. (C) The percentage of cells with a clear nucleation site was calculated. Graph is representative of one experiment.

5.3. DISCUSSION

Two recent studies have provided tantalizing evidence that there may be a role for EML4-ALK V3 at the centrosome. Firstly, it has been shown that cells expressing EML4-ALK V3 exhibit centrosome amplification in interphase and form multipolar spindles in mitosis (Lucken *et al.*, 2022). Moreover, these results were obtained in the isogenic BEAS-2B cell lines as well as the NSCLC cell lines suggesting that the presence of EML4-ALK V3 is somehow causative for centrosome amplification. Secondly, a separate study has shown that cells of the H2228 (V3) NSCLC cell line exhibit more rapid microtubule nucleation from the centrosome than H3122 (V1) cells (Sampson *et al.*, 2022). However, neither of these studies investigated whether EML4-ALK V3 localised to the centrosome, so this was the first question we set out to answer.

Strikingly, we found that EML4-ALK V3 strongly co-localised with centrosomes in the BEAS-2B inducible cell line ($R = 0.8084$). This was an unexpected finding as there is no evidence to date for localisation of wild-type ALK to centrosomes. A large number of protein kinases have been demonstrated to localise to centrosomes, including a number of tyrosine kinases, where their signalling is spatially organised (Arquint, Gabryjonczyk and Nigg, 2014; Ley *et al.*, 1994). Indeed, many cell cycle regulators are found to localise to the centrosome, including the CDK1/cyclin B complex, Aurora A and PLK1 (Bailey *et al.*, 1989; Dutertre *et al.*, 2004; Golsteyn *et al.*, 1995). This raises the question of whether EML4-ALK V3 is capable of signalling from the centrosome, in a similar manner to its signalling from liquid-liquid phase separated foci (Sampson *et al.*, 2021; Tulpule *et al.*, 2021; Qin *et al.*, 2021). This is an important area for future research as focused signalling of EML4-ALK V3 from the centrosome could increase activation of downstream targets.

In contrast, a lower degree of co-localisation was detected between endogenous EML4-ALK V3 and the centrosome in H2228 cells. However, the Pearson's correlation coefficient of co-localisation between ALK and γ -tubulin was marginally higher in the H2228 cell line compared to the H3122 cell line ($R = 0.3837$ and $R = 0.3260$, respectively). This may suggest that more EML4-ALK V3 is recruited to the centrosome than EML4-ALK V1 in the NSCLC cell

lines. Staining with an antibody against the N-terminal region of EML4, rather than ALK, would be beneficial to determine if this confirms increased localisation in the H2228 cell line compared to H3122 cells. This would add further weight to the argument that there is increased recruitment of EML4-ALK V3 to centrosomes compared to EML4-ALK V1.

Previous work from our laboratory revealed there is a signalling module comprised of EML4-ALK V3:NEK9:NEK7 that is localised to microtubules in interphase cells (O'Regan *et al.*, 2020). In addition, previous chapters of this thesis demonstrated that the kinesin motor protein, Eg5, is a downstream target of NEK7 in this signalling pathway. For this reason, we also investigated whether NEK7 and Eg5 were recruited to interphase centrosomes in addition to the EML4-ALK V3 protein. However, experiments presented here revealed there was no significant recruitment of either NEK7 or Eg5 to centrosomes in cells expressing EML4-ALK V3. This suggests that whatever role EML4-ALK V3 is performing at the centrosome, including in microtubule nucleation, is independent of the NEK9:NEK7:Eg5 signalling pathway and more likely to depend on ALK activity. Indeed, published work has demonstrated that the increased microtubule nucleation capacity of H2228 (V3) cells was reduced in the presence of the ALK inhibitor, ceritinib, supporting a dependence on ALK catalytic activity for this function (Sampson *et al.*, 2022).

It will be interesting to investigate whether localisation of EML4-ALK V3 to the centrosomes is required for deregulation of the centrosome duplication cycle and the amplification of centrosomes (Lucken *et al.*, 2022). The key residues that enable EML4-ALK V3 to localise to the centrosome could be determined and these residues could then be mutated to see if this alters both localisation and centrosome amplification. To determine if ALK catalytic activity is disrupting the centrosome cycle, centrosome amplification should be quantified in cells treated with ALK inhibitors. It will also be intriguing to know what proteins at the centrosome EML4-ALK V3 interacts with and whether EML4-ALK V3 might phosphorylate a regulator of the centrosome cycle.

It is well documented that p53 has a surveillance role in detecting cells with amplified centrosomes and preventing their proliferation (Nigg and Holland, 2018). Intriguingly, it has been found that patients with EML4-ALK V3 and p53 mutations have worse outcomes compared with patients with just EML4-ALK V3 or p53 mutations alone (Christopoulos *et al.*, 2019; Tanimoto *et al.*, 2021). This raises the question of whether the reason these patients have worse outcomes is due to the continual proliferation of cells with amplified centrosomes which are capable of evading p53-mediated arrest or death. p53 status may therefore be something to consider when selecting treatments for patients with EML4-ALK V3. It may be that an approach which combines standard chemotherapy with targeted ALK inhibitors would be more effective in these patients; however, further studies are needed to explore this. In addition, studies could be conducted that explore the use of centrosome targeting agents, either alone or in combination with ALK inhibitors. Interestingly, the H2228 cell line harbours a nonsense mutation in the *TP53* gene which likely results in a non-functional protein (Cancer.sanger.ac.uk, nd). This makes this cell line even more useful for pre-clinical studies from a translational perspective.

As recently described, expression of EML4-ALK V3 is associated with a greater microtubule nucleation capacity from centrosomes (Sampson *et al.*, 2022). This was shown to be the case in H2228 cells when compared to H3122 cells. However, as previously discussed, the H2228 cell line harbours many other genetic alterations in addition to expression of EML4-ALK V3. For this reason, we investigated whether there were any differences in microtubule nucleation in isogenic BEAS-2B cell lines, where the only difference was expression of EML4-ALK V3. Indeed, we did see an increase in microtubule nucleation in BEAS-2B cells expressing V3 compared to parental cells, as demonstrated by larger microtubule asters and a higher percentage of cells with distinct nucleation from the MTOC after 1 minute of regrowth. Likewise, we confirmed similar results in the NSCLC patient cell lines. Together, these results provide clear evidence that EML4-ALK V3 does somehow increase the nucleation of microtubules at centrosomes.

In the published study, microtubule nucleation was seen to depend on ALK activity, shown by a reduction in aster diameter after treatment with ceretinib (Sampson *et al.*, 2022). These experiments should be repeated in the BEAS-2B cell lines to confirm that ALK catalytic activity does indeed contribute to microtubule nucleation. In addition, microtubule regrowth could also be measured in cells transfected with a kinase dead EML4-ALK V3 mutant and compared to the wild type protein. If microtubule nucleation does rely on ALK activity, one would expect a smaller microtubule aster in cells expressing the kinase dead compared to wild type protein. If ALK activity is indeed required, this raises the question of what ALK is phosphorylating to promote microtubule nucleation. For example, could it phosphorylate a component of the γ -TuRC resulting in a conformational change required for microtubule nucleation? Or could its activity somehow increase the rate of microtubule polymerization to accelerate the formation of growing microtubules?

To conclude this chapter, we have obtained additional evidence for a role of EML4-ALK V3 at the centrosome. The recruitment of V3 to the centrosome is interesting in itself and raises many more questions such as how is it localising there and is this affecting the centrosome duplication cycle? However, it potentially does offer some explanation as to why centrosome amplification occurs in EML4-ALK V3 expressing cells (Lucken *et al.*, 2022), although further investigations to understand the mechanisms are needed. Furthermore, EML4-ALK V3 does appear to increase microtubule nucleation and this appears more likely to be dependent on ALK activity than the NEK7/Eg5 pathway. Exactly what ALK is doing to increase microtubule nucleation for now remains unknown.

CHAPTER 6

Discussion

6.1. Summary

This study aimed to investigate whether the mitotic kinesin Eg5 is a downstream target of the EML4-ALK V3:NEK9:NEK7 pathogenic signalling module. We found that Eg5 is recruited to interphase microtubules in cells expressing EML4-ALK V3, whereas Eg5 is normally only recruited to microtubules in dividing cells. Moreover, our results suggest that NEK7 phosphorylation of Eg5 may contribute to this unusual localisation. We discovered that Eg5 is required for the generation of a mesenchymal morphology in these cells and that this requires phosphorylation of Eg5 at S1033, a site known to be targeted by NEK7, as well as the motor activity of Eg5. We also present evidence that EML4-ALK V3 may be recruited to the centrosome and promote microtubule nucleation. These novel data add to our knowledge of the mechanisms that EML4-ALK V3 uses to promote cancer progression. They also indicate directions for future research into both the biology of EML4-ALK V3 cancers and avenues that might lead to effective new treatments for these patients.

6.2. EML4-ALK biology and current treatment of ALK rearranged NSCLC

The EML4-ALK oncogenic fusion was first identified in 2007 and was found to exist in approximately 5% of NSCLCs (Soda *et al.*, 2007). It has since been identified in other cancer types, such as colorectal, breast and pancreatic and as many as fifteen variants of this fusion have been identified which arise due to different breakpoints in the *EML4* gene (Lin *et al.*, 2009; Singhi *et al.*, 2017; Ou *et al.*, 2021; Sabir *et al.*, 2017). Importantly, due to alternative breakpoints in the *EML4* gene, the amount of the EML4 protein that is present in the fusions differs between variants, whilst all the variants contain the same portion of the ALK kinase which includes its tyrosine kinase domain (Bayliss *et al.*, 2016). The inclusion of the tyrosine kinase domain of ALK means that these fusions are all capable of oncogenic signalling and pathways activated downstream of EML4-ALK fusions include RAS/RAF/MEK/ERK, JAK/STAT and PI3K/Akt which drive cell proliferation and survival (Sabir *et al.*, 2017; Hallberg and Palmer, 2016).

The inclusion of distinct portions of EML4 gives EML4-ALK variants different properties. Variants can be categorised into long or short variants depending on which domains of the EML4 protein they contain. Shorter variants, such as V3 or V5, typically consist of the N-terminal trimerization domain and none of the EML4 TAPE domain. On the other hand, longer variants, such as V1 or V2, contain the trimerization domain in addition to a disrupted TAPE domain. As the TAPE domain is a highly structured region, a disrupted TAPE domain in longer EML4-ALK variants renders these fusions unstable and reliant on chaperone proteins such as HSP90 to maintain their expression (Richards *et al.*, 2014; Sabir *et al.*, 2017).

In addition to differences in protein stability, the intracellular localisation of EML4-ALK variants also varies. Shorter variants bind to interphase microtubules whereas longer variants remain in the cytoplasm (Richards *et al.*, 2015; O'Regan *et al.*, 2020). This is likely due to the reliance of longer variants on chaperone protein HSP90 which may physically block interaction with the microtubules or due to structural elements of the disrupted TAPE domain (Richards *et al.*, 2014; Sampson *et al.*, 2021). Interestingly, cells which express the shorter EML4-ALK variants exhibit excessive microtubule stabilisation, adopt more mesenchymal morphologies and display accelerated migration, which in the case of EML4-ALK V3 depend on the NEK9 and NEK7 kinases (O'Regan *et al.*, 2020). Collectively, the striking differences in the biology of the different EML4-ALK variants suggests that treatments of NSCLC patients with EML4-ALK cancers may need to be selected depending on which variant the patient presents with. In line with this, studies have shown that patients with EML4-ALK V3 often fare far worse than patients with longer EML4-ALK variants, highlighting the need to develop novel treatment approaches for this subset of patients (Christopoulos *et al.*, 2018).

ALK+ cancers are currently treated with targeted ALK inhibitors. Crizotinib was the first ALK inhibitor to be approved by the FDA in 2011 for the treatment of ALK rearranged lung cancers (Kazandjian *et al.*, 2014; Bayliss *et al.*, 2016; Lei *et al.*, 2022). Unfortunately, the success of this drug is limited due to the development of tumour resistance via secondary

mutations or activation of alternative signalling pathways (Choi *et al.*, 2010; Heuckmann *et al.*, 2011; Woo *et al.*, 2017; Lei *et al.*, 2022). Second and third generation ALK inhibitors, such as ceritinib or lorlatinib, have been developed to combat this problem but eventually face similar fates (Wu *et al.*, 2016). The most recent development in the ALK inhibitor field is the design of fourth generation inhibitors that are double-mutant active meaning in theory they can be used in the treatment of cancers with multiple ALK mutations that confer resistance to previous generations of ALK inhibitors (Ou *et al.*, 2021; Peng *et al.*, 2022; Lei *et al.*, 2022). Fourth generation inhibitors are currently in phase I/II clinical trials (Lei *et al.*, 2022). Moreover, the continual acquisition of secondary mutations makes it appealing to identify other proteins that potentially could be targeted either alone or in combination treatments with ALK inhibitors. The use of HSP90 inhibitors has previously been explored in the context of EML4-ALK cancers but with limited success (Katayama *et al.*, 2011; Sabir *et al.*, 2017). Not all patients respond well to HSP90 inhibitors and the increased stability of the shorter variants would further limit which patients could be treated with such inhibitors in the first place.

The discovery of the kinesin motor protein, Eg5, downstream of the short variant, EML4-ALK V3, raises the intriguing possibility that NSCLC patients with this variant might benefit from treatment with clinical Eg5 inhibitors either alone or in combination with ALK inhibitors (see section 6.5).

6.3. Eg5 is a downstream substrate of the EML4-ALK V3:NEK9:NEK7 signalling module

EML4-ALK V3 expressing cells have previously been shown to exhibit a more mesenchymal-like morphology which is dependent not only on an intact microtubule network but also the NEK9 and NEK7 kinases (O'Regan *et al.*, 2020). Furthermore, cells expressing EML4-ALK V3 have more stable microtubules compared to cells expressing other variants and display accelerated migration (O'Regan *et al.*, 2020). Although it was shown that EML4-ALK V3, NEK9 and NEK7 are recruited to interphase microtubules, it remained unclear exactly how this alters microtubule dynamics and promotes mesenchymal morphology and migration. Since there was strong evidence of involvement of the microtubule cytoskeleton, we

hypothesised that a microtubule regulator could be a downstream substrate of the EML4-ALK V3:NEK9:NEK7 signalling module. Our attention was drawn to Eg5 as it is known to be a substrate of NEK7, with its phosphorylation promoting centrosome separation in early mitosis (Bertran *et al.*, 2011; Rapley *et al.*, 2008). In addition, NEK7 phosphorylation of Eg5 is able to promote dendrite extension in non-dividing neuronal cells (Frexio *et al.*, 2018). For this reason, we began to explore whether Eg5 was a downstream substrate of the EML4-ALK V3:NEK9:NEK7 pathway and contributed to the mesenchymal-like phenotypic changes.

First, we found that Eg5 is recruited to interphase microtubules in cells expressing EML4-ALK V3 but not V1 or in the parental cell lines. This finding was highly suggestive of some involvement given that normally Eg5 only associates with microtubules of the mitotic spindle and not with interphase microtubules (Sawin and Mitchison, 1995). We also demonstrated that the untimely recruitment of Eg5 to interphase microtubules likely occurs downstream of NEK7. Depletion of NEK7 reduced the amount of Eg5 that co-localised with interphase microtubules in V3 cells. Moreover, we obtained preliminary evidence that NEK7 phosphorylation of S1033 in the tail domain of Eg5 may contribute to microtubule localisation of Eg5. Here, we found an Eg5-S1033D mutant transiently transfected into EML4-ALK V1 cells showed a higher percentage co-localisation with microtubules compared to a Eg5-WT protein. The development of an Eg5-pS1033 phosphoantibody that was able to specifically detect the phosphorylated protein by immunofluorescence microscopy would help to confirm this. Indeed, analysis of the level of phosphorylated Eg5 in the different cell lines by Western blot with an Eg5-pS1033 phosphoantibody, or quantitative mass spectrometry would also be valuable. In addition to this, the phosphorylation status of T926, the residue phosphorylated by CDK1 and most commonly associated with binding of Eg5 to mitotic microtubules, should also be checked by Western blot using a phosphospecific antibody in these cells. It would also be valuable to formally assess the activation status of NEK7 in our V3 cell lines, for example by immunoprecipitating NEK7 and performing *in vitro* kinase assays or developing a biosensor for measuring NEK7 activity in cells.

Eg5 expression is upregulated in many types of cancer, including NSCLC (Garcia-Saez and Skoufias, 2021; Castillo *et al.*, 2007; Saijo *et al.*, 2006). Interestingly, we found no significant difference in Eg5 expression in our BEAS-2B cell lines expressing EML4-ALK V1 or V3 as compared to the parental cells. However, Eg5 expression was reduced in the H2228 NSCLC patient-derived cell line compared to H3122 cells. This may be a consequence of EML4-ALK V3 expression but may equally result from the fact this cell line harbours a mutation in the *Kif11* gene, which encodes Eg5. Nevertheless, Eg5 expression may be an important prognostic marker based on recent research that investigated expression of the NEK9-Eg5 signalling axis in patient colorectal tumour samples (Kim *et al.*, 2023). Here, it was demonstrated by immunohistochemistry that Eg5 expression was upregulated in over half of high-grade colorectal tumour samples and was correlated with the presence of distant metastases (Kim *et al.*, 2023). Not only could Eg5 expression give an indication of the likelihood of a patient developing metastases, it was also demonstrated to predict response to chemotherapeutic treatment using anti-mitotic agents in combination with platinum compounds (Saijo *et al.*, 2006). Taken together, these findings and our data identify Eg5 as a potentially important clinical factor that could be targeted in future treatments of ALK rearranged cancer. Furthermore, immunohistochemical analysis of Eg5 expression in primary tumour samples may be a useful tool in the clinic in selecting which patients may benefit from Eg5 inhibitor treatment.

6.4. Eg5 activity is required for altered cell morphology in EML4-ALK V3 cells

Our finding that Eg5 is recruited to interphase microtubules in cells expressing EML4-ALK V3 led us to question whether it could be contributing to the phenotypic alterations exhibited by V3 cells. V3 cells develop a mesenchymal-like morphology with protrusions that contain stable microtubules (O'Regan *et al.*, 2020). Using Eg5 inhibitors which inhibited Eg5 motor activity and either strengthened or perturbed the interaction between Eg5 and the microtubules, we found that Eg5 does indeed promote cell elongation in a way that is dependent on its motor activity. Indeed, cell elongation was blocked with similar efficiencies with both categories of Eg5 inhibitor used. Interestingly, studies have demonstrated that Eg5 has microtubule polymerase activity (Chen and Hancock, 2015; Chen *et al.*, 2019). These studies showed that Eg5 present at the plus-end of a growing protofilament could step on to

an incoming tubulin dimer and change the conformation of tubulin in a way that stabilised the newly formed interaction (Chen and Hancock, 2015; Chen *et al.*, 2019). It is therefore possible that the presence of Eg5 on interphase microtubules in EML4-ALK V3 expressing cells results in cell elongation through microtubule polymerisation mediated by Eg5. However, there was no evidence from our localisation studies for a concentration of Eg5 at growing microtubule ends. Alternatively, as Eg5 facilitates microtubule crosslinking, it could be this that results in microtubule stabilization and cytoplasmic protrusion formation. Anti-parallel sliding of microtubules may also be important as kinesin-1 mediated microtubule sliding has previously been shown to promote neurite outgrowth (Lu *et al.*, 2013).

In addition to our finding that Eg5 inhibitors could inhibit cell elongation, we also found that cell length can be regulated by the phosphorylation of S1033 of Eg5. Expression of a phosphomimetic Eg5-S1033D mutant was able to rescue the length of EML4-ALK V3 cells that had been depleted of NEK7; however, this did not occur upon expression of an S1033A phosphonull mutant. This is similar to findings in neurons which demonstrated that dendrite length is also controlled by NEK7 phosphorylation of S1033 of Eg5 (Freixo *et al.*, 2018). Given that cancer cells are known to manipulate normal cellular pathways (Thiery, 2002), it may be that cancer cells expressing EML4-ALK V3 are mimicking the behaviour of neurons in a way that enhances their ability to develop mesenchymal-like properties which ultimately contribute to metastasis.

Although we provide evidence of Eg5 having a role in promoting a mesenchymal morphology, we believe the increased rate of migration displayed by EML4-ALK V3 expressing cells requires more than this. Treatment of BEAS-2B:EML4-ALK V3 cells with Eg5 inhibitors revealed no change in cell migration distance, speed or directionality and treatment of H2228 cells only resulted in minor reductions in migration distance and speed. Indeed, it is well established that the actin cytoskeleton performs essential roles in cell migration at both the front and rear of the cell. The actin cytoskeleton is required both for forming protrusions at the front of the cell, such as lamellipodia and filopodia, which push the cell membrane forward in the direction of migration and for contraction of the rear of

the cell which allows the rear of the cell to detach and pull itself forward (Rottner and Schaks, 2019; Etienne-Manneville, 2013). Moreover, it is now accepted that cooperation between the actin and microtubule cytoskeletons is required for efficient cell migration (Dogterom and Koenderink, 2019). It is therefore likely that alterations to the actin cytoskeleton downstream of EML4-ALK V3 are required in addition to microtubule alterations for the enhanced migration of these cells (Figure 6.1). This is consistent with data previously generated in our lab which demonstrated changes to the actin cytoskeleton in EML4-ALK V3 expressing cells and that NEK7 can also phosphorylate actin regulators (Richardson, 2021).

In addition to the phosphorylation of actin regulators, it may also be possible that NEK7 may interact with other regulators of the microtubule cytoskeleton that may contribute to cell migration. For example, EB1 (end-binding 1) is capable of regulating protrusions required for 3D cell migration (Jayatilaka *et al.*, 2018). Interestingly, *Aspergillus* NIMA depends on EB1 for its localisation to microtubule plus-ends, although an interaction between EB1 and a human NEK kinase is yet to be characterised (Govindaraghavan *et al.*, 2014; Hennessey *et al.*, 2020). Nonetheless, NEK7 can interact with multiple regulators of the microtubule cytoskeleton such as MAP2 or CLASP1/2 and can also regulate EML4 (de Souza *et al.*, 2014; Adib *et al.*, 2019). Furthermore, preliminary data from our lab suggests that EML4 expression regulates the localisation of EB proteins (Adib, 2019). It would therefore be interesting to investigate whether EB1 might be regulated by NEK7 in this context and may contribute to the migration of EML4-ALK V3 expressing cells.

We also investigated whether NEK7-mediated Eg5 phosphorylation in V3 cells led to an increase in microtubule stabilisation. Depleting NEK7 from EML4-ALK V3 cells reduced microtubule acetylation, indicative of less stable microtubules, suggesting that a downstream substrate of NEK7 is indeed involved in stabilising microtubules in these cells. However, when we transfected the Eg5-S1033 phosphomutants, neither the phosphomimetic nor phosphonull mutants were able to rescue the microtubule acetylation levels. This may suggest other proteins may also be involved in microtubule stabilisation

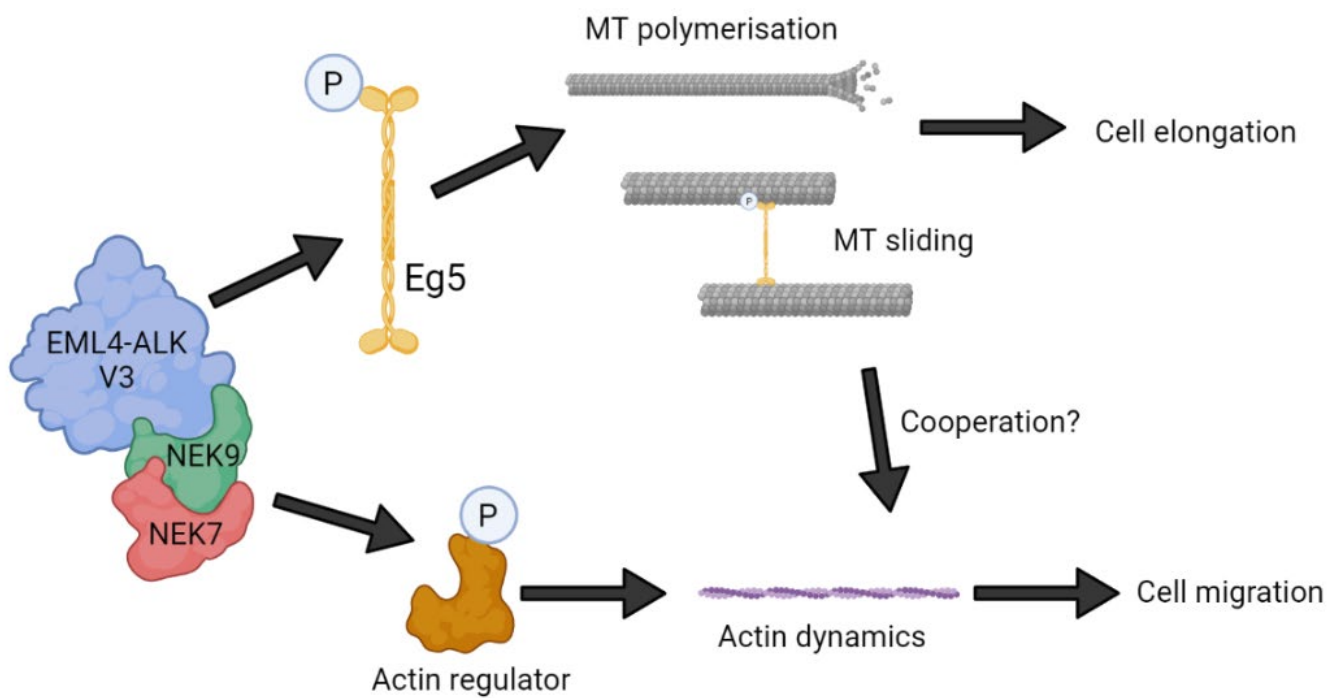


Figure 6.1. Schematic figure of how the EML4-ALK V3:NEK9:NEK7 complex may regulate microtubule and actin associated proteins. The EML4-ALK V3:NEK9:NEK7 complex is likely to have many downstream substrates, including regulators of both the microtubule and actin cytoskeleton. Eg5 may promote microtubule polymerisation or microtubule crosslinking or sliding which results in cell elongation. The regulation of actin regulators may be required for the increased migration of V3 cells.

downstream of NEK7. However, as previously mentioned, our methods of measuring acetylated tubulin intensity from immunofluorescence microscopy images may have been flawed as a result of the large differences in cell morphology. Therefore, further experiments including Western blots with acetylated tubulin antibodies are required to determine whether Eg5 affects microtubule stability in EML4-ALK V3 cells. In addition, previous studies that have shown Eg5 can promote microtubule stability have done so using rigor inhibitors that lock Eg5 in an immobile state on microtubules (Chen *et al.*, 2017; Freixo *et al.*, 2018). Hence, it could be that microtubule stabilisation only occurs when Eg5 is immobile.

6.5. Could Eg5 inhibitors be used in the treatment of lung cancer?

Conventional chemotherapy approaches used to treat NSCLC patients typically consist of platinum compounds and microtubule poisons (Zappa and Mousa, 2016). Whilst microtubule poisons prevent mitotic progression by interfering with mitotic spindle dynamics, they are also toxic to other dividing cells and specific differentiated cell types, such as gut epithelia and neurons, which results in unpleasant side effects for the patient (Shi and Mitchison, 2017). In addition, patient responses to microtubule poisons vary and tumours can acquire resistance to them (Shi and Mitchison, 2017). Recently, efforts have been made to find alternatives to microtubule poisons and a lot of focus has been on mitotic inhibitors which target proteins that are specifically involved with the mitotic spindle. Such targets include motor proteins, for example Eg5, or kinases such as Aurora kinases or PLKs. The benefit of these is that they selectively target dividing cells so may mitigate some of the distressing side effects caused by traditional chemotherapy (Shi and Mitchison, 2017).

Many different Eg5 inhibitors have been developed in academia and industry, some of which have progressed to clinical trials (Garcia-Saez and Skoufias, 2021). Unfortunately, many of these clinical trials have produced disappointing results with Eg5 inhibitors lacking sufficient efficacy (Shi and Mitchison, 2017; Garcia-Saez and Skoufias, 2021). However, one Eg5 inhibitor, filanesib, has recently reached phase III clinical trials for use in the treatment

of multiple myeloma (Indorato *et al.*, 2019). Excitingly, preclinical studies as well as phase I/II clinical trials have demonstrated synergy between filanesib, pomalidomide (a targeted cancer drug used to treat myeloma) and dexamethasone in the treatment of multiple myeloma, suggesting combination therapies may be superior to Eg5 inhibitor monotherapy (Hernández-García *et al.*, 2017; Ocio *et al.*, 2021).

Given our results that suggest Eg5 may promote the development of a mesenchymal phenotype, Eg5 inhibitors should be explored in the context of EML4-ALK V3 cancer. There is a possibility that by preventing the development of a mesenchymal morphology using Eg5 inhibitors, this could slow or block further metastasis of these cells. Combination therapies using Eg5 inhibitors with ALK inhibitors to block activation of other ALK-associated signalling pathways should also be explored. Given that microtubules are stabilised in EML4-ALK V3 expressing cells (O'Regan *et al.*, 2020; Sampson *et al.*, 2022) and the link between microtubule acetylation and cell migration (Boggs *et al.*, 2015; Bance *et al.*, 2019), the effect of Eg5 inhibitors on microtubule dynamics is something which should be considered when exploring potential combination treatments. Different types of Eg5 inhibitor (L5 or rigor) have been shown to have opposing effects on microtubule stability so this is something that needs to be carefully considered and investigated when attempting to treat EML4-ALK V3 driven cancers with Eg5 inhibitors (Chen *et al.*, 2017).

6.6. EML4-ALK V3 promotes microtubule nucleation at the centrosome

Cells expressing EML4-ALK V3 exhibit centrosome amplification and an increased microtubule nucleation capacity (Lucken *et al.*, 2022; Sampson *et al.*, 2022). We therefore set out to further investigate how EML4-ALK V3 might affect centrosome biology. Firstly, we analysed EML4-ALK V3 localisation with respect to the centrosome and found strong co-localisation in our BEAS-2B cell line and a weaker co-localisation in the H2228 cell line. Pearson's correlation coefficients of co-localisation measured in NSCLC patient cell lines were slightly higher in H2228 cells compared to H3122 cells, which may suggest a minor increase in recruitment of the EML4-ALK V3 as compared to the V1 protein to the centrosome. Going forward, it will be interesting to determine whether the localisation of

EML4-ALK V3 to the centrosome is somehow perturbing the centrosome cycle and contributing to centrosome amplification or indeed whether EML4-ALK V3 is capable of signalling from the centrosome, as many kinases are (Arquint, Gabryjonczyk and Nigg, 2014). Interestingly, this includes kinases involved with cell cycle regulation such as Aurora A, which incidentally has many targets in common with the NEK kinase family. These include NEDD1 which recruits the γ -TuRC to the centrosome, TACC proteins and ch-TOG which contribute to microtubule polymerisation from a microtubule aster (Magnaghi-Jaulin *et al.*, 2019).

Data suggesting that EML4-ALK V3 can increase microtubule nucleation in cells had previously been obtained from NSCLC patient cell lines, H3122 and H2228 (Sampson *et al.*, 2022). Due to the additional mutational burden of these cell lines, we examined microtubule nucleation in the isogenic BEAS-2B cell lines. Here, we found that BEAS-2B:EML4-ALK V3 cells had an increased microtubule nucleation capacity compared to the parental BEAS-2B cell line. This strengthens the argument that EML4-ALK V3 does indeed lead to an increase in the rate of microtubule nucleation.

Further experiments investigating the localisation of NEK7 and Eg5 with respect to the centrosome in interphase EML4-ALK V3 cells revealed there was no active recruitment of either of these proteins. This suggests that any change to centrosome biology and microtubule nucleation activity is likely to be dependent on ALK activity rather than the NEK9:NEK7:Eg5 signalling module. Consistent with this, it was also shown that the diameter of the microtubule aster formed upon microtubule regrowth in H2228 cells, but not H3122 cells, could be reduced using the ALK inhibitor, ceretinib (Sampson *et al.*, 2022). Further research into how EML4-ALK V3 might influence microtubule nucleation could seek to identify novel interacting partners or test the consequence of inhibitors of the well-known ALK signalling pathways. This might reveal alternative targets for therapeutic intervention that could interfere with the interaction of EML4-ALK V3 with the centrosome or block pathways that lead to deregulation of the centrosome cycle or microtubule nucleation.

Interestingly, as we hypothesise that NEK7 is activated by EML4-ALK V3, it was somewhat surprising to find that Eg5 was not recruited to the centrosome in these cells. Indeed, phosphorylation of Eg5 on S1033 by NEK7 was demonstrated to result in its accumulation at the centrosome in early mitosis (Bertran *et al.*, 2011; Rapley *et al.*, 2008). This may suggest that something else is required to make the centrosome accessible to Eg5 during mitosis that is missing in interphase cells, explaining why Eg5 was not seen localised with centrosomes of interphase EML4-ALK V3 cells. Alternatively, it has been suggested in previous studies that EML4-ALK is active when incorporated into phase separated foci but is inactive when bound to microtubules (Sampson *et al.*, 2021). With this in mind, perhaps EML4-ALK V3 is active at the centrosome and may be unable to form a complex with NEK9 and NEK7 when ALK is active, hence Eg5 is no longer phosphorylated. Further studies are needed to investigate this.

6.7. Implications and future perspectives

This work has identified Eg5 as a downstream component of the EML4-ALK V3:NEK9:NEK7 signalling pathway. Through NEK7-mediated phosphorylation of Eg5, we suspect that Eg5 may polymerise microtubules or facilitate microtubule crosslinking and/or sliding resulting in the development of a mesenchymal morphology in EML4-ALK V3 cells. Therapeutic targeting of Eg5 may therefore prevent cell elongation, as shown by our *in vitro* cell-based experiments. Although our experiments did not suggest a role for Eg5 in regulating migration in cultured cells, *in vivo* studies in mice would be beneficial to see if Eg5 inhibitors could slow or block metastasis. Future research should also focus on translational studies that test the use of Eg5 inhibitors for treatment of EML4-ALK V3 cancers.

Further basic research into potential crosstalk between microtubules and the actin cytoskeleton would also be beneficial to understand how cells that recruit EML4-ALK V3, NEK9 and NEK7 to microtubules become more migratory. Cell migration is controlled by complex mechanisms involving many different proteins which can regulate both microtubule and actin dynamics (Rottner and Schaks, 2019; Etienne-Manneville, 2013). Indeed, the inclusion of stable microtubules in protrusions formed by EML4-ALK V3

expressing cells may allow delivery of proteins required at the leading edge that organise the actin cytoskeleton in a way that promotes cell migration. Further studies investigating cytoskeleton ultrastructure and organisation in the leading edge by correlative light and electron microscopy may be valuable to explore the distribution of proteins that mediate actin-microtubule cross-talk in EML4-ALK V3 cells. One such group of proteins that have been strongly associated with actin-microtubule cross-talk are the Rho GTPases and their upstream guanine nucleotide exchange factors and it would be interesting to assess Rho GTPase activity in the EML4-ALK cell lines (Dogterom and Koenderink, 2019).

As previously discussed, further work is needed to understand whether Eg5 contributes to microtubule stabilisation in EML4-ALK V3 cells. Previous studies have shown that by locking Eg5 on to microtubules using rigor inhibitors, microtubule stabilisation is increased while the opposite is true when the Eg5-microtubule interaction is perturbed by L5 inhibitors (Chen *et al.*, 2017; Freixo *et al.*, 2018). Whether microtubule stabilisation is only increased when Eg5 is immobile on microtubules is something that should be investigated as this could reflect the purpose of NEK7 phosphorylation of the Eg5 tail domain. Understanding how Eg5 affects microtubule dynamics will also have impact beyond the field of this study, for example in neuronal development studies.

We have also added important information to the hypothesis that EML4-ALK V3 has a role at the centrosome. EML4-ALK V3 was seen to strongly co-localise with the interphase centrosome in BEAS-2B cells, which have previously been shown to exhibit centrosome amplification upon expression of this fusion protein (Lucken *et al.*, 2022). Future research could now focus on exploring whether EML4-ALK V3 recruitment to the centrosome is resulting in centrosome amplification in these cells, how it occurs (including whether it is associating with centrioles or the PCM) and whether the EML4-ALK protein localised to the centrosome could be therapeutically targeted to reduce the generation of genomic instability. In line with previous published data (Sampson *et al.*, 2022), we also show that cells expressing EML4-ALK V3 have a higher microtubule nucleation capacity as compared to V1 or parental cell lines. More research could be conducted to gain a greater understanding

of exactly how EML4-ALK V3 assists in nucleating microtubules and whether this somehow gives cancer cells an advantage, for example in promoting an invasive phenotype.

EML4-ALK fusions are found in approximately 5% of NSCLC, but have also been identified in other cancers such as breast, colorectal and pancreatic (Soda *et al.*, 2007; Lin *et al.*, 2009; Ou *et al.*, 2021; Singhi *et al.*, 2017). Therefore, wider implications of this work include the possibility that Eg5 could be involved in the tumorigenic properties of these cancers and benefit from Eg5-directed treatment. However, more research in these cancer types is required to determine which variants of the EML4-ALK fusion are expressed and whether they utilise the same signalling pathways as found in NSCLC.

6.8. Concluding statement

Here I have shown the mitotic kinesin Eg5 is a downstream target of the EML4-ALK V3:NEK9:NEK7 signalling module. Specifically, NEK7 phosphorylation of Eg5 on S1033 may contribute to its untimely recruitment to interphase microtubules and the microtubule dependent changes in cell morphology exhibited by EML4-ALK V3 expressing cells. Eg5 represents a potential novel target for the treatment of ALK+ NSCLC and future research on both mechanistic understanding and translational studies could build upon the findings presented in this thesis. I have also shown that EML4-ALK V3 may be recruited to the centrosome where it can promote microtubule nucleation. The centrosome may also therefore represent a potential target for therapeutic intervention in ALK+ cancers. Together, the hope is that this will ultimately lead to new options and better outcomes for lung cancer patients.

CHAPTER 7

Bibliography

- Acar, S., Carlson, D.B., Budamagunta, M.S., Yarov-Yarovoy, V., Correia, J.J., Niñonuevo, M.R., Jia, W., Tao, L., Leary, J.A., Voss, J.C., Evans, J.E. & Scholey, J.M.** (2013). The bipolar assembly domain of the mitotic motor kinesin-5. *Nature Communications*, 4(1):1343.
- Adib, R.** (2019). *EML4: Cell Cycle-Dependent Regulation And Function*. University of Leicester. Available from: https://figshare.com/articles/thesis/EML4_Cell_Cycle-Dependent_Regulation_And_Function/10239962
- Adib, R., Montgomery, J.M., Atherton, J., O'Regan, L., Richards, M.W., Straatman, K.R., Roth, D., Straube, A., Bayliss, R., Moores, C.A. & Fry, A.M.** (2019). Mitotic phosphorylation by NEK6 and NEK7 reduces the microtubule affinity of EML4 to promote chromosome congression. *Science Signaling*, 12(594):eaaw2939.
- Akhmanova, A. & Steinmetz, M.O.** (2010). Microtubule +TIPs at a glance. *Journal of Cell Science*, 123(20):3415-3419.
- Ananthakrishnan, R. & Ehrlicher, A.** (2007). The Forces Behind Cell Movement. *International Journal of Biological Sciences*:303-317.
- Arquint, C., Gabryjonczyk, A.-M. & Nigg, E.A.** (2014). Centrosomes as signalling centres. *Philosophical Transactions of the Royal Society B: Biological Sciences*, 369(1650):20130464.
- Artym, V.V. & Matsumoto, K.** (2010). Imaging Cells in Three-Dimensional Collagen Matrix. *Current Protocols in Cell Biology*, 48(1):10.18.11-10.18.12.
- Baas, P.W. & Lin, S.** (2011). Hooks and comets: The story of microtubule polarity orientation in the neuron. *Developmental Neurobiology*, 71(6):403-418.
- Bachus, S., Graves, D., Fulham, L., Akkerman, N., Stephanson, C., Shieh, J. & Pelka, P.** (2022). In Mitosis You Are Not: The NIMA Family of Kinases in Aspergillus, Yeast, and Mammals. *International Journal of Molecular Sciences*, 23(7):4041.
- Bailly, E., Dorée, M., Nurse, P. & Bornens, M.** (1989). p34cdc2 is located in both nucleus and cytoplasm; part is centrosomally associated at G2/M and enters vesicles at anaphase. *The EMBO journal*, 8(13):3985-3995.
- Bance, B., Seetharaman, S., Leduc, C., Boëda, B. & Etienne-Manneville, S.** (2019). Microtubule acetylation but not detyrosination promotes focal adhesion dynamics and astrocyte migration. *Journal of Cell Science*, 132(7):jcs225805.
- Bär, J., Popp, Y., Bucher, M. & Mikhaylova, M.** (2022). Direct and indirect effects of tubulin post-translational modifications on microtubule stability: Insights and regulations. *Biochimica et Biophysica Acta (BBA) - Molecular Cell Research*, 1869(6):119241.
- Barlan, K. & Gelfand, V.I.** (2017). Microtubule-Based Transport and the Distribution, Tethering, and Organization of Organelles. *Cold Spring Harbor Perspectives in Biology*, 9(5):a025817.
- Bayliss, R., Choi, J., Fennell, D.A., Fry, A.M. & Richards, M.W.** (2016). Molecular mechanisms that underpin EML4-ALK driven cancers and their response to targeted drugs. *Cellular and Molecular Life Sciences*, 73(6):1209-1224.
- Belham, C., Roig, J., Caldwell, J.A., Aoyama, Y., Kemp, B.E., Comb, M. & Avruch, J.** (2003). A Mitotic Cascade of NIMA Family Kinases. *Journal of Biological Chemistry*, 278(37):34897-34909.

- Bertran, M.T., Sdelci, S., Regué, L., Avruch, J., Caelles, C. & Roig, J.** (2011). Nek9 is a Plk1-activated kinase that controls early centrosome separation through Nek6/7 and Eg5. *The EMBO Journal*, 30(13):2634-2647.
- Blangy, A., Lane, H.A., D'Hérin, P., Harper, M., Kress, M. & Nigg, E.A.** (1995). Phosphorylation by p34cdc2 regulates spindle association of human Eg5, a kinesin-related motor essential for bipolar spindle formation in vivo. *Cell*, 83(7):1159-1169.
- Boggs, A.E., Vitolo, M.I., Whipple, R.A., Charpentier, M.S., Goloubeva, O.G., Ioffe, O.B., Tuttle, K.C., Slovic, J., Lu, Y., Mills, G.B. & Martin, S.S.** (2015). α -Tubulin Acetylation Elevated in Metastatic and Basal-like Breast Cancer Cells Promotes Microtentacle Formation, Adhesion, and Invasive Migration. *Cancer Research*, 75(1):203-215.
- Bossi, R.T., Saccardo, M.B., Ardini, E., Menichincheri, M., Rusconi, L., Magnaghi, P., Orsini, P., Avanzi, N., Borgia, A.L., Nesi, M., Bandiera, T., Fogliatto, G. & Bertrand, J.A.** (2010). Crystal Structures of Anaplastic Lymphoma Kinase in Complex with ATP Competitive Inhibitors. *Biochemistry*, 49(32):6813-6825.
- Bouchet, B.P., Noordstra, I., Van Amersfoort, M., Katrukha, E.A., Ammon, Y.-C., Ter Hoeve, N.D., Hodgson, L., Dogterom, M., Derksen, P.W.B. & Akhmanova, A.** (2016). Mesenchymal Cell Invasion Requires Cooperative Regulation of Persistent Microtubule Growth by SLAIN2 and CLASP1. *Developmental Cell*, 39(6):708-723.
- Bowne-Anderson, H., Zanic, M., Kauer, M. & Howard, J.** (2013). Microtubule dynamic instability: A new model with coupled GTP hydrolysis and multistep catastrophe. *BioEssays*, 35(5):452-461.
- Brinkley, B.R.** (2001). Managing the centrosome numbers game: from chaos to stability in cancer cell division. *Trends in Cell Biology*, 11(1):18-21.
- Cahu, J., Olichon, A., Hentrich, C., Schek, H., Drinjakovic, J., Zhang, C., Doherty-Kirby, A., Lajoie, G. & Surrey, T.** (2008). Phosphorylation by Cdk1 Increases the Binding of Eg5 to Microtubules In Vitro and in Xenopus Egg Extract Spindles. *PLoS ONE*, 3(12):e3936.
- Cancer Research UK**, nd. *Lung Cancer Statistics*. [online] Available at: <<https://www.cancerresearchuk.org/health-professional/cancer-statistics/statistics-by-cancer-type/lung-cancer#heading-One>> [Accessed 15 May 2023].
- Cancer.org**. 2022. *Lung Cancer Statistics | How Common is Lung Cancer?*. [online] Available at: <<https://www.cancer.org/cancer/lung-cancer/about/key-statistics.html>> [Accessed 16 March 2022].
- Cancer.org**. 2022. *What Is Lung Cancer? | Types of Lung Cancer*. [online] Available at: <<https://www.cancer.org/cancer/lung-cancer/about/what-is.html#:~:text=Non%2Dsmall%20cell%20lung%20cancer,carcinoma%2C%20and%20large%20cell%20carcinoma.>> [Accessed 16 March 2022].
- Cancer.sanger.ac.uk**. nd. *Sample overview for COSS687816*. [online] Available at: <https://cancer.sanger.ac.uk/cell_lines/sample/overview?id=687816#mut-spec> [Accessed 9 January 2023].
- Casey, J.P., Brennan, K., Scheidel, N., McGettigan, P., Lavin, P.T., Carter, S., Ennis, S., Dorkins, H., Ghali, N., Blacque, O.E., Mc Gee, M.M., Murphy, H. & Lynch, S.A.** (2016).

Recessive NEK9 mutation causes a lethal skeletal dysplasia with evidence of cell cycle and ciliary defects. *Human Molecular Genetics*, 25(9):1824-1835.

Castillo, A., Morse, H.C., III, Godfrey, V.L., Naeem, R. & Justice, M.J. (2007). Overexpression of Eg5 Causes Genomic Instability and Tumor Formation in Mice. *Cancer Research*, 67(21):10138-10147.

Cau, J. & Hall, A. (2005). Cdc42 controls the polarity of the actin and microtubule cytoskeletons through two distinct signal transduction pathways. *Journal of Cell Science*, 118(12):2579-2587.

Caviston, J.P. & Holzbaur, E.L.F. (2006). Microtubule motors at the intersection of trafficking and transport. *Trends in Cell Biology*, 16(10):530-537.

Chaaban, S. & Brouhard, G.J. (2017). A microtubule bestiary: structural diversity in tubulin polymers. *Molecular Biology of the Cell*, 28(22):2924-2931.

Chattopadhyay, S., Stewart, Alison L., Mukherjee, S., Huang, C., Hartwell, Kimberly A., Miller, Peter G., Subramanian, R., Carmody, Leigh C., Yusuf, Rushdia Z., Sykes, David B., Paulk, J., Vetere, A., Vallet, S., Santo, L., Cirstea, Diana D., Hideshima, T., Dančák, V., Majireck, Max M., Hussain, Mahmud M., Singh, S., Quiroz, R., Iaconelli, J., Karmacharya, R., Tolliday, Nicola J., Clemons, Paul A., Moore, Malcolm A.S., Stern, Andrew M., Shamji, Alykhan F., Ebert, Benjamin L., Golub, Todd R., Raje, Noopur S., Scadden, David T. & Schreiber, Stuart L. (2015). Niche-Based Screening in Multiple Myeloma Identifies a Kinesin-5 Inhibitor with Improved Selectivity over Hematopoietic Progenitors. *Cell Reports*, 10(5):755-770.

Chen, G.-Y., Cleary, J.M., Asenjo, A.B., Chen, Y., Mascaro, J.A., Arginteanu, D.F.J., Sosa, H. & Hancock, W.O. (2019). Kinesin-5 Promotes Microtubule Nucleation and Assembly by Stabilizing a Lattice-Competent Conformation of Tubulin. *Current Biology*, 29(14):2259-2269.e2254.

Chen, G.-Y., Kang, Y.J., Gayek, A.S., Youyen, W., Tüzel, E., Ohi, R. & Hancock, W.O. (2017). Eg5 Inhibitors Have Contrasting Effects on Microtubule Stability and Metaphase Spindle Integrity. *ACS Chemical Biology*, 12(4):1038-1046.

Chen, Y. & Hancock, W.O. (2015). Kinesin-5 is a microtubule polymerase. *Nature Communications*, 6(1):8160.

Chevallier, M., Borgeaud, M., Addeo, A. & Friedlaender, A. (2021). Oncogenic driver mutations in non-small cell lung cancer: Past, present and future. *World Journal of Clinical Oncology*, 12(4):217-237.

Choi, Y.L., Soda, M., Yamashita, Y., Ueno, T., Takashima, J., Nakajima, T., Yatabe, Y., Takeuchi, K., Hamada, T., Haruta, H., Ishikawa, Y., Kimura, H., Mitsudomi, T., Tanio, Y. & Mano, H. (2010). EML4-ALK Mutations in Lung Cancer That Confer Resistance to ALK Inhibitors. *New England Journal of Medicine*, 363(18):1734-1739.

Choi, Y.L., Takeuchi, K., Soda, M., Inamura, K., Togashi, Y., Hatano, S., Enomoto, M., Hamada, T., Haruta, H., Watanabe, H., Kurashina, K., Hatanaka, H., Ueno, T., Takada, S., Yamashita, Y., Sugiyama, Y., Ishikawa, Y. & Mano, H. (2008). Identification of Novel Isoforms of the EML4-ALK Transforming Gene in Non-Small Cell Lung Cancer. *Cancer Research*, 68(13):4971-4976.

- Christopoulos, P., Endris, V., Bozorgmehr, F., Elsayed, M., Kirchner, M., Ristau, J., Buchhalter, I., Penzel, R., Herth, F.J., Heussel, C.P., Eichhorn, M., Muley, T., Meister, M., Fischer, J.R., Rieken, S., Warth, A., Bischoff, H., Schirmacher, P., Stenzinger, A. & Thomas, M.** (2018). EML4-ALKfusion variant V3 is a high-risk feature conferring accelerated metastatic spread, early treatment failure and worse overall survival in ALK+non-small cell lung cancer. *International Journal of Cancer*, 142(12):2589-2598.
- Christopoulos, P., Kirchner, M., Bozorgmehr, F., Endris, V., Elsayed, M., Budczies, J., Ristau, J., Penzel, R., Herth, F.J., Heussel, C.P., Eichhorn, M., Muley, T., Meister, M., Fischer, J.R., Rieken, S., Lasitschka, F., Bischoff, H., Sotillo, R., Schirmacher, P., Thomas, M. & Stenzinger, A.** (2019). Identification of a highly lethal V3⁺TP53⁺subset in ALK⁺lung adenocarcinoma. *International Journal of Cancer*, 144(1):190-199.
- Cohen, S., Aizer, A., Shav-Tal, Y., Yanai, A. & Motro, B.** (2013). Nek7 kinase accelerates microtubule dynamic instability. *Biochimica et Biophysica Acta (BBA) - Molecular Cell Research*, 1833(5):1104-1113.
- Costes, S.V., Daelemans, D., Cho, E.H., Dobbin, Z., Pavlakis, G. & Lockett, S.** (2004). Automatic and Quantitative Measurement of Protein-Protein Colocalization in Live Cells. *Biophysical Journal*, 86(6):3993-4003.
- Cullati, S.N., Kabeche, L., Kettenbach, A.N. & Gerber, S.A.** (2017). A bifurcated signaling cascade of NIMA-related kinases controls distinct kinesins in anaphase. *Journal of Cell Biology*, 216(8):2339-2354.
- Dai, Y., Wei, Q., Schwager, C., Moustafa, M., Zhou, C., Lipson, K.E., Weichert, W., Debus, J. & Abdollahi, A.** (2015). Synergistic effects of crizotinib and radiotherapy in experimental EML4-ALK fusion positive lung cancer. *Radiotherapy and Oncology*, 114(2):173-181.
- De Keersmaecker, K., Graux, C., Odero, M.D., Mentens, N., Somers, R., Maertens, J., Wlodarska, I., Vandenberghe, P., Hagemeyer, A., Marynen, P. & Cools, J.** (2005). Fusion of EML1 to ABL1 in T-cell acute lymphoblastic leukemia with cryptic t(9;14)(q34;q32). *Blood*, 105(12):4849-4852.
- De Munck, S., Provost, M., Kurikawa, M., Omori, I., Mukohyama, J., Felix, J., Bloch, Y., Abdel-Wahab, O., Bazan, J.F., Yoshimi, A. & Savvides, S.N.** (2021). Structural basis of cytokine-mediated activation of ALK family receptors. *Nature*, 600(7887):143-147.
- De Souza, E.E., Hehnly, H., Perez, A.M., Meirelles, G.V., Smetana, J.H.C., Doxsey, S. & Kobarg, J.** (2015). Human Nek7-interactor RGS2 is required for mitotic spindle organization. *Cell Cycle*, 14(4):656-667.
- De Souza, E.E., Meirelles, G.V., Godoy, B.B., Perez, A.M., Smetana, J.H.C., Doxsey, S.J., McComb, M.E., Costello, C.E., Whelan, S.A. & Kobarg, J.** (2014). Characterization of the Human NEK7 Interactome Suggests Catalytic and Regulatory Properties Distinct from Those of NEK6. *Journal of Proteome Research*, 13(9):4074-4090.
- Deguchi, T., Iwanski, M.K., Schentarra, E.-M., Heidebrecht, C., Schmidt, L., Heck, J., Weihs, T., Schnorrenberg, S., Hoess, P., Liu, S., Chevreva, V., Noh, K.-M., Kapitein, L.C. & Ries, J.**

(2023). Direct observation of motor protein stepping in living cells using MINFLUX. *Science*, 379(6636):1010-1015.

del Rio, A., Perez-Jimenez, R., Liu, R., Roca-Cusachs, P., Fernandez, J.M. & Sheetz, M.P. (2009). Stretching single talin rod molecules activates vinculin binding. *Science*, 323(5914):638-641.

Della Corte, C.M., Viscardi, G., Di Liello, R., Fasano, M., Martinelli, E., Troiani, T., Ciardiello, F. & Morgillo, F. (2018). Role and targeting of anaplastic lymphoma kinase in cancer. *Molecular Cancer*, 17(1)

Desai, A. & Mitchison, T.J. (1997). MICROTUBULE POLYMERIZATION DYNAMICS. *Annual Review of Cell and Developmental Biology*, 13(1):83-117.

Díaz-Serrano, A., Gella, P., Jiménez, E., Zugazagoitia, J. & Paz-Ares Rodríguez, L. (2018). Targeting EGFR in Lung Cancer: Current Standards and Developments. *Drugs*, 78(9):893-911.

Dogterom, M. & Koenderink, G.H. (2019). Actin–microtubule crosstalk in cell biology. *Nature Reviews Molecular Cell Biology*, 20(1):38-54.

Du, X., Shao, Y., Qin, H.-F., Tai, Y.-H. & Gao, H.-J. (2018). ALK rearrangement in non-small-cell lung cancer (NSCLC). *Thoracic Cancer*, 9(4):423-430.

Dutertre, S.P., Cazales, M., Quaranta, M., Froment, C., Trabut, V., Dozier, C., Mirey, G., Bouché, J.-P., Theis-Febvre, N., Schmitt, E., Monsarrat, B., Prigent, C. & Ducommun, B. (2004). Phosphorylation of CDC25B by Aurora-A at the centrosome contributes to the G2–M transition. *Journal of Cell Science*, 117(12):2523-2531.

Eibes, S., Gallisà-Suñé, N., Rosas-Salvans, M., Martínez-Delgado, P., Vernos, I. & Roig, J. (2018). Nek9 Phosphorylation Defines a New Role for TPX2 in Eg5-Dependent Centrosome Separation before Nuclear Envelope Breakdown. *Current Biology*, 28(1):121-129.e124.

Eichenmüller, B., Everley, P., Palange, J., Lepley, D. & Suprenant, K.A. (2002). The Human EMAP-like Protein-70 (ELP70) Is a Microtubule Destabilizer That Localizes to the Mitotic Apparatus. *Journal of Biological Chemistry*, 277(2):1301-1309.

Elshatlawy, M., Sampson, J., Clarke, K. & Bayliss, R. (2023). <sc>EML4-ALK</sc> biology and drug resistance in <sc>non-small</sc> cell lung cancer: a new phase of discoveries. *Molecular Oncology*,

Etienne-Manneville, S. (2013). Microtubules in Cell Migration. *Annual Review of Cell and Developmental Biology*, 29(1):471-499.

Etienne-Manneville, S. (2004). Cdc42 - the centre of polarity. *Journal of Cell Science*, 117(8):1291-1300.

Etienne-Manneville, S. & Hall, A. (2002). Rho GTPases in cell biology. *Nature*, 420(6916):629-635.

Eudy, J.D., Ma-Edmonds, M., Yao, S., Talmadge, C.B., Kelley, P.M., Weston, M.D., Kimberling, W.J. & Sumegi, J. (1997). Isolation of a Novel Human Homologue of the Gene Coding for Echinoderm Microtubule-Associated Protein (EMAP) from the Usher Syndrome Type 1a Locus at 14q32. *Genomics*, 43(1):104-106.

Exertier, P., Javerzat, S., Wang, B., Franco, M., Herbert, J., Platonova, N., Winandy, M., Pujol, N., Nivelles, O., Ormenese, S., Godard, V., Becker, J., Bicknell, R., Pineau, R., Wilting,

- J., Bikfalvi, A. & Hagedorn, M.** (2013). Impaired angiogenesis and tumor development by inhibition of the mitotic kinesin Eg5. *Oncotarget*, 4(12):2302-2316.
- Ezratty, E.J., Partridge, M.A. & Gundersen, G.G.** (2005). Microtubule-induced focal adhesion disassembly is mediated by dynamin and focal adhesion kinase. *Nature Cell Biology*, 7(6):581-590.
- Falnikar, A., Tole, S. & Baas, P.W.** (2011). Kinesin-5, a mitotic microtubule-associated motor protein, modulates neuronal migration. *Molecular Biology of the Cell*, 22(9):1561-1574.
- Fang, X. & Svitkina, T.M.** (2022). Adenomatous Polyposis Coli (APC) in cell migration. *European Journal of Cell Biology*, 101(3):151228.
- Fletcher, C.**, 2019. *Diagnostic histopathology of tumors*. 5th ed. Elsevier, pp.225-272.
- Flevaris, P., Stojanovic, A., Gong, H., Chishti, A., Welch, E. & Du, X.** (2007). A molecular switch that controls cell spreading and retraction. *Journal of Cell Biology*, 179(3):553-565.
- Franco, S.J., Rodgers, M.A., Perrin, B.J., Han, J., Bennin, D.A., Critchley, D.R. & Huttenlocher, A.** (2004). Calpain-mediated proteolysis of talin regulates adhesion dynamics. *Nature Cell Biology*, 6(10):977-983.
- Freixo, F., Martinez Delgado, P., Manso, Y., Sánchez-Huertas, C., Lacasa, C., Soriano, E., Roig, J. & Lüders, J.** (2018). NEK7 regulates dendrite morphogenesis in neurons via Eg5-dependent microtubule stabilization. *Nature Communications*, 9(1)
- Fry, A.M., Bayliss, R. & Roig, J.** (2017). Mitotic Regulation by NEK Kinase Networks. *Front Cell Dev Biol*, 5:102.
- Fry, A.M., Mayor, T., Meraldi, P., Stierhof, Y.-D., Tanaka, K. & Nigg, E.A.** (1998). C-Nap1, a Novel Centrosomal Coiled-Coil Protein and Candidate Substrate of the Cell Cycle-regulated Protein Kinase Nek2. *Journal of Cell Biology*, 141(7):1563-1574.
- Fry, A.M., O'Regan, L., Montgomery, J., Adib, R. & Bayliss, R.** (2016). EML proteins in microtubule regulation and human disease. *Biochemical Society Transactions*, 44(5):1281-1288.
- Fry, A.M., O'Regan, L., Sabir, S.R. & Bayliss, R.** (2012). Cell cycle regulation by the NEK family of protein kinases. *Journal of Cell Science*, 125(19):4423-4433.
- Fukasawa, K.** (2005). Centrosome amplification, chromosome instability and cancer development. *Cancer Letters*, 230(1):6-19.
- Fukata, M., Watanabe, T., Noritake, J., Nakagawa, M., Yamaga, M., Kuroda, S., Matsuura, Y., Iwamatsu, A., Perez, F. & Kaibuchi, K.** (2002). Rac1 and Cdc42 Capture Microtubules through IQGAP1 and CLIP-170. *Cell*, 109(7):873-885.
- Gainor, J.F. & Shaw, A.T.** (2013). Emerging Paradigms in the Development of Resistance to Tyrosine Kinase Inhibitors in Lung Cancer. *Journal of Clinical Oncology*, 31(31):3987-3996.
- Gainor, J.F., Varghese, A.M., Ou, S.-H.I., Kabraji, S., Awad, M.M., Katayama, R., Pawlak, A., Mino-Kenudson, M., Yeap, B.Y., Riely, G.J., Iafrate, A.J., Arcila, M.E., Ladanyi, M., Engelman, J.A., Dias-Santagata, D. & Shaw, A.T.** (2013). *ALK* Rearrangements Are Mutually Exclusive with Mutations in *EGFR* or *KRAS*: An Analysis of 1,683 Patients with Non-Small Cell Lung Cancer. *Clinical Cancer Research*, 19(15):4273-4281.

- Garcia-Saez, I. & Skoufias, D.A.** (2021). Eg5 targeting agents: From new anti-mitotic based inhibitor discovery to cancer therapy and resistance. *Biochemical Pharmacology*, 184:114364.
- Garcin, C. & Straube, A.** (2019). Microtubules in cell migration. *Essays in Biochemistry*, 63(5):509-520.
- Gardner, M.K., Zanic, M. & Howard, J.** (2013). Microtubule catastrophe and rescue. *Current Opinion in Cell Biology*, 25(1):14-22.
- George, R.E., Sanda, T., Hanna, M., Fröhling, S., li, W.L., Zhang, J., Ahn, Y., Zhou, W., London, W.B., McGrady, P., Xue, L., Zozulya, S., Gregor, V.E., Webb, T.R., Gray, N.S., Gilliland, D.G., Diller, L., Greulich, H., Morris, S.W., Meyerson, M. & Look, A.T.** (2008). Activating mutations in ALK provide a therapeutic target in neuroblastoma. *Nature*, 455(7215):975-978.
- Gill, S.R., Schroer, T.A., Szilak, I., Steuer, E.R., Sheetz, M.P. & Cleveland, D.W.** (1991). Dynactin, a conserved, ubiquitously expressed component of an activator of vesicle motility mediated by cytoplasmic dynein. *Journal of Cell Biology*, 115(6):1639-1650.
- Godinho, S.A. & Pellman, D.** (2014). Causes and consequences of centrosome abnormalities in cancer. *Philosophical Transactions of the Royal Society B: Biological Sciences*, 369(1650):20130467.
- Golsteyn, R.M., Mundt, K.E., Fry, A.M. & Nigg, E.A.** (1995). Cell cycle regulation of the activity and subcellular localization of Plk1, a human protein kinase implicated in mitotic spindle function. *Journal of Cell Biology*, 129(6):1617-1628.
- Govindaraghavan, M., McGuire Anglin, S.L., Shen, K.-F., Shukla, N., De Souza, C.P. & Osmani, S.A.** (2014). Identification of Interphase Functions for the NIMA Kinase Involving Microtubules and the ESCRT Pathway. *PLoS Genetics*, 10(3):e1004248.
- Graziani, V., Rodriguez-Hernandez, I., Maiques, O. & Sanz-Moreno, V.** (2022). The amoeboid state as part of the epithelial-to-mesenchymal transition programme. *Trends in Cell Biology*, 32(3):228-242.
- Groen, A.C., Needleman, D., Brangwynne, C., Gradinaru, C., Fowler, B., Mazitschek, R. & Mitchison, T.J.** (2008). A novel small-molecule inhibitor reveals a possible role of kinesin-5 in anastral spindle-pole assembly. *Journal of Cell Science*, 121(14):2293-2300.
- Grosse, A., Grosse, C., Rechsteiner, M. & Soltermann, A.** (2019). Analysis of the frequency of oncogenic driver mutations and correlation with clinicopathological characteristics in patients with lung adenocarcinoma from Northeastern Switzerland. *Diagnostic Pathology*, 14(1)
- Guan, J., Umapathy, G., Yamazaki, Y., Wolfstetter, G., Mendoza, P., Pfeifer, K., Mohammed, A., Hugosson, F., Zhang, H., Hsu, A.W., Halenbeck, R., Hallberg, B. & Palmer, R.H.** (2015). FAM150A and FAM150B are activating ligands for anaplastic lymphoma kinase. *eLife*, 4
- Hafiyani, L.** (2022). *Investigating the regulation of EML proteins through their N-terminal domain*. University of Leicester. Available from:

[https://figshare.le.ac.uk/articles/thesis/Investigating the regulation of EML proteins through their N-terminal domain/22707943](https://figshare.le.ac.uk/articles/thesis/Investigating_the_regulation_of_EML_proteins_through_their_N-terminal_domain/22707943)

Haga, R.B. & Ridley, A.J. (2016). Rho GTPases: Regulation and roles in cancer cell biology. *Small GTPases*, 7(4):207-221.

Hallberg, B. & Palmer, R.H. (2016). The role of the ALK receptor in cancer biology. *Annals of Oncology*, 27:iii4-iii15.

Han, X., Na, T., Wu, T. & Yuan, B.-Z. (2020). Human lung epithelial BEAS-2B cells exhibit characteristics of mesenchymal stem cells. *PLOS ONE*, 15(1):e0227174.

Hanahan, D. & Weinberg, R.A. (2011). Hallmarks of Cancer: The Next Generation. *Cell*, 144(5):646-674.

Haq, T., Richards, M.W., Burgess, S.G., Gallego, P., Yeoh, S., O'Regan, L., Reverter, D., Roig, J., Fry, A.M. & Bayliss, R. (2015). Mechanistic basis of Nek7 activation through Nek9 binding and induced dimerization. *Nature Communications*, 6(1):8771.

Haque, S.A., Hasaka, T.P., Brooks, A.D., Lobanov, P.V. & Baas, P.W. (2004). Monastrol, a prototype anti-cancer drug that inhibits a mitotic kinesin, induces rapid bursts of axonal outgrowth from cultured postmitotic neurons. *Cell Motility and the Cytoskeleton*, 58(1):10-16.

He, Z., Ni, X., Xia, L. & Shao, Z. (2018). Overexpression of NIMA-related kinase 6 (NEK6) contributes to malignant growth and dismal prognosis in Human Breast Cancer. *Pathology - Research and Practice*, 214(10):1648-1654.

Hennessey, K.M., Alas, G.C.M., Rogiers, I., Li, R., Merritt, E.A. & Paredes, A.R. (2020). Nek8445, a protein kinase required for microtubule regulation and cytokinesis in *Giardia lamblia*. *Molecular Biology of the Cell*, 31(15):1611-1622.

Hernández-García, S., San-Segundo, L., González-Méndez, L., Corchete, L.A., Misiewicz-Krzeminska, I., Martín-Sánchez, M., López-Iglesias, A.-A., Algarín, E.M., Mogollón, P., Díaz-Tejedor, A., Paíno, T., Tunquist, B., Mateos, M.-V., Gutiérrez, N.C., Díaz-Rodríguez, E., Garayoa, M. & Ocio, E.M. (2017). The kinesin spindle protein inhibitor filanesib enhances the activity of pomalidomide and dexamethasone in multiple myeloma. *Haematologica*, 102(12):2113-2124.

Heuckmann, J.M., Balke-Want, H., Malchers, F., Peifer, M., Sos, M.L., Koker, M., Meder, L., Lovly, C.M., Heukamp, L.C., Pao, W., Küppers, R. & Thomas, R.K. (2012). Differential Protein Stability and ALK Inhibitor Sensitivity of EML4-ALK Fusion Variants. *Clinical Cancer Research*, 18(17):4682-4690.

Heuckmann, J.M., Hölzel, M., Sos, M.L., Heynck, S., Balke-Want, H., Koker, M., Peifer, M., Weiss, J., Lovly, C.M., Grütter, C., Rauh, D., Pao, W. & Thomas, R.K. (2011). ALK Mutations Conferring Differential Resistance to Structurally Diverse ALK Inhibitors. *Clinical Cancer Research*, 17(23):7394-7401.

Hill, M.A., Schedlich, L. & Gunning, P. (1994). Serum-induced signal transduction determines the peripheral location of beta-actin mRNA within the cell. *Journal of Cell Biology*, 126(5):1221-1229.

- Hirokawa, N., Noda, Y., Tanaka, Y. & Niwa, S.** (2009). Kinesin superfamily motor proteins and intracellular transport. *Nature Reviews Molecular Cell Biology*, 10(10):682-696.
- Hohmann & Dehghani.** (2019). The Cytoskeleton—A Complex Interacting Meshwork. *Cells*, 8(4):362.
- Hotta, T., McAlear, T.S., Yue, Y., Higaki, T., Haynes, S.E., Nesvizhskii, A.I., Sept, D., Verhey, K.J., Bechstedt, S. & Ohi, R.** (2022). EML2-S constitutes a new class of proteins that recognizes and regulates the dynamics of tyrosinated microtubules. *Current Biology*, 32(18):3898-3910.e3814.
- Houtman, S.H., Rutteman, M., De Zeeuw, C.I. & French, P.J.** (2007). Echinoderm microtubule-associated protein like protein 4, a member of the echinoderm microtubule-associated protein family, stabilizes microtubules. *Neuroscience*, 144(4):1373-1382.
- Huber, A.H., Nelson, W.J. & Weis, W.I.** (1997). Three-Dimensional Structure of the Armadillo Repeat Region of β -Catenin. *Cell*, 90(5):871-882.
- Hueston, J.L., Herren, G.P., Cueva, J.G., Buechner, M., Lundquist, E.A., Goodman, M.B. & Suprenant, K.A.** (2008). The *C. elegans*EMAP-like protein, ELP-1 is required for touch sensation and associates with microtubules and adhesion complexes. *BMC Developmental Biology*, 8(1):110.
- Indorato, R.-L., Talapatra, S.K., Lin, F., Haider, S., Mackay, S.P., Kozielski, F. & Skoufias, D.A.** (2019). Is the Fate of Clinical Candidate Arry-520 Already Sealed? Predicting Resistance in Eg5–Inhibitor Complexes. *Molecular Cancer Therapeutics*, 18(12):2394-2406.
- Innocenti, M.** (2018). New insights into the formation and the function of lamellipodia and ruffles in mesenchymal cell migration. *Cell Adhesion & Migration*:1-16.
- Iwahara, T., Fujimoto, J., Wen, D., Cupples, R., Bucay, N., Arakawa, T., Mori, S., Ratzkin, B. & Yamamoto, T.** (1997). Molecular characterization of ALK, a receptor tyrosine kinase expressed specifically in the nervous system. *Oncogene*, 14(4):439-449.
- Izumi, N., Fumoto, K., Izumi, S. & Kikuchi, A.** (2008). GSK-3 β Regulates Proper Mitotic Spindle Formation in Cooperation with a Component of the γ -Tubulin Ring Complex, GCP5. *Journal of Biological Chemistry*, 283(19):12981-12991.
- Jaber, N.** (2021). *FDA Approval of KRAS Inhibitor Sotorasib for Lung Cancer Hailed as Milestone*. Available from: <https://www.cancer.gov/news-events/cancer-currents-blog/2021/fda-sotorasib-lung-cancer-kras>
- Jana, S.C.** (2021). Centrosome structure and biogenesis: Variations on a theme? *Seminars in Cell & Developmental Biology*, 110:123-138.
- Janke, C. & Magiera, M.M.** (2020). The tubulin code and its role in controlling microtubule properties and functions. *Nature Reviews Molecular Cell Biology*, 21(6):307-326.
- Janke, C. & Montagnac, G.** (2017). Causes and Consequences of Microtubule Acetylation. *Current Biology*, 27(23):R1287-R1292.
- Jarmoskaite, I. & Russell, R.** (2011). DEAD-box proteins as RNA helicases and chaperones. *Wiley Interdisciplinary Reviews: RNA*, 2(1):135-152.

- Jayatilaka, H., Giri, A., Karl, M., Aifuwa, I., Trenton, N.J., Phillip, J.M., Khatau, S. & Wirtz, D.** (2018). EB1 and cytoplasmic dynein mediate protrusion dynamics for efficient 3-dimensional cell migration. *The FASEB Journal*, 32(3):1207-1221.
- Jin, Q., Huang, F., Wang, X., Zhu, H., Xian, Y., Li, J., Zhang, S. & Ni, Q.** (2017). High Eg5 expression predicts poor prognosis in breast cancer. *Oncotarget*, 8(37):62208-62216.
- Job, D., Valiron, O. & Oakley, B.** (2003). Microtubule nucleation. *Current Opinion in Cell Biology*, 15(1):111-117.
- Johnsson, A.-K. & Karlsson, R.** (2010). Microtubule-dependent localization of profilin I mRNA to actin polymerization sites in serum-stimulated cells. *European Journal of Cell Biology*, 89(5):394-401.
- Jolly, A.L., Kim, H., Srinivasan, D., Lakonishok, M., Larson, A.G. & Gelfand, V.I.** (2010). Kinesin-1 heavy chain mediates microtubule sliding to drive changes in cell shape. *Proceedings of the National Academy of Sciences*, 107(27):12151-12156.
- Jolly, M.K., Boareto, M., Huang, B., Jia, D., Lu, M., Ben-Jacob, E., Onuchic, J.N. & Levine, H.** (2015). Implications of the Hybrid Epithelial/Mesenchymal Phenotype in Metastasis. *Front Oncol*, 5:155.
- Juanes, M.A., Bouguenina, H., Eskin, J.A., Jaiswal, R., Badache, A. & Goode, B.L.** (2017). Adenomatous polyposis coli nucleates actin assembly to drive cell migration and microtubule-induced focal adhesion turnover. *Journal of Cell Biology*, 216(9):2859-2875.
- Jung, R., Radko, S. & Pelka, P.** (2016). The Dual Nature of Nek9 in Adenovirus Replication. *Journal of Virology*, 90(4):1931-1943.
- Kahn, O.I., Sharma, V., González-Billault, C. & Baas, P.W.** (2015). Effects of kinesin-5 inhibition on dendritic architecture and microtubule organization. *Molecular Biology of the Cell*, 26(1):66-77.
- Kalluri, R. & Weinberg, R.A.** (2009). The basics of epithelial-mesenchymal transition. *Journal of Clinical Investigation*, 119(6):1420-1428.
- Kapitein, L.C., Peterman, E.J.G., Kwok, B.H., Kim, J.H., Kapoor, T.M. & Schmidt, C.F.** (2005). The bipolar mitotic kinesin Eg5 moves on both microtubules that it crosslinks. *Nature*, 435(7038):114-118.
- Kashina, A.S., Baskin, R.J., Cole, D.G., Wedaman, K.P., Saxton, W.M. & Scholey, J.M.** (1996). A bipolar kinesin. *Nature*, 379(6562):270-272.
- Katayama, R., Khan, T.M., Benes, C., Lifshits, E., Ebi, H., Rivera, V.M., Shakespeare, W.C., Iafrate, A.J., Engelman, J.A. & Shaw, A.T.** (2011). Therapeutic strategies to overcome crizotinib resistance in non-small cell lung cancers harboring the fusion oncogene EML4-ALK. *Proceedings of the National Academy of Sciences*, 108(18):7535-7540.
- Kaverina, I., Rottner, K. & Small, J.V.** (1998). Targeting, Capture, and Stabilization of Microtubules at Early Focal Adhesions. *Journal of Cell Biology*, 142(1):181-190.
- Kazandjian, D., Blumenthal, G.M., Chen, H.-Y., He, K., Patel, M., Justice, R., Keegan, P. & Pazdur, R.** (2014). FDA Approval Summary: Crizotinib for the Treatment of Metastatic Non-Small Cell Lung Cancer With Anaplastic Lymphoma Kinase Rearrangements. *The Oncologist*, 19(10):e5-e11.

- Kielar, M., Tuy, F.P.D., Bizzotto, S., Lebrand, C., De Juan Romero, C., Poirier, K., Oegema, R., Mancini, G.M., Bahi-Buisson, N., Olaso, R., Le Moing, A.-G., Boutourlinsky, K., Boucher, D., Carpentier, W., Berquin, P., Deleuze, J.-F., Belvindrah, R., Borrell, V., Welker, E., Chelly, J., Croquelois, A. & Francis, F. (2014). Mutations in Eml1 lead to ectopic progenitors and neuronal heterotopia in mouse and human. *Nature Neuroscience*, 17(7):923-933.
- Kim, M., Jeong, H.J., Ju, H.-M., Song, J.-Y., Jang, S.J. & Choi, J. (2023). Overexpression of the NEK9–EG5 axis is a novel metastatic marker in pathologic stage T3 colon cancer. *Scientific Reports*, 13(1)
- Kim, S., Kim, S. & Rhee, K. (2011). NEK7 is essential for centriole duplication and centrosomal accumulation of pericentriolar material proteins in interphase cells. *Journal of Cell Science*, 124(22):3760-3770.
- King, S.J. & Schroer, T.A. (2000). Dynactin increases the processivity of the cytoplasmic dynein motor. *Nature Cell Biology*, 2(1):20-24.
- Kirschner, M. & Mitchison, T. (1986). Beyond self-assembly: From microtubules to morphogenesis. *Cell*, 45(3):329-342.
- Klymenko, Y., Kim, O., Loughran, E., Yang, J., Lombard, R., Alber, M. & Stack, M.S. (2017). Cadherin composition and multicellular aggregate invasion in organotypic models of epithelial ovarian cancer intraperitoneal metastasis. *Oncogene*, 36(42):5840-5851.
- Kollman, J.M., Merdes, A., Mourey, L. & Agard, D.A. (2011). Microtubule nucleation by γ -tubulin complexes. *Nature Reviews Molecular Cell Biology*, 12(11):709-721.
- Kollman, J.M., Polka, J.K., Zelter, A., Davis, T.N. & Agard, D.A. (2010). Microtubule nucleating γ -TuSC assembles structures with 13-fold microtubule-like symmetry. *Nature*, 466(7308):879-882.
- Krämer, A., Mailand, N., Lukas, C., Syljuåsen, R.G., Wilkinson, C.J., Nigg, E.A., Bartek, J. & Lukas, J. (2004). Centrosome-associated Chk1 prevents premature activation of cyclin-B–Cdk1 kinase. *Nature Cell Biology*, 6(9):884-891.
- Krendel, M., Zenke, F.T. & Bokoch, G.M. (2002). Nucleotide exchange factor GEF-H1 mediates cross-talk between microtubules and the actin cytoskeleton. *Nature Cell Biology*, 4(4):294-301.
- Kurioka, D., Takeshita, F., Tsuta, K., Sakamoto, H., Watanabe, S.-I., Matsumoto, K., Watanabe, M., Nakagama, H., Ochiya, T., Yokota, J., Kohno, T. & Tsuchiya, N. (2014). NEK9-dependent proliferation of cancer cells lacking functional p53. *Scientific Reports*, 4(1)
- Kwak, E.L., Bang, Y.-J., Camidge, D.R., Shaw, A.T., Solomon, B., Maki, R.G., Ou, S.-H.I., Dezube, B.J., Jänne, P.A., Costa, D.B., Varella-Garcia, M., Kim, W.-H., Lynch, T.J., Fidias, P., Stubbs, H., Engelman, J.A., Sequist, L.V., Tan, W., Gandhi, L., Mino-Kenudson, M., Wei, G.C., Shreeve, S.M., Ratain, M.J., Settleman, J., Christensen, J.G., Haber, D.A., Wilner, K., Salgia, R., Shapiro, G.I., Clark, J.W. & Iafrate, A.J. (2010). Anaplastic Lymphoma Kinase Inhibition in Non–Small-Cell Lung Cancer. *New England Journal of Medicine*, 363(18):1693-1703.
- Larson, A.G., Naber, N., Cooke, R., Pate, E. & Rice, S.E. (2010). The Conserved L5 Loop Establishes the Pre-Powerstroke Conformation of the Kinesin-5 Motor, Eg5. *Biophysical Journal*, 98(11):2619-2627.

- Lee, Christian C., Jia, Y., Li, N., Sun, X., Ng, K., Ambing, E., Gao, M.-Y., Hua, S., Chen, C., Kim, S., Michellys, P.-Y., Lesley, Scott A., Harris, Jennifer L. & Spraggon, G.** (2010). Crystal structure of the ALK (anaplastic lymphoma kinase) catalytic domain. *Biochemical Journal*, 430(3):425-437.
- Lee, M.-Y., Kim, H.-J., Kim, M.-A., Jee, H.J., Kim, A.J., Bae, Y.-S., Park, J.-I., Chung, J.H. & Yun, J.** (2008). Nek6 is involved in G₂/M phase cell cycle arrest through DNA damage-induced phosphorylation. *Cell Cycle*, 7(17):2705-2709.
- Lei, Y., Lei, Y., Shi, X. & Wang, J.** (2022). EML4-ALK fusion gene in non-small cell lung cancer (Review). *Oncology Letters*, 24(2)
- Lemjabbar-Alaoui, H., Hassan, O.U., Yang, Y.-W. & Buchanan, P.** (2015). Lung cancer: Biology and treatment options. *Biochimica et Biophysica Acta (BBA) - Reviews on Cancer*, 1856(2):189-210.
- Lepley, D.M., Palange, J.M. & Suprenant, K.A.** (1999). Sequence and expression patterns of a human EMAP-related protein-2 (HuEMAP-2). *Gene*, 237(2):343-349.
- Ley, S.C., Marsh, M., Bebbington, C.R., Proudfoot, K. & Jordan, P.** (1994). Distinct intracellular localization of Lck and Fyn protein tyrosine kinases in human T lymphocytes. *Journal of Cell Biology*, 125(3):639-649.
- Lin, E., Li, L., Guan, Y., Soriano, R., Rivers, C.S., Mohan, S., Pandita, A., Tang, J. & Modrusan, Z.** (2009). Exon Array Profiling Detects EML4-ALK Fusion in Breast, Colorectal, and Non-Small Cell Lung Cancers. *Molecular Cancer Research*, 7(9):1466-1476.
- Lin, H., Ren, G. & Liang, X.** (2018). A Novel EML6-ALK FBXO11-ALK Double Fusion Variant in Lung Adenocarcinoma and Response to Crizotinib. *Journal of Thoracic Oncology*, 13(11):e234-e236.
- Lin, M., Xie, S.S. & Chan, K.Y.** (2022). An updated view on the centrosome as a cell cycle regulator. *Cell Division*, 17(1)
- Liu, J., Kang, R. & Tang, D.** (2022). The KRAS-G12C inhibitor: activity and resistance. *Cancer Gene Therapy*, 29(7):875-878.
- Liu, M., Ran, J. & Zhou, J.** (2018). Non-canonical functions of the mitotic kinesin Eg5. *Thoracic Cancer*, 9(8):904-910.
- Liu, S., Huang, T., Liu, M., He, W., Zhao, Y., Yang, L., Long, Y., Zong, D., Zeng, H., Liu, Y., Liao, W., Duan, J., Gong, S. & Chen, S.** (2020). The Genomic Characteristics of ALK Fusion Positive Tumors in Chinese NSCLC Patients. *Frontiers in Oncology*, 10
- Liu, S., Lu, W., Obara, T., Kuida, S., Lehoczky, J., Dewar, K., Drummond, I.A. & Beier, D.R.** (2002). A defect in a novel Nek-family kinase causes cystic kidney disease in the mouse and in zebrafish. *Development*, 129(24):5839-5846.
- Loh, C.-Y., Chai, J., Tang, T., Wong, W., Sethi, G., Shanmugam, M., Chong, P. & Looi, C.** (2019). The E-Cadherin and N-Cadherin Switch in Epithelial-to-Mesenchymal Transition: Signaling, Therapeutic Implications, and Challenges. *Cells*, 8(10):1118.
- Lorén, C.E., Scully, A., Grabbe, C., Edeen, P.T., Thomas, J., McKeown, M., Hunter, T. & Palmer, R.H.** (2001). Identification and characterization of DAlk: a novel Drosophila

melanogaster RTK which drives ERK activation *in vivo*. *Genes to Cells*, 6(6):531-544.

Lu, W., Fox, P., Lakonishok, M., Michael & Vladimir. (2013). Initial Neurite Outgrowth in Drosophila Neurons Is Driven by Kinesin-Powered Microtubule Sliding. *Current Biology*, 23(11):1018-1023.

Lucken, K., O'Regan, L., Choi, J., Sampson, J., Pashley, S.L., Bayliss, R., Khan, S. & Fry, A.M. (2022). EML4-ALK variant 3 promotes mitotic errors and spindle assembly checkpoint deficiency leading to increased microtubule poison sensitivity EML4-ALK V3 sensitizes NSCLC cells to microtubule poisons. *Molecular Cancer Research*:OF1-OF13.

Luo, S.Y. & Lam, D.C. (2013). Oncogenic driver mutations in lung cancer. *Translational Respiratory Medicine*, 1(1):6.

Ma, N., Titus, J., Gable, A., Ross, J.L. & Wadsworth, P. (2011). TPX2 regulates the localization and activity of Eg5 in the mammalian mitotic spindle. *Journal of Cell Biology*, 195(1):87-98.

Magnaghi-Jaulin, L., Eot-Houllier, G., Gallaud, E. & Giet, R. (2019). Aurora A Protein Kinase: To the Centrosome and Beyond. *Biomolecules*, 9(1):28.

Mahjoub, M.R., Qasim Rasi, M. & Quarmby, L.M. (2004). A NIMA-related Kinase, Fa2p, Localizes to a Novel Site in the Proximal Cilia of *Chlamydomonas* and Mouse Kidney Cells. *Molecular Biology of the Cell*, 15(11):5172-5186.

Mann, B.J. & Wadsworth, P. (2019). Kinesin-5 Regulation and Function in Mitosis. *Trends in Cell Biology*, 29(1):66-79.

Marconi, G.D., Carradori, S., Ricci, A., Guglielmi, P., Cataldi, A. & Zara, S. (2019). Kinesin Eg5 Targeting Inhibitors as a New Strategy for Gastric Adenocarcinoma Treatment. *Molecules*, 24(21):3948.

Matsumoto, S., Fumoto, K., Okamoto, T., Kaibuchi, K. & Kikuchi, A. (2010). Binding of APC and dishevelled mediates Wnt5a-regulated focal adhesion dynamics in migrating cells. *The EMBO Journal*, 29(7):1192-1204.

Mattila, P.K. & Lappalainen, P. (2008). Filopodia: molecular architecture and cellular functions. *Nature Reviews Molecular Cell Biology*, 9(6):446-454.

Maziveyi, M. & Alahari, S.K. (2017). Cell matrix adhesions in cancer: The proteins that form the glue. *Oncotarget*, 8(29):48471-48487.

McIntosh, J.R., Molodtsov, M.I. & Ataullakhanov, F.I. (2012). Biophysics of mitosis. *Quarterly Reviews of Biophysics*, 45(2):147-207.

Meirelles, G.V., Perez, A.M., de Souza, E.E., Basei, F.L., Papa, P.F., Melo Hanchuk, T.D., Cardoso, V.B. & Kobarg, J. (2014). "Stop Ne(c)king around": How interactomics contributes to functionally characterize Nek family kinases. *World J Biol Chem*, 5(2):141-160.

Miki, H., Okada, Y. & Hirokawa, N. (2005). Analysis of the kinesin superfamily: insights into structure and function. *Trends in Cell Biology*, 15(9):467-476.

Mingle, L.A., Okuhama, N.N., Shi, J., Singer, R.H., Condeelis, J. & Liu, G. (2005). Localization of all seven messenger RNAs for the actin-polymerization nucleator Arp2/3 complex in the protrusions of fibroblasts. *Journal of Cell Science*, 118(11):2425-2433.

Mitchison, T. & Kirschner, M. (1984). Dynamic instability of microtubule growth. *Nature*, 312(5991):237-242.

Moniz, L., Dutt, P., Haider, N. & Stambolic, V. (2011). Nek family of kinases in cell cycle, checkpoint control and cancer. *Cell Division*, 6(1):18.

Morris, N.R. (1975). Mitotic mutants of *Aspergillus nidulans*. *Genetical Research*, 26(3):237-254.

Morris, S.W., Kirstein, M.N., Valentine, M.B., Dittmer, K.G., Shapiro, D.N., Saltman, D.L. & Look, A.T. (1994). Fusion of a Kinase Gene, *ALK*, to a Nucleolar Protein Gene, *NPM*, in Non-Hodgkin's Lymphoma. *Science*, 263(5151):1281-1284.

Morris, S.W., Naeve, C., Mathew, P., James, P.L., Kirstein, M.N., Cui, X. & Witte, D.P. (1997). ALK, the chromosome 2 gene locus altered by the t(2;5) in non-Hodgkin's lymphoma, encodes a novel neural receptor tyrosine kinase that is highly related to leukocyte tyrosine kinase (LTK). *Oncogene*, 14(18):2175-2188.

Mrozik, K.M., Blaschuk, O.W., Cheong, C.M., Zannettino, A.C.W. & Vandyke, K. (2018). N-cadherin in cancer metastasis, its emerging role in haematological malignancies and potential as a therapeutic target in cancer. *BMC Cancer*, 18(1)

Murray, B.W., Zhai, D., Deng, W., Zhang, X., Ung, J., Nguyen, V., Zhang, H., Barrera, M., Parra, A., Cowell, J., Lee, D.J., Aloysius, H. & Rogers, E. (2021). TPX-0131, a Potent CNS-penetrant, Next-generation Inhibitor of Wild-type ALK and ALK-resistant Mutations. *Molecular Cancer Therapeutics*, 20(9):1499-1507.

Myers, K.A. & Baas, P.W. (2007). Kinesin-5 regulates the growth of the axon by acting as a brake on its microtubule array. *Journal of Cell Biology*, 178(6):1081-1091.

Nadar, V.C., Ketschek, A., Myers, K.A., Gallo, G. & Baas, P.W. (2008). Kinesin-5 Is Essential for Growth-Cone Turning. *Current Biology*, 18(24):1972-1977.

Narumiya, S., Tanji, M. & Ishizaki, T. (2009). Rho signaling, ROCK and mDia1, in transformation, metastasis and invasion. *Cancer and Metastasis Reviews*, 28(1-2):65-76.

National Cancer Institute. 2022. *Non-Small Cell Lung Cancer Treatment (PDQ®)–Patient Version*. [online] Available at: <<https://www.cancer.gov/types/lung/patient/non-small-cell-lung-treatment-pdq>> [Accessed 16 March 2022].

NHS England. 2022. *Hundreds of patients to benefit from revolutionary lung cancer drug on the NHS*. Available from: <https://www.england.nhs.uk/2022/03/hundreds-of-patients-to-benefit-from-revolutionary-lung-cancer-drug-on-the-nhs/> (Accessed 1st March 2023).

NHS. 2019. *Lung cancer - Treatment*. [online] Available at: <<https://www.nhs.uk/conditions/lung-cancer/treatment/>> [Accessed 10 June 2022].

Nigg, E.A. & Holland, A.J. (2018). Once and only once: mechanisms of centriole duplication and their deregulation in disease. *Nature Reviews Molecular Cell Biology*, 19(5):297-312.

Nobre, A.R., Albergaria, A. & Schmitt, F. (2013). p40: A p63 Isoform Useful for Lung Cancer Diagnosis – A Review of the Physiological and Pathological Role of p63. *Acta Cytologica*, 57(1):1-8.

Noh, K.-W., Lee, M.-S., Lee, S.E., Song, J.-Y., Shin, H.-T., Kim, Y.J., Oh, D.Y., Jung, K., Sung, M., Kim, M., An, S., Han, J., Shim, Y.M., Zo, J.I., Kim, J., Park, W.-Y., Lee, S.-H. & Choi, Y.-L.

- (2017). Molecular breakdown: a comprehensive view of anaplastic lymphoma kinase (<i>ALK</i>)-rearranged non-small cell lung cancer. *The Journal of Pathology*, 243(3):307-319.
- O'Connor, V., Houtman, S.H., De Zeeuw, C.I., Bliss, T.V.P. & French, P.J.** (2004). Eml5, a novel WD40 domain protein expressed in rat brain. *Gene*, 336(1):127-137.
- O'Regan, L., Barone, G., Adib, R., Woo, C.G., Jeong, H.J., Richardson, E.L., Richards, M.W., Muller, P.A.J., Collis, S.J., Fennell, D.A., Choi, J., Bayliss, R. & Fry, A.M.** (2020). EML4-ALK V3 oncogenic fusion proteins promote microtubule stabilization and accelerated migration through NEK9 and NEK7. *Journal of Cell Science*, 133(9):jcs241505.
- O'Regan, L. & Fry, A.M.** (2009). The Nek6 and Nek7 Protein Kinases Are Required for Robust Mitotic Spindle Formation and Cytokinesis. *Molecular and Cellular Biology*, 29(14):3975-3990.
- O'Regan, L., Sampson, J., Richards, M.W., Knebel, A., Roth, D., Hood, F.E., Straube, A., Royle, S.J., Bayliss, R., Fry, A.M.** (2015). Hsp72 is targeted to the mitotic spindle by Nek6 to promote K-fiber assembly and mitotic progression. *Journal of Cell Biology* 209(3): 349-358.
- Oakley, B. & Morris, R.** (1983). A mutation in aspergillus nidulans that blocks the transition from interphase to prophase. *Journal of Cell Biology*, 96(4):1155-1158.
- Ocio, E.M., Motlló, C., Rodríguez-Otero, P., Martínez-López, J., Cejalvo, M.J., Martín-Sánchez, J., Bladé, J., García-Malo, M.D., Dourdil, M.V., García-Mateo, A., Arriba, F., García-Sanz, R., Rubia, J., Oriol, A., Lahuerta, J.J., San-Miguel, J.F. & Mateos, M.V.** (2021). Filanesib in combination with pomalidomide and dexamethasone in refractory MM patients: safety and efficacy, and association with alpha 1-acid glycoprotein (AAG) levels. Phase Ib/II Pomdefil clinical trial conducted by the Spanish MM group. *British Journal of Haematology*, 192(3):522-530.
- Ohashi, K., Nagata, K., Maekawa, M., Ishizaki, T., Narumiya, S. & Mizuno, K.** (2000). Rho-associated Kinase ROCK Activates LIM-kinase 1 by Phosphorylation at Threonine 508 within the Activation Loop. *Journal of Biological Chemistry*, 275(5):3577-3582.
- Oriolo, A.S., Wald, F.A., Canessa, G. & Salas, P.J.I.** (2007). GCP6 Binds to Intermediate Filaments: A Novel Function of Keratins in the Organization of Microtubules in Epithelial Cells. *Molecular Biology of the Cell*, 18(3):781-794.
- Osmani, N., Peglion, F., Chavrier, P. & Etienne-Manneville, S.** (2010). Cdc42 localization and cell polarity depend on membrane traffic. *Journal of Cell Biology*, 191(7):1261-1269.
- Osmani, S.A., Pu, R.T. & Morris, N.R.** (1988). Mitotic induction and maintenance by overexpression of a G2-specific gene that encodes a potential protein kinase. *Cell*, 53(2):237-244.
- Otto, E.A., Trapp, M.L., Schultheiss, U.T., Helou, J., Quarmby, L.M. & Hildebrandt, F.** (2008). NEK8 mutations affect ciliary and centrosomal localization and may cause nephronophthisis. *J Am Soc Nephrol*, 19(3):587-592.
- Ou, K., Liu, X., Li, W., Yang, Y., Ying, J. & Yang, L.** (2021). ALK Rearrangement-Positive Pancreatic Cancer with Brain Metastasis Has Remarkable Response to ALK Inhibitors: A Case Report. *Frontiers in Oncology*, 11

- Ou, S.-H.I., Nagasaka, M., Brazel, D., Hou, Y. & Zhu, V.W.** (2021). Will the clinical development of 4th-generation “double mutant active” ALK TKIs (TPX-0131 and NVL-655) change the future treatment paradigm of ALK+ NSCLC? *Translational Oncology*, 14(11):101191.
- Ouyang, M., Lu, S., Kim, T., Chen, C.-E., Seong, J., Leckband, D.E., Wang, F., Reynolds, A.B., Schwartz, M.A. & Wang, Y.** (2013). N-cadherin regulates spatially polarized signals through distinct p120ctn and β -catenin-dependent signalling pathways. *Nature Communications*, 4(1):1589.
- Owens, B.** (2013). Kinesin inhibitor marches toward first-in-class pivotal trial. *Nature Medicine*, 19(12):1550-1550.
- Palamidessi, A., Frittoli, E., Garré, M., Faretta, M., Mione, M., Testa, I., Diaspro, A., Lanzetti, L., Scita, G. & Di Fiore, P.P.** (2008). Endocytic Trafficking of Rac Is Required for the Spatial Restriction of Signaling in Cell Migration. *Cell*, 134(1):135-147.
- Papageorgiou, S., Pashley, S.L., O'Regan, L., Khan, S., Bayliss, R. & Fry, A.M.** (2022). Alternative Treatment Options to ALK Inhibitor Monotherapy for EML4-ALK-Driven Lung Cancer. *Cancers*, 14(14):3452.
- Parsons, J.T., Horwitz, A.R. & Schwartz, M.A.** (2010). Cell adhesion: integrating cytoskeletal dynamics and cellular tension. *Nature Reviews Molecular Cell Biology*, 11(9):633-643.
- Paterson, E.K. & Courtneidge, S.A.** (2018). Invadosomes are coming: new insights into function and disease relevance. *The FEBS Journal*, 285(1):8-27.
- Pelish, H.E., Tangpeerachaikul, A., Kohl, N.E., Porter, J.R., Shair, M.D. & Horan, J.C.** (2021). Abstract 1468: NUV-655 (NVL-655) is a selective, brain-penetrant ALK inhibitor with antitumor activity against the lorlatinib-resistant G1202R/L1196M compound mutation. *Cancer Research*, 81(13_Supplement):1468-1468.
- Peng, J., Wallar, B.J., Flanders, A., Swiatek, P.J. & Alberts, A.S.** (2003). Disruption of the Diaphanous-Related Formin Drf1 Gene Encoding mDia1 Reveals a Role for Drf3 as an Effector for Cdc42. *Current Biology*, 13(7):534-545.
- Peng, L., Zhu, L., Sun, Y., Stebbing, J., Selvaggi, G., Zhang, Y. & Yu, Z.** (2022). Targeting ALK Rearrangements in NSCLC: Current State of the Art. *Frontiers in Oncology*, 12
- Peris, L., They, M., Fauré, J., Saoudi, Y., Lafanechère, L., Chilton, J.K., Gordon-Weeks, P., Galjart, N., Bornens, M., Wordeman, L., Wehland, J., Andrieux, A. & Job, D.** (2006). Tubulin tyrosination is a major factor affecting the recruitment of CAP-Gly proteins at microtubule plus ends. *Journal of Cell Biology*, 174(6):839-849.
- Peris, L., Wagenbach, M., Lafanechère, L., Brocard, J., Moore, A.T., Kozielski, F., Job, D., Wordeman, L. & Andrieux, A.** (2009). Motor-dependent microtubule disassembly driven by tubulin tyrosination. *Journal of Cell Biology*, 185(7):1159-1166.
- Petry, S.** (2016). Mechanisms of Mitotic Spindle Assembly. *Annual Review of Biochemistry*, 85(1):659-683.
- Pillai, R.N. & Ramalingam, S.S.** (2018). Throwing More Cold Water on Heat Shock Protein 90 Inhibitors in NSCLC. *Journal of Thoracic Oncology*, 13(4):473-474.

- Pollmann, M., Parwaresch, R., Adam-Klages, S., Kruse, M.-L., Buck, F. & Heidebrecht, H.-J.** (2006). Human EML4, a novel member of the EMAP family, is essential for microtubule formation. *Experimental Cell Research*, 312(17):3241-3251.
- Portran, D., Schaedel, L., Xu, Z., Théry, M. & Maxence.** (2017). Tubulin acetylation protects long-lived microtubules against mechanical ageing. *Nature Cell Biology*, 19(4):391-398.
- Prosser, S.L. & Pelletier, L.** (2017). Mitotic spindle assembly in animal cells: a fine balancing act. *Nature Reviews Molecular Cell Biology*, 18(3):187-201.
- Qin, Z., Sun, H., Yue, M., Pan, X., Chen, L., Feng, X., Yan, X., Zhu, X. & Ji, H.** (2021). Phase separation of EML4–ALK in firing downstream signaling and promoting lung tumorigenesis. *Cell Discovery*, 7(1)
- Quarmby, L.M. & Mahjoub, M.R.** (2005). Caught Nek-ing: cilia and centrioles. *Journal of Cell Science*, 118(22):5161-5169.
- Rapley, J., Nicolàs, M., Groen, A., Regué, L., Bertran, M.T., Caelles, C., Avruch, J. & Roig, J.** (2008). The NIMA-family kinase Nek6 phosphorylates the kinesin Eg5 at a novel site necessary for mitotic spindle formation. *Journal of Cell Science*, 121(23):3912-3921.
- Raucher, D. & Sheetz, M.P.** (2000). Cell Spreading and Lamellipodial Extension Rate Is Regulated by Membrane Tension. *Journal of Cell Biology*, 148(1):127-136.
- Regué, L., Sdelci, S., Bertran, M.T., Caelles, C., Reverter, D. & Roig, J.** (2011). DYNLL/LC8 Protein Controls Signal Transduction through the Nek9/Nek6 Signaling Module by Regulating Nek6 Binding to Nek9. *Journal of Biological Chemistry*, 286(20):18118-18129.
- Reininger, L., Tewari, R., Fennell, C., Holland, Z., Goldring, D., Ranford-Cartwright, L., Billker, O. & Doerig, C.** (2009). An Essential Role for the Plasmodium Nek-2 Nima-related Protein Kinase in the Sexual Development of Malaria Parasites. *Journal of Biological Chemistry*, 284(31):20858-20868.
- Reshetnyak, A.V., Murray, P.B., Shi, X., Mo, E.S., Mohanty, J., Tome, F., Bai, H., Gunel, M., Lax, I. & Schlessinger, J.** (2015). Augmentor α and β (FAM150) are ligands of the receptor tyrosine kinases ALK and LTK: Hierarchy and specificity of ligand–receptor interactions. *Proceedings of the National Academy of Sciences*, 112(52):15862-15867.
- Reshetnyak, A.V., Rossi, P., Myasnikov, A.G., Sowaileh, M., Mohanty, J., Nourse, A., Miller, D.J., Lax, I., Schlessinger, J. & Kalodimos, C.G.** (2021). Mechanism for the activation of the anaplastic lymphoma kinase receptor. *Nature*, 600(7887):153-157.
- Richards, M.W., Law, E.W.P., Rennalls, L.P., Busacca, S., O'Regan, L., Fry, A.M., Fennell, D.A. & Bayliss, R.** (2014). Crystal structure of EML1 reveals the basis for Hsp90 dependence of oncogenic EML4-ALK by disruption of an atypical γ -propeller domain. *Proceedings of the National Academy of Sciences*, 111(14):5195-5200.
- Richards, M.W., O'Regan, L., Mas-Droux, C., Blot, J.M.Y., Cheung, J., Hoelder, S., Fry, A.M. & Bayliss, R.** (2009). An Autoinhibitory Tyrosine Motif in the Cell-Cycle-Regulated Nek7 Kinase Is Released through Binding of Nek9. *Molecular Cell*, 36(4):560-570.
- Richards, M.W., O'Regan, L., Roth, D., Montgomery, J.M., Straube, A., Fry, A.M. & Bayliss, R.** (2015). Microtubule association of EML proteins and the EML4-ALK variant 3 oncoprotein require an N-terminal trimerization domain. *Biochemical Journal*, 467(3):529-536.

- Richardson, E.L.** (2021). *The role and regulation of cortactin in EML4-ALK V3 non-small cell lung cancer*. University of Leicester. Available from: <https://ethos.bl.uk/OrderDetails.do?uin=uk.bl.ethos.842898>
- Ridley, A.J. & Hall, A.** (1992). The small GTP-binding protein rho regulates the assembly of focal adhesions and actin stress fibers in response to growth factors. *Cell*, 70(3):389-399.
- Roberts, A.J., Kon, T., Knight, P.J., Sutoh, K. & Burgess, S.A.** (2013). Functions and mechanics of dynein motor proteins. *Nature Reviews Molecular Cell Biology*, 14(11):713-726.
- Roche, J.** (2018). The Epithelial-to-Mesenchymal Transition in Cancer. *Cancers*, 10(2):52.
- Roig, J., Groen, A., Caldwell, J. & Avruch, J.** (2005). Active Ncrcc1 Protein Kinase Concentrates at Centrosomes Early in Mitosis and Is Necessary for Proper Spindle Assembly. *Molecular Biology of the Cell*, 16(10):4827-4840.
- Roig, J., Mikhailov, A., Belham, C. & Avruch, J.** (2002). Ncrcc1, a mammalian NIMA-family kinase, binds the Ran GTPase and regulates mitotic progression. *Genes & Development*, 16(13):1640-1658.
- Rolfo, C., Passiglia, F., Castiglia, M., Raez, L.E., Germonpre, P., Gil-Bazo, I., Zwaenepoel, K., De Wilde, A., Bronte, G., Russo, A., Van Meerbeeck, J.P., Van Schil, P. & Pauwels, P.** (2014). ALK and crizotinib: after the honeymoon...what else? Resistance mechanisms and new therapies to overcome it. *Transl Lung Cancer Res*, 3(4):250-261.
- Rooney, C., White, G., Nazgiewicz, A., Woodcock, S.A., Anderson, K.I., Ballestrem, C. & Malliri, A.** (2010). The Rac activator STEF (Tiam2) regulates cell migration by microtubule-mediated focal adhesion disassembly. *EMBO reports*, 11(4):292-298.
- Rottner, K. & Schaks, M.** (2019). Assembling actin filaments for protrusion. *Current Opinion in Cell Biology*, 56:53-63.
- Sabir, S., Yeoh, S., Jackson, G. & Bayliss, R.** (2017). EML4-ALK Variants: Biological and Molecular Properties, and the Implications for Patients. *Cancers*, 9(9):118.
- Saijo, T., Ishii, G., Ochiai, A., Yoh, K., Goto, K., Nagai, K., Kato, H., Nishiwaki, Y., Saijo, N.** (2006). Eg5 expression is closely correlated with the response of advanced non-small cell lung cancer to antimitotic agents combined with platinum chemotherapy. *Lung Cancer*, 54(2):217-225.
- Sampson, J., Ju, H.-M., Song, J.-Y., Fry, A.M., Bayliss, R. & Choi, J.** (2022). A Polytherapy Strategy Using Vincristine and ALK Inhibitors to Sensitise EML4-ALK-Positive NSCLC. *Cancers*, 14(3):779.
- Sampson, J., O'Regan, L., Dyer, M.J.S., Bayliss, R. & Fry, A.M.** (2017). Hsp72 and Nek6 Cooperate to Cluster Amplified Centrosomes in Cancer Cells. *Cancer Research*, 77(18):4785-4796.
- Sampson, J., Richards, M.W., Choi, J., Fry, A.M. & Bayliss, R.** (2021). Phase-separated foci of EML4-ALK facilitate signalling and depend upon an active kinase conformation. *EMBO reports*,
- Sasaki, T., Rodig, S.J., Chirieac, L.R. & Jänne, P.A.** (2010). The biology and treatment of EML4-ALK non-small cell lung cancer. *European Journal of Cancer*, 46(10):1773-1780.

- Satir, P. & Christensen, S.T.** (2007). Overview of Structure and Function of Mammalian Cilia. *Annual Review of Physiology*, 69(1):377-400.
- Sawin, K.E., Leguellec, K., Philippe, M. & Mitchison, T.J.** (1992). Mitotic spindle organization by a plus-end-directed microtubule motor. *Nature*, 359(6395):540-543.
- Sawin, K.E. & Mitchison, T.J.** (1995). Mutations in the kinesin-like protein Eg5 disrupting localization to the mitotic spindle. *Proceedings of the National Academy of Sciences*, 92(10):4289-4293.
- Schroer, T.A. & Sheetz, M.P.** (1991). Two activators of microtubule-based vesicle transport. *The Journal of Cell Biology*, 115(5):1309-1318.
- Sdelci, S., Schütz, M., Pinyol, R., M, Regué, L., Caelles, C., Vernos, I. & Roig, J.** (2012). Nek9 Phosphorylation of NEDD1/GCP-WD Contributes to Plk1 Control of γ -Tubulin Recruitment to the Mitotic Centrosome. *Current Biology*, 22(16):1516-1523.
- Serrano-Gomez, S.J., Maziveyi, M. & Alahari, S.K.** (2016). Regulation of epithelial-mesenchymal transition through epigenetic and post-translational modifications. *Molecular Cancer*, 15(1)
- Seyfried, T.N. & Huysentruyt, L.C.** (2013). On the Origin of Cancer Metastasis. *Critical Reviews[®] in Oncogenesis*, 18(1 - 2):43-73.
- Shao, Q. & Gao, Y.Q.** (2006). On the hand-over-hand mechanism of kinesin. *Proceedings of the National Academy of Sciences*, 103(21):8072-8077.
- Shao, Y.-Y., Sun, N.-Y., Jeng, Y.-M., Wu, Y.-M., Hsu, C., Hsu, C.-H., Hsu, H.-C., Cheng, A.-L. & Lin, Z.-Z.** (2021). Eg5 as a Prognostic Biomarker and Potential Therapeutic Target for Hepatocellular Carcinoma. *Cells*, 10(7):1698.
- Sharif, H., Wang, L., Wang, W.L., Magupalli, V.G., Andreeva, L., Qiao, Q., Hauenstein, A.V., Wu, Z., Núñez, G., Mao, Y. & Wu, H.** (2019). Structural mechanism for NEK7-licensed activation of NLRP3 inflammasome. *Nature*, 570(7761):338-343.
- Shaw, A.T., Kim, D.-W., Nakagawa, K., Seto, T., Crinó, L., Ahn, M.-J., De Pas, T., Besse, B., Solomon, B.J., Blackhall, F., Wu, Y.-L., Thomas, M., O'Byrne, K.J., Moro-Sibilot, D., Camidge, D.R., Mok, T., Hirsh, V., Riely, G.J., Iyer, S., Tassell, V., Polli, A., Wilner, K.D. & Jänne, P.A.** (2013). Crizotinib versus Chemotherapy in AdvancedALK-Positive Lung Cancer. *New England Journal of Medicine*, 368(25):2385-2394.
- Shi, J. & Mitchison, T.J.** (2017). Cell death response to anti-mitotic drug treatment in cell culture, mouse tumor model and the clinic. *Endocrine-Related Cancer*, 24(9):T83-T96.
- Singhi, A.D., Ali, S.M., Lacy, J., Hendifar, A., Nguyen, K., Koo, J., Chung, J.H., Greenbowe, J., Ross, J.S., Nikiforova, M.N., Zeh, H.J., Sarkaria, I.S., Dasyam, A. & Bahary, N.** (2017). Identification of Targetable ALK Rearrangements in Pancreatic Ductal Adenocarcinoma. *Journal of the National Comprehensive Cancer Network*, 15(5):555-562.
- Skoufias, D.A., Debonis, S., Saoudi, Y., Lebeau, L., Crevel, I., Cross, R., Wade, R.H., Hackney, D. & Kozielski, F.** (2006). S-Trityl-L-cysteine Is a Reversible, Tight Binding Inhibitor of the Human Kinesin Eg5 That Specifically Blocks Mitotic Progression. *Journal of Biological Chemistry*, 281(26):17559-17569.

- Soda, M., Choi, Y.L., Enomoto, M., Takada, S., Yamashita, Y., Ishikawa, S., Fujiwara, S.-I., Watanabe, H., Kurashina, K., Hatanaka, H., Bando, M., Ohno, S., Ishikawa, Y., Aburatani, H., Niki, T., Sohara, Y., Sugiyama, Y. & Mano, H. (2007).** Identification of the transforming EML4–ALK fusion gene in non-small-cell lung cancer. *Nature*, 448(7153):561-566.
- Solomon, B.J., Mok, T., Kim, D.-W., Wu, Y.-L., Nakagawa, K., Mekhail, T., Felip, E., Cappuzzo, F., Paolini, J., Usari, T., Iyer, S., Reisman, A., Wilner, K.D., Tursi, J. & Blackhall, F. (2014).** First-Line Crizotinib versus Chemotherapy in <i>ALK</i>-Positive Lung Cancer. *New England Journal of Medicine*, 371(23):2167-2177.
- Spigel, D.R., Reynolds, C., Waterhouse, D., Garon, E.B., Chandler, J., Babu, S., Thurmes, P., Spira, A., Jotte, R., Zhu, J., Lin, W.H. & Blumenschein, G. (2018).** Phase 1/2 Study of the Safety and Tolerability of Nivolumab Plus Crizotinib for the First-Line Treatment of Anaplastic Lymphoma Kinase Translocation — Positive Advanced Non–Small Cell Lung Cancer (CheckMate 370). *Journal of Thoracic Oncology*, 13(5):682-688.
- Stehbens, S. & Wittmann, T. (2012).** Targeting and transport: How microtubules control focal adhesion dynamics. *Journal of Cell Biology*, 198(4):481-489.
- Stenhouse, G., Fyfe, N., King, G., Chapman, A. & Kerr, K.M. (2004).** Thyroid transcription factor 1 in pulmonary adenocarcinoma. *Journal of Clinical Pathology*, 57(4):383-387.
- Stiff, T., Echegaray-Iturra, F.R., Pink, H.J., Herbert, A., Reyes-Aldasoro, C.C. & Hochegger, H. (2020).** Prophase-Specific Perinuclear Actin Coordinates Centrosome Separation and Positioning to Ensure Accurate Chromosome Segregation. *Cell Rep*, 31(8):107681.
- Stone, M.C., Roegiers, F. & Rolls, M.M. (2008).** Microtubules Have Opposite Orientation in Axons and Dendrites of Drosophila Neurons. *Molecular Biology of the Cell*, 19(10):4122-4129.
- Sun, J.J., Huang, M., Xiao, F. & Xi, Z.Q. (2015).** Echinoderm microtubule-associated protein - like protein 5 in anterior temporal neocortex of patients with intractable epilepsy. *Iran J Basic Med Sci*, 18(10):1008-1013.
- Sun, X.-D., Shi, X.-J., Sun, X.-O., Luo, Y.-G., Wu, X.-J., Yao, C.-F., Yu, H.-Y., Li, D.-W., Liu, M. & Zhou, J. (2011).** Dimethylenastron suppresses human pancreatic cancer cell migration and invasion in vitro via allosteric inhibition of mitotic kinesin Eg5. *Acta Pharmacologica Sinica*, 32(12):1543-1548.
- Sun, Z., Gong, W., Zhang, Y. & Jia, Z. (2020).** Physiological and Pathological Roles of Mammalian NEK7. *Frontiers in Physiology*, 11
- Suprenant, K.A., Dean, K., McKee, J. & Hake, S. (1993).** EMAP, an echinoderm microtubule-associated protein found in microtubule-ribosome complexes. *Journal of Cell Science*, 104(2):445-450.
- Suprenant, K.A., Tuxhorn, J.A., Daggett, M.A.F., Ahrens, D.P., Hostetler, A., Palange, J.M., Vanwinkle, C.E. & Livingston, B.T. (2000).** Conservation of the WD-repeat, microtubule-binding protein, EMAP, in sea urchins, humans, and the nematode *C. elegans*. *Development, Genes and Evolution*, 210(1):2-10.
- Tanimoto, A., Matsumoto, S., Takeuchi, S., Arai, S., Fukuda, K., Nishiyama, A., Yoh, K., Ikeda, T., Furuya, N., Nishino, K., Ohe, Y., Goto, K. & Yano, S. (2021).** Proteasome Inhibition

Overcomes ALK-TKI Resistance in ALK-Rearranged/TP53-Mutant NSCLC via Noxa Expression. *Clinical Cancer Research*, 27(5):1410-1420.

Tao, W., South, V.J., Zhang, Y., Davide, J.P., Farrell, L., Kohl, N.E., Sepp-Lorenzino, L. & Lobell, R.B. (2005). Induction of apoptosis by an inhibitor of the mitotic kinesin KSP requires both activation of the spindle assembly checkpoint and mitotic slippage. *Cancer Cell*, 8(1):49-59.

Targeted Oncology. 2017. *Nonbiomarker, Nonsquamous NSCLC: Diagnosis, Statistics, Staging, and Testing*. [online] Available at: <<https://www.targetedonc.com/view/nonbiomarker-nonsquamous-nsclc-diagnosis-statistics-staging-and-testing>> [Accessed 16 March 2022].

Tegha-Dunghu, J., Neumann, B., Reber, S., Krause, R., Erfle, H., Walter, T., Held, M., Rogers, P., Hupfeld, K., Ruppert, T., Ellenberg, J. & Gruss, O.J. (2008). EML3 is a nuclear microtubule-binding protein required for the correct alignment of chromosomes in metaphase. *Journal of Cell Science*, 121(10):1718-1726.

Thawani, A. & Petry, S. (2021). Molecular insight into how γ -TuRC makes microtubules. *Journal of Cell Science*, 134(14)

Theisen, U., Straube, E. & Straube, A. (2012). Directional Persistence of Migrating Cells Requires Kif1C-Mediated Stabilization of Trailing Adhesions. *Developmental Cell*, 23(6):1153-1166.

The Open Lab Book v1.0. (n.d) Measuring cell fluorescence using ImageJ. Available at: <https://theolb.readthedocs.io/en/latest/imaging/measuring-cell-fluorescence-using-imagej.html> (Accessed: 09 May 2023).

Thiery, J.P. (2002). Epithelial–mesenchymal transitions in tumour progression. *Nature Reviews Cancer*, 2(6):442-454.

Thiery, J.P., Acloque, H., Huang, R.Y.J. & Nieto, M.A. (2009). Epithelial-Mesenchymal Transitions in Development and Disease. *Cell*, 139(5):871-890.

Tomasek, J.J. & Hay, E.D. (1984). Analysis of the role of microfilaments and microtubules in acquisition of bipolarity and elongation of fibroblasts in hydrated collagen gels. *Journal of Cell Biology*, 99(2):536-549.

Tulpule, A., Guan, J., Neel, D.S., Allegakoen, H.R., Lin, Y.P., Brown, D., Chou, Y.-T., Heslin, A., Chatterjee, N., Perati, S., Menon, S., Nguyen, T.A., Debnath, J., Ramirez, A.D., Shi, X., Yang, B., Feng, S., Makhija, S., Huang, B. & Bivona, T.G. (2021). Kinase-mediated RAS signaling via membraneless cytoplasmic protein granules. *Cell*, 184(10):2649-2664.e2618.

Vallee, R.B., Williams, J.C., Varma, D. & Barnhart, L.E. (2004). Dynein: An ancient motor protein involved in multiple modes of transport. *Journal of Neurobiology*, 58(2):189-200.

Wadsworth, P. (1999). Regional regulation of microtubule dynamics in polarized, motile cells. *Cell Motil Cytoskeleton*, 42(1):48-59.

Waitzman, J.S. & Rice, S.E. (2014). Mechanism and regulation of kinesin-5, an essential motor for the mitotic spindle. *Biology of the Cell*, 106(1):1-12.

- Wang, G., Jiang, Q. & Zhang, C.** (2014). The role of mitotic kinases in coupling the centrosome cycle with the assembly of the mitotic spindle. *Journal of Cell Science*, 127(19):4111-4122.
- Waterman-Storer, C.M., Karki, S.B., Kuznetsov, S.A., Tabb, J.S., Weiss, D.G., Langford, G.M. & Holzbaur, E.L.F.** (1997). The interaction between cytoplasmic dynein and dynactin is required for fast axonal transport. *Proceedings of the National Academy of Sciences*, 94(22):12180-12185.
- Waterman-Storer, C.M., Worthylake, R.A., Liu, B.P., Burridge, K. & Salmon, E.D.** (1999). Microtubule growth activates Rac1 to promote lamellipodial protrusion in fibroblasts. *Nature Cell Biology*, 1(1):45-50.
- Woo, C.G., Seo, S., Kim, S.W., Jang, S.J., Park, K.S., Song, J.Y., Lee, B., Richards, M.W., Bayliss, R., Lee, D.H. & Choi, J.** (2017). Differential protein stability and clinical responses of EML4-ALK fusion variants to various ALK inhibitors in advanced ALK-rearranged non-small cell lung cancer. *Annals of Oncology*, 28(4):791-797.
- Woodruff, J.B., Wueseke, O. & Hyman, A.A.** (2014). Pericentriolar material structure and dynamics. *Philosophical Transactions of the Royal Society B: Biological Sciences*, 369(1650):20130459.
- Wu, J., Savooji, J. & Liu, D.** (2016). Second- and third-generation ALK inhibitors for non-small cell lung cancer. *Journal of Hematology & Oncology*, 9(1)
- Xiang, Y., Zhang, S., Fang, X., Jiang, Y., Fang, T., Liu, J. & Lu, K.** (2022). Therapeutic Advances of Rare ALK Fusions in Non-Small Cell Lung Cancer. *Current Oncology*, 29(10):7816-7831.
- Xu, Z., Schaedel, L., Portran, D., Aguilar, A., Gaillard, J., Marinkovich, M.P., Théry, M. & Nachury, M.V.** (2017). Microtubules acquire resistance from mechanical breakage through intraluminal acetylation. *Science*, 356(6335):328-332.
- Zappa, C. & Mousa, S.A.** (2016). Non-small cell lung cancer: current treatment and future advances. *Translational Lung Cancer Research*, 5(3):288-300.
- Zhang, H., Pao, L.I., Zhou, A., Brace, A.D., Halenbeck, R., Hsu, A.W., Bray, T.L., Hestir, K., Bosch, E., Lee, E., Wang, G., Liu, H., Wong, B.R., Kavanaugh, W.M. & Williams, L.T.** (2014). Deorphanization of the human leukocyte tyrosine kinase (LTK) receptor by a signaling screen of the extracellular proteome. *Proceedings of the National Academy of Sciences*, 111(44):15741-15745.
- Zhang, R., Alushin, G.M., Brown, A. & Nogales, E.** (2015). Mechanistic Origin of Microtubule Dynamic Instability and Its Modulation by EB Proteins. *Cell*, 162(4):849-859.
- Zhou, L., Wang, Z., Xu, X., Wan, Y., Qu, K., Fan, H., Chen, Q., Sun, X. & Liu, C.** (2016). Nek7 is overexpressed in hepatocellular carcinoma and promotes hepatocellular carcinoma cell proliferation in vitro and in vivo. *Oncotarget*, 7(14):18620-18630.